

University of Mississippi

eGrove

Electronic Theses and Dissertations

Graduate School

1-1-2016

Performance Evaluation and Improvement of Wireless Amplify-and-Forward Cooperative-Based Systems under Nodes Mobility and Imperfect CSI Estimation Impacts

Yazid Khattabi

University of Mississippi

Follow this and additional works at: <https://egrove.olemiss.edu/etd>



Part of the [Electrical and Electronics Commons](#)

Recommended Citation

Khattabi, Yazid, "Performance Evaluation and Improvement of Wireless Amplify-and-Forward Cooperative-Based Systems under Nodes Mobility and Imperfect CSI Estimation Impacts" (2016). *Electronic Theses and Dissertations*. 1387.

<https://egrove.olemiss.edu/etd/1387>

This Dissertation is brought to you for free and open access by the Graduate School at eGrove. It has been accepted for inclusion in Electronic Theses and Dissertations by an authorized administrator of eGrove. For more information, please contact egrove@olemiss.edu.

PERFORMANCE EVALUATION AND IMPROVEMENT OF WIRELESS
AMPLIFY-AND-FORWARD COOPERATIVE-BASED SYSTEMS UNDER NODES
MOBILITY AND IMPERFECT CSI ESTIMATION IMPACTS

A Dissertation
presented in partial fulfillment of requirements
for the degree of DOCTOR OF PHILOSOPHY
in the Department of Electrical Engineering
The University of Mississippi

by
YAZID KHATTABI

August 2016

ABSTRACT

Cooperative communication techniques have been introduced in wireless networks to achieve spacial diversity-gain via the readiness of multiple users (via relays) to assist a source forwarding its data to a final destination. Cooperative communication techniques have shown their capability in improving system reliability and extending coverage area, and hence, it is believable that they will act as a promising technology for the coming fifth-generation (5G). Nevertheless, most existing work reported in literature on performance studies of wireless cooperative-based systems are based on the assumptions that the multipath fading channels among systems cooperating nodes are quasi-static (i.e., fading channels coefficients are constant over a number of consecutive signaling periods) and channel-state-information (CSI) estimation processes at systems receivers are perfect. Nowadays, however, there is an increased number of users riding high-speed public transportation vehicles and demanding wireless data services through their own terminals. As a result of such high mobility wireless terminals, the assumption of time-selective (i.e., non quasi-static) fading is more realistic. This time-selective fading environment would severely deteriorate the performance of existing wireless cooperative systems that have been already designed based on the assumption of quasi-static fading (low users speeds). Further, due to impairments associated with practical receiver tracking-loops implementation issues, it is more general to assume that CSI estimations at systems receiving sides are imperfect.

The scope of this dissertation is to provide comprehensive performance evaluation study for several emerging models of wireless amplify-and-forward (AF) cooperative-based communication systems that operate under the effects of the more general scenarios of high nodes mobility (time-selective fading) and imperfect channel estimations. This performance evaluation study is conducted by deriving closed-form expressions for different performance

metrics; including error probability, outage probability and channel capacity. Monte Carlo simulations are also provided to complement and validate the analytical analyses. All of the obtained results in this dissertation are novel and general for mobile as well as non-moving nodes and for imperfect as well as perfect CSI estimations. Moreover, in this dissertation we develop innovative and applicable solutions and receiver designs that are capable of mitigating the detrimental impacts of the high nodes mobility on the performance of the cooperative system models under study.

DEDICATION

To my parents, my wife, and my kids.

ACKNOWLEDGEMENTS

First and foremost, without reconciling God, this work would not have been accomplished successfully.

My sincere grateful goes to my parents and my wife for their prayers, encouragements, patience and emotional support.

I would like to thank my academic advisor, Prof. Mustafa M. Matalgah, for his endless help and continuous support during my Ph.D study and dissertation work. I am most thankful for his valuable guidance and comments that helped in completing this work and publishing several technical papers as part of it.

I would like to extend my thankfulness and appreciation to my Ph.D. examining committee: Prof. Ramanarayanan “Vish” Viswanathan, Prof. Dwight Waddell and Prof. Hailin Sang for their advice and supportive comments. I would also like to thank Prof. Lei Cao, for his serving on the committee of this work prospectus, and our administration team at the Department of Electrical Engineering, Stefanie Delmastro and Dwight O’Dell, and especially, the department chairman Prof. Ramanarayanan “Vish” Viswanathan for the financial support provided during my study.

University, Mississippi

Yazid Khattabi

August, 2016

TABLE OF CONTENTS

ABSTRACT	ii
DEDICATION	iv
ACKNOWLEDGEMENTS	v
LIST OF TABLES	x
LIST OF FIGURES	xi
PREFACE	xiv
Part I: Amplify-and-Forward (AF) Cooperative Communication Systems with Mobile	
Nodes and Imperfect CSI Estimation	1
Introduction	2
1.1 Literature Review	2
1.2 Work Summery	4
Regular M -Relay Variable-Gain AF Cooperative Systems With Mobile Nodes and Perfect	
CSI Estimation: SNR Derivation and Performance Analysis	6
2.1 Chapter Overview	6
2.2 System and Channel Model	7
2.3 Preliminary Results: Effective SNR and pdf	12
2.4 System Performance Evaluation	19
2.5 Nodes Mobility and CSI Estimation Rates Effects	25
2.6 Numerical Results and Simulation	30

2.7 Conclusion	37
Regular M -Relay Variable-Gain AF Cooperative Systems with Mobile Nodes and Im-	
perfect CSI Estimation: SNR Derivation and Performance Analysis	42
3.1 Chapter Overview	42
3.2 System and Channel Model	42
3.3 Preliminary Results: Effective SNR and pdf	43
3.4 System Performance Evaluation	49
3.5 Numerical Results and Simulation	52
3.6 Conclusion	54
Best-Relay-Selection M -Relay Variable-Gain AF Cooperative Systems with Mobile Nodes	
and Imperfect CSI Estimation: SNR Derivation and Performance Analysis	56
4.1 Chapter Overview	56
4.2 System and Channel Model	56
4.3 Total SNR Derivation and Probability Density Function	57
4.4 System Performance Evaluation	60
4.5 Numerical Results and Simulation	66
4.6 Conclusion	69
Part II: Alamouti-Type OSTBC Based Amplify-and-Forward (AF) Cooperative Com-	
munication Systems with Mobile Nodes and Imperfect CSI Estimation	71
Introduction	72
5.1 Literature Review	72
5.2 Work Summery	73
Alamouti-OSTBC Based M -Relay Fixed-Gain AF Cooperative Systems with Mobile	
Nodes and Perfect CSI Estimation: SINR Derivation and SEP Analysis	75
6.1 Chapter Overview	75

6.2	System Model	76
6.3	System Conditional SEP Analysis	84
6.4	System Average SEP Analysis	90
6.5	System Performance under Static Nodes Case	91
6.6	Numerical Results and Simulation	94
6.7	Conclusion	95

Improved Performance Zero-Forcing Space-Time Decoder (ZFSTD) for High Mobility Alamouti-Type OSTBC Based AF Cooperative Systems: Decoder Design and SEP Analysis	99
--	----

7.1	Chapter Overview	99
7.2	System Model	100
7.3	ZFSTD Decoding Matrix Design	100
7.4	ZFSTD Output Decision Statistics	101
7.5	ZFSTD SEP Performance	102
7.6	ZFSTD under Static-Nodes Case	103
7.7	Numerical Results and Simulation	104
7.8	Conclusion	104

Improved Performance Low-Complexity Sub-Optimal Space-Time-Decoder (SOSTD) for High Mobility Alamouti-Type OSTBC Based AF Cooperative Systems: Decoder Design and SEP Analysis	107
--	-----

8.1	Chapter Overview	107
8.2	System Model	107
8.3	SOSTD Decoding Matrix Design	108
8.4	SOSTD Output Decision Statistics	112
8.5	SOSTD SEP Performance	114
8.6	SOSTD under Static-Nodes Case	115

8.7	Numerical and Simulation Results	116
8.8	Conclusion	119
Alamouti-OSTBC Based M -Relay Fixed-Gain AF Cooperative Systems with Mobile		
	Nodes and Imperfect CSI Estimation: SINR Derivation and SEP Analysis	120
9.1	Chapter Overview	120
9.2	System Model	121
9.3	ALD Decision Variables	124
9.4	System Conditional SEP Analysis	130
9.5	System Average SEP Analysis	144
9.6	Numerical Results and Simulation	145
9.7	Conclusion	149
Part III: Dissertation Conclusions and Proposed Future Work		151
Dissertation Conclusions and Proposed Future Work		152
10.1	Dissertation Conclusions	152
10.2	Proposed Future Work	154
BIBLIOGRAPHY		156
APPENDIX		162
Approximating $I_3^{\theta_1} \mathcal{S}_1$ as ZMCSCG		163
Approximating $I_6^{\xi_1} \mathcal{S}_1$ and $I_{12}^{\xi_1} \mathcal{S}_1$ as ZMCSCG		165
VITA		167

LIST OF TABLES

2.1	Different Correlation parameter values obtained using (2.2.5) for different relative speeds in mph and transmission data rates in kbps with carrier frequency of 1.9 GHz.	10
2.2	Different Correlation parameter values obtained using (2.2.5) for different relative speeds in mph and transmission data rates in kbps with carrier frequency of 5 GHz.	10

LIST OF FIGURES

2.1	System model: M -relay regular-protocol amplify-and-forward wireless cooperative network with time-selective fading channels.	8
2.2	BPSK BER versus E_s/N_o with 2% CSI estimation rates ($N = 50$) for number of relays $M = 1, 2$ and 3. In dB: $\mathbb{E}[h_{s,d}(1) ^2] = 1$, $\mathbb{E}[h_{s,\ell}(1) ^2] = \{1.5, 2.5, 3.5\}$ and $\mathbb{E}[h_{\ell,d}(1) ^2] = \{2.5, 3.5, 4.5\}$. The Source is mobile and the other nodes are static corresponding to correlation parameters of $\rho_{s,d} = \rho_{s,\ell} = 0.9997$ and $\rho_{i,d} = 1$	32
2.3	BPSK lower bound BER versus E_s/N_o with 5% CSI estimation rates ($N = 20$). In dB: $\mathbb{E}[h_{s,d}(1) ^2] = 1$, $\mathbb{E}[h_{s,\ell}(1) ^2] = \{1.5, 2.5, 3.5\}$ and $\mathbb{E}[h_{\ell,d}(1) ^2] = \{4.5, 5.5, 6.5\}$. The corresponding correlation parameter is 0.9986.	33
2.4	BPSK lower bound BER versus E_s/N_o with 2% CSI estimation rates ($N = 50$) and $M = 2$. In dB: first hop=second hop: $\mathbb{E}[h_{s,\ell}(1) ^2] = \mathbb{E}[h_{\ell,d}(1) ^2] = \{0.5, 0.8, 0.1.2\}$, first hop>second hop: $\mathbb{E}[h_{s,\ell}(1) ^2] = \{4.5, 5.5, 6.5\}$ and $\mathbb{E}[h_{\ell,d}(1) ^2] = \{1.5, 2.5, 3.5\}$, second hop>first hop: $\mathbb{E}[h_{s,\ell}(1) ^2] = \{1.5, 2.5, 3.5\}$ and $\mathbb{E}[h_{\ell,d}(1) ^2] = \{4.5, 5.5, 6.5\}$. The corresponding correlation parameter is 0.9989.	34
2.5	BPSK lower bound BER versus E_s/N_o for $M = 3$. In dB: $\mathbb{E}[h_{s,d}(1) ^2] = 1$, $\mathbb{E}[h_{s,\ell}(1) ^2] = \{4.5, 5.5, 6.5\}$ and $\mathbb{E}[h_{\ell,d}(1) ^2] = \{1.5, 2.5, 3.5\}$. The corresponding correlation parameter is 0.9969.	35
2.6	Outage probability versus E_s/N_o with 2% CSI estimation rates ($N = 50$). In dB: $\mathbb{E}[h_{s,d}(1) ^2] = 1$, $\mathbb{E}[h_{s,\ell}(1) ^2] = \{2.5, 3.5\}$ and $\mathbb{E}[h_{\ell,d}(1) ^2] = \{3.5, 4.5\}$. The Source is mobile and the other nodes are static corresponding to correlation parameters of $\rho_{s,d} = \rho_{s,\ell} = 0.9997$ and $\rho_{i,d} = 1$	36
2.7	Theoretical lower bound outage probability versus E_s/N_o with $M = 2$ and 2% CSI estimation rate. In dB: $\mathbb{E}[h_{s,d}(1) ^2] = 1$, $\mathbb{E}[h_{s,\ell}(1) ^2] = \{1.5, 2.5\}$ and $\mathbb{E}[h_{\ell,d}(1) ^2] = \{4.5, 5.5\}$. The corresponding correlation parameter is 0.9980.	37
2.8	Theoretical lower bound outage probability versus E_s/N_o with $M = 2$. In dB: $\mathbb{E}[h_{s,d}(1) ^2] = 1$, $\mathbb{E}[h_{s,\ell}(1) ^2] = \{1.5, 2.5\}$ and $\mathbb{E}[h_{\ell,d}(1) ^2] = \{4.5, 5.5\}$. The corresponding correlation parameter is 0.9980.	38
2.9	Average upper bound normalized capacity versus E_s/N_o with 2% CSI estimation rates ($N = 50$). In dB: $\mathbb{E}[h_{s,d}(1) ^2] = 1$, $\mathbb{E}[h_{s,\ell}(1) ^2] = \{2.5, 3.5\}$ and $\mathbb{E}[h_{\ell,d}(1) ^2] = \{3.5, 4.5\}$. The Source is mobile and the other nodes are static corresponding to correlation parameters of $\rho_{s,d} = \rho_{s,\ell} = 0.9997$ and $\rho_{i,d} = 1$	39
2.10	Theoretical upper bound average normalized capacity versus E_s/N_o with $M = 2$ and 2% CSI estimation rates. In dB: $\mathbb{E}[h_{s,d}(1) ^2] = 1$, $\mathbb{E}[h_{s,\ell}(1) ^2] = \{2, 3\}$ and $\mathbb{E}[h_{\ell,d}(1) ^2] = \{4, 2\}$. Correlation parameter of 0.9999 for 10 mph speed and 0.9990 for 75 mph speed.	40

2.11	Theoretical upper bound average normalized capacity versus E_s/N_o with $M = 2$. In dB: $\mathbb{E}[h_{s,\ell}(1) ^2] = \{2, 3, 1\}$ and $\mathbb{E}[h_{\ell,d}(1) ^2] = \{4, 2, 2\}$. The corresponding correlation parameter is 0.9986.	41
3.1	BPSK BER versus E_s/N_o with 2% CSI estimation rates ($N = 50$) and $M = 1, 2$ and 3. In dB: $\mathbb{E}[h_{s,d}(1) ^2] = 1$, $\mathbb{E}[h_{s,\ell}(1) ^2] = \{1.5, 2.5, 3.5\}$ and $\mathbb{E}[h_{\ell,d}(1) ^2] = \{2.5, 3.5, 4.5\}$. The Source is mobile and the other nodes are static corresponding to correlation parameters of $\rho_{s,d} = \rho_{s,\ell} = 0.9997$ and $\rho_{i,d} = 1$. In case of imperfect channel estimation: $\sigma_{e_{a,b}}^2 = 0.02 \forall(a, b)$	53
3.2	Per-block-average outage probability versus E_s/N_o with and $N = 30$ and $M = 1$ and 2. In dB: $\mathbb{E}[h_{s,d}(1) ^2] = 1$, $\mathbb{E}[h_{s,\ell}(1) ^2] = \{1.5, 2.5\}$ and $\mathbb{E}[h_{\ell,d}(1) ^2] = \{2.5, 3.5\}$. The corresponding correlation parameter is 0.9990. In case of imperfect estimation: $\sigma_{e_{a,b}}^2 = 0.03 \forall(a, b)$	54
3.3	Per-block-average upper-bound normalized capacity versus E_s/N_o with $N = 100$ and $M = 1, 2$ and 3. In dB: $\mathbb{E}[h_{s,d}(1) ^2] = 1$, $\mathbb{E}[h_{s,\ell}(1) ^2] = \{1.5, 2.5, 3.5\}$ and $\mathbb{E}[h_{\ell,d}(1) ^2] = \{2.5, 3.5, 4.5\}$. Imperfect estimation with $\sigma_{e_{a,b}}^2 = 0.01 \forall(a, b)$	55
4.1	System model: M -relay best-relay-selection amplify-and-forward wireless cooperative system with time-selective fading channels.	57
4.2	Best-relay selection BPSK BER versus E_s/N_o with $N = 25$ and 1 and $M = 1$ and 2. In dB: $\mathbb{E}[h_{s,d}(1) ^2] = \mathbb{E}[h_{s,\ell}(1) ^2] = \mathbb{E}[h_{\ell,d}(1) ^2] = 1$. The Source is mobile and the other nodes are static corresponding to correlation parameters of $\rho_{s,d} = \rho_{s,\ell} = 0.999$ and $\rho_{i,d} = 1$. Channel estimation is perfect ($\sigma_{e_{a,b}}^2 = 0 \forall(a, b)$).	66
4.3	Regular and best-relay-selection cooperative protocols BPSK BER versus E_s/N_o with $N = 50$ and $M = 2$. In dB: $\mathbb{E}[h_{s,d}(1) ^2] = 1$, $\mathbb{E}[h_{s,\ell}(1) ^2] = \{1.5, 2.5\}$ and $\mathbb{E}[h_{\ell,d}(1) ^2] = \{2.5, 3.5\}$. Mobile nodes corresponding to correlation parameter of 0.9998. Channel estimation is perfect ($\sigma_{e_{a,b}}^2 = 0 \forall(a, b)$).	67
4.4	Regular and best-relay-selection cooperative protocols BPSK error floors versus the correlation parameter ρ for $M = 2$ and $N = 10$ and 80. In dB: $\mathbb{E}[h_{s,d}(1) ^2] = 1$, $\mathbb{E}[h_{s,\ell}(1) ^2] = \{1.5, 2.5\}$ and $\mathbb{E}[h_{\ell,d}(1) ^2] = \{2.5, 3.5\}$	68
4.5	Best-relay-selection per-block-average upper bound system normalized capacity versus E_s/N_o with $B = 1$, $N = 50$ and $M = 2$. In dB: $\mathbb{E}[h_{a,b}(1) ^2] = 1 \forall(a, b)$	69
4.6	Best-relay-selection per-block-average lower-bound outage probability with and without estimation error. $N = 40$, $M = 1$ and 2, and $R = 1$. In dB: $\mathbb{E}[h_{a,b}(1) ^2] = 1 \forall(a, b)$	70
6.1	System model: Alamouti-OSTBC Transmission over M -relay fixed-gain amplify-and-forward wireless cooperative system with time-selective fading channels.	76
6.2	Average SEP versus E_s/N_o for $M = 1, 4$ and 64 QAM constellations, transmission data-rate $R_s = 9.6$ kbps, carrier frequency $f_c = 2.4$ GHz, path-loss exponent $n = 3$, normalized nodes distances $d_{s,\ell} = 1$ and $d_{\ell,d} = 2$	95
6.3	Average SEP versus E_s/N_o for $M = 1, 4$ and 64 QAM constellations, transmission data-rate $R_s = 64$ kbps, carrier frequency $f_c = 2.4$ GHz, path-loss exponent $n = 3$, normalized nodes distances $d_{s,\ell} = 1$ and $d_{\ell,d} = 2$	96

6.4	Average SEP versus E_s/N_o for $M = 1, 2$ and 3 , 16-QAM constellations, transmission data-rate $R_s = 25$ kbps, carrier frequency $f_c = 2.4$ GHz, path-loss exponent $n = 2$, normalized nodes distances $d_{s,\ell} = 2$ and $d_{\ell,d} = 1$	97
6.5	ALD Semi-analytic Average SEP versus E_s/N_o for $M = 2, 16$ and 256 QAM constellations, different transmission data-rates, carrier frequency $f_c = 2.4$ GHz, path-loss exponent $n = 2$, normalized nodes distances $d_{s,\ell} = 1$ and $d_{\ell,d} = 2$	98
7.1	Average SEP versus E_s/N_o for both ZFSTD and ALD. $M = 1, 2$ and 3 , QAM constellations size of 16 , transmission data-rate $R_s = 25$ kbps, carrier frequency $f_c = 2.4$ GHz, path-loss exponent $n = 3$, normalized nodes distances $d_{s,\ell} = 2$ and $d_{\ell,d} = 1$	105
7.2	Average SEP versus nodes relative speeds for both ZFSTD and ALD with $E_s/N_o = 20$ dB, different transmission data-rate values, $M = 1$ and 2 , QAM constellations size of 64 , carrier frequency $f_c = 2.4$ GHz, path-loss exponent $n = 3$, normalized nodes distances $d_{s,\ell} = 2$ and $d_{\ell,d} = 1$	106
8.1	Average SEP versus E_s/N_o for both ALD and SOSTD with 0 and 70 mph relative speeds, number of relays $M = 1, 2$ and 3 , QAM constellations size of 16 , transmission data-rate $R_s = 25$ kbps, carrier frequency $f_c = 2.4$ GHz, path-loss exponent $n = 2$, normalized nodes distances $d_{s,\ell} = 2$ and $d_{\ell,d} = 1$	116
8.2	Average SEP versus E_s/N_o for both ALD and SOSTD with 0 and 60 mph relative speeds, number of relays $M = 2$, QAM constellation sizes of 16 and 64 , transmission data-rate $R_s = 20$ kbps, carrier frequency $f_c = 2.4$ GHz, path-loss exponent $n = 3$, normalized nodes distances $d_{s,\ell} = 1$ and $d_{\ell,d} = 2$	117
8.3	Average SEP versus nodes relative speeds for both SOSTD and ALD with $E_s/N_o = 25$ dB, different transmission data-rate values of 9.6 and 25 kbps, $M = 1$, QAM constellations size of 4 and 16 , carrier frequency $f_c = 2.4$ GHz, path-loss exponent $n = 2$, normalized nodes distances $d_{s,\ell} = 1$ and $d_{\ell,d} = 2$	118
8.4	Average SEP versus transmission data-rate for both SOSTD and ALD with $E_s/N_o = 25$ dB, different nodes relative speeds of 10 and 75 mph, $M = 2$, $16 -$ QAM constellation, carrier frequency $f_c = 2.4$ GHz, path-loss exponent $n = 2$, normalized nodes distances $d_{s,\ell} = 1$ and $d_{\ell,d} = 2$	119
9.1	Average SEP versus E_s/N_o for $M = 1$ and 4 and 64 -QAM, transmission data-rate $R_s = 44$ kbps, carrier frequency $f_c = 1.9$ GHz, path-loss exponent $n = 2$, normalized nodes distances $d_{s,\ell} = 1$ and $d_{\ell,d} = 2$	146
9.2	Average SEP versus E_s/N_o for $M = 1$ and 2 , 16 QAM constellations, transmission data-rate $R_b = 44$ kbps, carrier frequency $f_c = 1.9$ GHz, path-loss exponent $n = 2$, normalized nodes distances $d_{s,\ell} = 1$ and $d_{\ell,d} = 2$	147
9.3	Average SEP versus nodes relative speeds in mph with $E_s/N_o = 25$ dB, different transmission data-rate values of 9.6 and 25 kbps, $M = 1$, QAM constellations size of 16 and 64 , carrier frequency $f_c = 2.4$ GHz, path-loss exponent $n = 3$, normalized nodes distances $d_{s,\ell} = 1$ and $d_{\ell,d} = 2$	148
9.4	Average SEP versus transmission data-rate in kbps with $E_s/N_o = 25$ dB, different nodes relative speeds of $10, 75$ and 120 mph, $M = 1$, $16 -$ QAM constellation, carrier frequency $f_c = 2.4$ GHz, path-loss exponent $n = 2$, normalized nodes distances $d_{s,\ell} = 1$ and $d_{\ell,d} = 2$	149

PREFACE

Modern wireless communication systems require reliable communication with very low error rates, in order to achieve very high data rates, and simple designs with less processing at mobile nodes. Achieving these requirements is mainly challenged by the multipath fading nature of the wireless channels, which greatly affects the quality of received signals and impairs overall system performance. Alleviating these multipath fading detrimental impacts in wireless systems is possible by employing diversity. The idea of diversity is based on transmitting same information-bearing signals over multiple independent fading channels and then combining all received replicas via appropriate diversity combining receiver. This technique has great capability of reducing the probability of having deep fading and of improving the combined received signal quality. Diversity techniques have been intensively studied in literature and several approaches have been proposed, which are already employed in current communication systems. One of these approaches is what so called antenna diversity (or spacial diversity), in which spaced sufficiently far enough multiple antennas can be located at the transmitter, the receiver or both. Based on where antennas are located in communication systems terminals, antenna diversity techniques can be classified into receive-diversity, using single transmit antenna and multiple receive antennas (so-called as single-input-multiple-output (SIMO) systems), and transmit-diversity, using multiple transmit antennas and single receive antenna (so-called as multiple-input-single-output (MISO) systems). Moreover, the combination of both is applicable and the resulted system is what so called multiple-input-multiple-output (MIMO) system. In SIMO systems, efficient combining methodologies are required at the receiving side to combine all received signals and

obtain the intended diversity gain. Among these combining methodologies that have been widely studied in communications literature are maximal-ratio-combining (MRC), equal-gain-combining (EGC) and selection-combining (SC). In MISO systems, diversity gain can be achieved at receiving sides if transmit data symbols are distributed among the transmit antennas in an efficient design that guarantees propagating them over multiple independent channels. Among these efficient designs is space-time-coding (STC). In STC-based communication systems, transmit data stream is encoded across transmit antennas and several signaling periods such that redundant reception of same information-bearing data symbols over independent fading channels is guaranteed. In MIMO systems design problems, there is a tradeoff between improving overall system performance (via extracting spacial diversity gain) or achieving higher spectral efficiency and data throughput (via extracting spacial multiplexing gain). Employing STC in MIMO systems is an oriented design approach toward maximizing system diversity gain and improving its performance. On the other hand, designing and employing vertical Bell-labs-layered-space-time (V-BLAST) receiving equalizers in MIMO systems is an oriented design approach toward maximizing system throughput.

Achieving MIMO spacial diversity and/or multiplexing gains at some wireless devices might be impractical due to their size, cost and energy limitations. Therefore, during the past decade, an alternative of what so-called cooperative communication has been proposed to achieve diversity without modifications on power and size constraints of mobile wireless terminals. This could be achieved by allowing multiple users (called relays) to cooperate and effectively share their antennas, as a virtual antenna array, and other resources to assist the source node (transmitter) forwarding its data to a final destination. In general, two common scenarios of relaying can be applied in cooperative networks; amplify-and-forward (AF) and decode-and-forward (DF). In AF system, the relays only amplify the received signals broadcasted from the source and retransmit them to the ultimate destination without any detection or decoding of the original data. In DF systems, the received signals at the relays are decoded to recover the information bearing data, and then retransmitted once again

toward the destination. It has been demonstrated that cooperative diversity techniques can achieve a diversity gain equal to the number of paths between the source and the ultimate destination even though all cooperating nodes are equipped with single antennas. Further, the transmission of space-time-codes over wireless cooperative networks has gained great interest in the research community. By this combination, the STC transmit diversity gain achieved at the receiving node can be increased proportionally with the number of the relays without affecting the design of the STC decoders. Recently, cooperative diversity is a promising technique that has found its way in several recent mobile wireless communication systems, e.g., IEEE 802.11s and 3GPP LTE. It is also expected to be included as a feature in the coming fifth-generation (5G) standards.

Performance analysis of cooperative diversity systems has attracted a huge research interest in the communications literature community. Nevertheless, most of reported research results are based on the the assumptions that the fading channels among the cooperating nodes are quasi-static (i.e., their fading coefficients are assumed to be constant over a number of consecutive signaling periods) and the channel-state-information (CSI) estimation processes at the systems receivers (the relays and destination) are perfect. However, in practical wireless networks applications, these assumptions are not fairly realistic. For example, nowadays, number of users using wireless terminals while they are riding high-speed public transportation vehicles (e.g., cars, buses, trains, subways, or airplanes) is increasing. In such high mobility wireless systems, and according to Jakes' autocorrelation model, increasing the relative speed between any two communicating nodes reduces the correlation between any two time-adjacent coefficients of their fading channels. This is basically as a result of the increased Doppler spread by nodes mobility. For example, a mobile moving at a speed of 70 mph, transmitting a data rate of 10 kilo-symbols-per-second (ksps) and operating at a carrier frequency of 5 GHz can introduce a Doppler shift of 550 Hz. Furthermore, the 3G European cellular standard (i.e., higher data-rate systems) works on trains as fast as 300 mile-per-hour (mph), which introduces a Doppler shift of up to 800 Hz for a carrier frequency

of 2 GHz. There are also some military applications like unmanned airborne vehicles (UAV) systems in which higher Doppler shifts is encountered. Therefore, in all of these applications, the assumption of time-selective (non quasi-static) fading is more realistic. Moreover, due to impairments associated with practical receiver implementation issues, it is more practical to assume that estimated fading channel coefficients at systems receivers are corrupted by estimation errors (i.e, CSI estimation is imperfect). These facts motivate us to investigate in this dissertation the impact of high nodes mobility (the time-selective fading) and the imperfect CSI estimation on the performance of different cooperative based wireless communication system scenarios and to propose innovative and realistic solutions to overcome with these impacts. This dissertation is partitioned into two main parts and each part is divided into chapters. In the following, we summarize the research contribution behind this dissertation by providing a summery for each part conducted work.

In Part I of this dissertation, we are concerned in analyzing and investigating the performance of wireless amplify-and-forward (AF) cooperative communication systems with single-antenna nodes under the impacts of the time-selective fading (due to high nodes mobility) and the imperfect CSI estimation. This part includes three main research problems. In the first one (chapter 2), we consider such a time-selective fading AF cooperative system model but with multiple relays, variable amplification gains at the relays, negligible CSI estimation errors (perfect estimation) at the receivers, and regular cooperative protocol (in which all relays signals are combined at the destination via MRC combining). In this chapter, we analyze the performance of this cooperative based system model in terms of three metrics; the bit error rate (BER), the outage probability and the system Shannon capacity. More specifically, we derive novel closed-form tight approximate expressions for the per-block-average of these three performance metrics, which are further verified through exact Monte Carlo simulations. The derived expressions in this chapter are general functions of both the cooperating nodes speeds (in terms of the links correlation parameters) and the

receivers' tracking loops CSI estimation rates¹ (in terms of the transmitted block length). Thus, these expressions are valid for mobile as well as static nodes for both low and high CSI estimation rates. We use these expressions to analytically investigate the system performance under the impacts of several nodes mobility scenarios. Further, these expressions are used to investigate the role of the receiver's tracking loops speeds in mitigating the high nodes mobility impact on the system performance. In the second research problem of part I (chapter 3), we consider same cooperative based system model considered in chapter 2, but, along with the practical assumption of nodes mobility (time-selective fading), we follow the more realistic assumption of imperfect CSI estimation at the relays and the destination receivers. Under these assumptions, we, in chapter 3, similarly analyze the overall system performance by deriving closed-form expressions for the system per-block-average BER, outage probability, and Shannon capacity. The performance metric expressions obtained in chapter 3 are functions of the fading channels correlation parameters as well as of the channel estimation errors, and thus, they generalize their corresponding performance metric expressions in chapter 2. It should be noted that the regular cooperative protocol (which is employed in chapters 2 and 3 of part I of this dissertation) has a drawback that the second phase data transmission from the relays to the destination requires number of orthogonal channels equivalent to the number of the system relays. This yields an inefficient use of the system channel resources and reduction in its spectral efficiency. An alternative to the regular cooperative protocol that can tackle this problem without reducing the achieved full diversity gain is the best-relay-selection. In this protocol, the relay that achieves the highest effective signal-to-noise-ratio (SNR) at the destination is the only relay that retransmits to the destination. By this scheme, the number of the required transmission channels is dropped to two, and thus, results in reduced required channel resources. However, in communication systems literature, performance evaluation of best-relay-selection cooperative based systems has been conducted with negligible nodes mobility and imperfect channel estimation effects.

¹By CSI estimation rate we mean how much the receivers' tracking loops are fast enough to catch up and estimate the fading channels coefficients over the individual signaling periods.

Thus, chapter 4 of this dissertation is dedicated to fill this literature gap by evaluating the performance of the best-relay-selection cooperative protocol considering both practical assumptions of mobile nodes and imperfect channel estimation. In chapter 4, we consider same system model as in chapter 3, but instead of employing the regular cooperative scheme we employ the best-relay-selection one and analyze its overall performance by deriving novel and general closed-form expressions for its BER, outage probability and Shannon capacity.

Part II of this dissertation includes four research problems, in which, we provide analytical symbol error probability (SEP) performance evaluation and improvement for wireless multiple-relay fixed-amplification-gain AF cooperative communication systems that employ Alamouti-type orthogonal-space-time-block-code (OSTBC) transmission at the source and operate in high mobility environment along with either perfect or imperfect CSI estimation. In chapter 6, we consider such a mobile cooperative system model with perfect CSI estimation assumption and employ the classical Alamouti space-time decoder (ALD) at the destination. We then show that the time-selective fading (or the high nodes mobility) destroys the orthogonality and the optimality of this ALD decoder as a result of its output correlated and non-separable (with inter-transmit-antenna-interference (ITAI)) decision statistics. Starting from these decision statistics, we derive exact general conditional SEP expression for the system under study and use it to semi-analytically evaluate the system average SEP performance. We show that this ALD based system average SEP performance is severely affected by high nodes mobility and experiences irreducible error floors. In order to overcome with this nodes mobility effect, in chapter 7, we design a zero-forcing-space-time-decoder (ZFSTD) that could be employed at the system destination (instead of the ALD) such that it is capable of providing decision statistics without ITAI terms. In chapter 7, we evaluate the average SEP performance of this proposed ZFSTD based system and show its perfect immunity against the high nodes mobility by completely suppressing the error floors. We also show, however, that this proposed ZFSTD has a drawback that its achieved error performance improvement over that of the ALD system comes at the expense

of additional decoding complexity at the destination. Therefore, in order to address this drawback, we propose in chapter 7 another space-time decoder that has high capability of reducing the nodes mobility impact on the system error performance, but without any additional decoding complexity (i.e., has decoding complexity level equal to that of the ALD but with improved error performance). In particular, we derive the decoding matrix of this proposed decoder, employ it at the destination and show that it achieves the required target by providing separable decision statistics and improved error performance. The proposed decoder in chapter 8 is sub-optimal because it provides correlated statistics, and hence, we refer to it as sub-optimal-space-time-decoder (SOSTD). In chapter 9 of the dissertation, we generalize the ALD system model studied in chapter 6 by assuming (along with assumption that the system fading channels are time-selective) that the channel estimation processes at the system relays and destination are imperfect. For this extended system, we derive tight approximate expression for its conditional SEP performance, which generalizes the one derived in chapter 6 and helps in investigating the impact of both nodes mobility and channel estimation errors on the performance of mobile AF cooperative communication systems that employs Alamouti-type OSTBC coding and decoding.

Part I:

Amplify-and-Forward (AF) Cooperative Communication Systems with Mobile Nodes and
Imperfect CSI Estimation

CHAPTER 1

Introduction

1.1 Literature Review

Performance evaluation of wireless cooperative communication networks under the impact of the more practical scenarios of imperfect (or outdated) channel estimation and/or time-selective fading (due to high nodes mobility or Doppler spread effect) has been considered in several locations in literature. In [1] and [2], the effects of practical channel estimation schemes, in terms of estimator design and pilot symbol spacing based upon realistic channel models, on the performance of quasi-static fading AF cooperative communication systems have been investigated. In [3], the impact of both imperfect channel estimation and Doppler spread on the performance of a single-relay AF cooperative system has been studied, where closed-form expression for the system symbol error rate (SER) performance has been derived. The authors of [4] have considered dual-hop AF cooperative system with quasi-static fading environment and investigated the effect of the imperfect channel estimation at the relay's receiver on the system error and outage probabilities. In [5], the authors have derived closed-form SER expressions for a multiple-relay DF cooperative network operating in time-selective fading environment but with perfect channel estimation. The work in [6] has focused on studying the harmful effects of the unknown and time-varying fading channels on the information rate of a single-relay AF cooperative system. The results reported in [3] and [5] have shown that the imperfect channel estimation and/or the time-selective fading assumptions severely degrade the coherent-detection error performance of the systems under study, where such degradation is mainly represented by irreducible error floors. It is worthwhile to mention that the analyses in [3]–[6] are conducted under the employment of

the pilot-symbol-assisted modulation (PSAM) technique to model the time-selective (time-varying) fading channels. In literature, PSAM technique has been proposed to estimate the gains of the time-varying fading channels and it is practically implemented by periodically inserting known pilot symbols to the transmitted data sequences [7], [8]. An alternative to PSAM, to model the time-varying fading channels or the channel estimation processes, is the first-order autoregressive (AR1) model. The information theoretic results reported in [9] have shown that the AR1 model is a sufficiently accurate model for the time-varying fading channels. The issue of estimating the parameters of the AR1 model have been studied in several places in literature [10], [11], [12]. In [10] and [11], the work is devoted to channel estimation and tracking of the AR1 model parameters in non-cooperative based systems. In [12], the authors have analysed these estimation and tracking processes for an AF cooperative system based on Kalman filter (KF) based algorithm. In [13], outdated channel estimates (due to feedback delay) have been assumed and modeled via the AR1 process, and its impact on the performance of relay selection AF cooperative system has been evaluated. In this modeling of the outdated channel estimates, the AR1 process is utilized to represent the correlation between the delayed (estimated) and the current (actual) fading channel coefficients. In [14] and [15], the AR1 model has been exploited to model the time-varying fading channels (by expressing the correlation between the actual time-adjacent channel coefficients) in cooperative systems. In [14], a partially coherent detector for AF and DF single-relay cooperative network has been proposed to mitigate the error floors appeared in case of coherent detections. In [15], the authors have considered a multiple-relay AF cooperative diversity system and employed the differential coherent detection at the destination in order to overcome with the time-varying fading channels impact. In the system model assumed in [15] the CSI is not required at the relays and the destination and the amplification gains at the relay nodes are not adaptive to the channel gains (i.e., fixed gains).

1.2 Work Summery

Based on the above aforementioned literature review and to the best of our knowledge, none of the work reported has addressed the performance evaluation of a multiple-relay AF wireless cooperative communication system with maximal-ratio-combining (MRC) at the destination under the effect of the time-selective fading and CSI estimation rates (i.e., how much the receivers are fast enough to track and estimate the channel gains over individual time slots). In the first three chapters of this part, we consider such a system model with a source node (S), M -relays (R_1, R_2, \dots, R_M) and a destination node (D) and use the AR1 process to model the system time-selective fading channels among the communicating nodes. Unlike the work in [15], we consider variable amplification gain at the relays, coherent MRC detection at the destination where the CSI knowledge is required at the system receivers. We first derive novel expressions for the direct and the i th indirect (end-to-end) paths instantaneous SNRs, which are general for the links temporal characteristics. We then exploit the moment generating function (MGF) approach to derive the probability density functions (pdf) of the upper bounded total effective SNR obtained at the output of the MRC destination. We use same pdf to derive general closed-form expressions for the per-block-average system BER, considering binary phase shift keying (BPSK) transmission, outage probability, and system Shannon capacity as well as their asymptotic limits. Using these derived expressions, we analytically and numerically investigate the impact of different nodes mobility scenarios as well as the effect of CSI estimation rates on the overall system performance. These analyses are conducted in this part for both assumptions of perfect (in chapter 2) and imperfect (in chapters 3 and 4) channel estimations. The analyses conducted in chapter 3, are repeated in chapter 4 but considering the best-relay-selection (BRS) scheme instead of the regular one. The remainder of this part of this dissertation is organized as follows. In chapter 2 we present the multiple-relay system and channel model and discusses the AR1 process used to model the fading channels, the variable-gains considered at the relays, and the CSI estimations at the relays and the destination. In this chapter, we employ the regular

cooperative protocol and analyze the overall system performance considering perfect channel estimation at the network's receivers. Chapter 3 extends the analysis in chapter 2 by following the more general assumption of imperfect channel estimation. In chapter 4, we reanalyze the performance of the system model under study but by employing the best-relay-selection cooperative protocol instead of the regular one along with imperfect channel estimation.

CHAPTER 2

Regular M -Relay Variable-Gain AF Cooperative Systems With Mobile Nodes and Perfect CSI Estimation: SNR Derivation and Performance Analysis

2.1 Chapter Overview

In this chapter, we consider a dual-hop multiple-relay variable-gain amplify-and-forward (AF) cooperative system with maximal ratio combining (MRC) at the destination and investigate the effects of both the cooperating-nodes mobility and the receivers' estimation rates of the channel state information (CSI) on its performance. By CSI estimation rates we mean how much the receivers' tracking loops are fast enough to catch up and estimate the fading channels gains over the individual signaling periods. Also, the estimation processes at the network's receivers (the relays and the destination) are assumed to be perfect, i.e., the channel estimation error is negligible. In addition, we employ in this chapter the regular cooperative protocol, in which all relays are active and participate in the relaying process via orthogonal transmissions. The fading links between any two cooperating nodes in this network are assumed to be frequency-flat (frequency-nonselective), time-selective (as a result of the nodes mobility), Rayleigh, independent but not identically distributed (i.n.i.d), and modeled by a first-order autoregressive (AR1) process.

Under these considerations, we first derive exact expressions for the destination's effective signal-to-noise-ratios (SNRs) through the direct (source-to-destination) and the i th-indirect (end-to-end) paths. Moreover, we derive approximate closed-form expression for the probability density function (pdf) of the total effective SNR at the destination's MRC output. Using this pdf, We derive closed-form tight approximate expressions for the system's per-block-average bit error rate (BER), outage probability, and system capacity in Shannon's

sense. These expressions are generic enough and valid for time-selective as well as quasi-static fading links for both low and high CSI estimation rates. We analytically show that, due to relatively high speeds of the cooperating-nodes, the system BER, outage probability, and capacity are severely degraded and, in some particular network circumstances, experience asymptotic limits. When both of the source and the destination are static, the system performance does not experience asymptotic limits even though the relays are in motion. On the other hand, despite that the relays are static, the mobility of either the source or the destination severely impact the system performance by asymptotic limits. Moreover, the difference between the impact of the source mobility and the destination mobility depends on the symmetrical conditions of the network two hops fading gains powers.

Moreover, we assume the scenario that the relays and the destination receivers are equipped with fast tracking and estimation loops, and show that the harmful impact of the nodes mobility (or the time-selective fading) can be completely eliminated. Simulation and numerical results are also provided to verify the accuracy of the derived analytical expressions.

2.2 System and Channel Model

2.2.1 Signal and link model

As depicted in Fig. 2.1, we consider a mobile cooperative network with a source node S communicates with a destination node D via a direct link (S - D) and M dual-hop indirect paths through M AF relays $R_i, i = 1, 2, \dots, M$ (S - R_i - D). We assume that the source transmits consequent data blocks each with N symbols length. Over the k th signaling-period, two phases of transmissions are accomplished throughout the network. In the first phase of cooperation, the source broadcasts the signal $x(k)$, and with average transmit energy E_s , to the destination and the relays. The received signals at the destination and at the i th relay

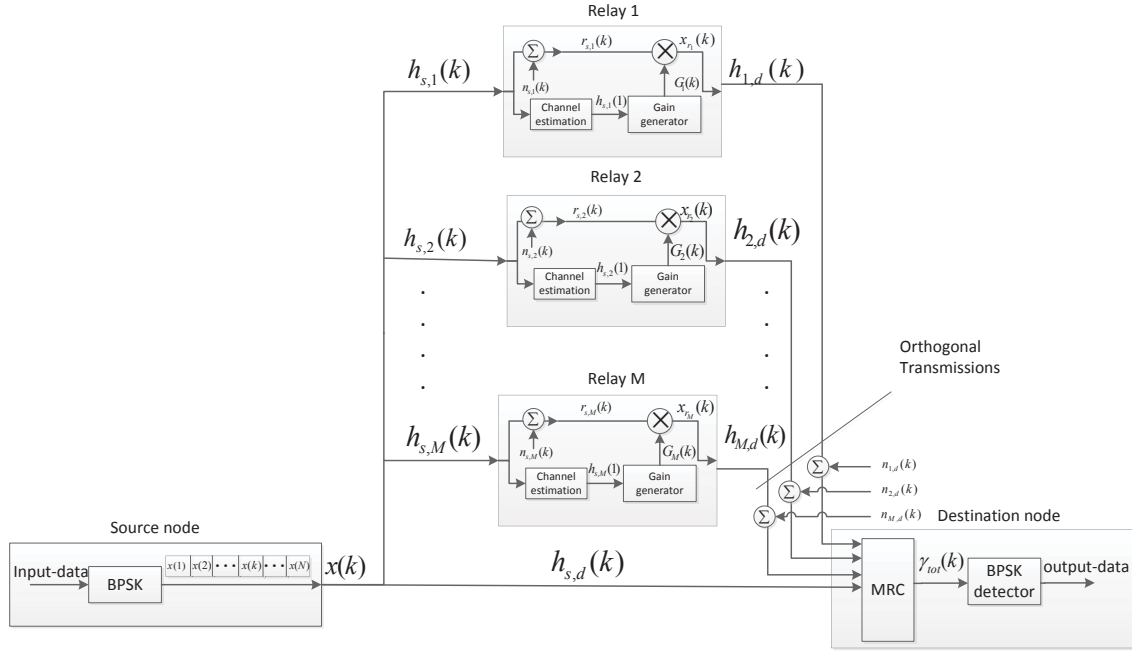


Figure 2.1. System model: M -relay regular-protocol amplify-and-forward wireless cooperative network with time-selective fading channels.

during this phase are, respectively, given by

$$r_{s,d}(k) = h_{s,d}(k)x(k) + n_{s,d}(k) \quad (2.2.1)$$

and,

$$r_{s,i}(k) = h_{s,i}(k)x(k) + n_{s,i}(k). \quad (2.2.2)$$

For AF relaying, the i th relay multiplies its received signal $r_{s,i}(k)$ by the amplifying gain $\mathcal{G}_i(k)$ and, in the second phase of cooperation, retransmits it toward the destination as $x_{r_i}(k) = \mathcal{G}_i(k)r_{s,i}(k)$. In this chapter we consider regular cooperative protocol, and thus these transmissions from all relays are required to be orthogonal (either via TDMA, FDMA

or CDMA) in order to travel through independent paths. However, the received signal at the destination from the i th relay can be written as

$$r_{i,d}(k) = h_{i,d}(k)x_{r_i}(k) + n_{i,d}(k). \quad (2.2.3)$$

The gains $h_{s,d}(k)$, $h_{s,i}(k)$ and $h_{i,d}(k)$ represent the small-scale fading coefficients corresponding to the k th transmitted symbol during the S - D , S - R_i and R_i - D fading links, respectively, which are distributed as complex Gaussian (i.e., Rayleigh envelope and uniform phase). Each of $n_{s,d}(k)$, $n_{s,i}(k)$ and $n_{i,d}(k)$ is a zero-mean circularly symmetric complex Gaussian (ZMCSCG) additive white noise with variance N_o ($\mathcal{CN}(0, N_o)$) and they, respectively, corrupt S - D , S - R_i and R_i - D links.

Because we consider mobile network, we assume that the relative speed between any two communicating nodes is significant, and according to Jakes' model [16], the variation in the time-adjacent channel gains of their associated fading links can be considered significant. In order to take this variation into account, we assume that each fading link between any two communicating nodes is characterized as time-selective and modeled by the first-order autoregressive (AR1) process [9] as

$$h_{a,b}(k) = \rho_{a,b}h_{a,b}(k-1) + \sqrt{1 - \rho_{a,b}^2}e_{a,b}(k) \quad (2.2.4)$$

where the pair a, b denotes for one of the following pairs; s, d , s, r_i and r_i, d . The random process $e_{a,b}(k)$ represents the varying component of the associated link and assumed to be ZMCSCG with a density of $\mathcal{CN}(0, \sigma_{a,b}^2)$. The coefficient $\rho_{a,b} \in [0, 1]$, represents the correlation parameter of the associated link and takes values between 0 and 1. According to Jakes' autocorrelation model [16], it is function of the communicating nodes relative speed ν , the transmitted symbol duration T_s , the carrier frequency f_c and the speed of light c as

$$\rho = \mathcal{J}_0\left(\frac{2\pi f_c \nu T_s}{c}\right) \quad (2.2.5)$$

where $\mathcal{J}_0(.)$ is the zeroth-order Bessel function of the first kind. It is clear from (2.2.5) that, at a certain value of the carrier frequency f_c , the parameter ρ is inversely proportional with the relative speed ν while it is directly proportional with the transmission data-rate $R_s = \frac{1}{T_s}$. Tables 2.1 and 2.2 shows different practical values for ρ as a function of the relative speed and the transmission data-rate at carrier frequencies of $f_c = 1.9$ GHz and $f_c = 5$ GHz, respectively.

Table 2.1. Different Correlation parameter values obtained using (2.2.5) for different relative speeds in mph and transmission data rates in kbps with carrier frequency of 1.9 GHz.

speed (mph)	10 kbps	44 kbps	64 kbps	144 kbps	1400 kbps
0	1	1	1	1	1
30	0.99968357	0.99998365	0.99999227	0.99999847	0.99999998
50	0.99802311	0.99989784	0.99995171	0.99999046	0.99999999
80	0.99494306	0.99973848	0.99987639	0.99997558	0.99999974
120	0.98863989	0.99941163	0.99972188	0.99994506	0.99999942
250	0.95116121	0.99744757	0.99879317	0.99976156	0.99999748

Table 2.2. Different Correlation parameter values obtained using (2.2.5) for different relative speeds in mph and transmission data rates in kbps with carrier frequency of 5 GHz.

speed (mph)	10 kbps	44 kbps	64 kbps	144 kbps	1400 kbps
0	1	1	1	1	1
30	0.99780966	0.9998868	0.9999465	0.99998943	0.99999989
50	0.9863496	0.99929263	0.99966563	0.99993395	0.9999993
80	0.9652415	0.99818963	0.99914411	0.99983091	0.99999821
120	0.922647	0.99592897	0.99807477	0.99961956	0.99999597
250	0.68579394	0.98239063	0.99165738	0.99834931	0.99998253

It should be noted that the set of the signals in (2.2.1), (2.2.2), and (2.2.3) summarizes the operations taking place for the k th transmitted symbol from the source ($x(k)$). This is because of our consideration that each fading link between any two nodes is time-selective, and consequently, the transmitted symbol at the k th signaling period experiences its own corresponding channel gains over the network.

2.2.2 Channel estimation and estimation-rate concept

Because the fading links in our network are time-selective (i.e., time varying), we assume that the relays and the destination estimation (or tracking) loops can not catch up with their time-varying channel gains over the individual signaling periods. However, we assume that these loops update their estimations only once every N transmitted symbols, and therefore, they can estimate (using a pilot signal¹) the fading gain over the first signaling period of each transmitted block from the source (i.e., $h_{a,b}(1) \forall a, b$) as $\hat{h}_{a,b}(1)$). We can now mean by CSI estimation rate as how much the receivers' tracking loops are fast enough to catch up with the rapid time-varying channel gains. In percentage, we quantify the CSI estimation rate as $(\frac{1}{N})100\%$. For example, 100% estimation rate means that the receivers can perfectly track and estimate all of the individual adjacent channel gains (i.e., $N=1$). In this chapter, we assume perfect-estimation of the fading links' gains, therefore, we can write $\hat{h}_{a,b}(1) = h_{a,b}(1)$ (the estimation error is negligible).

2.2.3 The amplification-gain

We consider variable amplification gains at the relays such that the instantaneous CSI is required at each relay. As stated in [18], the amplification gain is constrained to satisfy the following average energy constraint

$$\mathcal{E}(|x_{r_i}(k)|^2) = E_s. \quad (2.2.6)$$

Therefore, the amplification-gain at the i th relay of our time-selective fading system model, corresponding to the k th transmitted symbol, that can satisfy the constrain in (2.2.6) can be given by

$$\mathcal{G}_i(k) = \sqrt{\frac{E_s}{|h_{s,i}(k)|^2 E_s + N_o}}. \quad (2.2.7)$$

¹The work in [17] is conducted in the CSI estimation over wireless relying systems.

It is clear that the amplification-gain in (2.2.7) requires estimating $h_{s,i}(k)$. However, because the relays update their estimations only once every N transmitted symbols, the i th relay uses the estimated channel gain $h_{s,i}(1)$ instead of $h_{s,i}(k)$ to compute the amplification-gain in (2.2.7) as

$$\mathcal{G}_i(k) = \sqrt{\frac{E_s}{|h_{s,i}(1)|^2 E_s + N_o}}. \quad (2.2.8)$$

It is clear that the amplification-gain in (2.2.8) does not satisfy the required constraint in (2.2.6) unless the relative speed between the source and the i th relay is zero (or the S - R_i fading link is quasi-static with $\rho_{s,i} = 1$).

2.2.4 Regular cooperative protocol and Maximal Ratio Combining destination

In our network model, we assume that the destination employs MRC receiver, which combines the direct-path received signal with the M orthogonal received signals forwarded from the M relays. In addition, we assume symbol-by-symbol coherent detection process for the resulted MRC combined signal, i.e., MRC symbol-by-symbol detection. For such a detection process for the k th transmitted symbol $x(k)$, it is required from the destination to obtain estimated versions of $h_{a,b}(k) \forall a, b$ to be used in the MRC combining [19]. However, because, as we assumed above, the network receivers only estimates the gains $h_{a,b}(1) \forall a, b$, the destination receiver uses these estimated gains, instead of $\hat{h}_{a,b}(k)$, for the MRC detection process of $x(k)$. As will be shown later, this leads to sever performance degradation that represents the impact of the nodes' mobility (or of the time-selective fading).

2.3 Preliminary Results: Effective SNR and pdf

First, in order to mathematically show the time-selective fading impact on the destination received signals and to simplify the derivations of the effective SNRs, we derive, with the help of (2.2.4), the following relationship between $h_{a,b}(k)$ and $h_{a,b}(1)$

$$h_{a,b}(k) = \rho_{a,b}^{k-1} h_{a,b}(1) + \sqrt{1 - \rho_{a,b}^2} \sum_{j=1}^{k-1} \rho_{a,b}^{k-j-1} e_{a,b}(j) \quad (2.3.1)$$

2.3.1 destination direct-path effective SNR

First, by substituting (2.3.1), with the s, d pair, into (2.2.1), we can expand $r_{s,d}(k)$, showing the different noise terms, as

$$r_{s,d}(k) = \underbrace{\rho_{s,d}^{k-1} h_{s,d}(1) x(k)}_{\text{desired signal}} + \underbrace{x(k) \sqrt{1 - \rho_{s,d}^2} \sum_{j=1}^{k-1} \rho_{s,d}^{k-j-1} e_{s,d}(j)}_{\text{nodes' mobility noise}} + \underbrace{n_{s,d}(k)}_{\text{white noise}}. \quad (2.3.2)$$

Since $n_{s,d}(k)$ and $e_{s,d}(j)$ are independent ZMCSCG processes and the process $e_{s,d}(j)$ is i.i.d, the sum of the noise terms in (2.3.2) is also ZMCSCG and has a variance, $\sigma_{eff_{s,d}}^2$, which can be evaluated as

$$\begin{aligned} \sigma_{eff_{s,d}}^2 &= E_s (1 - \rho_{s,d}^2) \sum_{j=1}^{k-1} \rho_{s,d}^{2(k-j-1)} \text{Var}\{e_{s,d}(j)\} + \text{Var}\{n_{s,d}(k)\} \\ &= (1 - \rho_{s,d}^{2(k-1)}) \sigma_{s,d}^2 E_s + N_o. \end{aligned} \quad (2.3.3)$$

From (2.3.2) and (2.3.3), we can obtain the direct path destination SNR, corresponding to the k th signaling period, $\gamma_{s,d}(k)$ as

$$\begin{aligned} \gamma_{s,d}(k) &= \frac{\text{desired signal instantaneous power}}{\text{effective noise power}} = \frac{|\rho_{s,d}^{k-1} h_{s,d}(1) x(k)|^2}{\sigma_{eff_{s,d}}^2} \\ &= \frac{\rho_{s,d}^{2(k-1)} |h_{s,d}(1)|^2 E_s}{(1 - \rho_{s,d}^{2(k-1)}) \sigma_{s,d}^2 E_s + N_o}. \end{aligned} \quad (2.3.4)$$

It should be noted that if the S - D link is quasi-static, i.e., $\rho_{s,d} = 1$, then the nodes' mobility noise in (2.3.2) reduces to zero. Moreover, under such special case, $\gamma_{s,d}(k)$ in (2.3.4) reduces to $\gamma_{s,d} = \frac{|h_{s,d}(1)|^2 E_s}{N_o}$, which is a well know expression.

Because $|h_{s,d}(1)|$ is Rayleigh, $\gamma_{s,d}(k)$ has an exponential pdf, which can be given as

$$f_{\gamma_{s,d}(k)}(\gamma) = \frac{1}{\bar{\gamma}_{s,d}(k)} \exp\left(-\frac{\gamma}{\bar{\gamma}_{s,d}(k)}\right) \quad (2.3.5)$$

where

$$\bar{\gamma}_{s,d}(k) = \mathbb{E}[\gamma_{s,d}(k)] = \frac{\rho_{s,d}^{2(k-1)} E_s \mathbb{E}[|h_{s,d}(1)|^2]}{(1 - \rho_{s,d}^{2(k-1)}) \sigma_{s,d}^2 E_s + N_o}$$

and \mathbb{E} denotes the statistical mean operator.

2.3.2 destination end-to-end path effective SNR

We start deriving the effective SNR at the destination through the i th-relay indirect path (or the i th end-to-end path) and corresponding to the k th transmitting symbol, $\gamma_{s,i,d}(k)$, by first substituting (2.2.2) into (2.2.3) to write $r_{i,d}(k)$ as

$$r_{i,d}(k) = \mathcal{G}_i(k)x(k)h_{s,i}(k)h_{i,d}(k) + \mathcal{G}_i(k)h_{i,d}(k)n_{s,i}(k) + n_{i,d}(k). \quad (2.3.6)$$

By expanding $h_{s,i}(k)$ and $h_{i,d}(k)$ as in (2.3.1) and then substituting the obtained expansions into (2.3.6), we can expand $r_{i,d}(k)$ showing the desired signal and the overall noise terms as

$$\begin{aligned} r_{i,d}(k) = & \overbrace{\mathcal{G}_i(k)\rho_{s,i}^{k-1}\rho_{i,d}^{k-1}h_{s,i}(1)h_{i,d}(1)x(k)}^{\text{desired signal}} \\ & \overbrace{+\mathcal{G}_i(k)x(k)\rho_{s,i}^{k-1}h_{s,i}(1)\sqrt{1-\rho_{i,d}^2}\sum_{j=1}^{k-1}\rho_{i,d}^{k-j-1}e_{i,d}(j)}^{\text{overall effective noise}} \\ & +\rho_{i,d}^{k-1}h_{i,d}(1)\sqrt{1-\rho_{s,i}^2}\sum_{j=1}^{k-1}\rho_{s,i}^{k-j-1}e_{s,i}(j) + n_{i,d}(k) \\ & +\sqrt{1-\rho_{s,i}^2}\sum_{j=1}^{k-1}\rho_{s,i}^{k-j-1}e_{s,i}(j)\sqrt{1-\rho_{i,d}^2}\sum_{j=1}^{k-1}\rho_{i,d}^{k-j-1}e_{i,d}(j) \\ & +\mathcal{G}_i n_{s,i}(k)(\rho_{i,d}^{k-1}h_{i,d}(1) + \sqrt{1-\rho_{i,d}^2}\sum_{j=1}^{k-1}\rho_{i,d}^{k-j-1}e_{s,i}(j)). \end{aligned} \quad (2.3.7)$$

Similarly, the overall effective noise term in (2.3.7) is ZMCSCG, which we can obtain its variance, $\sigma_{eff_{s,i,d}}^2$, as

$$\begin{aligned}\sigma_{eff_{s,i,d}}^2 &= (1 - \rho_{s,i}^{2(k-1)})\sigma_{s,i}^2\rho_{i,d}^{2(k-1)}E_s\mathcal{G}_i^2(k)|h_{i,d}(1)|^2 + (1 - \rho_{i,d}^{2(k-1)})\sigma_{i,d}^2\rho_{s,i}^{2(k-1)}E_s \\ &\quad \times \mathcal{G}_i^2(k)|h_{s,i}(1)|^2 + \mathcal{G}_i^2(k)\rho_{i,d}^{2(k-1)}|h_{i,d}(1)|^2 N_o + N_o.\end{aligned}\quad (2.3.8)$$

From (2.3.7), we can obtain $\gamma_{s,i,d}(k)$ as

$$\begin{aligned}\gamma_{s,i,d}(k) &= \frac{|\mathcal{G}_i(k)\rho_{s,i}^{k-1}\rho_{i,d}^{k-1}h_{i,d}(1)h_{s,i}(1)x(k)|^2}{\sigma_{eff_{s,i,d}}^2} \\ &= \left(\mathcal{G}_i^2(k)\rho_{s,i}^{2(k-1)}\rho_{i,d}^{2(k-1)}|h_{i,d}(1)|^2|h_{s,i}(1)|^2E_s \right) / \left((1 - \rho_{s,i}^{2(k-1)})\sigma_{s,i}^2\rho_{i,d}^{2(k-1)} \right. \\ &\quad \times E_s\mathcal{G}_i^2(k)|h_{i,d}(1)|^2 + (1 - \rho_{i,d}^{2(k-1)})\sigma_{i,d}^2\rho_{s,i}^{2(k-1)}E_s\mathcal{G}_i^2(k)|h_{s,i}(1)|^2 + \mathcal{G}_i^2(k)\rho_{i,d}^{2(k-1)} \\ &\quad \times |h_{i,d}(1)|^2 N_o + N_o \Big). \end{aligned}\quad (2.3.9)$$

It is obvious that the SNR in (2.3.9) is instantaneous (random variable) in terms of the estimated channel gains $h_{s,i}(1)$ and $h_{i,d}(1)$, and obtaining its pdf from this form is not easily tractable. Therefore, in the following we rewrite (2.3.9) in more tractable form that helps in obtaining its pdf in closed-form expression. By substituting the amplification-gain given by (2.2.8) into (2.3.9), and after doing some manipulations and simplifications, we can write $\gamma_{s,i,d}(k)$ in the following form

$$\gamma_{s,i,d}(k) = \frac{\gamma_{s,i}(k)\gamma_{i,d}(k)}{\beta_i(k)\gamma_{s,i}(k) + \gamma_{i,d}(k) + \phi_i(k)} \quad (2.3.10)$$

where

$$\gamma_{s,i}(k) = \frac{E_s\rho_{s,i}^{2(k-1)}|h_{s,i}(1)|^2}{(1 - \rho_{s,i}^{2(k-1)})\sigma_{s,i}^2E_s + N_o} \quad (2.3.11)$$

$$\gamma_{i,d}(k) = \frac{E_s\rho_{i,d}^{2(k-1)}|h_{i,d}(1)|^2}{(1 - \rho_{i,d}^{2(k-1)})\sigma_{i,d}^2E_s + N_o}. \quad (2.3.12)$$

$$\beta_i(k) = \frac{(1 - \rho_{i,d}^{2(k-1)})\sigma_{i,d}^2 E_s + (N_o/\rho_{i,d}^{2(k-1)})}{(1 - \rho_{i,d}^{2(k-1)})\sigma_{i,d}^2 E_s + N_o} \quad (2.3.13)$$

$$\phi_i(k) = \frac{(1 - \rho_{s,i}^{2(k-1)})(1 - \rho_{i,d}^{2(k-1)})\sigma_{s,i}^2 \sigma_{i,d}^2 E_s^2 + (1 - \rho_{i,d}^{2(k-1)})\sigma_{i,d}^2 N_o E_s + N_o^2}{((1 - \rho_{s,i}^{2(k-1)})\sigma_{s,i}^2 E_s + N_o)((1 - \rho_{i,d}^{2(k-1)})\sigma_{i,d}^2 E_s + N_o)} \quad (2.3.14)$$

The SNRs $\gamma_{s,i}(k)$ and $\gamma_{i,d}(k)$ represent the effective SNRs of S - R_i and R_i - D links, respectively. The SNR expression in (2.3.10) is novel and has not been reported in literature before. It is function of the indirect links correlation parameters, $\rho_{s,i}$ and $\rho_{i,d}$, which are dependent on the mobile cooperating-nodes speeds. As a special case, when the links of the i th indirect path are quasi-static, i.e., ($\rho_{s,i} = \rho_{i,d} = 1$) the expression in (2.3.10) reduces to

$$\gamma_{s,i,d} = \frac{\gamma_{s,i}\gamma_{i,d}}{\gamma_{s,i} + \gamma_{i,d} + 1} \quad (2.3.15)$$

where $\gamma_{s,i} = \frac{E_s|h_{s,i}|^2}{N_o}$ and $\gamma_{i,d} = \frac{E_s|h_{i,d}|^2}{N_o}$. The SNR in (2.3.15) is well known in literature for dual-hop AF cooperative network over quasi-static fading links [20] and [21], and it is clear that it is not function of the symbol position k because, in the quasi-static fading assumption, all of the transmitted symbols experience equal channel gains over time.

Simplifying $\gamma_{s,i,d}(k)$ from the form in (2.3.9) to the form in (2.3.10) is intended in order to simplify the problem of obtaining mathematically tractable closed-form expression for its pdf. This is possible if we first propose the following upper-bound ² on $\gamma_{s,i,d}(k)$ as

$$\gamma_{s,i,d}(k) \leq \min(\gamma_{s,i}(k), \gamma_{i,d}(k)). \quad (2.3.16)$$

In this chapter, we continue our analysis based on approximating $\gamma_{s,i,d}(k)$ by its upper bound as

$$\gamma_{s,i,d}(k) \approx \gamma_{\text{up},i}(k) = \min(\gamma_{s,i}(k), \gamma_{i,d}(k)) \quad (2.3.17)$$

²This approximation has been applied in several locations in literature (see e.g., [19] and [22]) on the end-to-end effective SNR in (2.3.15) for the quasi-static fading case.

which has the following exponential pdf

$$f_{\gamma_{\text{up},i}(k)}(\gamma) = \frac{1}{\bar{\gamma}_{\text{up},i}(k)} \exp\left(-\frac{\gamma}{\bar{\gamma}_{\text{up},i}(k)}\right) \quad (2.3.18)$$

where

$$\bar{\gamma}_{\text{up},i}(k) = \frac{\bar{\gamma}_{s,i}(k)\bar{\gamma}_{i,d}(k)}{(\bar{\gamma}_{s,i}(k) + \bar{\gamma}_{i,d}(k))}. \quad (2.3.19)$$

2.3.3 MRC destination overall SNR

In regular cooperative protocol, all relays in the network participate in the transmission process and forward their amplified signals toward the destination. The destination combines all these signals with the direct path signal using MRC. The overall (total) effective SNR at the output of the destination's MRC combiner, corresponding to the k th transmitted symbol, can be written now as

$$\gamma_{\text{tot}}(k) = \gamma_{s,d}(k) + \sum_{i=1}^M \gamma_{s,i,d}(k). \quad (2.3.20)$$

By approximating $\gamma_{s,i,d}(k)$ as in (2.3.17), we can approximate $\gamma_{\text{tot}}(k)$ in (2.3.20) as

$$\gamma_{\text{tot}}(k) \approx \gamma_{\text{tot,up}}(k) = \gamma_{s,d}(k) + \sum_{i=1}^M \gamma_{\text{up},i}(k) \quad (2.3.21)$$

It is clear that $\gamma_{\text{tot,up}}(k)$ is a sum of independent exponential random variables, and by using the moment generating function (MGF) approach, we can find its pdf $f_{\gamma_{\text{tot,up}}(k)}(\gamma)$ as

$$f_{\gamma_{\text{tot,up}}(k)}(\gamma) = \mathcal{L}^{-1}\{\mathbf{M}_{\gamma_{\text{tot,up}}(k)}(s)\} \quad (2.3.22)$$

where \mathcal{L}^{-1} denotes the Inverse Laplace Transform (ILT) and $\mathbf{M}_X(s) = E[e^{-sx}]$ is the MGF. Given that fact that the MGF of an exponential random variable with mean λ is given as

$\frac{1}{1+\lambda s}$, we can obtain $\mathbf{M}_{\gamma_{\text{tot,up}}(k)}$ as

$$\mathbf{M}_{\gamma_{\text{tot,up}}(k)}(s) = \mathbf{M}_{\gamma_{s,d}(k)}(s) \prod_{i=1}^M \mathbf{M}_{\gamma_{\text{up},i}(k)}(s) = \frac{1}{(1 + s\bar{\gamma}_{s,d}(k)) \prod_{i=1}^M (1 + s\bar{\gamma}_{\text{up},i}(k))}. \quad (2.3.23)$$

We can now decompose $\mathbf{M}_{\gamma_{\text{tot,up}}(k)}(s)$ in (2.3.23) into its partial fraction terms as

$$\mathbf{M}_{\gamma_{\text{tot,up}}(k)}(s) = \frac{\xi_{\text{up}}}{1 + s\bar{\gamma}_{s,d}(k)} + \sum_{i=1}^M \frac{\xi_{\text{up},i}}{1 + s\bar{\gamma}_{\text{up},i}(k)} \quad (2.3.24)$$

where

$$\xi_{\text{up}} = \mathbf{M}_{\gamma_{\text{tot,up}}(k)}(s)(1 + s\bar{\gamma}_{s,d}(k))|_{s=-\frac{1}{\bar{\gamma}_{s,d}(k)}} = \frac{\bar{\gamma}_{s,d}^M(k)}{\prod_{i=1}^M (\bar{\gamma}_{s,d}(k) - \bar{\gamma}_{\text{up},i}(k))} \quad (2.3.25)$$

and

$$\begin{aligned} \xi_{\text{up},i} &= \mathbf{M}_{\gamma_{\text{tot,up}}(k)}(s)(1 + s\bar{\gamma}_{\text{up},i}(k))|_{s=-\frac{1}{\bar{\gamma}_{\text{up},i}(k)}} \\ &= \frac{\bar{\gamma}_{\text{up},i}^M(k)}{(\bar{\gamma}_{\text{up},i}(k) - \bar{\gamma}_{s,d}(k)) \prod_{i=1, i \neq j}^M (\bar{\gamma}_{\text{up},i}(k) - \bar{\gamma}_{\text{up},j}(k))}. \end{aligned} \quad (2.3.26)$$

By substituting (2.3.24) into (2.3.22) and solving for the ILT based on the fact that $\mathcal{L}^{-1}\{\frac{1}{1+as}\} = \frac{1}{a} \exp(-\frac{x}{a})$, we can obtain $f_{\gamma_{\text{tot,up}}(k)}(\gamma)$ in its ultimate closed-form as

$$f_{\gamma_{\text{tot,up}}(k)}(\gamma) = \frac{\xi_{\text{up}} e^{\left(\frac{-\gamma}{\bar{\gamma}_{s,d}(k)}\right)}}{\bar{\gamma}_{s,d}(k)} + \sum_{i=1}^M \frac{\xi_{\text{up},i} e^{\left(\frac{-\gamma}{\bar{\gamma}_{\text{up},i}(k)}\right)}}{\bar{\gamma}_{\text{up},i}(k)}. \quad (2.3.27)$$

As a special case of quasi-static fading environment within the network, i.e., $\rho_{s,d} = \rho_{s,i} = \rho_{i,d} = 1$, (2.3.27) reduces to [23, Eq. (17)]. This means that our derived pdf in (2.3.27) generalizes what has been obtained in the literature from the quasi-static fading case to the more general case of time-selective fading.

In the next section, we use the pdf in (2.3.27) to derive analytical closed-form general expressions for the system per-block-average BPSK BER, outage probability, and Shannon

capacity as well as their corresponding asymptotic limits.

2.4 System Performance Evaluation

In this section we use the pdf given by (2.3.27) to derive closed-form analytical expressions for the system per-block-average BER considering BPSK transmission at the source, outage probability, and Shannon capacity. These expressions are functions of the number of relays (M), the CSI estimation rates at the network receivers (in terms of the block length N), and the relative speeds among the cooperating nodes in terms of the time-selective fading links's correlation parameters $\rho_{a,b} \forall(a, b)$.

2.4.1 Error probability

In this subsection, we consider BPSK transmission over the network and derive lower-bound closed-form expression for the per-block-average BER at the output of the BPSK demodulator that follows the MRC combiner. Since BPSK modulation scheme is considered, the k th transmitted symbol $x(k)$ is given as $\pm\sqrt{E_s}$ and the conditional BER is given by $Q(\sqrt{2\gamma_{\text{tot}}(k)})$ where $Q(x)$ is the Q-function. Assuming equiprobable N symbols in the transmitted block, the per-block-average BER can be given as

$$\overline{P}_e = \frac{1}{N} \sum_{k=1}^N \mathbb{E}[Q(\sqrt{2\gamma_{\text{tot}}(k)})] = \frac{1}{N} \sum_{k=1}^N \left(\int_0^\infty Q(\sqrt{2\gamma}) f_{\gamma_{\text{tot}}(k)}(\gamma) d\gamma \right). \quad (2.4.1)$$

If we consider the approximated total SNR $\gamma_{\text{tot,up}}(k)$, along with its pdf in (2.3.27), in evaluating (2.4.1) instead of the $\gamma_{\text{tot}}(k)$, we can obtain the lower-bound per-block-average

BER as

$$\begin{aligned}
\bar{P}_{e,\text{Low}} &= \frac{1}{N} \sum_{k=1}^N \left(\int_0^\infty Q(\sqrt{2\gamma}) f_{\gamma_{\text{tot},\text{up}}(k)}(\gamma) d\gamma \right) \\
&= \frac{1}{N} \sum_{k=1}^N \left(\frac{\xi_{\text{up}}}{\bar{\gamma}_{s,d}(k)} \int_0^\infty Q(\sqrt{2\gamma}) e^{\frac{-\gamma}{\bar{\gamma}_{s,d}(k)}} d\gamma \right. \\
&\quad \left. + \sum_{i=1}^M \left(\frac{\xi_{\text{up},i}}{\bar{\gamma}_{\text{up},i}(k)} \int_0^\infty Q(\sqrt{2\gamma}) e^{\frac{-\gamma}{\bar{\gamma}_{\text{up},i}(k)}} d\gamma \right) \right) \\
&= \frac{1}{2N} \sum_{k=1}^N \left(\xi_{\text{up}} \left[1 - \sqrt{\frac{\bar{\gamma}_{s,d}(k)}{1 + \bar{\gamma}_{s,d}(k)}} \right] + \sum_{i=1}^M \xi_{\text{up},i} \left[1 - \sqrt{\frac{\bar{\gamma}_{\text{up},i}(k)}{1 + \bar{\gamma}_{\text{up},i}(k)}} \right] \right). \tag{2.4.2}
\end{aligned}$$

The integrals in (2.4.2) were evaluated using the by-parts integration technique. In order to analytically support our claims about the performance degradation due to the nodes mobility (i.e., time-selective links), it is informative to derive the asymptotic BER floor, which can be found by evaluating the limit in (2.4.2) at very high values of the per-symbol average SNR i.e., $\frac{E_s}{N_o}$. To simplify the evaluation of this limit we need first to write (2.4.2) in terms of $\frac{E_s}{N_o}$. By substituting the expressions of $\bar{\gamma}_{s,d}(k)$, $\bar{\gamma}_{s,i}(k)$, and $\bar{\gamma}_{i,d}(k)$, from (2.3.10), (2.3.11) and (2.3.12), respectively, into (2.4.2), and after doing some manipulations and simplifications, we obtain³

$$\begin{aligned}
\bar{P}_{e,\text{Low}} &= \frac{1}{2N} \sum_{k=1}^N \left(\alpha^M \left[1 - \sqrt{\frac{\alpha \frac{E_s}{N_o}}{\zeta \frac{E_s}{N_o} + 1}} \right] \prod_{i=1}^M \left(\frac{\eta_i \frac{E_s}{N_o} + \beta_i}{\mu_i \frac{E_s}{N_o} + \lambda_i} \right) \right. \\
&\quad \left. - \sum_{i=1}^M \left(\left[1 - \sqrt{\frac{\delta_i \frac{E_s}{N_o}}{\chi_i \frac{E_s}{N_o} + \beta_i}} \right] \frac{(\delta_i)^M (\kappa \frac{E_s}{N_o} + 1)}{\mu_i \frac{E_s}{N_o} + \lambda_i} \prod_{j=1, j \neq i}^M \left(\frac{\eta_j \frac{E_s}{N_o} + \beta_j}{\nu_{i,j} \frac{E_s}{N_o} + \omega_{i,j}} \right) \right) \right) \tag{2.4.3}
\end{aligned}$$

³The parameters ξ_{up} and $\xi_{\text{up},i}$ in (2.4.2) are also functions of $\bar{\gamma}_{s,d}(k)$, $\bar{\gamma}_{s,i}(k)$ and $\bar{\gamma}_{i,d}(k)$ (see (2.3.25) and (2.3.26)).

where

$$\begin{aligned}
\zeta &= \alpha + \kappa \\
\mu_i &= \alpha\eta_i - \delta_i\kappa \\
\lambda_i &= \alpha\beta_i - \delta_i \\
\chi_i &= \eta_i + \delta_i \\
\nu_{i,j} &= \delta_i\eta_j - \delta_j\eta_i \\
\omega_{i,j} &= \delta_i\beta_j - \delta_j\beta_i \\
\alpha &= \rho_{s,d}^{2(k-1)}\mathbb{E}[|h_{s,d}(1)|^2] \\
\kappa &= 1 - \rho_{s,d}^{2(k-1)} \\
\eta_\ell &= \rho_{s,\ell}^{2(k-1)}(1 - \rho_{\ell,d}^{2(k-1)})\mathbb{E}[|h_{s,\ell}(1)|^2] \\
&\quad + \rho_{\ell,d}^{2(k-1)}(1 - \rho_{s,\ell}^{2(k-1)})\mathbb{E}[|h_{\ell,d}(1)|^2] \\
\beta_\ell &= \rho_{s,\ell}^{2(k-1)}\mathbb{E}[|h_{s,\ell}(1)|^2] + \rho_{\ell,d}^{2(k-1)}\mathbb{E}[|h_{\ell,d}(1)|^2] \\
\delta_\ell &= \rho_{s,\ell}^{2(k-1)}\rho_{\ell,d}^{2(k-1)}\mathbb{E}[|h_{s,\ell}(1)|^2]\mathbb{E}[|h_{\ell,d}(1)|^2], \quad \forall \ell = 1, 2, \dots, M.
\end{aligned}$$

In order to analytically support our claims about the performance degradation due to the nodes' mobility and the constrained CSI estimation rates, it is informative to derive the irreducible BER floor, which can be found by evaluating the limit of (2.4.3) at very high values of the per-symbol average SNR, $\frac{E_s}{N_o}$, as

$$\begin{aligned}
\lim_{\frac{E_s}{N_o} \rightarrow \infty} \bar{P}_{e,\text{Low}} &= \frac{1}{2N} \sum_{k=1}^N \left(\alpha^M \left[1 - \sqrt{\frac{\alpha}{\zeta}} \right] \prod_{i=1}^M \left(\frac{\eta_i}{\mu_i} \right) \right. \\
&\quad \left. - \sum_{i=1}^M \frac{\kappa(\delta_i)^M \left[1 - \sqrt{\frac{\delta_i}{\chi_i}} \right] \prod_{j=1, j \neq i}^M \frac{\eta_j}{\nu_{i,j}}}{\mu_i} \right). \tag{2.4.4}
\end{aligned}$$

2.4.2 Outage probability

For our M -relay cooperative network model, the mutual information between the source and the destination, corresponding to the k th transmitted symbol, can be expressed as [18]

$$I(k) = \frac{1}{M+1} \log_2(1 + \gamma_{\text{tot}}(k)). \quad (2.4.5)$$

The reason for the $\frac{1}{M+1}$ factor in (2.4.5) is that the transmission process in a regular cooperative protocol takes place in $M+1$ orthogonal channels or time-slots. The outage probability for the k th transmitted symbol, say $P_{\text{out}}(k)$, is defined as the probability that the channel mutual information, $I(k)$, falls below the required rate R , which can be expressed as

$$P_{\text{out}}(k) = Pr\{I(k) \leq R\} = Pr\{\gamma_{\text{tot}}(k) < \gamma_{th}\} = \int_0^{\gamma_{th}} f_{\gamma_{\text{tot}}(k)}(\gamma) d\gamma \quad (2.4.6)$$

where $\gamma_{th} = 2^{(M+1)R} - 1$. By assuming equiprobable N symbols in the transmitted block, we can obtain the per-block-average outage probability for our system model as

$$P_{\text{out}} = \frac{1}{N} \sum_{k=1}^N \left(\int_0^{\gamma_{th}} f_{\gamma_{\text{tot}}(k)}(\gamma) d\gamma \right). \quad (2.4.7)$$

By using the pdf given by (2.3.27) in evaluating (2.4.7), we can obtain the lower-bound per-block-average outage probability as

$$\begin{aligned} P_{\text{out,Low}} &= \frac{1}{N} \sum_{k=1}^N \left(\int_0^{\gamma_{th}} f_{\gamma_{\text{tot,up}}(k)}(\gamma) d\gamma \right) \\ &= \frac{1}{N} \sum_{k=1}^N \left(\frac{\xi_{\text{up}}}{\bar{\gamma}_{s,d}(k)} \int_0^{\gamma_{th}} e^{\left(\frac{-\gamma}{\bar{\gamma}_{s,d}(k)}\right)} d\gamma + \sum_{i=1}^M \frac{\xi_{\text{up},i}}{\bar{\gamma}_{\text{up},i}(k)} \int_0^{\gamma_{th}} e^{\left(\frac{-\gamma}{\bar{\gamma}_{\text{up},i}(k)}\right)} d\gamma \right) \\ &= \frac{1}{N} \sum_{k=1}^N \left(\xi_{\text{up}} \left(1 - e^{\frac{-\gamma_{th}}{\bar{\gamma}_{s,d}(k)}} \right) + \sum_{i=1}^M \left(\xi_{\text{up},i} \left(1 - e^{\frac{-\gamma_{th}}{\bar{\gamma}_{\text{up},i}(k)}} \right) \right) \right). \end{aligned} \quad (2.4.8)$$

and then by substituting the expressions of $\bar{\gamma}_{s,d}(k)$, $\bar{\gamma}_{s,i}(k)$, and $\bar{\gamma}_{i,d}(k)$, from (2.3.10), (2.3.11) and (2.3.12), respectively, into (2.4.8), and after some manipulations and simplifications, we

can write $P_{\text{out,Low}}$ in terms of $\frac{E_s}{N_o}$ as

$$P_{\text{out,Low}} = \frac{1}{N} \sum_{k=1}^N \left(\alpha^M \left(1 - e^{-\frac{\kappa \frac{E_s}{N_o} + 1}{\alpha \frac{E_s}{N_o}} \gamma_{th}} \right) \prod_{i=1}^M \left(\frac{\eta_i \frac{E_s}{N_o} + \beta_i}{\mu_i \frac{E_s}{N_o} + \lambda_i} \right) \right. \\ \left. - \sum_{i=1}^M \left(\left(1 - e^{-\frac{\eta_i \frac{E_s}{N_o} + \beta_i}{\delta_i \frac{E_s}{N_o}} \gamma_{th}} \right) \frac{(\delta_i)^M (\kappa \frac{E_s}{N_o} + 1)}{\mu_i \frac{E_s}{N_o} + \lambda_i} \prod_{j=1, j \neq i}^M \left(\frac{\eta_j \frac{E_s}{N_o} + \beta_j}{\nu_{i,j} \frac{E_s}{N_o} + \omega_{i,j}} \right) \right) \right). \quad (2.4.9)$$

Due to the assumption of the time-selective fading, the outage probability performance also experiences outage floor, which can be obtained as

$$\lim_{\frac{E_s}{N_o} \rightarrow \infty} P_{\text{out,Low}} = \frac{1}{N} \sum_{k=1}^N \left(\alpha^M \left(1 - e^{-\frac{\kappa}{\alpha} \gamma_{th}} \right) \prod_{i=1}^M \left(\frac{\eta_i}{\mu_i} \right) \right. \\ \left. - \sum_{i=1}^M \left(\frac{\kappa (\delta_i)^M}{\mu_i} \left(1 - e^{-\frac{\eta_i}{\delta_i} \gamma_{th}} \right) \prod_{j=1, j \neq i}^M \frac{\eta_j}{\nu_{i,j}} \right) \right). \quad (2.4.10)$$

2.4.3 System Shannon capacity

The system Shannon capacity is an important performance measure because it gives information about the maximum allowable transmission rate under which error free communication system could be designed. In cooperative networks with regular protocol, the average Shannon's sense channel capacity can be expressed as [18]

$$\overline{C} = \frac{B}{M+1} \int_0^\infty \log_2(1 + \gamma) f_\gamma(\gamma) d\gamma \quad (2.4.11)$$

where B is the channel bandwidth in Hz. The reason for the $\frac{1}{M+1}$ factor is that the transmission process takes place in $M+1$ orthogonal frequency channels or time-slots. For our network model, the system Shannon capacity corresponding to the k th transmitted symbol is given as

$$\overline{C}(k) = \frac{B}{M+1} \int_0^\infty \log_2(1 + \gamma) f_{\gamma_{\text{tot}}(k)}(\gamma) d\gamma. \quad (2.4.12)$$

Unlike the BER and the outage probability, using the pdf given by (2.3.27) in (2.4.12) leads to the upper bound capacity. Therefore, using (2.3.27) for the pdf in (2.4.12), and then taking the average overall the block (assuming equiprobable transmission) gives the upper bound per-block-average capacity as follows

$$\begin{aligned}
\overline{C}_{\text{up}} &= \frac{1}{N} \sum_{k=1}^N \left(\frac{B}{M+1} \int_0^\infty \log_2(1+\gamma) f_{\gamma_{\text{tot,up}}(k)}(\gamma) d\gamma \right) \\
&= \frac{B}{N(M+1)} \sum_{k=1}^N \left(\int_0^\infty \log_2(1+\gamma) \frac{\xi_{\text{up}} e^{\frac{-\gamma}{\overline{\gamma}_{s,d}(k)}}}{\overline{\gamma}_{s,d}(k)} d\gamma \right. \\
&\quad \left. + \sum_{i=1}^M \int_0^\infty \log_2(1+\gamma) \frac{\xi_{\text{up},i} e^{\frac{-\gamma}{\overline{\gamma}_{\text{up},i}(k)}}}{\overline{\gamma}_{\text{up},i}(k)} d\gamma \right).
\end{aligned} \tag{2.4.13}$$

By evaluating the last integrals in (2.4.13) in closed-form as in [24, Eq. (38)], we can obtain \overline{C}_{up} as

$$\begin{aligned}
\overline{C}_{\text{up}} &= \frac{B \log_2(e)}{N(M+1)} \sum_{k=1}^N \left(\xi_{\text{up}} e^{1/\overline{\gamma}_{s,d}(k)} E_1 \left(\frac{1}{\overline{\gamma}_{s,d}(k)} \right) \right. \\
&\quad \left. + \sum_{i=1}^M \xi_{\text{up},i} e^{1/\overline{\gamma}_{i,\text{up}}(k)} E_1 \left(\frac{1}{\overline{\gamma}_{i,\text{up}}(k)} \right) \right)
\end{aligned} \tag{2.4.14}$$

where $E_1(x) = \int_1^\infty \frac{e^{-xt}}{t} dt$. Similarly, by substituting the expressions of $\overline{\gamma}_{s,d}(k)$, $\overline{\gamma}_{s,i}(k)$, and $\overline{\gamma}_{i,d}(k)$, from (2.3.10), (2.3.11) and (2.3.12), respectively, into (2.4.14), and after some manipulations and simplifications, we can write \overline{C}_{up} in terms of $\frac{E_s}{N_o}$ as

$$\begin{aligned}
\overline{C}_{\text{up}} &= \frac{B \log_2(e)}{N(M+1)} \sum_{k=1}^N \left(\alpha^M e^{\frac{\kappa \frac{E_s}{N_o} + 1}{\alpha \frac{E_s}{N_o}}} E_1 \left(\frac{\kappa \frac{E_s}{N_o} + 1}{\alpha \frac{E_s}{N_o}} \right) \prod_{i=1}^M \left(\frac{\eta_i \frac{E_s}{N_o} + \beta_i}{\mu_i \frac{E_s}{N_o} + \lambda_i} \right) \right. \\
&\quad \left. - \sum_{i=1}^M \left(e^{\frac{\eta_i \frac{E_s}{N_o} + \beta_i}{\delta_i \frac{E_s}{N_o}}} E_1 \left(\frac{\eta_i \frac{E_s}{N_o} + \beta_i}{\delta_i \frac{E_s}{N_o}} \right) \frac{(\delta_i)^M (\kappa \frac{E_s}{N_o} + 1)}{\mu_i \frac{E_s}{N_o} + \lambda_i} \prod_{j=1, j \neq i}^M \left(\frac{\eta_j \frac{E_s}{N_o} + \beta_j}{\nu_{i,j} \frac{E_s}{N_o} + \omega_{i,j}} \right) \right) \right).
\end{aligned} \tag{2.4.15}$$

The limit of (2.4.15) as $\frac{E_s}{N_o} \rightarrow \infty$ also exists and given by

$$\lim_{\frac{E_s}{N_o} \rightarrow \infty} \bar{C}_{\text{up}} = \frac{B \log_2(e)}{N(M+1)} \sum_{k=1}^N \left(\alpha^M e^{\frac{\kappa}{\alpha}} E_1 \left(\frac{\kappa}{\alpha} \right) \prod_{i=1}^M \left(\frac{\eta_i}{\mu_i} \right) - \sum_{i=1}^M \left(e^{\frac{\eta_i}{\delta_i}} E_1 \left(\frac{\eta_i}{\delta_i} \right) \left(\frac{(\delta_i)^M \kappa}{\mu_i} \right) \prod_{j=1, j \neq i}^M \left(\frac{\eta_j}{\nu_{i,j}} \right) \right) \right). \quad (2.4.16)$$

This means that the time-selective fading also impacts the system channel capacity by a ceiling.

All of the above derived expressions are novel and have not reported in literature before and they are general for the network fading links temporal characteristics in terms of their corresponding correlation parameters that are dependent on the cooperating-nodes speeds. They are also functions of the receivers' CSI estimation rates, in terms of the block length N . Therefore, these expressions are useful in investigating the system performance under the effects of different nodes mobility scenarios and CSI estimation rates.

2.5 Nodes Mobility and CSI Estimation Rates Effects

In this section, we investigate the effects of different cooperating-nodes mobility scenarios and CSI estimation rates on the system performance analyzed in Sec. 2.4. We provide our results based on the obtained expressions for the lower bounds per-block-average BER and outage probability and the upper bound per-block-average channel capacity and their corresponding asymptotic limits.

2.5.1 Nodes mobility effects

All nodes static

From (2.2.4), when the relative speed between any two nodes in the network is zero, i.e., the two nodes are static, the correlation parameter of their corresponding fading link is one, and hence, this link is considered quasi-static. Therefore, in our network model, when all of the nodes are static (zero speeds), all of the network links are considered quasi-static

because $\rho_{s,d} = \rho_{s,\ell} = \rho_{\ell,d} = 1, \forall \ell$. Considering this condition in (2.4.3), (2.4.9) and (2.4.15), we obtain the lower bound per-block-average quasi BER, the lower bound per-block-average quasi outage probability and the upper bound per-block-average quasi channel capacity, respectively, as follows

$$\begin{aligned} \overline{P}_{e,\text{Low}}^{\text{quasi}} &= \frac{(\alpha')^M}{2} \left[1 - \sqrt{\frac{\alpha' \frac{E_s}{N_o}}{\alpha' \frac{E_s}{N_o} + 1}} \right] \prod_{i=1}^M \left(\frac{\beta'_i}{\lambda'_i} \right) \\ &\quad - \sum_{i=1}^M \left(\frac{1}{2} \left[1 - \sqrt{\frac{\delta'_i \frac{E_s}{N_o}}{\delta'_i \frac{E_s}{N_o} + \beta'_i}} \right] \frac{(\delta'_i)^M}{\lambda'_i} \prod_{j=1, j \neq i}^M \left(\frac{\beta'_j}{\omega'_{i,j}} \right) \right) \end{aligned} \quad (2.5.1)$$

$$\begin{aligned} P_{\text{out,Low}}^{\text{quasi}} &= (\alpha')^M \left(1 - e^{-\frac{\gamma_{th}}{\alpha' \frac{E_s}{N_o}}} \right) \prod_{i=1}^M \left(\frac{\beta'_i}{\lambda'_i} \right) \\ &\quad - \sum_{i=1}^M \left(\left(1 - e^{-\frac{\beta'_i \gamma_{th}}{\delta'_i \frac{E_s}{N_o}}} \right) \frac{(\delta'_i)^M}{\lambda'_i} \prod_{j=1, j \neq i}^M \left(\frac{\beta'_j}{\omega'_{i,j}} \right) \right) \end{aligned} \quad (2.5.2)$$

and,

$$\begin{aligned} \overline{C}_{\text{up}}^{\text{quasi}} &= \frac{B \log_2(e)}{M+1} \left(\alpha'^M e^{\frac{1}{\alpha' \frac{E_s}{N_o}}} E_1 \left(\frac{1}{\alpha' \frac{E_s}{N_o}} \right) \prod_{i=1}^M \left(\frac{\beta'_i}{\lambda'_i} \right) \right. \\ &\quad \left. - \sum_{i=1}^M \left(e^{\frac{\beta'_i}{\delta'_i \frac{E_s}{N_o}}} E_1 \left(\frac{\beta'_i}{\delta'_i \frac{E_s}{N_o}} \right) \frac{(\delta'_i)^M}{\lambda'_i} \prod_{j=1, j \neq i}^M \left(\frac{\beta'_j}{\omega'_{i,j}} \right) \right) \right) \end{aligned} \quad (2.5.3)$$

where

$$\begin{aligned} \lambda'_i &= \alpha' \beta'_i - \delta'_i \\ \omega'_{i,j} &= \delta'_i \beta'_j - \delta'_j \beta'_i \\ \alpha' &= \mathbb{E}[|h_{s,d}(1)|^2] \\ \beta'_\ell &= \mathbb{E}[|h_{s,\ell}(1)|^2] + \mathbb{E}[|h_{\ell,d}(1)|^2] \\ \delta'_\ell &= \mathbb{E}[|h_{s,\ell}(1)|^2] \mathbb{E}[|h_{\ell,d}(1)|^2] \quad \forall \ell = 1, 2, \dots, M. \end{aligned}$$

It should be noted that the limits of (2.5.1) and (2.5.2) as $\frac{E_s}{N_o} \rightarrow \infty$ are zero (floor disappears), while the limit of (2.5.3) as $\frac{E_s}{N_o} \rightarrow \infty$ is infinity (ceiling disappears), as both are expected since the nodes mobility impact is absent.

Mobile relays, static source and destination

Corollary 2.5.1. *In amplify-and-forward regular cooperative networks with direct link and adaptive-gains at the relays employing MRC at the destination, even though the relays are in motion, the system does not experience BER floor, outage floor or capacity ceiling as long as both of the source and the destination are static.*

Proof. When the source and the destination are static, the correlation parameter of the direct link $\rho_{s,d}$ equals 1. On the other hand, because of the relays mobility, the first and the second fading hops of the ℓ th indirect path are time-selective, i.e., $\rho_{s,\ell}$ and $\rho_{\ell,d}$ are $< 1 \forall \ell$. Considering this condition in (2.4.3), (2.4.9) and (2.4.15) reduces them, respectively, to

$$\begin{aligned} \bar{P}_{e,\text{Low}} = & \frac{1}{2N} \sum_{k=1}^N \left((\alpha')^M \left[1 - \sqrt{\frac{\alpha' \frac{E_s}{N_o}}{\alpha' \frac{E_s}{N_o} + 1}} \right] \prod_{i=1}^M \left(\frac{\eta_i \frac{E_s}{N_o} + \beta_i}{\alpha' \eta_i \frac{E_s}{N_o} + (\alpha' \beta_i - \delta_i)} \right) \right. \\ & \left. - \sum_{i=1}^M \left(\left[1 - \sqrt{\frac{\delta_i \frac{E_s}{N_o}}{\chi_i \frac{E_s}{N_o} + \beta_i}} \right] \frac{(\delta_i)^M}{\alpha' \eta_i \frac{E_s}{N_o} + (\alpha' \beta_i - \delta_i)} \prod_{j=1, j \neq i}^M \left(\frac{\eta_j \frac{E_s}{N_o} + \beta_j}{\nu_{i,j} \frac{E_s}{N_o} + \omega_{i,j}} \right) \right) \right) \end{aligned} \quad (2.5.4)$$

$$\begin{aligned} P_{\text{out,Low}} = & \frac{1}{N} \sum_{k=1}^N \left((\alpha')^M \left(1 - e^{-\frac{\gamma_{th}}{\alpha' \frac{E_s}{N_o}}} \right) \prod_{i=1}^M \left(\frac{\eta_i \frac{E_s}{N_o} + \beta_i}{\alpha' \eta_i \frac{E_s}{N_o} + (\alpha' \beta_i - \delta_i)} \right) \right. \\ & \left. - \sum_{i=1}^M \left(1 - e^{-\frac{\eta_i \frac{E_s}{N_o} + \beta_i}{\delta_i \frac{E_s}{N_o}} \gamma_{th}} \right) \frac{(\delta_i)^M}{\alpha' \eta_i \frac{E_s}{N_o} + (\alpha' \beta_i - \delta_i)} \prod_{j=1, j \neq i}^M \left(\frac{\eta_j \frac{E_s}{N_o} + \beta_j}{\nu_{i,j} \frac{E_s}{N_o} + \omega_{i,j}} \right) \right) \end{aligned} \quad (2.5.5)$$

and,

$$\begin{aligned} \overline{C}_{\text{up}} = & \frac{B \log_2(e)}{N(M+1)} \sum_{k=1}^N \left((\alpha')^M e^{\frac{1}{\alpha' \frac{E_s}{N_o}}} E_1 \left(\frac{1}{\alpha' \frac{E_s}{N_o}} \right) \prod_{i=1}^M \left(\frac{\eta_i \frac{E_s}{N_o} + \beta_i}{\alpha' \eta_i \frac{E_s}{N_o} + (\alpha' \beta_i - \delta_i)} \right) \right. \\ & \left. - \sum_{i=1}^M \left(e^{\frac{\eta_i \frac{E_s}{N_o} + \beta_i}{\delta_i \frac{E_s}{N_o}}} E_1 \left(\frac{\eta_i \frac{E_s}{N_o} + \beta_i}{\delta_i \frac{E_s}{N_o}} \right) \frac{(\delta_i)^M}{\alpha' \eta_i \frac{E_s}{N_o} + (\alpha' \beta_i - \delta_i)} \prod_{j=1, j \neq i}^M \left(\frac{\eta_j \frac{E_s}{N_o} + \beta_j}{\nu_{i,j} \frac{E_s}{N_o} + \omega_{i,j}} \right) \right) \right) \end{aligned} \quad (2.5.6)$$

Now, by taking the limits of (2.5.4) and (2.5.5) as $\frac{E_s}{N_o} \rightarrow \infty$ we obtain zero⁴, and the limit of (2.5.6) as $\frac{E_s}{N_o} \rightarrow \infty$ we obtain infinity⁵. This means that these three performance criteria do not experience asymptotic limits, which completes the proof. \square

Despite that both scenarios 1 and 2 do not provide asymptotic limits, this does not mean that they provide same results in terms of the BER, outage and capacity over all the non-infinite SNR range because (2.5.4), (2.5.5) and (2.5.6) quantitatively differ from (2.5.1), (2.5.2) and (2.5.3), respectively. Later in the numerical results section, we will show that scenario 2 provides worse BER, outage and capacity performance than scenario 1 due to the mobility of relays.

Static relays, either source or destination is mobile

Corollary 2.5.2. *In amplify-and-forward regular cooperative networks with direct link and adaptive-gains at the relays employing MRC at the destination, even though all the relays are static, the system performance is severely degraded by BER floor, outage floor and capacity ceiling as long as either the source or the destination is in motion.*

Proof. This scenario is divided into two cases:

The first case is when the source node is in motion and the other nodes are static; i.e., $\rho_{\ell,d} = 1$ while $\rho_{s,d}$ and $\rho_{s,\ell}$ are $< 1 \forall \ell$. In this case the BER, the outage probability and

⁴We can also obtain same results by substituting $\kappa = 0$ in (2.4.4) and (2.4.10).

⁵We can also obtain same result by substituting $\kappa = 0$ in (2.4.16).

the system capacity are, respectively, given by (2.4.3), (2.4.9) and (2.4.15), and their corresponding limits are, respectively, given by (2.4.4), (2.4.10) and (2.4.16) with the following modified parameters: $\delta_\ell = \rho_{s,\ell}^{2(k-1)} \mathbb{E}[|h_{s,\ell}(1)|^2] \mathbb{E}[|h_{\ell,d}(1)|^2]$, $\eta_\ell = (1 - \rho_{s,\ell}^{2(k-1)}) \mathbb{E}[|h_{\ell,d}(1)|^2]$, and $\beta_\ell = \rho_{s,\ell}^{2(k-1)} \mathbb{E}[|h_{s,\ell}(1)|^2] + \mathbb{E}[|h_{\ell,d}(1)|^2]$.

The second case is when the destination node is in motion and the other nodes are static; i.e., $\rho_{s,\ell} = 1$ while $\rho_{s,d}$ and $\rho_{\ell,d}$ are $< 1 \forall \ell$. Similarly, the BER, the outage probability and the system capacity are, respectively, given by (2.4.3), (2.4.9) and (2.4.15), and their corresponding limits are, respectively, given by (2.4.4), (2.4.10) and (2.4.16) but with the following modified parameters: $\delta_\ell = \rho_{\ell,d}^{2(k-1)} \mathbb{E}[|h_{s,\ell}(1)|^2] \mathbb{E}[|h_{\ell,d}(1)|^2]$, $\eta_\ell = (1 - \rho_{\ell,d}^{2(k-1)}) \mathbb{E}[|h_{s,\ell}(1)|^2]$ and $\beta_\ell = \mathbb{E}[|h_{s,\ell}(1)|^2] + \rho_{\ell,d}^{2(k-1)} \mathbb{E}[|h_{\ell,d}(1)|^2]$.

From the above two cases we conclude that the BER and the outage floors and the capacity ceiling exist, which completes the proof. \square

We can conclude from the last proof that when the two hops of the network indirect paths are symmetrical, i.e., $\mathbb{E}[|h_{s,\ell}(1)|^2] = \mathbb{E}[|h_{\ell,d}(1)|^2]$, $\forall \ell$, then either the source mobility or the destination mobility, with same speed, provides same system performance. In addition, the source mobility degrades the performance more than the destination mobility when the powers of the first hop fading gains are greater than that of the second hop, i.e., $\mathbb{E}[|h_{s,\ell}(1)|^2] > \mathbb{E}[|h_{\ell,d}(1)|^2]$, $\forall \ell$. On the other hand, the destination mobility degrades the performance more than the source mobility when the powers of the first hop fading gains are less than that of the second hop, i.e., $\mathbb{E}[|h_{s,\ell}(1)|^2] < \mathbb{E}[|h_{\ell,d}(1)|^2]$, $\forall \ell$.

2.5.2 Receivers' CSI estimation rates effect

In Sec. 2.4 all of the derived expressions are functions of the transmitted block length N . This parameter reflects the CSI estimation rate which is quantified as $\frac{1}{N}100\%$ (as discussed in subsection 2.2.2). As we have shown above, due to the cooperating-nodes mobility, the system performance is degraded and in some scenarios it is severely degraded by asymptotic limits. In order to reduce these degradations, we can increase the relays and the

destination receivers CSI estimation rates (i.e., reducing N in our analytical expressions). It will be shown, in the numerical results section, that increasing this rate improves the performance and reduces the asymptotic limits. The effect of 100% CSI estimation rates is stated in the following corollary.

Corollary 2.5.3. *In amplify-and-forward regular cooperative networks with direct link and adaptive-gains at the relays employing MRC at the destination while nodes are in motion (time-varying links), if all of the network receivers (the relays and the destination) have 100% CSI estimation rates, the system performance degradation in terms of BER, outage probability and capacity, that is generated due to the nodes mobility, is completely removed and the performance reduces to that of the all nodes static scenario.*

Proof. By substituting $N = 1$ into the expressions given by (2.4.3), (2.4.9) and (2.4.15) and computing their first summation, these expressions, respectively, reduce into (2.5.1), (2.5.2) and (2.5.3), which completes the proof. \square

It should be noted that 100% CSI estimation rate can be achieved in the case of time-varying fading links by transmitting a non-informative pilot signal accompanied with each transmitted symbol in the block (via training). However, this is not feasible because it causes a tremendous amount of reduction in the spectral efficiency and tremendously increased overhead. Another way to achieve that is by equipping the relays and the destination receivers by fast tracking loops (i.e., more complex receivers) that can catch up with the rapid time-varying channel gains. The work in [25] is devoted to tracking and estimation of time-varying fading links.

2.6 Numerical Results and Simulation

In this section, we present numerical results for the under study system per-block-average BPSK BER, outage probability and Shannon capacity using (2.4.3), (2.4.9) and (2.4.15), respectively, and verify them by exact simulation results. We consider $\sigma_{s,d}^2 = \sigma_{s,i}^2$

$= \sigma_{i,d}^2 = 1$, $\mathbb{E}[|h_{s,d}(1)|^2] = 1$ and $R = 1$. In all of the plots, $\frac{E_s}{N_o}$ represents the per symbol average SNR (in dB) where E_s is the transmit energy per symbol which is assumed to be 1.

Fig. 2.2 compares between the approximate theoretical and the exact simulation results obtained for the network per-block-average BER performance. The source is mobile while the other nodes are static. It is clear that increasing the number of relays, M , improves the BER performance since the MRC diversity gain and the virtual antenna gain are monotonically increasing functions of M . However, for any number of relays, the performance experiences error floor at high values of SNR due to the effect of the source mobility and the constrained CSI estimation rates of 2%. We can also notice that, as compared with the exact simulation, the tightness of the derived lower-bound, in particular, at medium and high SNR regions.

Fig. 2.3 shows the BER performance (using the theoretical lower bound) for $M = 1$ and 3 under the different nodes mobility scenarios that have been discussed in subsection 2.5.1. It is obvious from this figure that when all of the nodes are static (all of the network fading links are quasi-static), the BER performance does not experience floor because the effect of the nodes mobility is absent. Also, when both of the source and the destination are static, the relays mobility degrades the BER performance, as compared with the all nodes static case, but it does not causes asymptotic error floor. On the other hand, a severe BER performance degradation with error floor occurs when either the source or the destination is in motion. Furthermore, the mobility of all the nodes provides the worst BER performance.

Fig. 2.4 shows that the difference between the impacts of the source and the destination mobilities depends on the network symmetrical properties. It is clear that, when the channel is symmetrical (i.e., in each indirect path, the powers of the first hop fading gains equals that of the second hop), the impacts of the source mobility and the destination mobility are equivalent. On the other hand, the impact of the source mobility is greater than that of the destination mobility when the powers of the first hops fading gains are greater than that of the second hops and the opposite is true.

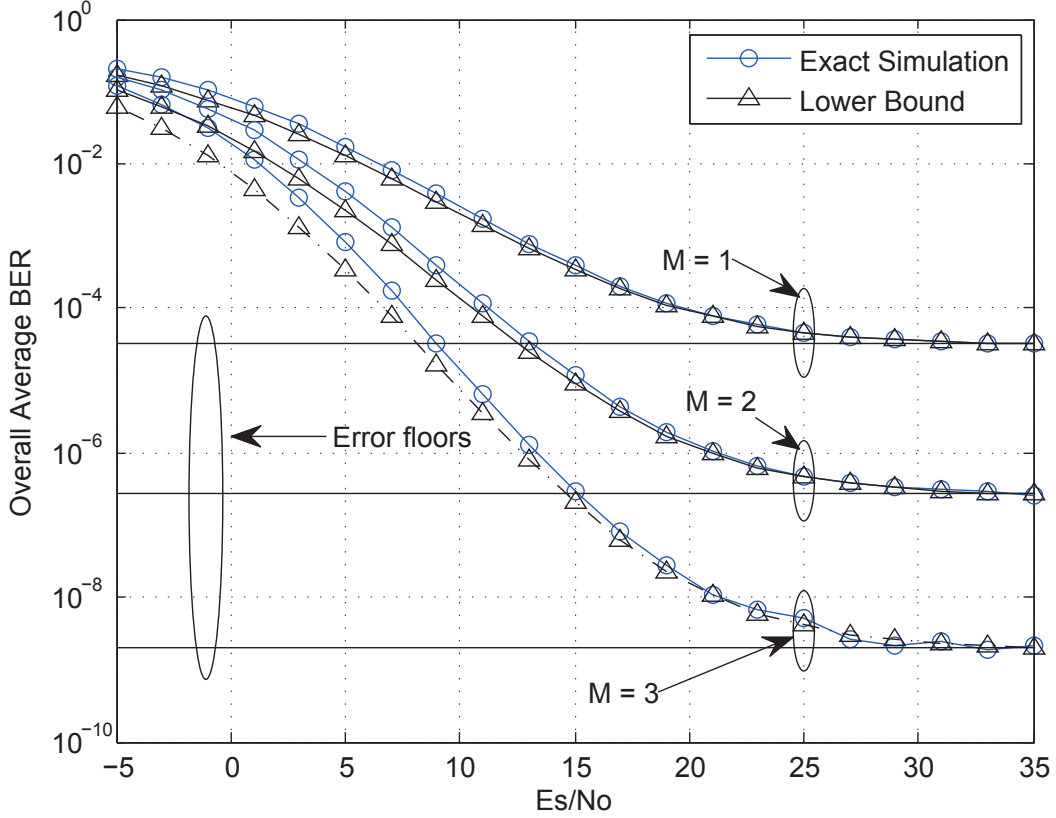


Figure 2.2. BPSK BER versus E_s/N_o with 2% CSI estimation rates ($N = 50$) for number of relays $M = 1, 2$ and 3 . In dB: $\mathbb{E}[|h_{s,d}(1)|^2] = 1$, $\mathbb{E}[|h_{s,\ell}(1)|^2] = \{1.5, 2.5, 3.5\}$ and $\mathbb{E}[|h_{\ell,d}(1)|^2] = \{2.5, 3.5, 4.5\}$. The Source is mobile and the other nodes are static corresponding to correlation parameters of $\rho_{s,d} = \rho_{s,\ell} = 0.9997$ and $\rho_{i,d} = 1$.

In Fig. 2.5, we show the effect of the receiving nodes' CSI estimation rates on the BER performance. Increasing this rate means increasing the abilities of the relays and the destination receivers' tracking loops to catch up with the rapid time-varying channel gains. We can notice from this figure that the BER performance is improved and the severe impact (error floor) of the cooperating-nodes high speeds is reduced by increasing the CSI estimation rates. In addition, when the CSI estimation rates are 100%, the impact of the nodes mobility on the BER performance vanishes and the performance is improved and matches with that of the all static nodes case.

Fig. 2.6 compares between the approximate theoretical and the exact simulation results obtained for the network per-block-average outage probability. It is clear that the

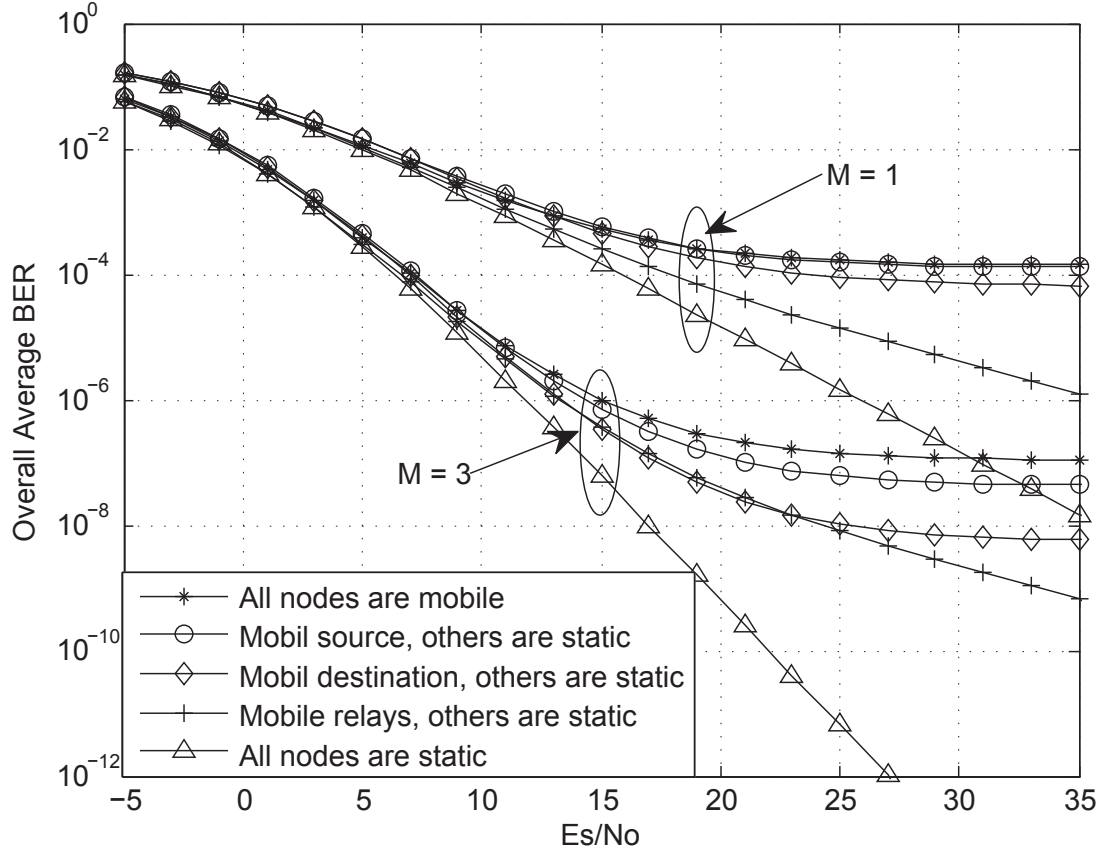


Figure 2.3. BPSK lower bound BER versus E_s/N_o with 5% CSI estimation rates ($N = 20$). In dB: $\mathbb{E}[|h_{s,d}(1)|^2] = 1$, $\mathbb{E}[|h_{s,\ell}(1)|^2] = \{1.5, 2.5, 3.5\}$ and $\mathbb{E}[|h_{\ell,d}(1)|^2] = \{4.5, 5.5, 6.5\}$. The corresponding correlation parameter is 0.9986.

lower bound is tight at medium and high SNR regions. At low values of the SNR, the outage performance degrades with increasing M because the data transmission over the network requires $M+1$ orthogonal channels or time slots which consequently reduces the network mutual information. However, for any number of relays, the outage performance experiences outage floor at high values of SNR due to the effect of the source mobility and the constrained CSI estimation rate of 2%.

Fig. 2.7 shows the outage performance under the different mobility scenarios that have been discussed in subsection 2.5.1. When all of the nodes are static, the outage performance does not suffer from outage floor. Also, the outage performance does not suffer from outage floor in the case of mobile relays and static source and destination, but it is worse than that

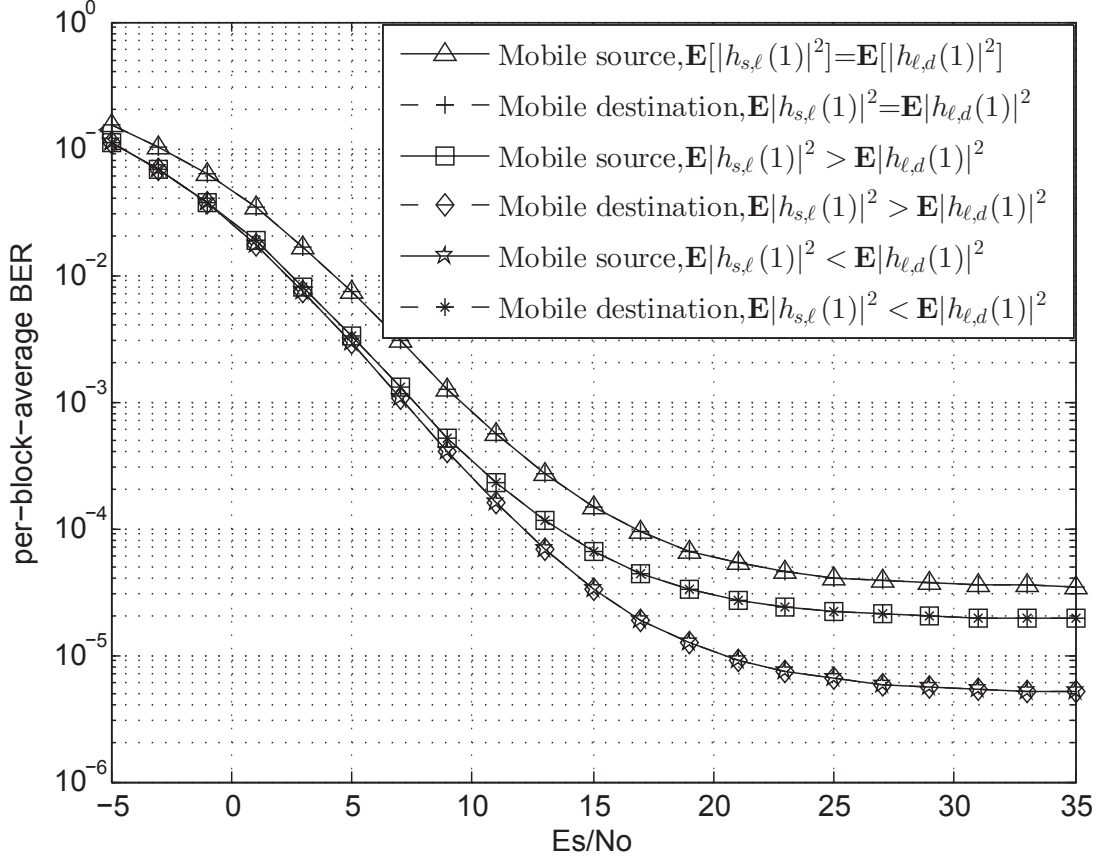


Figure 2.4. BPSK lower bound BER versus E_s/N_o with 2% CSI estimation rates ($N = 50$) and $M = 2$. In dB: first hop=second hop: $\mathbb{E}[|h_{s,\ell}(1)|^2] = \mathbb{E}[|h_{\ell,d}(1)|^2] = \{0.5, 0.8, 0.2\}$, first hop>second hop: $\mathbb{E}[|h_{s,\ell}(1)|^2] = \{4.5, 5.5, 6.5\}$ and $\mathbb{E}[|h_{\ell,d}(1)|^2] = \{1.5, 2.5, 3.5\}$, second hop>first hop: $\mathbb{E}[|h_{s,\ell}(1)|^2] = \{1.5, 2.5, 3.5\}$ and $\mathbb{E}[|h_{\ell,d}(1)|^2] = \{4.5, 5.5, 6.5\}$. The corresponding correlation parameter is 0.9989.

of the all static nodes case. We can also notice that, a severe outage performance degradation occurs when either the source or the destination is in motion as compared with the above cases.

In Fig. 2.8, we show the effect of the receiving nodes CSI estimation rates on the outage performance. It is obvious that increasing the CSI estimation rates reduces the outage floor that is generated from the destination mobility, and this floor is completely eliminated by 100% CSI estimation rates. Also, it is clear that the outage performance degradation due to the relays mobility is reduced by increasing the CSI estimation rates.

Fig. 2.9 compares between the approximate theoretical and the exact simulation

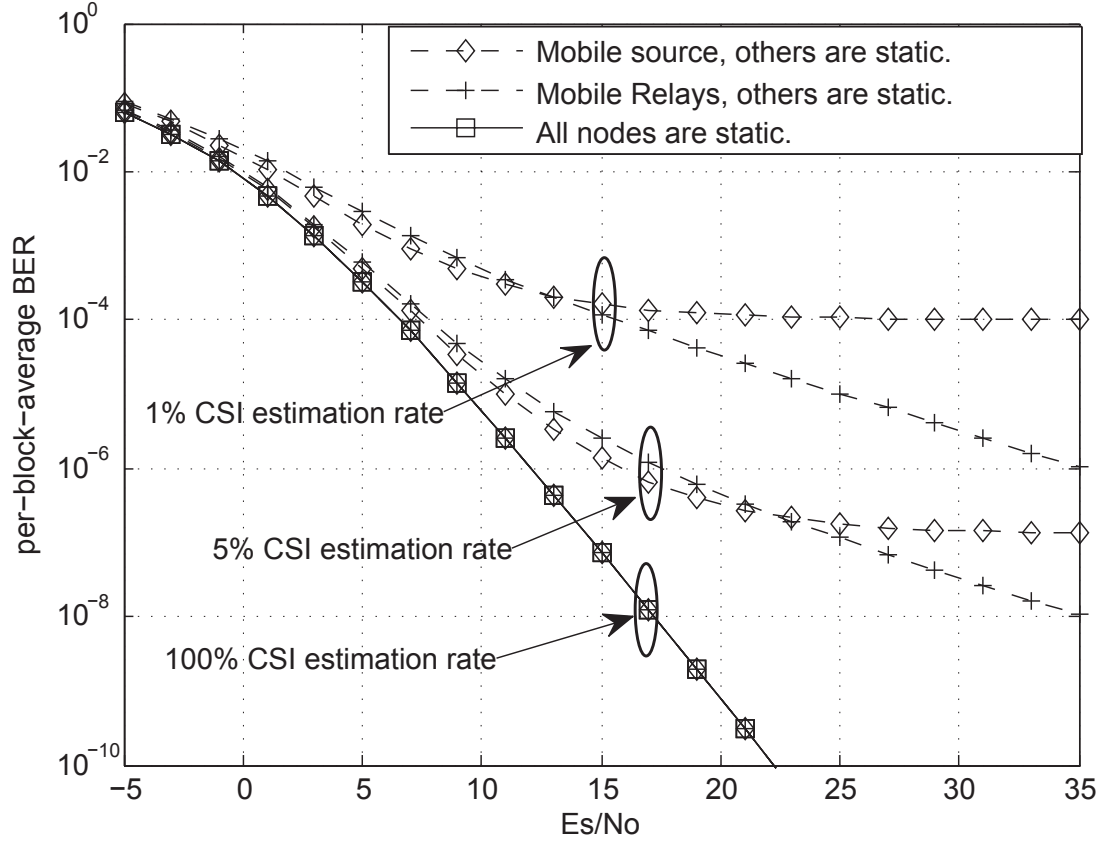


Figure 2.5. BPSK lower bound BER versus E_s/N_o for $M = 3$. In dB: $\mathbb{E}[|h_{s,d}(1)|^2] = 1$, $\mathbb{E}[|h_{s,\ell}(1)|^2] = \{4.5, 5.5, 6.5\}$ and $\mathbb{E}[|h_{\ell,d}(1)|^2] = \{1.5, 2.5, 3.5\}$. The corresponding correlation parameter is 0.9969..

results obtained for the network per-block-average normalized capacity (\bar{C}/B) where the tightness of the derived upper bound is clear at medium and high per-symbol average SNR values. The reason for capacity decreasing with increasing M is the $M + 1$ orthogonal frequency channels or time slots that are required for data transmission from the source to the destination through the network. Due to the source speed of 20 mph and the low CSI estimation rates of 2%, the normalized capacity cannot exceed a certain capacity ceiling.

In Fig. 2.10 we show the difference between the impact of the destination mobility and the relays mobility on the capacity performance. It is clear that when both the destination and the source are static, the capacity performance does not experience capacity ceiling even though all of the relays are in motion. It is also obvious that the mobility of the destination

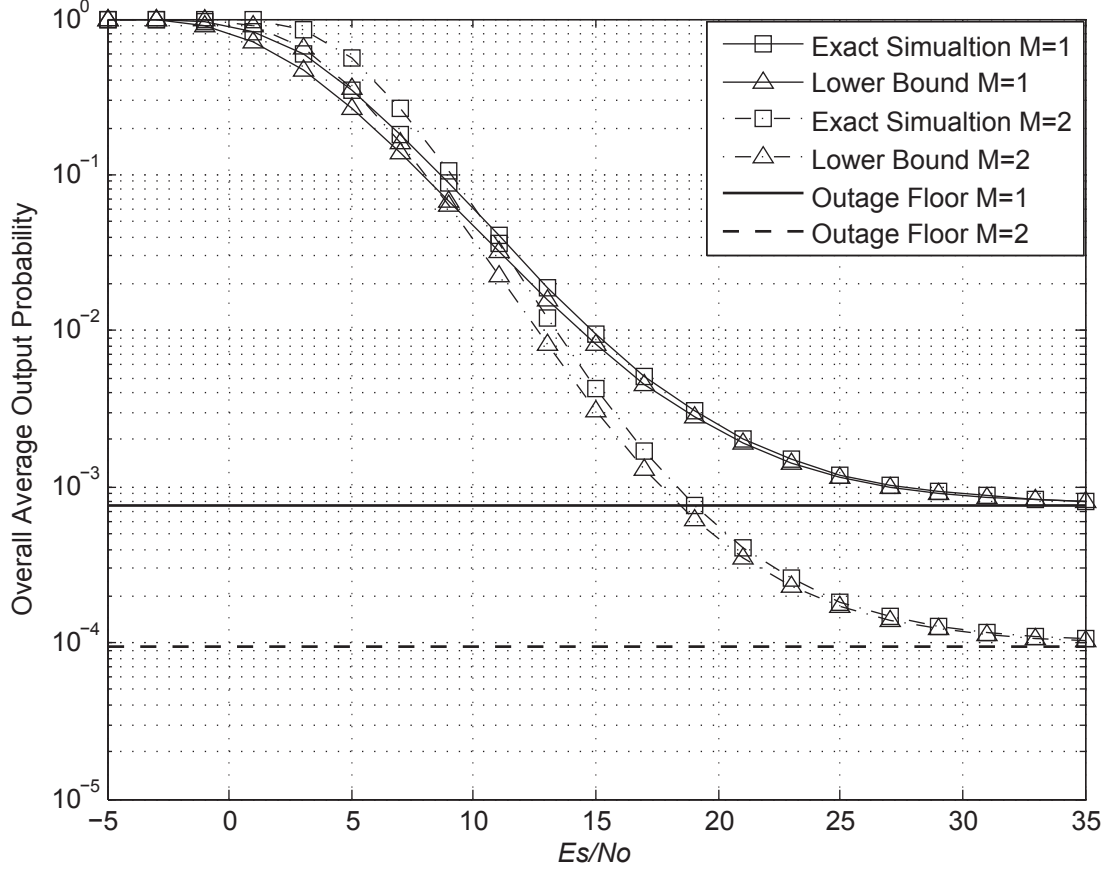


Figure 2.6. Outage probability versus E_s/N_o with 2% CSI estimation rates ($N = 50$). In dB: $\mathbb{E}[|h_{s,d}(1)|^2] = 1$, $\mathbb{E}[|h_{s,\ell}(1)|^2] = \{2.5, 3.5\}$ and $\mathbb{E}[|h_{\ell,d}(1)|^2] = \{3.5, 4.5\}$. The Source is mobile and the other nodes are static corresponding to correlation parameters of $\rho_{s,d} = \rho_{s,\ell} = 0.9997$ and $\rho_{i,d} = 1$.

severely degrades the capacity performance by a ceiling particularly at relatively high speed (e.g. 75 mph as compared with 10 mph).

In Fig. 2.11 we show the effect of the CSI estimation rates on the system capacity performance. We can notice from this figure that by increasing the CSI estimation rates, the capacity performance is also improved and the capacity ceiling, due to the source mobility, reduces. Furthermore, 100 % CSI estimation rates completely eliminates the capacity ceiling and improves the capacity performance to be as similar as that of the all nodes static case.

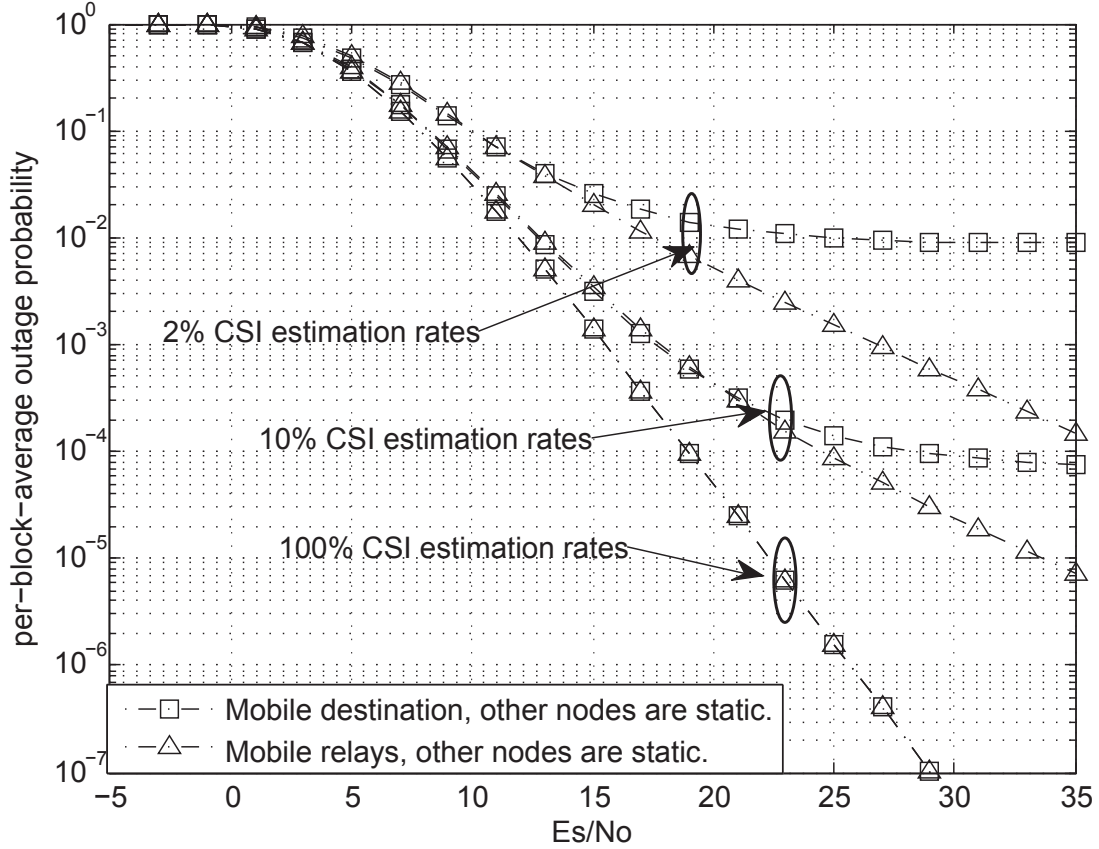


Figure 2.7. Theoretical lower bound outage probability versus E_s/N_o with $M = 2$ and 2% CSI estimation rate. In dB: $\mathbb{E}[|h_{s,d}(1)|^2] = 1$, $\mathbb{E}[|h_{s,\ell}(1)|^2] = \{1.5, 2.5\}$ and $\mathbb{E}[|h_{s,\ell}(1)|^2] = \{4.5, 5.5\}$. The corresponding correlation parameter is 0.9980.

2.7 Conclusion

In this chapter, we have considered a multiple-relay amplify-and-forward cooperative network over time-selective (due to nodes' mobility) Rayleigh fading links with MRC diversity and analyzed its performance by deriving closed-form expressions for the per-block-average of the BER, the outage probability and the system Shannon capacity. The first-order autoregressive process (AR1) has been used to model the fading link between any two nodes in the network. The derived expressions are general functions of both the cooperating-nodes speeds, in terms of the links correlation parameters, and the receivers' tracking loops CSI estimation rates, in terms of the transmitted block length. Due to the nodes mobility the system performance degraded and experiences asymptotic limits which have been also derived.

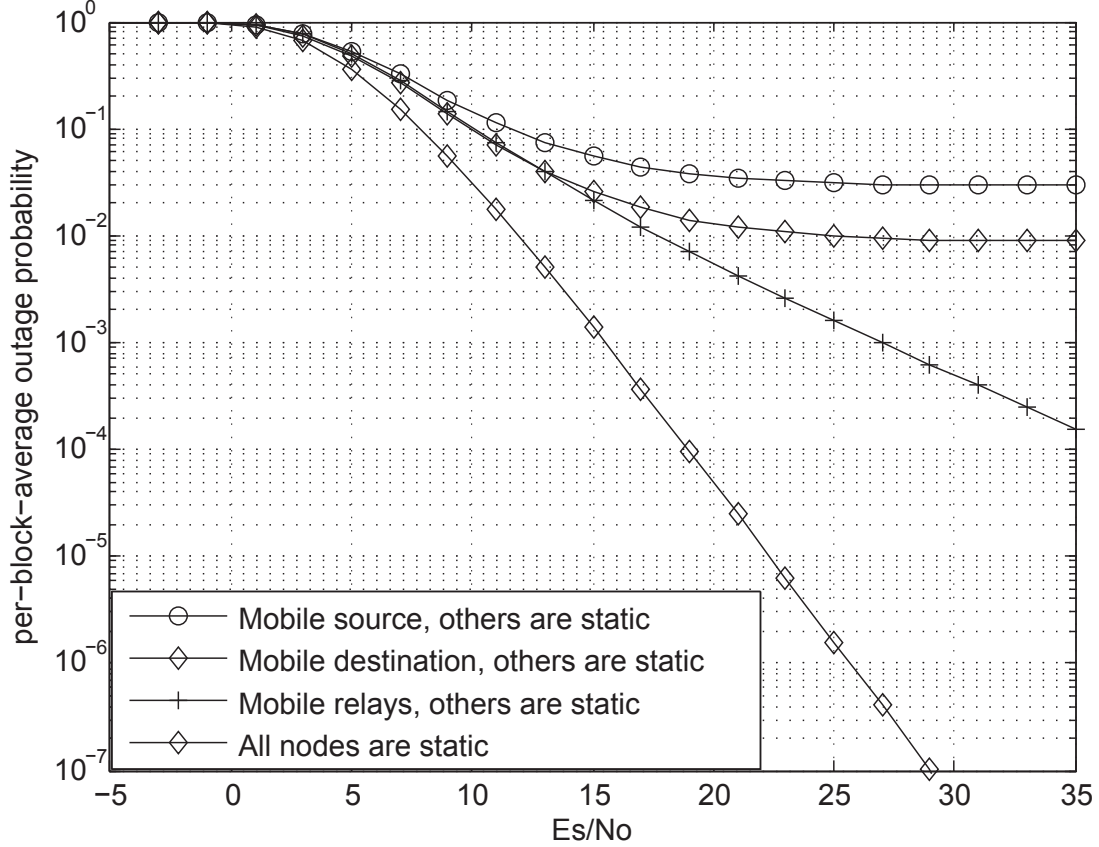


Figure 2.8. Theoretical lower bound outage probability versus E_s/N_o with $M = 2$. In dB: $\mathbb{E}[|h_{s,d}(1)|^2] = 1$, $\mathbb{E}[|h_{s,\ell}(1)|^2] = \{1.5, 2.5\}$ and $\mathbb{E}[|h_{s,\ell}(1)|^2] = \{4.5, 5.5\}$. The corresponding correlation parameter is 0.9980.

As a special case, when all of the cooperating-nodes are static, these expressions reduce to their correspondences in the quasi-static fading links case and hence the asymptotic limits are absent. Moreover, the effects of different nodes mobility scenarios on the system performance have been analytically investigated and novel useful observations have been obtained. For example, the mobility of the relays degrades the performance with no asymptotic limits if both the source and the destination are static, but the mobility of either the source or the destination severely impacts the performance with asymptotic limits no matter what the relays mobility situations are. We also have shown that the difference between the impacts of the source and the destination mobilities depends on the network power symmetrical properties. In addition, the scenario of equipping the receivers with fast tracking loops feature has

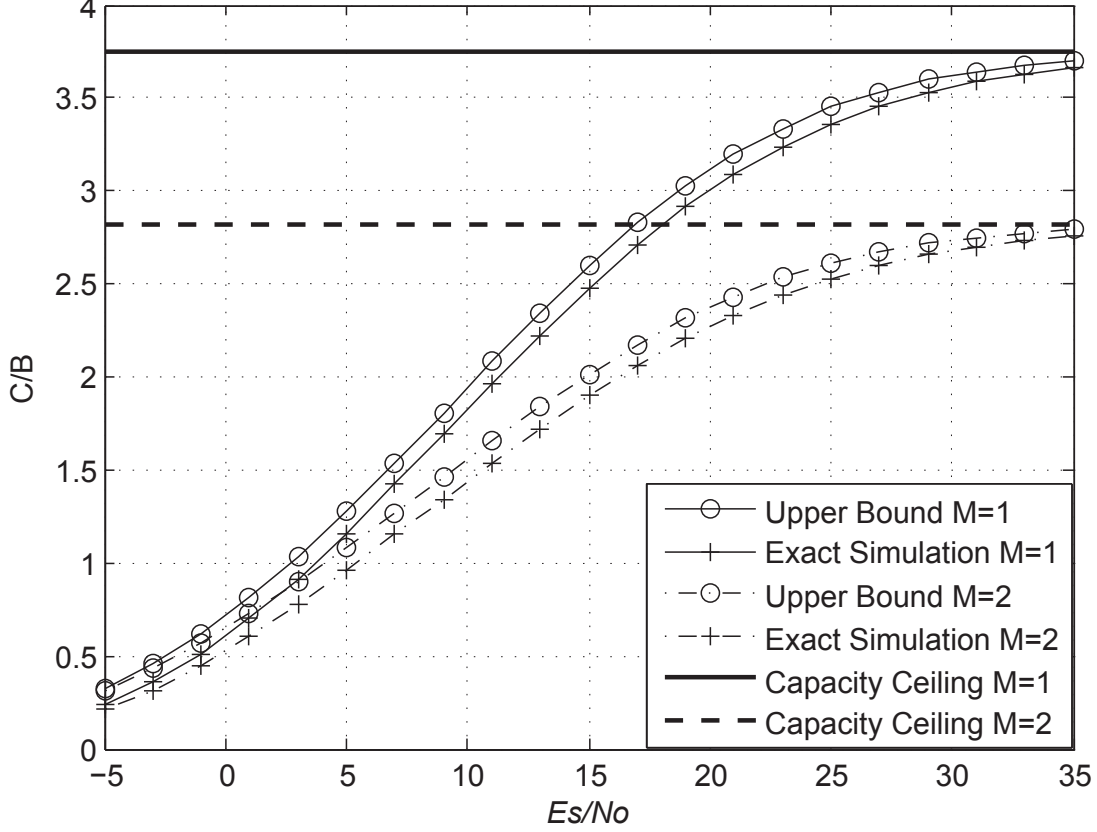


Figure 2.9. Average upper bound normalized capacity versus E_s/N_o with 2% CSI estimation rates ($N = 50$). In dB: $\mathbb{E}[|h_{s,d}(1)|^2] = 1$, $\mathbb{E}[|h_{s,\ell}(1)|^2] = \{2.5, 3.5\}$ and $\mathbb{E}[|h_{\ell,d}(1)|^2] = \{3.5, 4.5\}$. The Source is mobile and the other nodes are static corresponding to correlation parameters of $\rho_{s,d} = \rho_{s,\ell} = 0.9997$ and $\rho_{i,d} = 1$.

been assumed where such assumption clearly improves the system performance and reduces the asymptotic limits. In 100% CSI estimation rates case, the system performance reduces to that of the quasi-static fading case whatever the cooperating-nodes situation either mobile or static. Comprehensive numerical results have been presented to show the system performance and demonstrate how it is affected by the analyzed scenarios of nodes mobility and CSI estimation rates. We also have provided Monte-Carlo computer simulation results to verify the accuracy of the analytical results.

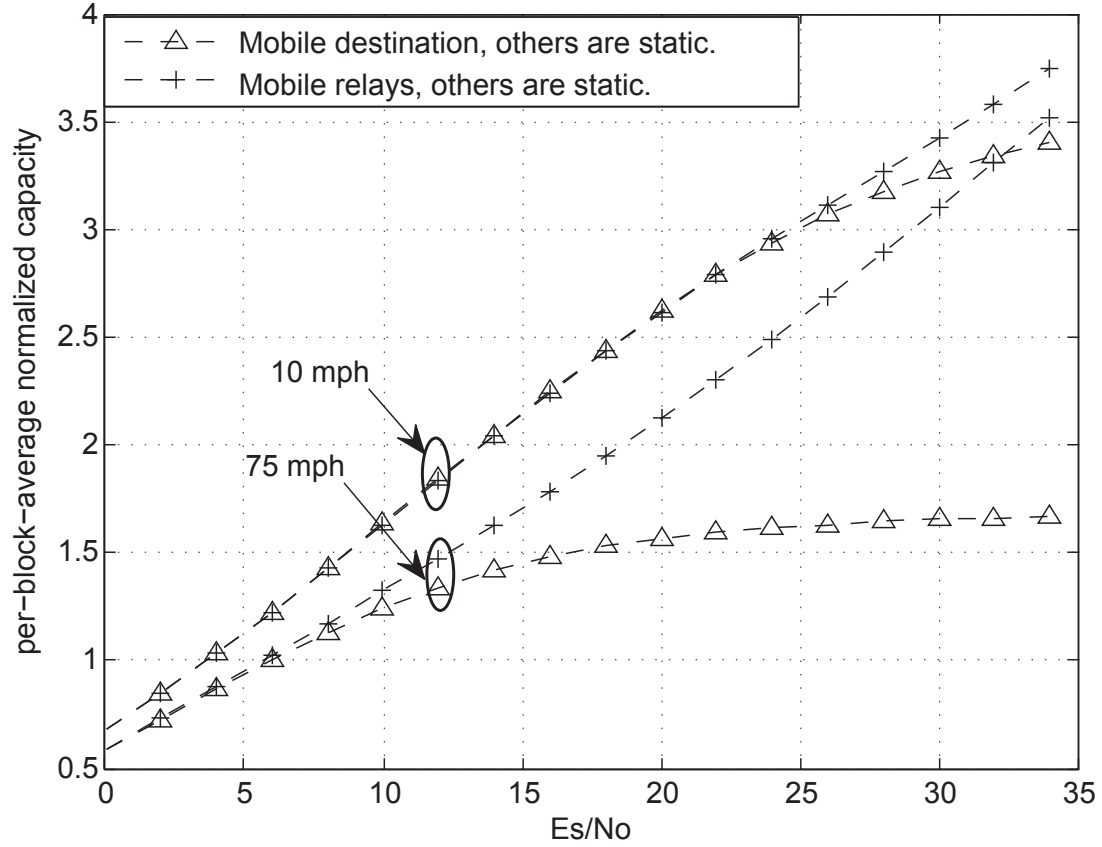


Figure 2.10. Theoretical upper bound average normalized capacity versus E_s/N_o with $M = 2$ and 2% CSI estimation rates. In dB: $\mathbb{E}[|h_{s,d}(1)|^2] = 1$, $\mathbb{E}[|h_{s,\ell}(1)|^2] = \{2, 3\}$ and $\mathbb{E}[|h_{\ell,d}(1)|^2] = \{4, 2\}$. Correlation parameter of 0.9999 for 10 mph speed and 0.9990 for 75 mph speed.

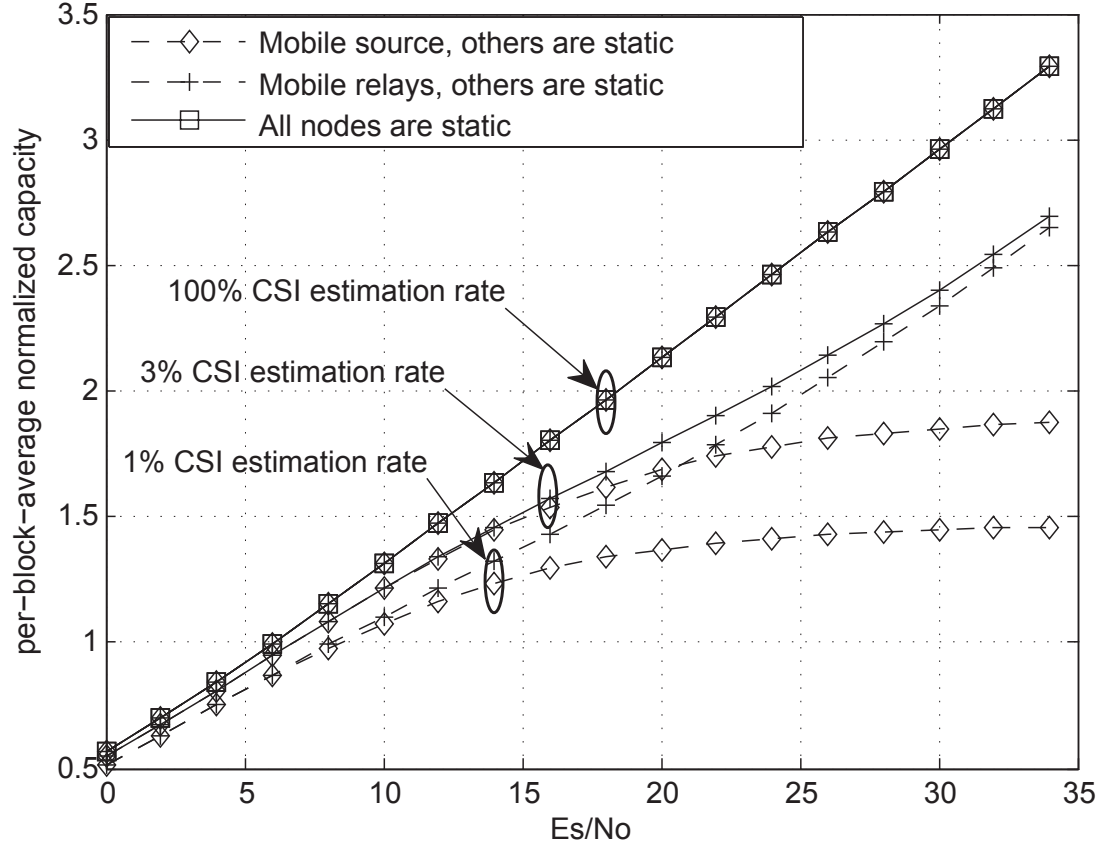


Figure 2.11. Theoretical upper bound average normalized capacity versus E_s/N_o with $M = 2$. In dB: $\mathbb{E}[|h_{s,\ell}(1)|^2] = \{2, 3, 1\}$ and $\mathbb{E}[|h_{\ell,d}(1)|^2] = \{4, 2, 2\}$. The corresponding correlation parameter is 0.9986.

CHAPTER 3

Regular M -Relay Variable-Gain AF Cooperative Systems with Mobile Nodes and Imperfect CSI Estimation: SNR Derivation and Performance Analysis

3.1 Chapter Overview

Similarly as in chapter 1, we consider in this chapter a multiple-relay amplify-and-forward wireless cooperative system with mobile nodes (i.e., time-selective fading), regular protocol and MRC destination but, unlike chapter 1, we consider imperfect channel estimation at the relays and the destination receivers. By this we add additional realistic assumption along with that of nodes' mobility. For such a system model and assumptions, we first derive novel exact closed-form expressions for the destination's direct-path and end-to-end instantaneous signal-to-noise ratios (SNRs) along with their pdfs. These SNRs are function of the links' correlation parameters and the estimation errors variances. After that, we obtain closed-form expression for the pdf of the total effective SNR at the destination's MRC output. This pdf generalizes the one derived in chapter 1 for the case of perfect channel estimation. In this chapter, we also derive closed-form tight approximate expressions for the system per-block-average BPSK BER, outage probability, and Shannon capacity, which also generalize the ones derived in chapter 1 for the perfect channel estimation case. Finally, we provide numerical results for these derived expressions along with their exact simulation.

3.2 System and Channel Model

In this chapter, we consider the same system and channel model and assumptions as in chapter 1 but we assume here that the estimation error at the network receivers (the relays and the destination) is significant, i.e., imperfect channel estimation is assumed. Therefore,

the estimated channel gain over the first signaling period $\hat{h}_{a,b}(1)$ is related to the actual one $h_{a,b}(1)$ as follows

$$h_{a,b}(1) = \hat{h}_{a,b}(1) + h_{\epsilon_{a,b}}(1) \quad (3.2.1)$$

where $h_{\epsilon_{a,b}}(1)$ is the estimation error, which is assumed to be ZMCSCG with variance $\sigma_{\epsilon_{a,b}}^2$, i.e., $\sim \mathcal{CN}(0, \sigma_{\epsilon_{a,b}}^2)$. In addition, we consider in this chapter that the i th relay computes the amplification gain that satisfies the power constraint described in (2.2.6). Therefore, we consider the following amplification gain at the i th relay

$$\mathcal{G}_i(k) = \sqrt{\frac{E_s}{\mathcal{E}(h_{s,i}(k))E_s + N_o}}. \quad (3.2.2)$$

It should be noted that the gain in (3.2.2) is assumed to require from the relays to estimate the average power of the channel gains over the individual signaling periods.

3.3 Preliminary Results: Effective SNR and pdf

First, by substituting (3.2.1) into (2.3.1), we can write a relationship between the actual channel gain over the k th signaling period $h_{a,b}(k)$ and the estimated one over the first signaling period $\hat{h}_{a,b}(1)$ as

$$h_{a,b}(k) = \underbrace{\rho_{a,b}^{k-1} \hat{h}_{a,b}(1) + \sqrt{1 - \rho_{a,b}^2} \sum_{j=1}^{k-1} \rho_{a,b}^{k-j-1} e_{a,b}(j)}_{\hat{h}_{a,b}(k)} + \underbrace{\rho_{a,b}^{k-1} h_{\epsilon_{a,b}}(1)}_{h_{\epsilon_{a,b}}(k)} \quad (3.3.1)$$

where $\hat{h}_{a,b}(k)$ is estimated version of $h_{a,b}(k)$ and $h_{\epsilon_{a,b}}(k)$ is its estimation error. In the next section we use the relationship in (3.3.1) to expand the destination to mathematically show the nodes-mobility (or the time-selective fading) and the imperfect-CSI estimation impacts on the destination received signals and SNRs.

3.3.1 destination direct-path effective SNR

First, with the help of (3.3.1), we can expand the received signal at the destination through the direct path, $r_{s,d}(k)$, given in ((2.2.1)), showing the desired signal terms and the noise terms generated from the time-selective fading, imperfect-CSI estimation and additive white noise, as

$$r_{s,d}(k) = \underbrace{\rho_{s,d}^{k-1} \hat{h}_{s,d}(1)x(k)}_{\text{desired signal}} + \underbrace{\overbrace{\sqrt{1 - \rho_{s,d}^2} \sum_{j=1}^{k-1} \rho_{s,d}^{k-j-1} e_{a,b}(j)x(k)}^{\text{time-selective fading noise}} + \overbrace{\rho_{s,d}^{k-1} h_{\epsilon_{s,d}}(1)x(k)}^{\text{estimation error noise}} + \underbrace{n_{s,d}(k)}_{\text{white noise}}}_{\text{overall effective noise}} \quad (3.3.2)$$

Because $e_{s,d}(j)$, $h_{\epsilon_{s,d}}(1)$ and $n_{s,d}(k)$ are independent ZMCSCG processes, the overall effective noise term in (3.3.2) has a variance of

$$\sigma_{eff_{s,d}}^{2\text{im}} = (1 - \rho_{s,d}^{2(k-1)})\sigma_{s,d}^2 E_s + \rho_{s,d}^{2(k-1)}\sigma_{e_{s,d}}^2 E_s + N_o. \quad (3.3.3)$$

From (3.3.2), we can write the direct-path effective SNR in case of imperfect-estimation, $\gamma_{s,d}^{\text{im}}(k)$, as

$$\gamma_{s,d}^{\text{im}}(k) = \frac{|\rho_{s,d}^{k-1} \hat{h}_{s,d}(1)x(k)|^2}{\sigma_{eff_{s,d}}^{2\text{im}}} = \frac{\rho_{s,d}^{2(k-1)} |\hat{h}_{s,d}(1)|^2 E_s}{((1 - \rho_{s,d}^{2(k-1)})\sigma_{s,d}^2 + \rho_{s,d}^{2(k-1)}\sigma_{e_{s,d}}^2) E_s + N_o}. \quad (3.3.4)$$

Because $|\hat{h}_{s,d}(1)|$ is Rayleigh, $\gamma_{s,d}^{\text{im}}(k)$ in (3.3.4) has an exponential pdf, which can be given as

$$f_{\gamma_{s,d}^{\text{im}}(k)}(\gamma) = \frac{1}{\bar{\gamma}_{s,d}^{\text{im}}(k)} \exp\left(-\frac{\gamma}{\bar{\gamma}_{s,d}^{\text{im}}(k)}\right) \quad (3.3.5)$$

where

$$\bar{\gamma}_{s,d}^{\text{im}}(k) = \mathbb{E}[\gamma_{s,d}^{\text{im}}(k)] = \frac{\rho_{s,d}^{2(k-1)} E_s}{((1 - \rho_{s,d}^{2(k-1)})\sigma_{s,d}^2 + \rho_{s,d}^{2(k-1)}\sigma_{e_{s,d}}^2) E_s + N_o}.$$

3.3.2 destination end-to-end path effective SNR

In order to derive the end-to-end effective SNR in the case of imperfect estimation, say $\gamma_{s,i,d}^{\text{im}}(k)$, we first expand $h_{s,i}(k)$ and $h_{i,d}(k)$ as in (3.3.1) and then substitute the obtained expansions into (2.3.6) to expand $r_{i,d}(k)$ as

$$\begin{aligned}
r_{i,d}(k) = & \overbrace{\mathcal{G}_i(k)\rho_{s,i}^{k-1}\rho_{i,d}^{k-1}\hat{h}_{s,i}(1)\hat{h}_{i,d}(1)x(k)}^{\text{desired signal}} \\
& \underbrace{+ \mathcal{G}_i(k)x(k)\rho_{s,i}^{k-1}\hat{h}_{s,i}(1)\left(\sqrt{1-\rho_{i,d}^2}\sum_{j=1}^{k-1}\rho_{i,d}^{k-j-1}e_{i,d}(j) + h_{\epsilon_{i,d}}(1)\right) + \rho_{i,d}^{k-1}\hat{h}_{i,d}(1)}_{\text{overall effective noise}} \\
& \times \left(\sqrt{1-\rho_{s,i}^2}\sum_{j=1}^{k-1}\rho_{s,i}^{k-j-1}e_{s,i}(j) + h_{\epsilon_{s,i}}(1)\right) + \left(\sqrt{1-\rho_{i,d}^2}\sum_{j=1}^{k-1}\rho_{i,d}^{k-j-1}e_{i,d}(j)\right. \\
& \left.+ h_{\epsilon_{i,d}}(1)\right)\left(\sqrt{1-\rho_{s,i}^2}\sum_{j=1}^{k-1}\rho_{s,i}^{k-j-1}e_{s,i}(j) + h_{\epsilon_{s,i}}(1)\right) + \mathcal{G}_i(k)n_{s,i}(k)\left(\rho_{i,d}^{k-1}\hat{h}_{i,d}(1)\right. \\
& \left.+ \sqrt{1-\rho_{i,d}^2}\sum_{j=1}^{k-1}\rho_{i,d}^{k-j-1}e_{i,d}(j)h_{\epsilon_{i,d}}(1)\right) + n_{i,d}(k). \tag{3.3.6}
\end{aligned}$$

The effective noise term in (3.3.6) is a also ZMCSCG process, which we can obtain its variance $\sigma_{effs,i,d}^{2\text{im}}$ as

$$\begin{aligned}
\sigma_{effs,i,d}^{2\text{im}} = & ((1-\rho_{s,i}^{2(k-1)})\sigma_{s,i}^2E_s + \rho_{s,i}^{2(k-1)}\sigma_{e_{s,i}}^2E_s + N_o)\rho_{i,d}^{2(k-1)}\mathcal{G}_i^2(k)|\hat{h}_{i,d}(1)|^2 \\
& + ((1-\rho_{i,d}^{2(k-1)})\sigma_{i,d}^2E_s + \rho_{i,d}^{2(k-1)}\sigma_{e_{i,d}}^2E_s)\rho_{s,i}^{2(k-1)}\mathcal{G}_i^2(k)|\hat{h}_{s,i}(1)|^2 \\
& + N_o + (1-\rho_{s,i}^{2(k-1)})\sigma_{s,i}^2((1-\rho_{i,d}^{2(k-1)})\sigma_{i,d}^2E_s + E_s\rho_{i,d}^{2(k-1)}\sigma_{e_{i,d}}^2)\mathcal{G}_i^2(k) \\
& + (1-\rho_{i,d}^{2(k-1)})\rho_{s,i}^{2(k-1)}\sigma_{e_{s,i}}^2\sigma_{i,d}^2E_s\mathcal{G}_i^2(k) + \rho_{s,i}^{2(k-1)}\sigma_{e_{s,i}}^2\rho_{i,d}^{2(k-1)}\sigma_{e_{i,d}}^2 \\
& \times E_s\mathcal{G}_i^2(k) + (1-\rho_{i,d}^{2(k-1)})\sigma_{i,d}^2N_o\mathcal{G}_i^2(k) + \rho_{i,d}^{2(k-1)}\sigma_{e_{i,d}}^2N_o\mathcal{G}_i^2(k). \tag{3.3.7}
\end{aligned}$$

From (3.3.6), we can obtain $\gamma_{s,i,d}^{\text{im}}(k)$ as

$$\gamma_{s,i,d}^{\text{im}}(k) = \frac{|\mathcal{G}_i(k)\rho_{s,i}^{k-1}\rho_{i,d}^{k-1}\hat{h}_{i,d}(1)\hat{h}_{s,i}(1)x(k)|^2}{\sigma_{effs,i,d}^{2\text{im}}}. \tag{3.3.8}$$

In order to write the SNR in (3.3.8) in more tractable form that helps in evaluating its pdf, we need first to evaluate the amplification gain described in (3.2.2). Because we assume imperfect estimation in this chapter, the gain in (3.2.2) can be rewritten as

$$\mathcal{G}_i^{\text{im}}(k) = \sqrt{\frac{E_s}{\mathcal{E}(\hat{h}_{s,i}(k))E_s + N_o}} \quad (3.3.9)$$

With the help of (3.3.1), we can write $\hat{h}_{s,i}(k) = \rho_{s,i}^{k-1}\hat{h}_{s,i}(1) + \sqrt{1 - \rho_{s,i}^2} \sum_{j=1}^{k-1} \rho_{s,i}^{k-j-1} e_{s,i}(j)$, and thus, its energy $\mathcal{E}(\hat{h}_{s,i}(k))$ can be given as

$$\mathcal{E}(\hat{h}_{s,i}(k)) = \rho_{s,i}^{2(k-1)}|\hat{h}_{s,i}(1)|^2 + (1 - \rho_{s,i}^{2(k-1)})\sigma_{s,i}^2. \quad (3.3.10)$$

By substituting now (3.3.10) into (3.3.9), we can obtain $\mathcal{G}_i^{\text{im}}(k)$ in its ultimate form as

$$\mathcal{G}_i^{\text{im}}(k) = \sqrt{\frac{E_s}{(\rho_{s,i}^{2(k-1)}|\hat{h}_{s,i}(1)|^2 + (1 - \rho_{s,i}^{2(k-1)})\sigma_{s,i}^2)E_s + N_o}} \quad (3.3.11)$$

Now, by substituting (3.3.11) for the amplification gain in (3.3.8), and after doing some manipulations and simplifications, we can write $\gamma_{s,i,d}^{\text{im}}(k)$ in the following intended ultimate form

$$\gamma_{s,i,d}^{\text{im}}(k) = \frac{\gamma_{s,i}^{\text{im}}(k)\gamma_{i,d}^{\text{im}}(k)}{\gamma_{s,i}^{\text{im}}(k) + \gamma_{i,d}^{\text{im}}(k) + \Psi_i(k)} \quad (3.3.12)$$

where

$$\gamma_{s,i}^{\text{im}}(k) = \frac{E_s \rho_{s,i}^{2(k-1)}|\hat{h}_{s,i}(1)|^2}{((1 - \rho_{s,i}^{2(k-1)})\sigma_{s,i}^2 + \rho_{s,i}^{2(k-1)}\sigma_{e_{s,i}}^2)E_s + N_o}$$

and

$$\gamma_{i,d}^{\text{im}}(k) = \frac{E_s \rho_{i,d}^{2(k-1)}|\hat{h}_{i,d}(1)|^2}{((1 - \rho_{i,d}^{2(k-1)})\sigma_{i,d}^2 + \rho_{i,d}^{2(k-1)}\sigma_{e_{i,d}}^2)E_s + N_o}$$

are the effective SNRs of S - R_i and R_i - D links, respectively, and

$$\begin{aligned}\Psi_i(k) = & \left((1 - \rho_{s,i}^{2(k-1)}) \sigma_{s,i}^2 E_s^2 \left((1 - \rho_{i,d}^{2(k-1)}) \sigma_{i,d}^2 + \rho_{i,d}^{2(k-1)} \sigma_{e_{i,d}}^2 + \frac{N_o}{E_s} \right) + (1 - \rho_{i,d}^{2(k-1)}) \right. \\ & \times \sigma_{i,d}^2 E_s \left(\rho_{s,i}^{2(k-1)} \sigma_{e_{s,i}}^2 E_s + N_o \right) + \rho_{s,i}^{2(k-1)} \sigma_{e_{s,i}}^2 \rho_{i,d}^{2(k-1)} \sigma_{e_{i,d}}^2 E_s^2 + \rho_{i,d}^{2(k-1)} \sigma_{e_{i,d}}^2 E_s N_o \\ & + N_o^2 \Big) / \left(\left((1 - \rho_{s,i}^{2(k-1)}) \sigma_{s,i}^2 E_s + N_o + \rho_{s,i}^{2(k-1)} \sigma_{e_{s,i}}^2 E_s \right) \left((1 - \rho_{i,d}^{2(k-1)}) \sigma_{i,d}^2 E_s + N_o \right. \right. \\ & \left. \left. + \rho_{i,d}^{2(k-1)} \sigma_{e_{i,d}}^2 E_s \right) \right).\end{aligned}\quad (3.3.13)$$

As a special case of quasi-static fading ($\rho_{a,b} = 1 \ \forall(a,b)$) and perfect channel estimation ($\sigma_{e_{s,i}}^2 = \sigma_{e_{i,d}}^2 = 0$), the effective end-to-end SNR in (3.3.12) also reduces to (2.3.15).

The cdf and the pdf of $\gamma_{s,i,d}^{\text{im}}(k)$, in (3.3.12), can be evaluated in exact form, with the help of [26], respectively, as

$$\begin{aligned}F_{\gamma_{s,i,d}^{\text{im}}(k)}(\gamma) = & 1 - 2(\bar{\gamma}_{s,i}^{\text{im}})^3(k) \exp \left(- \left(\frac{\bar{\gamma}_{s,i}^{\text{im}}(k) + \bar{\gamma}_{i,d}^{\text{im}}(k)}{\bar{\gamma}_{s,i}^{\text{im}}(k) \bar{\gamma}_{i,d}^{\text{im}}(k)} \right) \gamma \right) \sqrt{\frac{\gamma^2 + \Psi_i(k) \gamma}{\bar{\gamma}_{s,i}^{\text{im}}(k) \bar{\gamma}_{i,d}^{\text{im}}(k)}} \\ & \times K_1 \left(2 \sqrt{\frac{\gamma^2 + \Psi_i(k) \gamma}{\bar{\gamma}_{s,i}^{\text{im}}(k) \bar{\gamma}_{i,d}^{\text{im}}(k)}} \right)\end{aligned}\quad (3.3.14)$$

and

$$\begin{aligned}f_{\gamma_{s,i,d}^{\text{im}}(k)}(\gamma) = & \frac{2}{\bar{\gamma}_{s,i}^{\text{im}}(k)} \exp \left(- \left(\frac{\bar{\gamma}_{s,i}^{\text{im}}(k) + \bar{\gamma}_{i,d}^{\text{im}}(k)}{\bar{\gamma}_{s,i}^{\text{im}}(k) \bar{\gamma}_{i,d}^{\text{im}}(k)} \right) \gamma \right) \left[\frac{2\gamma + \Psi_i(k)}{\bar{\gamma}_{i,d}^{\text{im}}(k)} \right. \\ & K_o \left(2 \sqrt{\frac{\gamma^2 + \Psi_i(k) \gamma}{\bar{\gamma}_{s,i}^{\text{im}}(k) \bar{\gamma}_{i,d}^{\text{im}}(k)}} \right) + \left(\frac{\bar{\gamma}_{s,i}^{\text{im}}(k) + \bar{\gamma}_{i,d}^{\text{im}}(k)}{\bar{\gamma}_{s,i}^{\text{im}}(k) \bar{\gamma}_{i,d}^{\text{im}}(k)} \right) \sqrt{\frac{(\gamma^2 + \Psi_i(k) \gamma) \bar{\gamma}_{s,i}^{\text{im}}(k)}{\bar{\gamma}_{i,d}^{\text{im}}(k)}} \\ & \left. K_1 \left(2 \sqrt{\frac{\gamma^2 + \Psi_i(k) \gamma}{\bar{\gamma}_{s,i}^{\text{im}}(k) \bar{\gamma}_{i,d}^{\text{im}}(k)}} \right) \right]\end{aligned}\quad (3.3.15)$$

where $K_n(k)$ is the n th order modified bessel function of the second kind, $\bar{\gamma}_{s,i}^{\text{im}}(k) = \mathbb{E}[\gamma_{s,i}^{\text{im}}(k)]$ and $\bar{\gamma}_{i,d}^{\text{im}}(k) = \mathbb{E}[\gamma_{i,d}^{\text{im}}(k)]$. In order to simplify the following analysis, we propose to approximate (as similar as the approximation we have considered in (2.3.17)) $\gamma_{s,i,d}^{\text{im}}(k)$ in (3.3.12)

as

$$\gamma_{s,i,d}^{\text{im}}(k) \approx \gamma_{\text{up},i}^{\text{im}}(k) = \min(\gamma_{s,i}^{\text{im}}(k), \gamma_{i,d}^{\text{im}}(k)) \quad (3.3.16)$$

which we obtain its pdf as

$$f_{\gamma_{\text{up},i}^{\text{im}}(k)}(\gamma) = \frac{1}{\bar{\gamma}_{\text{up},i}^{\text{im}}(k)} \exp\left(-\frac{\gamma}{\bar{\gamma}_{\text{up},i}^{\text{im}}(k)}\right) \quad (3.3.17)$$

where

$$\bar{\gamma}_{\text{up},i}^{\text{im}}(k) = \frac{\bar{\gamma}_{s,i}^{\text{im}}(k) \bar{\gamma}_{i,d}^{\text{im}}(k)}{(\bar{\gamma}_{s,i}^{\text{im}}(k) + \bar{\gamma}_{i,d}^{\text{im}}(k))}. \quad (3.3.18)$$

In the following we continue our analysis based on this approximation, which, as will be shown later in the numerical results section, helps in obtaining tight closed-form system performance expressions.

3.3.3 MRC destination Overall SNR

Because the destination combines all received signals through the direct and the end-to-end paths via MRC, we can write the effective SNR at the MRC output in case of imperfect-estimation as

$$\gamma_{\text{tot}}^{\text{im}}(k) = \gamma_{s,d}^{\text{im}}(k) + \sum_{i=1}^M \gamma_{s,i,d}^{\text{im}}(k) \quad (3.3.19)$$

If we consider now the approximation of $\gamma_{s,i,d}^{\text{im}}(k)$ as in (3.3.16), we can approximate $\gamma_{\text{tot}}^{\text{im}}(k)$ in (3.3.19) as

$$\gamma_{\text{tot}}^{\text{im}}(k) \approx \gamma_{\text{tot,up}}^{\text{im}}(k) = \gamma_{s,d}^{\text{im}}(k) + \sum_{i=1}^M \gamma_{\text{up},i}^{\text{im}}(k) \quad (3.3.20)$$

By following same MGF method we have followed to obtain the pdf in (2.3.27), we can obtain the pdf of $\gamma_{\text{tot,up}}^{\text{im}}(k)$ in (3.3.20) as

$$f_{\gamma_{\text{tot,up}}^{\text{im}}(k)}(\gamma) = \frac{\xi_{\text{up}}^{\text{im}} e^{\left(\frac{-\gamma}{\bar{\gamma}_{s,d}^{\text{im}}(k)}\right)}}{\bar{\gamma}_{s,d}^{\text{im}}(k)} + \sum_{i=1}^M \frac{\xi_{\text{up},i}^{\text{im}} e^{\left(\frac{-\gamma}{\bar{\gamma}_{\text{up},i}^{\text{im}}(k)}\right)}}{\bar{\gamma}_{\text{up},i}^{\text{im}}(k)} \quad (3.3.21)$$

where

$$\xi_{\text{up}}^{\text{im}} = \frac{(\bar{\gamma}_{s,d}^{\text{im}}(k))^M}{\prod_{i=1}^M (\bar{\gamma}_{s,d}^{\text{im}}(k) - \bar{\gamma}_{\text{up},i}^{\text{im}}(k))} \quad (3.3.22)$$

and

$$\xi_{\text{up},i}^{\text{im}} = \frac{(\bar{\gamma}_{\text{up},i}^{\text{im}}(k))^M}{(\bar{\gamma}_{\text{up},i}^{\text{im}}(k) - \bar{\gamma}_{s,d}^{\text{im}}(k)) \prod_{i=1, i \neq j}^M (\bar{\gamma}_{\text{up},i}^{\text{im}}(k) - \bar{\gamma}_{\text{up},j}^{\text{im}}(k))}. \quad (3.3.23)$$

In case of perfect estimation assumption, the pdf in (3.3.21) reduces to the one in (2.3.27).

3.4 System Performance Evaluation

In this section we use the pdf in (3.3.21) to derive closed-form expressions for the per-block-average BPSK BER, outage probability and Shannon capacity of the system model described in Sec 3.2. These obtained expressions generalize the ones derived in chapter 1 for the case of perfect-estimation.

3.4.1 Error probability

By using the pdf given by (3.3.21) in evaluating (2.4.1), and solving the integration by parts and then doing some manipulation and simplifications, we obtain closed-form expression for the lower bound per-block-average BPSK BER, of our system model in case of error estimation, in terms of $\frac{E_s}{N_o}$ as

$$\begin{aligned} \bar{P}_{e,\text{Low}}^{\text{im}} = & \frac{1}{2N} \sum_{k=1}^N \left(\tilde{\alpha}^M \left[1 - \sqrt{\frac{\tilde{\alpha} \frac{E_s}{N_o}}{\tilde{\zeta} \frac{E_s}{N_o} + 1}} \right] \prod_{i=1}^M \left(\frac{\tilde{\eta}_i \frac{E_s}{N_o} + \tilde{\beta}_i}{\tilde{\mu}_i \frac{E_s}{N_o} + \tilde{\lambda}_i} \right) \right. \\ & \left. - \sum_{i=1}^M \left(\left[1 - \sqrt{\frac{\tilde{\delta}_i \frac{E_s}{N_o}}{\tilde{\chi}_i \frac{E_s}{N_o} + \tilde{\beta}_i}} \right] \frac{(\tilde{\delta}_i)^M (\tilde{\kappa} \frac{E_s}{N_o} + 1)}{\tilde{\mu}_i \frac{E_s}{N_o} + \tilde{\lambda}_i} \prod_{j=1, j \neq i}^M \left(\frac{\tilde{\eta}_j \frac{E_s}{N_o} + \tilde{\beta}_j}{\tilde{\nu}_{i,j} \frac{E_s}{N_o} + \tilde{\omega}_{i,j}} \right) \right) \right) \end{aligned} \quad (3.4.1)$$

where

$$\begin{aligned}
\tilde{\zeta} &= \tilde{\alpha} + \tilde{\kappa} \\
\tilde{\mu}_i &= \tilde{\alpha}\tilde{\eta}_i - \tilde{\delta}_i\tilde{\kappa} \\
\tilde{\lambda}_i &= \tilde{\alpha}\tilde{\beta}_i - \tilde{\delta}_i \\
\tilde{\chi}_i &= \tilde{\eta}_i + \tilde{\delta}_i \\
\tilde{\nu}_{i,j} &= \tilde{\delta}_i\tilde{\eta}_j - \tilde{\delta}_j\tilde{\eta}_i \\
\tilde{\omega}_{i,j} &= \tilde{\delta}_i\tilde{\beta}_j - \tilde{\delta}_j\tilde{\beta}_i \\
\tilde{\alpha} &= \rho_{s,d}^{2(k-1)}\mathbb{E}[|\hat{h}_{s,d}(1)|^2] \\
\tilde{\kappa} &= (1 - \rho_{s,d}^{2(k-1)})\sigma_{s,d}^2 + \sigma_{e_{s,d}}^2 \\
\tilde{\eta}_\ell &= \rho_{s,\ell}^{2(k-1)}((1 - \rho_{\ell,d}^{2(k-1)})\sigma_{\ell,d}^2 + \tilde{\sigma}_{e_{\ell,d}}^2)\mathbb{E}[|\hat{h}_{s,\ell}(1)|^2] \\
&\quad + \rho_{\ell,d}^{2(k-1)}((1 - \rho_{s,\ell}^{2(k-1)})\sigma_{s,\ell}^2 + \sigma_{e_{s,\ell}}^2)\mathbb{E}[|\hat{h}_{\ell,d}(1)|^2] \\
\tilde{\beta}_\ell &= \rho_{s,\ell}^{2(k-1)}\mathbb{E}[|\hat{h}_{s,\ell}(1)|^2] + \rho_{\ell,d}^{2(k-1)}\mathbb{E}[|\hat{h}_{\ell,d}(1)|^2] \\
\tilde{\delta}_\ell &= \rho_{s,\ell}^{2(k-1)}\rho_{\ell,d}^{2(k-1)}\mathbb{E}[|\hat{h}_{s,\ell}(1)|^2]\mathbb{E}[|\hat{h}_{\ell,d}(1)|^2], \quad \forall \ell = 1, 2, \dots, M.
\end{aligned}$$

Similarly as the BER in (2.4.3), the BER in (3.4.1) also experiences asymptotic floor, which can be given as

$$\begin{aligned}
\lim_{\frac{E_s}{N_0} \rightarrow \infty} \bar{P}_{e,\text{Low}}^{\text{im}} &= \frac{1}{2N} \sum_{k=1}^N \left(\tilde{\alpha}^M \left[1 - \sqrt{\frac{\tilde{\alpha}}{\tilde{\zeta}}} \right] \prod_{i=1}^M \left(\frac{\tilde{\eta}_i}{\tilde{\mu}_i} \right) \right. \\
&\quad \left. - \sum_{i=1}^M \left(\frac{\tilde{\kappa}(\tilde{\delta}_i)^M}{\tilde{\mu}_i} \left[1 - \sqrt{\frac{\tilde{\delta}_i}{\tilde{\chi}_i}} \right] \prod_{j=1, j \neq i}^M \frac{\tilde{\eta}_j}{\tilde{\nu}_{i,j}} \right) \right)
\end{aligned} \tag{3.4.2}$$

It is worthwhile to mention that this floor is not only due to the assumption of time-selective fading within the network but also due to that of imperfect channel estimation at the network receivers.

3.4.2 Outage probability

By using the pdf given by (3.3.21) in evaluating (2.4.7), and after doing some manipulation and simplifications, we can obtain closed-form expression for the system per-block-average outage probability in the case of imperfect-estimation as

$$\begin{aligned}
P_{\text{out,Low}}^{\text{im}} &= \frac{1}{N} \sum_{k=1}^N \left(\int_0^{\gamma_{th}} f_{\gamma_{\text{tot,up}}^{(k)}}(\gamma) d\gamma \right) \\
&= \frac{1}{N} \sum_{k=1}^N \left(\tilde{\alpha}^M \left(1 - e^{-\frac{\tilde{\kappa} \frac{E_s}{N_o} + 1}{\tilde{\alpha} \frac{E_s}{N_o}} \gamma_{th}} \right) \prod_{i=1}^M \left(\frac{\tilde{\eta}_i \frac{E_s}{N_o} + \tilde{\beta}_i}{\tilde{\mu}_i \frac{E_s}{N_o} + \tilde{\lambda}_i} \right) \right. \\
&\quad \left. - \sum_{i=1}^M \left(\left(1 - e^{-\frac{\tilde{\eta}_i \frac{E_s}{N_o} + \tilde{\beta}_i}{\tilde{\delta}_i \frac{E_s}{N_o}} \gamma_{th}} \right) \frac{(\tilde{\delta}_i)^M (\tilde{\kappa} \frac{E_s}{N_o} + 1)}{\tilde{\mu}_i \frac{E_s}{N_o} + \tilde{\lambda}_i} \prod_{j=1, j \neq i}^M \left(\frac{\tilde{\eta}_j \frac{E_s}{N_o} + \tilde{\beta}_j}{\tilde{\nu}_{i,j} \frac{E_s}{N_o} + \tilde{\omega}_{i,j}} \right) \right) \right)
\end{aligned} \tag{3.4.3}$$

which is also suffers from floor, as a result of the time-selective fading and the imperfect-estimation, that can be given as

$$\begin{aligned}
\lim_{\frac{E_s}{N_o} \rightarrow \infty} P_{\text{out,Low}}^{\text{im}} &= \frac{1}{N} \sum_{k=1}^N \left(\tilde{\alpha}^M \left(1 - e^{-\frac{\tilde{\kappa}}{\tilde{\alpha}} \gamma_{th}} \right) \prod_{i=1}^M \left(\frac{\tilde{\eta}_i}{\tilde{\mu}_i} \right) \right. \\
&\quad \left. - \sum_{i=1}^M \left(\frac{(\tilde{\delta}_i)^M}{\tilde{\mu}_i} \left(1 - e^{-\frac{\tilde{\eta}_i}{\tilde{\delta}_i} \gamma_{th}} \right) \prod_{j=1, j \neq i}^M \left(\frac{\tilde{\eta}_j}{\tilde{\nu}_{i,j}} \right) \right) \right).
\end{aligned} \tag{3.4.4}$$

3.4.3 System Shannon capacity

By using the pdf given by (3.3.21) in evaluating the first line in (2.4.13), and performing some manipulation and simplifications, we can obtain closed-form expression the

upper-bound per-block-average capacity in the case of imperfect-estimation as

$$\begin{aligned}
\bar{C}_{\text{up}}^{\text{im}} &= \frac{1}{N} \sum_{k=1}^N \left(\frac{B}{M+1} \int_0^\infty \log_2(1+\gamma) f_{\gamma_{\text{tot,up}}^{(k)}}(\gamma) d\gamma \right) \\
&= \frac{B \log_2(e)}{N(M+1)} \sum_{k=1}^N \left(\tilde{\alpha}^M e^{\frac{\tilde{\kappa} \frac{E_s}{N_o} + 1}{\tilde{\alpha} \frac{E_s}{N_o}}} E_1 \left(\frac{\tilde{\kappa} \frac{E_s}{N_o} + 1}{\tilde{\alpha} \frac{E_s}{N_o}} \right) \prod_{i=1}^M \left(\frac{\tilde{\eta}_i \frac{E_s}{N_o} + \tilde{\beta}_i}{\tilde{\mu}_i \frac{E_s}{N_o} + \tilde{\lambda}_i} \right) \right. \\
&\quad \left. - \sum_{i=1}^M \left(e^{\frac{\tilde{\eta}_i \frac{E_s}{N_o} + \tilde{\beta}_i}{\tilde{\delta}_i \frac{E_s}{N_o}}} E_1 \left(\frac{\tilde{\eta}_i \frac{E_s}{N_o} + \tilde{\beta}_i}{\tilde{\delta}_i \frac{E_s}{N_o}} \right) \frac{(\tilde{\delta}_i)^M (\tilde{\kappa} \frac{E_s}{N_o} + 1)}{\tilde{\mu}_i \frac{E_s}{N_o} + \tilde{\lambda}_i} \prod_{j=1, j \neq i}^M \left(\frac{\tilde{\eta}_j \frac{E_s}{N_o} + \tilde{\beta}_j}{\tilde{\nu}_{i,j} \frac{E_s}{N_o} + \tilde{\omega}_{i,j}} \right) \right) \right)
\end{aligned} \tag{3.4.5}$$

The capacity in (3.4.5) is limited by a ceiling as a result of both time-selective fading and imperfect-estimation, which can be given as

$$\begin{aligned}
\lim_{\frac{E_s}{N_o} \rightarrow \infty} \bar{C}_{\text{up}}^{\text{im}} &= \frac{B \log_2(e)}{N(M+1)} \sum_{k=1}^N \left(\tilde{\alpha}^M e^{\frac{\tilde{\kappa}}{\tilde{\alpha}}} E_1 \left(\frac{\tilde{\kappa}}{\tilde{\alpha}} \right) \prod_{i=1}^M \left(\frac{\tilde{\eta}_i}{\tilde{\mu}_i} \right) \right. \\
&\quad \left. - \sum_{i=1}^M \left(e^{\frac{\tilde{\eta}_i}{\tilde{\delta}_i}} E_1 \left(\frac{\tilde{\eta}_i}{\tilde{\delta}_i} \right) \left(\frac{(\tilde{\delta}_i)^M \tilde{\kappa}}{\tilde{\mu}_i} \right) \prod_{j=1, j \neq i}^M \left(\frac{\tilde{\eta}_j}{\tilde{\nu}_{i,j}} \right) \right) \right).
\end{aligned} \tag{3.4.6}$$

3.5 Numerical Results and Simulation

Fig. 3.1 is a plot for the theoretical lower-bound BPSK BER performance of the system model described in Sec. 3.2 (using (3.4.1)) along with the exact simulation. The plotted error floors in this figure are using (3.4.2). The tightness of the lower-bound is obvious, in particular, at medium and high average SNR regions. It is also clear that the BER performance experiences error floor due to the source mobility along with constrained CSI estimation rates of 2% ($N = 50$). In case of imperfect channel estimation, the error floor increases, which means further performance degradation.

In Fig. 3.2, we plot the exact simulation outage probability for the system model under study along with the theoretical lower-bound outage expression given by (3.4.3) and the outage floor expression given by (3.4.4). Similarly, this figure shows that the outage performance is degraded due to nodes mobility, imperfect estimation and low CSI estimation

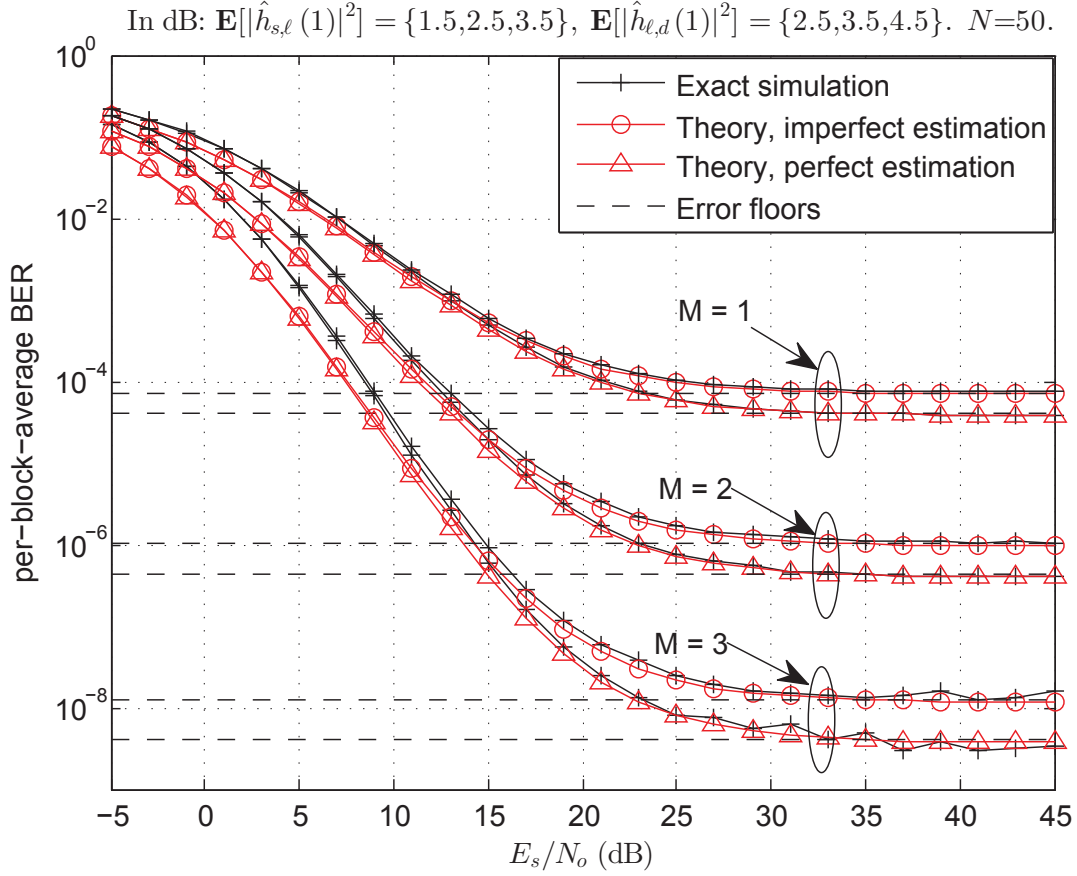


Figure 3.1. BPSK BER versus E_s/N_o with 2% CSI estimation rates ($N = 50$) and $M = 1, 2$ and 3. In dB: $\mathbf{E}[|h_{s,d}(1)|^2] = 1$, $\mathbf{E}[|h_{s,\ell}(1)|^2] = \{1.5, 2.5, 3.5\}$ and $\mathbf{E}[|h_{\ell,d}(1)|^2] = \{2.5, 3.5, 4.5\}$. The Source is mobile and the other nodes are static corresponding to correlation parameters of $\rho_{s,d} = \rho_{s,\ell} = 0.9997$ and $\rho_{i,d} = 1$. In case of imperfect channel estimation: $\sigma_{e_{a,b}}^2 = 0.02 \forall(a, b)$.

rate of $N = 30$. Moreover, in case of quasi-static fading (all nodes are static), the outage floor is removed as long as the estimation is perfect.

Fig. 3.3 is a plot for the system normalized Shannon capacity expression given by (3.4.5), verified via exact simulation, and the capacity ceiling expression given by (3.4.6) for 1% CSI imperfect estimation rate ($N = 100$). First, we can notice the tightness of the theoretical derived expressions as compared with the exact simulation. In addition, for higher nodes mobility the capacity ceiling decreases.

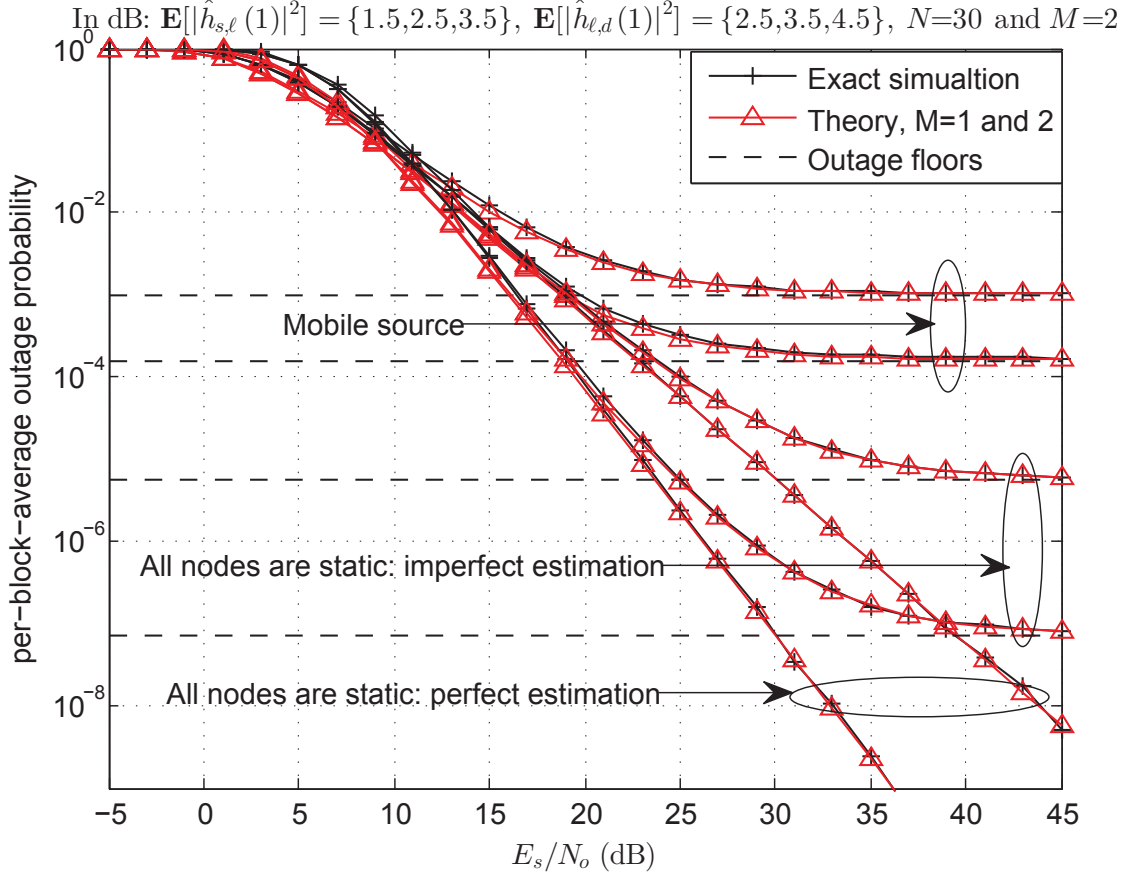


Figure 3.2. Per-block-average outage probability versus E_s/N_o with and $N = 30$ and $M = 1$ and 2. In dB: $\mathbb{E}[|h_{s,d}(1)|^2] = 1$, $\mathbb{E}[|h_{s,\ell}(1)|^2] = \{1.5, 2.5\}$ and $\mathbb{E}[|h_{s,\ell}(1)|^2] = \{2.5, 3.5\}$. The corresponding correlation parameter is 0.9990. In case of imperfect estimation: $\sigma_{e_{a,b}}^2 = 0.03 \forall(a, b)$.

3.6 Conclusion

In this chapter, we have analyzed the performance of M -relay AF cooperative network taking into account the impacts of the nodes mobility, the estimation errors, and the speed of the receivers' tracking loops. We have derived exact expressions for the destination's SNRs, through the direct and the end-to-end paths, and approximate expressions for the system average BER, outage probability, and capacity. The derived expressions are general, which are valid for mobile and static nodes, imperfect and perfect channel estimations, and slow and fast receiver's tracking loops. Numerical and simulation results have been presented to show the system performance and demonstrate how it is affected by the different scenarios

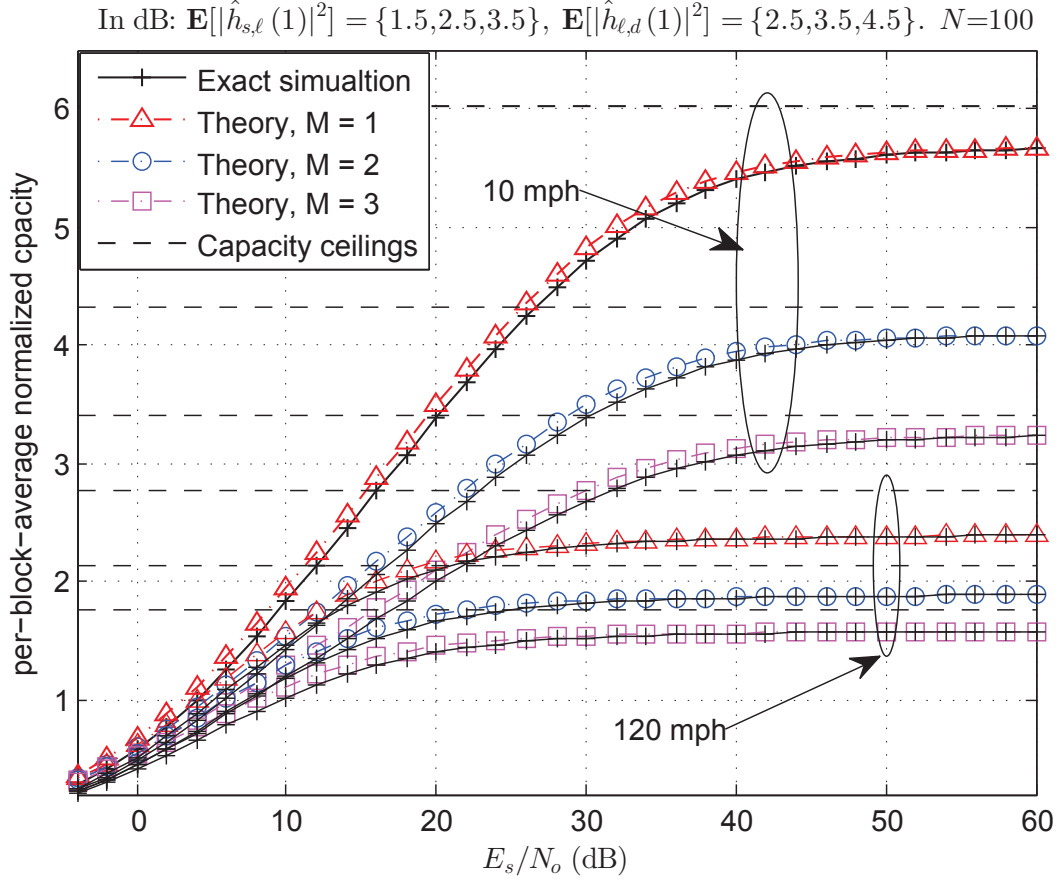


Figure 3.3. Per-block-average upper-bound normalized capacity versus E_s/N_o with $N = 100$ and $M = 1, 2$ and 3 . In dB: $\mathbf{E}[|h_{s,d}(1)|^2] = 1$, $\mathbf{E}[|h_{s,\ell}(1)|^2] = \{1.5, 2.5, 3.5\}$ and $\mathbf{E}[|h_{\ell,d}(1)|^2] = \{2.5, 3.5, 4.5\}$. Imperfect estimation with $\sigma_{e_{a,b}}^2 = 0.01 \forall(a, b)$.

of nodes mobility and channel estimation rates.

CHAPTER 4

Best-Relay-Selection M -Relay Variable-Gain AF Cooperative Systems with Mobile Nodes and Imperfect CSI Estimation: SNR Derivation and Performance Analysis

4.1 Chapter Overview

In this chapter, we consider the variable-gain M -relay amplify-and-forward (AF) cooperative system with best-relay-selection protocol, in which the relay (the best) that achieves the highest effective signal-to-noise-ratio (SNR) at the destination only retransmits to the destination, and investigate its performance under the impacts of the nodes' mobility and the channel estimation error. Specifically, we derive approximate closed-form expression for the pdf of the total effective SNR at the output of the destination's MRC combiner. Starting from this pdf, we derive closed-form tight approximate expressions for this system per-block-average BER, outage probability, and Shannon capacity. Our analysis reveals that due to the cooperating-nodes mobility and error estimation, the best-relay-selection cooperative system performance is severely degraded and experiences asymptotic limits. In addition, as compared with the regular cooperative system, we found that the best-relay-selection protocol provides higher asymptotic error floors. We finally provide simulation and numerical results to verify the accuracy of the derived analytical expressions.

4.2 System and Channel Model

Here, we consider the same system model as in chapter 2 but, instead of employing the regular cooperative protocol, we employ the best-relay-selection one [27]. In this protocol, the destination selects the signal from the relay that achieved the highest effective SNR and combine it with the direct-path signal via MRC (see Fig. 4.1).

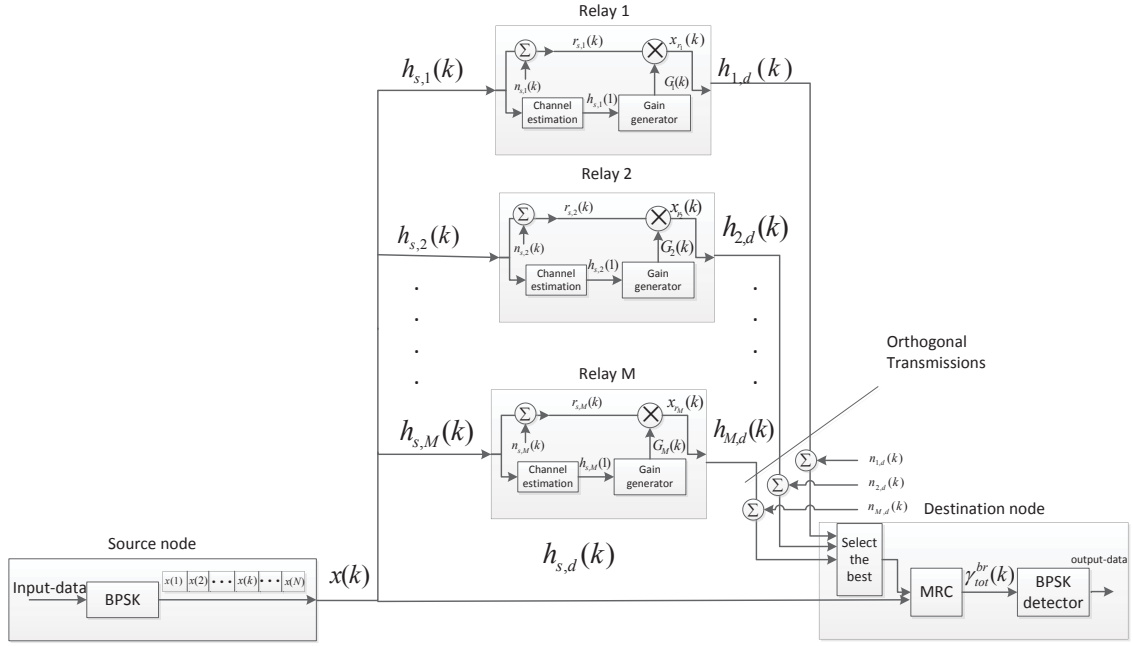


Figure 4.1. System model: M -relay best-relay-selection amplify-and-forward wireless cooperative system with time-selective fading channels.

4.3 Total SNR Derivation and Probability Density Function

In the best-relay-selection protocol, the MRC receiver at the destination combines the received signal through the direct-path with the signal from the relay the achieves the highest effective SNR at the destination. Therefore, under this protocol along with the assumption of imperfect channel estimation at the network receivers, the total effective SNR at the output of the MRC combiner corresponding to the k th signaling period, say $\gamma_{\text{tot}}^{\text{im,br}}(k)$, can be expressed as [28]

$$\gamma_{\text{tot}}^{\text{im,br}}(k) = \gamma_{s,d}^{\text{im}}(k) + \gamma_{\text{max}}(k) \quad (4.3.1)$$

where

$$\gamma_{\text{max}}(k) = \max_i (\gamma_{s,i,d}^{\text{im}}(k)). \quad (4.3.2)$$

The SNRs $\gamma_{s,d}^{\text{im}}(k)$ and $\gamma_{s,i,d}^{\text{im}}(k)$ are given in (3.3.4) and (3.3.12), respectively. If we substitute for $\gamma_{s,i,d}^{\text{im}}(k)$ in (4.3.2) by its approximation $\gamma_{\text{up},i}^{\text{im}}(k)$ as described in (3.3.16), we can approximate $\gamma_{\text{tot}}^{\text{im,br}}(k)$ in (4.3.1) as

$$\gamma_{\text{tot}}^{\text{im,br}}(k) \approx \gamma_{\text{tot,up}}^{\text{im,br}}(k) = \gamma_{s,d}^{\text{im}}(k) + \gamma_{\text{max,up}}(k) \quad (4.3.3)$$

where

$$\gamma_{\text{max,up}}(k) = \max_i (\gamma_{\text{up},i}^{\text{im}}(k)). \quad (4.3.4)$$

In this chapter we continue our analysis based on the approximated total SNR $\gamma_{\text{tot,up}}^{\text{im,br}}(k)$ instead of $\gamma_{\text{tot}}^{\text{im,br}}(k)$, which we need now to find closed-form expression for its pdf, say $f_{\gamma_{\text{tot,up}}^{\text{im,br}}(k)}(\gamma)$. To accomplish this purpose, in the following we use the MGF method. First, the MGF of $\gamma_{\text{tot,up}}^{\text{im,br}}(k)$ can be given as

$$\mathbf{M}_{\gamma_{\text{tot,up}}^{\text{im,br}}(k)}(s) = \mathbf{M}_{\gamma_{s,d}^{\text{im}}(k)}(s) \mathbf{M}_{\gamma_{\text{max,up}}(k)}(s) \quad (4.3.5)$$

where

$$\mathbf{M}_{\gamma_{s,d}^{\text{im}}(k)}(s) = \frac{1}{1 + \bar{\gamma}_{s,d}^{\text{im}}(k)s} \quad (4.3.6)$$

and $\mathbf{M}_{\gamma_{\text{max,up}}(k)}(s)$ is the MGF of $\gamma_{\text{max,up}}(k)$, which can be obtained as

$$\mathbf{M}_{\gamma_{\text{max,up}}(k)}(s) = \int_0^\infty e^{-s\gamma} f_{\gamma_{\text{max,up}}(k)}(\gamma) d\gamma \quad (4.3.7)$$

where $f_{\gamma_{\text{max,up}}(k)}(\gamma)$ is the pdf of $\gamma_{\text{max,up}}(k)$, which can be obtained as

$$\begin{aligned} f_{\gamma_{\text{max,up}}(k)}(\gamma) &= \frac{d}{d\gamma} (Pr\{\gamma_{\text{max,up}}(k) < \gamma\}) = \frac{d}{d\gamma} \left(\prod_{i=1}^M Pr\{\gamma_{\text{up},i}^{\text{im}}(k) < \gamma\} \right) \\ &= \frac{d}{d\gamma} \left(\prod_{i=1}^M \int_0^\gamma f_{\gamma_{\text{up},i}^{\text{im}}(k)}(\gamma) d\gamma \right). \end{aligned} \quad (4.3.8)$$

By substituting (3.3.17) into (4.3.8) and evaluating the integration, we can obtain the pdf

$f_{\gamma_{\max, \text{up}}(k)}(\gamma)$ as

$$f_{\gamma_{\max, \text{up}}(k)}(\gamma) = \frac{d}{d\gamma} \left(\prod_{i=1}^M (1 - e^{-\frac{\gamma}{\bar{\gamma}_{\text{up}, i}^{\text{im}}(k)}}) \right) \quad (4.3.9)$$

and after doing some manipulations it can be written as

$$\begin{aligned} f_{\gamma_{\max, \text{up}}(k)}(\gamma) &= \sum_{i=1}^M (-1)^{i+1} \sum_{\ell_1=1}^{M-i+1} \sum_{\ell_2=\ell_1+1}^{M-i+2} \cdots \sum_{\ell_i=\ell_{i-1}+1}^M \\ &\times \left(\mathcal{K} \prod_{j=1}^i \exp \left(-\gamma \frac{\bar{\gamma}_{s, \ell_j}^{\text{im}}(k) + \bar{\gamma}_{\ell_j, d}^{\text{im}}(k)}{\gamma_{s, \ell_j}^{\text{im}}(k) \bar{\gamma}_{\ell_j, d}^{\text{im}}(k)} \right) \right) \end{aligned} \quad (4.3.10)$$

where

$$\mathcal{K} = \sum_{j=1}^i \frac{\bar{\gamma}_{s, \ell_j}^{\text{im}}(k) + \bar{\gamma}_{\ell_j, d}^{\text{im}}(k)}{\gamma_{s, \ell_j}^{\text{im}}(k) \bar{\gamma}_{\ell_j, d}^{\text{im}}(k)}. \quad (4.3.11)$$

By substituting (4.3.10) into (4.3.7) and evaluating the integration, we can obtain the MGF

$\mathbf{M}_{\gamma_{\max, \text{up}}(k)}(s)$ as

$$\mathbf{M}_{\gamma_{\max, \text{up}}(k)}(s) = \sum_{i=1}^M (-1)^{i+1} \sum_{\ell_1=1}^{M-i+1} \sum_{\ell_2=\ell_1+1}^{M-i+2} \cdots \sum_{\ell_i=\ell_{i-1}+1}^M \left(\frac{\mathcal{K}}{\mathcal{K} + s} \right). \quad (4.3.12)$$

By substituting now (4.3.6) and (4.3.12) into (4.3.5), we obtain $\mathbf{M}_{\gamma_{\text{tot}, \text{up}}^{\text{im}, \text{br}}(k)}(s)$ as

$$\mathbf{M}_{\gamma_{\text{tot}, \text{up}}^{\text{im}, \text{br}}(k)}(s) = \sum_{i=1}^M (-1)^{i+1} \sum_{\ell_1=1}^{M-i+1} \sum_{\ell_2=\ell_1+1}^{M-i+2} \cdots \sum_{\ell_i=\ell_{i-1}+1}^M \left(\frac{\frac{1}{\bar{\gamma}_{s, d}^{\text{im}}(k)}}{\frac{1}{\bar{\gamma}_{s, d}^{\text{im}}(k)} + s} \right) \left(\frac{\mathcal{K}}{\mathcal{K} + s} \right). \quad (4.3.13)$$

Now, by finding the inverse Laplace Transform of (4.3.13), using the partial fractions method, we obtain $f_{\gamma_{\text{tot,up}}(k)}^{\text{im,br}}(\gamma)$ in its ultimate form as

$$f_{\gamma_{\text{tot,up}}(k)}^{\text{im,br}}(\gamma) = \sum_{i=1}^M (-1)^{i+1} \sum_{\ell_1=1}^{M-i+1} \sum_{\ell_2=\ell_1+1}^{M-i+2} \cdots \sum_{\ell_i=\ell_{i-1}+1}^M \left(\frac{\mathcal{K}}{1 - \mathcal{K}\bar{\gamma}_{s,d}^{\text{im}}(k)} (e^{-\mathcal{K}\gamma} - e^{-\frac{\gamma}{\bar{\gamma}_{s,d}^{\text{im}}(k)}}) \right). \quad (4.3.14)$$

As a special case of quasi-static fading ($\rho_{a,b} = 1 \ \forall(a,b)$) and perfect channel estimation ($\sigma_{e_{a,b}}^2 = 0 \ \forall(a,b)$), the best-relay-selection case pdf in (4.3.14) reduces to [28, Eq. (16)].

In the next section, we use the pdf in (4.3.14) to analyze the performance of our AF wireless cooperative system with best-relay-selection protocol and imperfect channel estimation. This analysis is in terms of the per-block-average lower-bound BPSK BER, lower-bound outage probability and upper-bound Shannon capacity.

4.4 System Performance Evaluation

4.4.1 Error probability

By assuming equiprobable N symbols in the transmitted block with BPSK modulation and using the pdf given by (4.3.14), we can obtain the lower-bound per-block-average BER at the output of the MRC combiner for the best-relay-selection protocol with imperfect estimation as

$$\begin{aligned} \bar{P}_{e,\text{Low}}^{\text{im,br}} &= \frac{1}{N} \sum_{k=1}^N \left(\int_0^\infty Q(\sqrt{2\gamma(k)}) f_{\gamma_{\text{tot,up}}(k)}^{\text{im,br}}(\gamma) d\gamma \right) \\ &= \frac{1}{N} \sum_{k=1}^N \left(\sum_{i=1}^M (-1)^{i+1} \sum_{\ell_1=1}^{M-i+1} \sum_{\ell_2=\ell_1+1}^{M-i+2} \cdots \sum_{\ell_i=\ell_{i-1}+1}^M \left(\frac{\mathcal{K}}{1 - \mathcal{K}\bar{\gamma}_{s,d}^{\text{im}}(k)} \right. \right. \\ &\quad \left. \left. \times \left(\int_0^\infty Q(\sqrt{2\gamma(k)}) e^{-\mathcal{K}\gamma} d\gamma - \int_0^\infty Q(\sqrt{2\gamma(k)}) e^{-\frac{\gamma}{\bar{\gamma}_{s,d}^{\text{im}}(k)}} d\gamma \right) \right) \right). \end{aligned} \quad (4.4.1)$$

By solving the last two integrals in (4.4.1) by parts technique and after doing some manipulations and simplification, we can obtain $\bar{P}_{e,\text{Low}}^{\text{im,br}}$ in its ultimate form in terms of $\frac{E_s}{N_o}$ as

$$\begin{aligned} \bar{P}_{e,\text{Low}}^{\text{im,br}} = & \frac{1}{2N} \sum_{k=1}^N \sum_{i=1}^M (-1)^{i+1} \sum_{\ell_1=1}^{M-i+1} \sum_{\ell_2=\ell_1+1}^{M-i+2} \cdots \sum_{\ell_i=\ell_{i-1}+1}^M \left(1 - \sqrt{\frac{1}{1 + \sum_{j=1}^i \frac{\ddot{\chi}_{\ell_j} \frac{E_s}{N_o} + \ddot{\lambda}_{\ell_j}}{\ddot{\omega}_{\ell_j} \frac{E_s}{N_o}}}} \right. \\ & \times \frac{\ddot{\kappa}_{s,d} \frac{E_s}{N_o} + 1}{\ddot{\kappa}_{s,d} \frac{E_s}{N_o} + 1 - \ddot{\alpha}_{s,d} \frac{E_s}{N_o} \sum_{j=1}^i \frac{\ddot{\chi}_{\ell_j} \frac{E_s}{N_o} + \ddot{\lambda}_{\ell_j}}{\ddot{\omega}_{\ell_j} \frac{E_s}{N_o}}} + \frac{\ddot{\alpha}_{s,d} \frac{E_s}{N_o} \sum_{j=1}^i \frac{\ddot{\chi}_{\ell_j} \frac{E_s}{N_o} + \ddot{\lambda}_{\ell_j}}{\ddot{\omega}_{\ell_j} \frac{E_s}{N_o}}}{\ddot{\kappa}_{s,d} \frac{E_s}{N_o} + 1 - \ddot{\alpha}_{s,d} \frac{E_s}{N_o} \sum_{j=1}^i \frac{\ddot{\chi}_{\ell_j} \frac{E_s}{N_o} + \ddot{\lambda}_{\ell_j}}{\ddot{\omega}_{\ell_j} \frac{E_s}{N_o}}} \\ & \left. \times \sqrt{\frac{\ddot{\alpha}_{s,d} \frac{E_s}{N_o}}{(\ddot{\alpha}_{s,d} + \ddot{\kappa}_{s,d}) \frac{E_s}{N_o} + 1}} \right) \end{aligned} \quad (4.4.2)$$

where

$$\begin{aligned} \ddot{\chi}_{\ell_j} &= \ddot{\alpha}_{s,\ell_j} \ddot{\kappa}_{\ell_j,d} + \ddot{\alpha}_{\ell_j,d} \ddot{\kappa}_{s,\ell_j} \\ \ddot{\lambda}_{\ell_j} &= \ddot{\alpha}_{s,\ell_j} + \ddot{\alpha}_{\ell_j,d} \\ \ddot{\omega}_{\ell_j} &= \ddot{\alpha}_{s,\ell_j} \ddot{\alpha}_{\ell_j,d} \\ \ddot{\alpha}_{a,b} &= \rho_{a,b}^{2(k-1)} \mathbb{E}[|\hat{h}_{a,b}(1)|^2] \\ \ddot{\kappa}_{a,b} &= (1 - \rho_{a,b}^{2(k-1)}) \sigma_{a,b}^2 + \rho_{a,b}^{2(k-1)} \sigma_{e_{a,b}}^2, \quad \forall \ell = 1, 2, \dots, M. \end{aligned} \quad (4.4.3)$$

As a result of the nodes' mobility (or the time-selective fading within the network) and the imperfect channel estimation, the BER performance of the best-relay-selection protocol also degraded at high $\frac{E_s}{N_o}$ values and suffers from irreducible floor, which is given by

$$\begin{aligned} \lim_{\frac{E_s}{N_o} \rightarrow \infty} \bar{P}_{e,\text{Low}}^{\text{im,br}} = & \frac{1}{2N} \sum_{k=1}^N \sum_{i=1}^M (-1)^{i+1} \sum_{\ell_1=1}^{M-i+1} \sum_{\ell_2=\ell_1+1}^{M-i+2} \cdots \sum_{\ell_i=\ell_{i-1}+1}^M \left(1 - \frac{\ddot{\kappa}_{s,d}}{\ddot{\kappa}_{s,d} - \ddot{\alpha}_{s,d} \sum_{j=1}^i \frac{\ddot{\chi}_{\ell_j}}{\ddot{\omega}_{\ell_j}}} \right. \\ & \times \sqrt{\frac{1}{1 + \sum_{j=1}^i \frac{\ddot{\chi}_{\ell_j}}{\ddot{\omega}_{\ell_j}}}} + \frac{\ddot{\alpha}_{s,d} \sum_{j=1}^i \frac{\ddot{\chi}_{\ell_j}}{\ddot{\omega}_{\ell_j}}}{\ddot{\kappa}_{s,d} - \ddot{\alpha}_{s,d} \sum_{j=1}^i \frac{\ddot{\chi}_{\ell_j}}{\ddot{\omega}_{\ell_j}}} \sqrt{\frac{\ddot{\alpha}_{s,d}}{\ddot{\alpha}_{s,d} + \ddot{\kappa}_{s,d}}} \Big). \end{aligned} \quad (4.4.4)$$

It is worthwhile to mention that in the literature (e.g. [28]), it has been shown that the best-relay-selection protocol provides better BER performance over the regular protocol over the entire range of $\frac{E_s}{N_o}$. However, this is no longer valid under the nodes' mobility and the imperfect-CSI impacts. As will be shown later in the numerical results section, the error floor in (4.4.4) has larger values than that in (3.4.2), which means that the best-relay-selection protocol provides worse BER performance than that of the regular protocol at the high values of $\frac{E_s}{N_o}$ under our system model assumptions.

4.4.2 Outage probability

For our M -relay cooperative network model with best-relay-selection protocol, the mutual information between the source and the destination, corresponding to the k th transmitted symbol, can be expressed as [28, Eq. (17)]

$$I^{\text{br}}(k) = \frac{1}{2} \log_2(1 + \gamma_{\text{tot}}^{\text{im,br}}(k)). \quad (4.4.5)$$

Unlike the factor $\frac{1}{M+1}$ in the mutual information expression given by (2.4.5), the reason for the $\frac{1}{2}$ factor in (4.4.5) is that the transmission process in the best-relay-selection cooperative protocol takes place in 2 orthogonal channels or time-slots; one for the direct-path transmission and the other for the indirect-path transmission through the best relay. We can now write the outage probability for the best-relay-selection protocol corresponding to the k th transmitted symbol, $P_{\text{out}}^{\text{br}}(k)$, as

$$P_{\text{out}}^{\text{im,br}}(k) = Pr\{I^{\text{br}}(k) \leq R\} = Pr\{\gamma_{\text{tot}}^{\text{im,br}}(k) < \gamma_{th}^{\text{br}}\} = \int_0^{\gamma_{th}^{\text{br}}} f_{\gamma_{\text{tot}}^{\text{im,br}}(k)}(\gamma) d\gamma \quad (4.4.6)$$

where $\gamma_{th}^{\text{br}} = 2^{2R} - 1$ and R is the required rate. By assuming equiprobable N symbols in the transmitted block and using the pdf in (4.3.14), we can obtain the lower-bound per-block-

average outage probability for the best-relay-selection protocol as

$$\begin{aligned}
P_{\text{out,Low}}^{\text{im,br}} &= \frac{1}{N} \sum_{k=1}^N \left(\int_0^{\gamma_{th}^{\text{br}}} f_{\gamma_{\text{tot,up}}^{\text{im,br}}(k)}(\gamma) d\gamma \right) \\
&= \frac{1}{N} \sum_{k=1}^N \left(\sum_{i=1}^M (-1)^{i+1} \sum_{\ell_1=1}^{M-i+1} \sum_{\ell_2=\ell_1+1}^{M-i+2} \cdots \sum_{\ell_i=\ell_{i-1}+1}^M \left(\frac{\mathcal{K}}{1 - \mathcal{K} \bar{\gamma}_{s,d}^{\text{im}}(k)} \right. \right. \\
&\quad \times \left. \left(\int_0^{\gamma_{th}^{\text{br}}} e^{-\mathcal{K}\gamma} d\gamma - \int_0^{\gamma_{th}^{\text{br}}} e^{-\frac{\gamma}{\bar{\gamma}_{s,d}^{\text{im}}(k)}} d\gamma \right) \right) \Bigg) \\
&= \frac{1}{N} \sum_{k=1}^N \sum_{i=1}^M (-1)^{i+1} \sum_{\ell_1=1}^{M-i+1} \sum_{\ell_2=\ell_1+1}^{M-i+2} \cdots \sum_{\ell_i=\ell_{i-1}+1}^M \left(\frac{\mathcal{K}}{1 - \mathcal{K} \bar{\gamma}_{s,d}^{\text{im}}(k)} \right. \\
&\quad \times \left. \left(\frac{e^{-\mathcal{K}\gamma_{th}^{\text{br}}}}{\mathcal{K}} - \frac{e^{-\frac{\gamma_{th}^{\text{br}}}{\bar{\gamma}_{s,d}^{\text{im}}(k)}}}{\frac{1}{\bar{\gamma}_{s,d}^{\text{im}}(k)}} \right) \right). \tag{4.4.7}
\end{aligned}$$

After doing some manipulations and simplification, we can write (4.4.7) explicitly as a function of $\frac{E_s}{N_o}$ as

$$\begin{aligned}
P_{\text{out,Low}}^{\text{im,br}} &= \frac{1}{N} \sum_{k=1}^N \sum_{i=1}^M (-1)^{i+1} \sum_{\ell_1=1}^{M-i+1} \sum_{\ell_2=\ell_1+1}^{M-i+2} \cdots \sum_{\ell_i=\ell_{i-1}+1}^M \\
&\quad \times \left(1 - \frac{(\ddot{\kappa}_{s,d} \frac{E_s}{N_o} + 1) \exp\left(-\gamma_{th} \sum_{j=1}^i \frac{\ddot{\chi}_{\ell_j} \frac{E_s}{N_o} + \ddot{\lambda}_{\ell_j}}{\ddot{\omega}_{\ell_j} \frac{E_s}{N_o}}\right)}{\ddot{\kappa}_{s,d} \frac{E_s}{N_o} + 1 - \ddot{\alpha}_{s,d} \frac{E_s}{N_o} \sum_{j=1}^i \frac{\ddot{\chi}_{\ell_j} \frac{E_s}{N_o} + \ddot{\lambda}_{\ell_j}}{\ddot{\omega}_{\ell_j} \frac{E_s}{N_o}}} \right. \\
&\quad \left. + \frac{\ddot{\alpha}_{s,d} \frac{E_s}{N_o} \sum_{j=1}^i \frac{\ddot{\chi}_{\ell_j} \frac{E_s}{N_o} + \ddot{\lambda}_{\ell_j}}{\ddot{\omega}_{\ell_j} \frac{E_s}{N_o}} \exp\left(-\gamma_{th} \frac{\ddot{\kappa}_{s,d} \frac{E_s}{N_o} + 1}{\ddot{\alpha}_{s,d} \frac{E_s}{N_o}}\right)}{\ddot{\kappa}_{s,d} \frac{E_s}{N_o} + 1 - \ddot{\alpha}_{s,d} \frac{E_s}{N_o} \sum_{j=1}^i \frac{\ddot{\chi}_{\ell_j} \frac{E_s}{N_o} + \ddot{\lambda}_{\ell_j}}{\ddot{\omega}_{\ell_j} \frac{E_s}{N_o}}} \right). \tag{4.4.8}
\end{aligned}$$

The limit of $P_{\text{out,Low}}^{\text{im,br}}$ as $\frac{E_s}{N_o} \rightarrow \infty$ also exists and given by

$$\begin{aligned} \lim_{\frac{E_s}{N_o} \rightarrow \infty} P_{\text{out,Low}}^{\text{im,br}} &= \frac{1}{N} \sum_{k=1}^N \sum_{i=1}^M (-1)^{i+1} \sum_{\ell_1=1}^{M-i+1} \sum_{\ell_2=\ell_1+1}^{M-i+2} \cdots \sum_{\ell_i=\ell_{i-1}+1}^M \\ &\times \left(1 - \ddot{\kappa}_{s,d} \frac{\exp\left(-\gamma_{th} \sum_{j=1}^i \frac{\ddot{\chi}_{\ell_j}}{\ddot{\omega}_{\ell_j}}\right)}{\ddot{\kappa}_{s,d} - \ddot{\alpha}_{s,d} \sum_{j=1}^i \frac{\ddot{\chi}_{\ell_j}}{\ddot{\omega}_{\ell_j}}} + \frac{\ddot{\alpha}_{s,d} \sum_{j=1}^i \frac{\ddot{\chi}_{\ell_j}}{\ddot{\omega}_{\ell_j}} \exp\left(-\gamma_{th} \frac{\ddot{\kappa}_{s,d}}{\ddot{\alpha}_{s,d}}\right)}{\ddot{\kappa}_{s,d} - \ddot{\alpha}_{s,d} \sum_{j=1}^i \frac{\ddot{\chi}_{\ell_j}}{\ddot{\omega}_{\ell_j}}} \right) \end{aligned} \quad (4.4.9)$$

which means that the outage performance of the best-relay-selection cooperative system also degrades at high $\frac{E_s}{N_o}$ values when the fading links are time-selective and the estimation processes are imperfect.

4.4.3 Shannon Capacity

The system shannon capacity of cooperative networks with best-relay-selection protocol can be described as [29]

$$\overline{C}^{\text{br}} = \frac{B}{2} \int_0^\infty \log_2(1 + \gamma) f_{\gamma_{\text{tot}}}(\gamma) d\gamma \quad (4.4.10)$$

where B is the channel bandwidth in Hz and γ is the total effective SNR at the destination. Similarly as (4.4.5), the factor $\frac{1}{2}$ in (4.4.10) is due to the two channels (or time-slots) required for data transmission in the best-relay-selection protocol. For our time-selective fading network model, the system Shannon capacity in case of imperfect-estimation and best-relay-selection, corresponding to the k th transmitted symbol, can be given as

$$\overline{C}(k) = \frac{B}{2} \int_0^\infty \log_2(1 + \gamma_{\text{tot}}^{\text{im,br}}(k)) f_{\gamma_{\text{tot}}^{\text{im,br}}(k)}(\gamma) d\gamma. \quad (4.4.11)$$

If we use now the pdf given by (4.3.14) in (4.4.11) and assume equiprobable symbols in the transmitted block, we can obtain upper-bound per-block-average system capacity as

$$\begin{aligned}
\bar{C}_{\text{up}}^{\text{im,br}} &= \frac{1}{N} \sum_{k=1}^N \left(\frac{B}{2} \int_0^\infty \log_2(1+\gamma) f_{\gamma_{\text{tot,up}}(k)}^{\text{im,br}}(\gamma) d\gamma \right) \\
&= \frac{B}{2N} \sum_{k=1}^N \sum_{i=1}^M (-1)^{i+1} \sum_{\ell_1=1}^{M-i+1} \sum_{\ell_2=\ell_1+1}^{M-i+2} \cdots \sum_{\ell_i=\ell_{i-1}+1}^M \left(\frac{\mathcal{K}}{1 - \mathcal{K} \bar{\gamma}_{s,d}^{\text{im}}(k)} \right. \\
&\quad \left. \left(\int_0^\infty \log_2(1+\gamma) e^{-\mathcal{K}\gamma} d\gamma - \int_0^\infty \log_2(1+\gamma) e^{-\frac{\gamma}{\bar{\gamma}_{s,d}^{\text{im}}(k)}} d\gamma \right) \right). \quad (4.4.12)
\end{aligned}$$

By evaluating the last integrals in (4.4.12) in closed-form as in [24, Eq. (38)] and doing some manipulations and simplification, we can obtain $\bar{C}_{\text{up}}^{\text{im,br}}$ in its ultimate closed-form expression as

$$\begin{aligned}
\bar{C}_{\text{up}}^{\text{im,br}} &= \frac{B \log_2(e)}{2N} \sum_{k=1}^N \sum_{i=1}^M (-1)^{i+1} \sum_{\ell_1=1}^{M-i+1} \sum_{\ell_2=\ell_1+1}^{M-i+2} \cdots \sum_{\ell_i=\ell_{i-1}+1}^M \left(\exp \left(\sum_{j=1}^i \frac{\ddot{\chi}_{\ell_j} \frac{E_s}{N_o} + \ddot{\lambda}_{\ell_j}}{\ddot{\omega}_{\ell_j} \frac{E_s}{N_o}} \right) \right. \\
&\quad \times \frac{\ddot{\kappa}_{s,d} \frac{E_s}{N_o} + 1}{\ddot{\kappa}_{s,d} \frac{E_s}{N_o} + 1 - \ddot{\alpha}_{s,d} \frac{E_s}{N_o} \sum_{j=1}^i \frac{\ddot{\chi}_{\ell_j} \frac{E_s}{N_o} + \ddot{\lambda}_{\ell_j}}{\ddot{\omega}_{\ell_j} \frac{E_s}{N_o}}} E_1 \left(\sum_{j=1}^i \frac{\ddot{\chi}_{\ell_j} \frac{E_s}{N_o} + \ddot{\lambda}_{\ell_j}}{\ddot{\omega}_{\ell_j} \frac{E_s}{N_o}} \right) \exp \left(\frac{\ddot{\kappa}_{s,d} \frac{E_s}{N_o} + 1}{\ddot{\alpha}_{s,d} \frac{E_s}{N_o}} \right) \\
&\quad \times E_1 \left(\frac{\ddot{\kappa}_{s,d} \frac{E_s}{N_o} + 1}{\ddot{\alpha}_{s,d} \frac{E_s}{N_o}} \right) + \frac{\ddot{\alpha}_{s,d} \frac{E_s}{N_o} \sum_{j=1}^i \frac{\ddot{\chi}_{\ell_j} \frac{E_s}{N_o} + \ddot{\lambda}_{\ell_j}}{\ddot{\omega}_{\ell_j} \frac{E_s}{N_o}}}{\ddot{\kappa}_{s,d} \frac{E_s}{N_o} + 1 - \ddot{\alpha}_{s,d} \frac{E_s}{N_o} \sum_{j=1}^i \frac{\ddot{\chi}_{\ell_j} \frac{E_s}{N_o} + \ddot{\lambda}_{\ell_j}}{\ddot{\omega}_{\ell_j} \frac{E_s}{N_o}}} \Bigg). \quad (4.4.13)
\end{aligned}$$

The limit of $\bar{C}_{\text{up}}^{\text{im,br}}$ as $\frac{s}{N_o} \rightarrow \infty$ also exists and given by

$$\begin{aligned}
\lim_{\frac{E_s}{N_o} \rightarrow \infty} \bar{C}_{\text{up}}^{\text{im,br}} &= \frac{B \log_2(e)}{2N} \sum_{k=1}^N \sum_{i=1}^M (-1)^{i+1} \sum_{\ell_1=1}^{M-i+1} \sum_{\ell_2=\ell_1+1}^{M-i+2} \cdots \sum_{\ell_i=\ell_{i-1}+1}^M \\
&\quad \times \left(\frac{\ddot{\kappa}_{s,d} \exp \left(\sum_{j=1}^i \frac{\ddot{\chi}_{\ell_j}}{\ddot{\omega}_{\ell_j}} \right) E_1 \left(\sum_{j=1}^i \frac{\ddot{\chi}_{\ell_j}}{\ddot{\omega}_{\ell_j}} \right)}{\ddot{\kappa}_{s,d} - \ddot{\alpha}_{s,d} \sum_{j=1}^i \frac{\ddot{\chi}_{\ell_j}}{\ddot{\omega}_{\ell_j}}} + \frac{\alpha_{s,d} \sum_{j=1}^i \frac{\chi_{\ell_j}}{\omega_{\ell_j}} \exp \left(\frac{\kappa_{s,d}}{\alpha_{s,d}} \right) E_1 \left(\frac{\ddot{\kappa}_{s,d}}{\ddot{\alpha}_{s,d}} \right)}{\ddot{\kappa}_{s,d} - \ddot{\alpha}_{s,d} \sum_{j=1}^i \frac{\ddot{\chi}_{\ell_j}}{\ddot{\omega}_{\ell_j}}} \right). \quad (4.4.14)
\end{aligned}$$

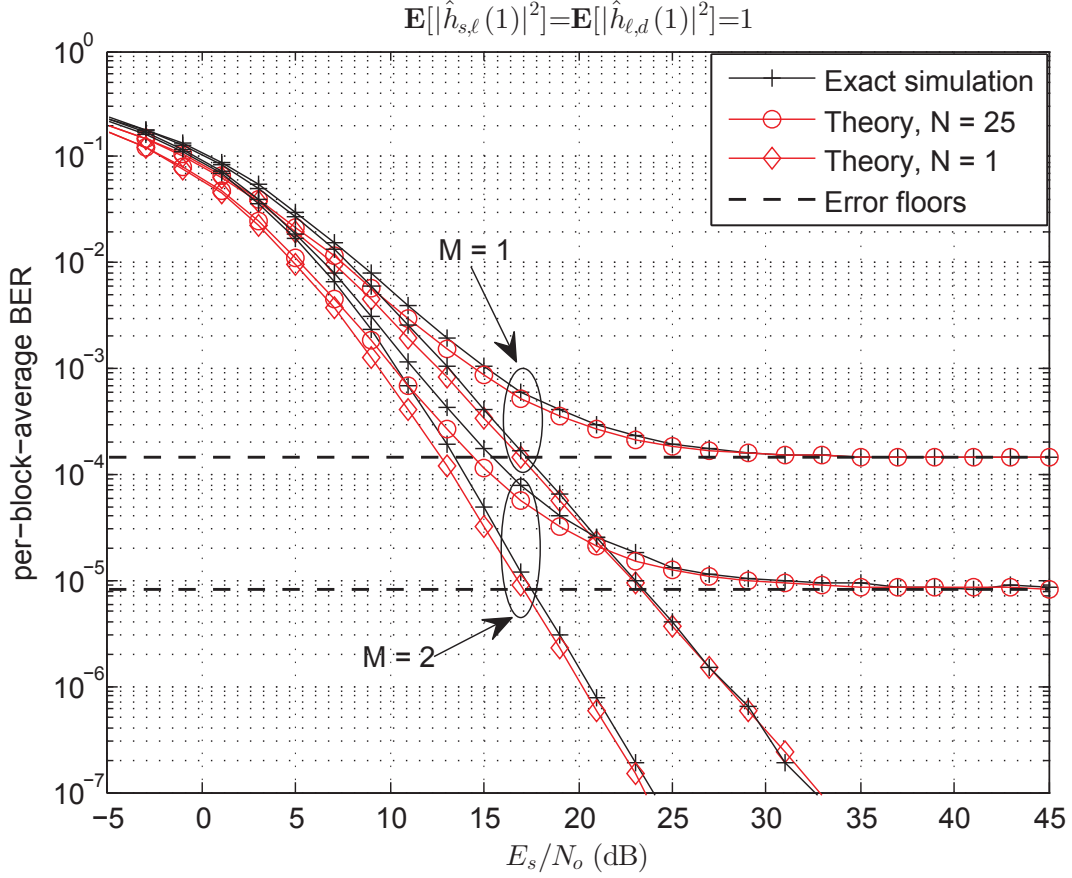


Figure 4.2. Best-relay selection BPSK BER versus E_s/N_o with $N = 25$ and 1 and $M = 1$ and 2 . In dB: $\mathbb{E}[|h_{s,d}(1)|^2] = \mathbb{E}[|h_{s,\ell}(1)|^2] = \mathbb{E}[|h_{\ell,d}(1)|^2] = 1$. The Source is mobile and the other nodes are static corresponding to correlation parameters of $\rho_{s,d} = \rho_{s,\ell} = 0.999$ and $\rho_{i,d} = 1$. Channel estimation is perfect ($\sigma_{e_{a,b}}^2 = 0 \forall(a, b)$).

which means that the capacity of a cooperative system with best-relay-selection protocol and error channel estimation degraded and bounded by a ceiling.

4.5 Numerical Results and Simulation

Fig. 4.2 is a plot for the best-relay-selection cooperative system theoretical lower-bound BPSK BER performance along with the exact simulation and the floors. The theoretical lower-bound BER plot is using (4.4.9) and the floors are using (4.4.10). It is clear from this figure that, the source mobility with low CSI estimation rate of 4% ($N = 25$) causes severe BER performance degradation with error floors whatever the number of relays

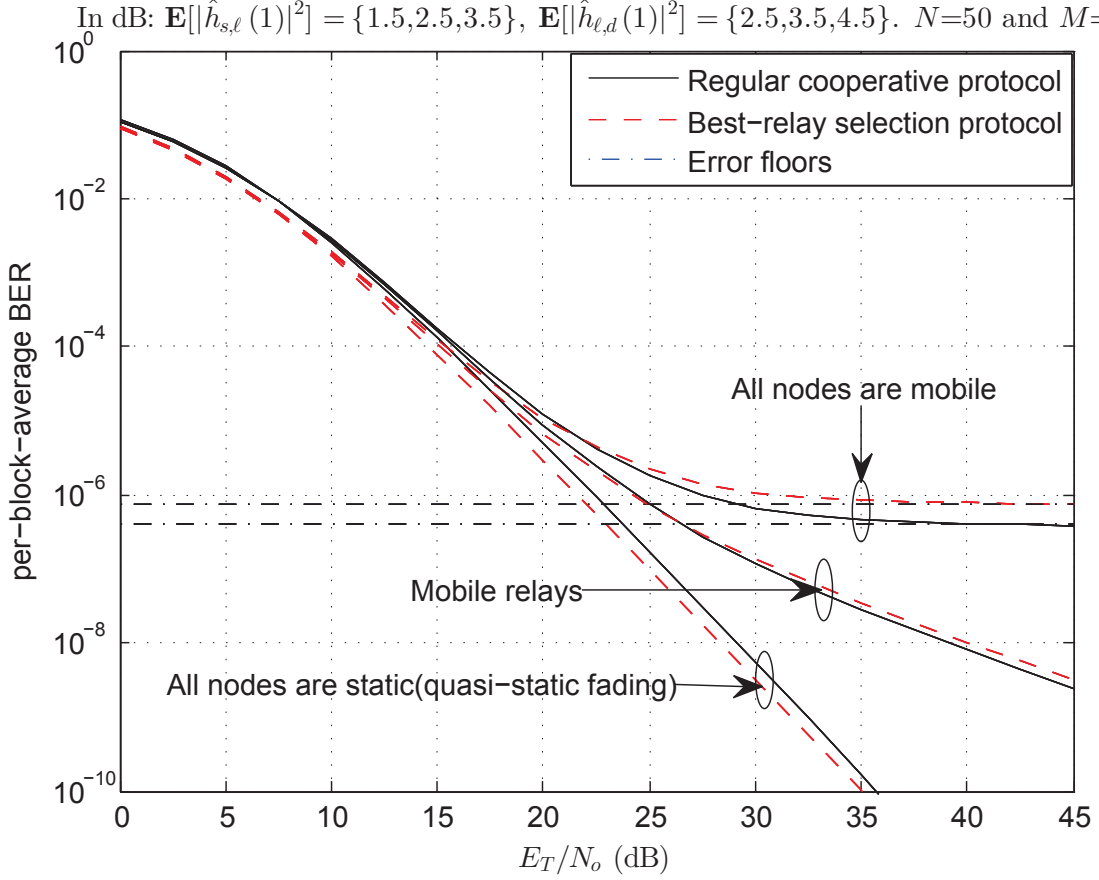


Figure 4.3. Regular and best-relay-selection cooperative protocols BPSK BER versus E_s/N_o with $N = 50$ and $M = 2$. In dB: $\mathbb{E}[|h_{s,d}(1)|^2] = 1$, $\mathbb{E}[|h_{s,\ell}(1)|^2] = \{1.5, 2.5\}$ and $\mathbb{E}[|h_{\ell,d}(1)|^2] = \{2.5, 3.5\}$. Mobile nodes corresponding to correlation parameter of 0.9998. Channel estimation is perfect ($\sigma_{e_{a,b}}^2 = 0 \forall(a, b)$).

is. Further, we can also notice that 100% CSI estimation rate ($N = 1$) completely removes the floors despite of the source mobility.

From Fig. 4.3, we can notice that in the case that all nodes are static, the best-relay-selection protocol outperforms the regular one over the entire SNR region where such result is known in literature in quasi-static fading case; see [28, Figure. 4]. However, in the case of mobile nodes, this result is no longer valid because the best-relay-selection protocol performance is degraded much than that of regular protocol at the high SNR values. Fig. 4.4 supports this result and shows that the error floor of best-relay protocol is higher than that of regular protocol for any $\rho < 1$ and $N > 1$ (i.e., time-selective fading and constraint

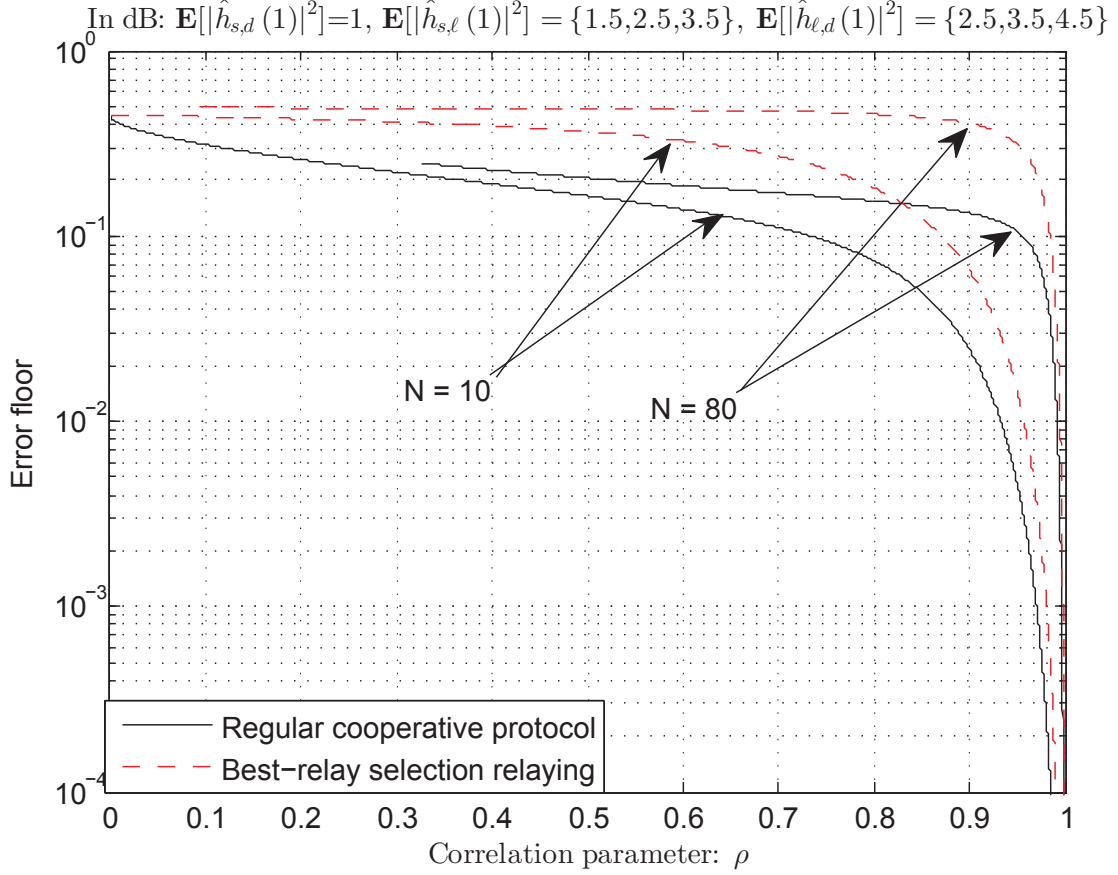


Figure 4.4. Regular and best-relay-selection cooperative protocols BPSK error floors versus the correlation parameter ρ for $M = 2$ and $N = 10$ and 80 . In dB: $\mathbb{E}[|h_{s,d}(1)|^2] = 1$, $\mathbb{E}[|h_{s,\ell}(1)|^2] = \{1.5, 2.5\}$ and $\mathbb{E}[|h_{\ell,d}(1)|^2] = \{2.5, 3.5\}$

CSI estimation rate). In addition, we can notice from Fig. 4.3 that the system performance does not experience error floor as long as the source and the destination are static (relays only are mobile), however, its performance is still worse than that for the case of all nodes are static.

Fig. 4.5 is a plot for the per-block-average capacity performance of the best-relay-selection protocol cooperative system for different fading environments. First, this figure shows the tightness of the derived upper-bound in (4.4.13) as compared with the exact simulation one. This figure also shows that as an impact of the time-selective fading ($\rho_{a,b} < 1$), the system capacity performance is severely degraded and bounded by a ceiling. As special case of slow-fading environment, this ceiling is disappeared. Similarly, Fig. 4.6 shows

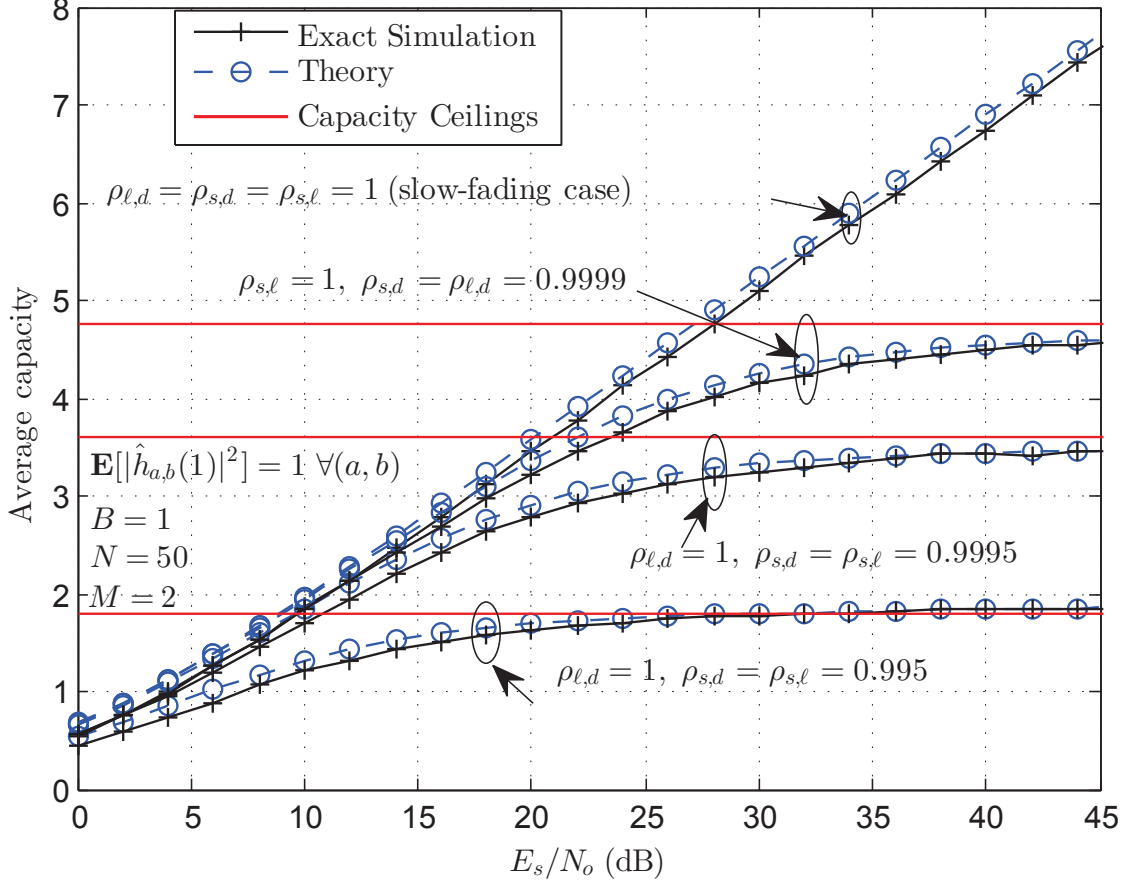


Figure 4.5. Best-relay-selection per-block-average upper bound system normalized capacity versus E_s/N_o with $B = 1$, $N = 50$ and $M = 2$. In dB: $\mathbb{E}[|h_{a,b}(1)|^2] = 1 \forall(a, b)$.

the tightness of the derived lower bound outage probability expression in (4.4.8) in particular at medium and high values of E_s/N_o . This figure also shows that due to time-selective fading, the system outage performance is also limited by floors whatever the number of relays is. These floors become higher (i.e., severer degradation) if the time-selective fading is combined with imperfect-estimation.

4.6 Conclusion

In this chapter, we have analyzed the BER, outage probability and Shannon capacity of the best-relay-selection scheme employed at amplify-and-forward time-selective fading cooperative networks with imperfect channel estimation. The obtained closed-form analytical expressions are tight enough and valid for both time-selective and quasi-static fading envi-

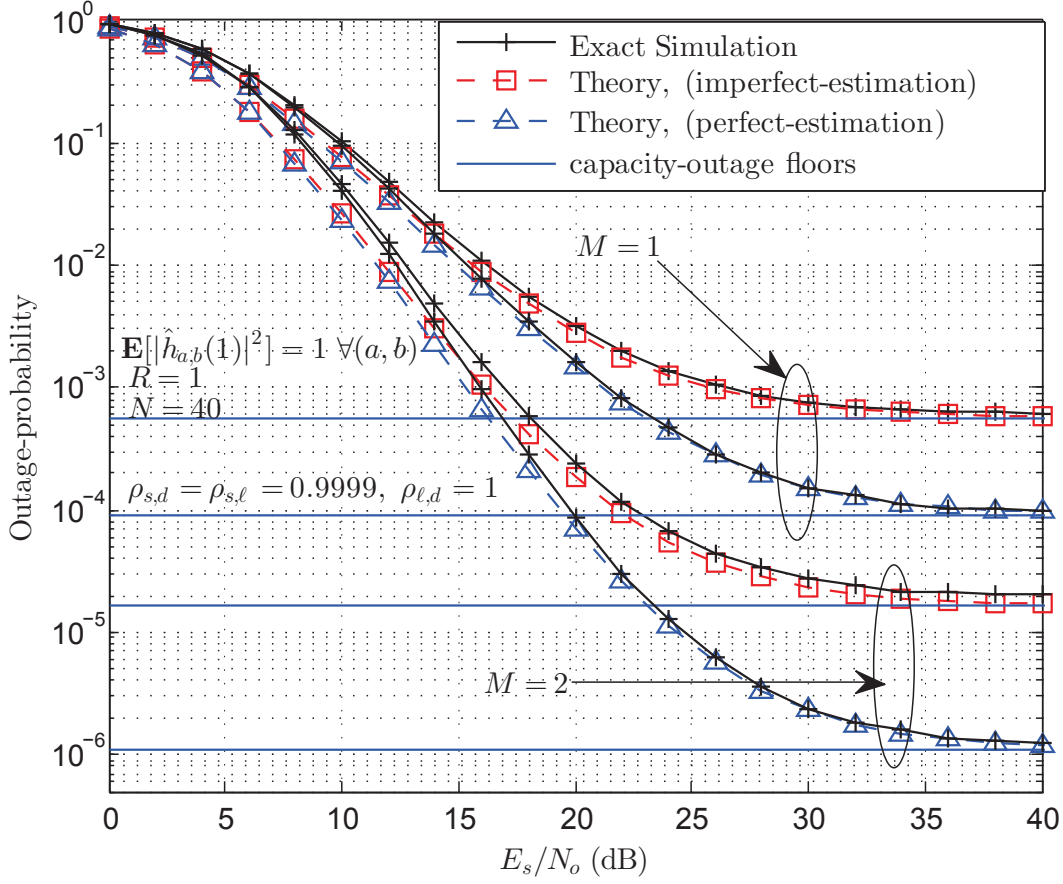


Figure 4.6. Best-relay-selection per-block-average lower-bound outage probability with and without estimation error. $N = 40$, $M = 1$ and 2 , and $R = 1$. In dB: $\mathbb{E}[|h_{a,b}(1)|^2] = 1 \forall(a, b)$.

ronments for perfect and imperfect estimations. We have also shown that the time-selective fading degrades the system performance by asymptotic limits whatever the number of relays is.

Part II:

Alamouti-Type OSTBC Based Amplify-and-Forward (AF) Cooperative Communication
Systems with Mobile Nodes and Imperfect CSI Estimation

CHAPTER 5

Introduction

5.1 Literature Review

Cooperative communication, multiple-input-multiple-output (MIMO) links, space-time codes, and a combination of them are among the successfully employed techniques in modern wireless communications systems that require higher link reliability. In [30] and [31], it has been proven that cooperative-based MIMO systems (i.e., cooperative-MIMO) are efficient for improved system performance and higher spectral efficiency. The techniques of Space-time-block coding (STBC) play a significant role in the developments of the new cellular networks generations [32], in particular, the techniques of Orthogonal-STBCs (OSTBCs). OSTBCs are capable of providing full spacial diversity gain with low decoding complexity that results from the optimal maximum-likelihood (ML) decoder [33] and [34]. The transmission of OSTBCs over cooperative networks has gained great interest in the research community. By this combination, the OSTBC transmit diversity gain, achieved at the receiving side, can be heighten by the the number of relays without destroying the optimality and simplicity of the OSTBCs decoders [26], [35], [36]. Reported results in [26], [35], [36] have been obtained based on the assumption that the fading channels among the nodes are quasi-static (i.e., their channel gains are constant over a number of consecutive signaling periods). This assumption is required in order to maintain the orthogonality of the OSTBCs and to guarantee the optimality of their corresponding ML decoders at the ultimate system destination. However, this assumption is not always realistic in some network applications. For example, in the Fourth Generation cellular technology (4G), frequent users' transitions between integrated systems occur [37] which leads to time variations in the

users' fading channels characteristics (i.e., time-selective fading is present). Furthermore, according to Jakes' model [16], high relative speed between any two communicating nodes makes their fading links characterize as time-selective. Under such fading channels conditions, the channel gain matrices of the OSTBCs are no longer orthogonal, and hence, their corresponding decoders are no longer optimal ML and experiences inter-transmit-antenna-interference (ITAI) that appears as terms in their output decision statistics. The effect of the time-selective fading on the performance of point-to-point (non-cooperative) communication systems that employ OSTBCs has been addressed in several locations in literature. In [38] the Kalman filter has been introduced in the Alamouti-type OSTBC decoders to track and estimate the time-selective fading channel gains. The proposed decoder in [38] has not shown a capability of suppressing the ITAI terms appeared as a result of time selective fading, and thus, its error performance suffers from floor at high values of the per-bit SNR. In [39] the authors have proposed an iterative-ITAI-cancellation based decoder that provides improved error performance with no floors. In [40] and [41] explicit decoders that are capable of providing separable decision statistics with removed ITAI, but at the price of a loss in the transmit diversity gain, have been proposed. The authors of [42] and [43] have proposed a modified OSTBC that can compensate for the performance degradation caused by time-selective fading.

5.2 Work Summery

However, the contribution in this part of this dissertation is three-fold. Firstly, in chapter 6, we investigate the impact of the time-selective fading in destroying the optimality of the traditional Alamouti space-time decoder employed at the destination of a multiple-relay cooperative-based system with Alamouti-OSTBC transmission at the source, and analyse its symbol-error-probability (SEP) performance. Secondly, in chapters 7 and 8, we are concerned in mitigating this impact of the time-selective fading on the overall system performance by proposing and designing alternative and efficient space-time decoders that can

be applied instead of Alamuti's decoder and provide remarkable performance improvement. Finally, in chapter 9, we consider the same system model as in chapter 6 and, along with the effect of the time-selective fading, we study the effect of the imperfect channel estimation on the system SEP performance.

CHAPTER 6

Alamouti-OSTBC Based M -Relay Fixed-Gain AF Cooperative Systems with Mobile Nodes and Perfect CSI Estimation: SINR Derivation and SEP Analysis

6.1 Chapter Overview

In this chapter, we study the effects of the cooperating nodes mobility on the symbol error probability (SEP) performance of a multiple-relay fixed-gain amplify-and-forward (AF) wireless cooperative network with Alamouti-type orthogonal-space-time-block-code (Alamouti-OSTBC) transmission at the source and its traditional decoder (ALD) at the destination. The multipath wireless environment is characterized in the small-scale fading as Rayleigh, frequency-flat and time-selective (due to nodes mobility), and it follows the path-loss model in the large-scale fading. We first show that the time-selective fading destroys the optimality of the ALD as a result of non-independent (statistically correlated) and non-separable decision statistics (with inter-transmit-antenna-interference (ITAI)). Then, by dealing this ITAI as an extra noise component, in addition to the effective background white noise, we derive exact expressions for the decision statistics' conditional signal-to-interference-plus-noise-ratios (SINRs). From these SINRs we obtain closed-form expression for the system's SEP performance conditioned on the channel gains in the end-to-end channel gain matrix. Based on this conditional SEP expression, we obtain its average by using computer Monte Carlo simulation, which are also verified via real link-level simulation.

From these analyzed results, we observe that the SEP performance of the system under study is severely degraded by node's mobility, in particular, at low transmission data-rates. This degradation is basically represented by irreducible SEP floors that appear at high values of the per-symbol average signal-to-noise-ratio (SNR) whatever the number of

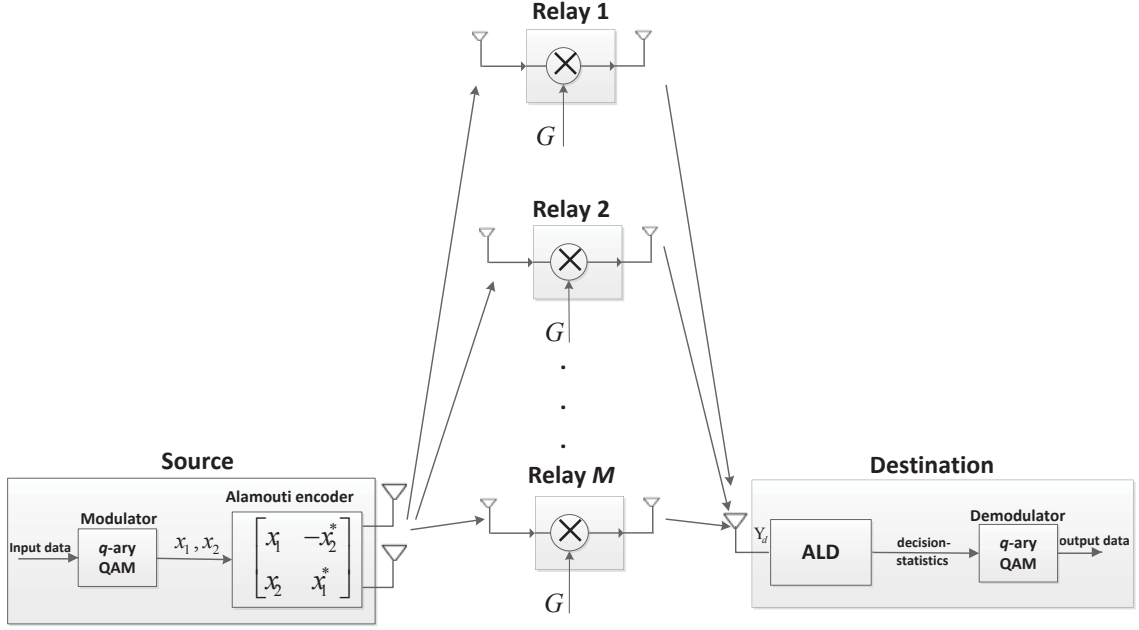


Figure 6.1. System model: Alamouti-OSTBC Transmission over M -relay fixed-gain amplify-and-forward wireless cooperative system with time-selective fading channels.

relays is. We also show that, as a special case of non moving nodes (i.e., quasi-static fading network), the decision statistics' statistical-correlation, the ITAI and the error floors reduce to zero. This means that the ALD is in its optimal version in such situation. Moreover, in such special case, our derived SINRs reduce to well known SNRs derived in the literature for such a system model with quasi-static fading.

6.2 System Model

6.2.1 Fading channel model

As shown in Fig. 6.1, we consider a wireless cooperative network with M number of relays (R_ℓ , $\ell \in \{1, 2, \dots, M\}$) which are ready to assist a source S in forwarding its data to a destination D via orthogonal transmissions where the direct path between S and D is assumed to be absent. The source is equipped with two transmit antennas (e.g., corresponding to a base station), while the relays and the destination are equipped with single antenna and work as mobile terminals. We consider an aggregate fading wireless channel

model which takes into account both large-scale and small-scale fading models. Let $h_{i,\ell}$ and $h_{\ell,d}$ denote the channel gains for the links from the source i th transmit antenna ($i \in \{1, 2\}$) to the ℓ th relay's receive antenna and from the ℓ th relay's transmit antenna to the destination's receive antenna, respectively. We assume that $h_{i,\ell}$ and $h_{\ell,d}$ have Rayleigh envelope and uniform phase, and thus, they can be distributed as zero-mean-circularly-symmetric-complex-Gaussian (ZMCSCG), i.e., $h_{i,\ell} \sim \mathcal{CN}(0, \sigma_{i,\ell}^2)$ and $h_{\ell,d} \sim \mathcal{CN}(0, \sigma_{\ell,d}^2)$. To take into account the effect of the path-loss large-scale fading, $\sigma_{i,\ell}^2$ and $\sigma_{\ell,d}^2$ are given as $1/d_{s,\ell}^n$ and $1/d_{\ell,d}^n$, respectively, where $d_{s,\ell}$ and $d_{\ell,d}$ are the S - R_ℓ and R_ℓ - D distances and n is the path-loss exponent. For the small scale-fading model, all of the network fading links are considered to be frequency-flat, so we consider narrowband network scenario. In addition, the relative speed between any two communicating nodes in the network is assumed to be significant, and according to Jakes' model [16], the time-adjacent channel gains of their associated fading links can be considered uncorrelated with correlation parameter of $\rho = \mathcal{J}_0(\frac{2\pi f_c \nu}{R_s c})$, where ν is the relative speed, $R_s = \frac{1}{T_s}$ is the transmission symbol rate, T_s is the signaling period length, f_c is the carrier frequency, c is the speed of light and $\mathcal{J}_0(\cdot)$ is the zeroth-order Bessel function of the first kind. In other words, time-selective (time-variant) fading is present. In this work, we adopt the first order autoregressive process (AR1) [9] to model the relationship between any two time-adjacent channel gains as

$$h_{a,b}(\tau_1) = \rho_{a,b} h_{a,b}(\tau_2) + \sqrt{1 - \rho_{a,b}^2} e_{a,b}(\tau_2) \quad (6.2.1)$$

where the pair $(a, b) \in \{(i, \ell), (\ell, d)\}$ denotes the link between antennas a and b , and τ_1 and τ_2 denote any two adjacent signaling period positions. The process $e_{a,b}(k)$ represents the varying-component of the associated link and assumed to be independent and identically distributed (i.i.d.) ZMCSCG with variance $\sigma_{a,b}^2$, i.e., $\sim \mathcal{CN}(0, \sigma_{a,b}^2)$. We also assume that $\rho_{1,\ell}$ and $\rho_{2,\ell}$ are equal and indicated as $\rho_{s,\ell}$.

6.2.2 Alamouti space-time-encoder and signal model

As depicted in Fig. 6.1, the binary input message at the source is first modulated¹, and then, the modulated complex symbol sequence $\{x_i\}$ is parsed into code vectors $\mathbf{x} = [x_1, x_2]^T$ and then arranged over space and time as Alamouti-OSTBC matrix [33]

$$\mathbf{X} = \begin{bmatrix} x_1 & -x_2^* \\ x_2 & x_1^* \end{bmatrix} \quad (6.2.2)$$

where the first column's symbols are transmitted simultaneously at the k th signaling period by the source two transmit antennas while that of the second column are transmitted at the $(k+1)$ th signaling period in the same manner. We assume radiation power limited system; therefore, the modulated symbol energy E_s is halved such that the overall source transmit energy from both antennas is kept E_s . Throughout data transmissions between S and D two phases are accomplished. In the first phase, S transmits the OSTBC matrix in (6.2.2) while each relay, R_ℓ , receives two signals over the k th and $(k+1)$ th signaling periods, respectively, as

$$y_{s,\ell}(k) = h_{1,\ell}(k)x_1 + h_{2,\ell}(k)x_2 + n_{s,\ell}(k) \quad (6.2.3)$$

$$y_{s,\ell}(k+1) = -h_{1,\ell}(k+1)x_2^* + h_{2,\ell}(k+1)x_1^* + n_{s,\ell}(k+1) \quad (6.2.4)$$

where $n_{s,\ell}(k)$ and $n_{s,\ell}(k+1)$ are ZMCSCG white noise samples with equal variance N_o , i.e., $\sim \mathcal{CN}(0, N_o)$. In the second transmission phase, the ℓ th relay amplifies its received signals in (6.2.3) and (6.2.4) by the following fixed amplification gain [44]

$$\mathcal{G} = \sqrt{\frac{E_r}{E_s + N_o}} \quad (6.2.5)$$

¹In this work, we consider a rectangular q -ary quadrature amplitude modulator (q -QAM) such that the constellation size q equals 2^b where b is an even integer.

where E_r is the overall relay transmit energy. After that, it sequentially transmits $\mathcal{G}y_{s,\ell}(k)$ and $\mathcal{G}y_{s,\ell}(k+1)$ towards the destination which results in received signals, over the k th and $(k+1)$ th signaling periods, respectively, as

$$y_{\ell,d}(k) = h_{\ell,d}(k)(\mathcal{G}y_{s,\ell}(k)) + n_{\ell,d}(k) \quad (6.2.6)$$

$$y_{\ell,d}(k+1) = h_{\ell,d}(k+1)(\mathcal{G}y_{s,\ell}(k+1)) + n_{\ell,d}(k+1) \quad (6.2.7)$$

where $n_{\ell,d}(k)$ and $n_{\ell,d}(k+1)$ are also $\sim \mathcal{CN}(0, N_o)$. Now, by substituting the signals given by (6.2.3) and (6.2.4) into (6.2.6) and (6.2.7), respectively, we can write the destination received signals in terms of the transmitted symbols x_1 and x_2 , over the k th and $(k+1)$ th signaling periods, respectively, as

$$y_{\ell,d}(k) = (\mathcal{G}h_{1,\ell}(k)h_{\ell,d}(k))x_1 + (\mathcal{G}h_{2,\ell}(k)h_{\ell,d}(k))x_2 + \mathcal{G}h_{\ell,d}(k)n_{s,\ell}(k) + n_{\ell,d}(k) \quad (6.2.8)$$

$$\begin{aligned} y_{\ell,d}(k+1) = & -(\mathcal{G}h_{1,\ell}(k+1)h_{\ell,d}(k+1))x_2^* + (\mathcal{G}h_{2,\ell}(k+1)h_{\ell,d}(k+1))x_1^* \\ & + \mathcal{G}h_{\ell,d}(k+1)n_{s,\ell}(k+1) + n_{\ell,d}(k+1). \end{aligned} \quad (6.2.9)$$

In Alamouti's work [33], it has been assumed that the receiver takes the complex conjugate (*) of the second received signal as a first step of his proposed decoder. By following same assumption and taking the complex conjugate of (6.2.9), we can write the destination's received signals from all of the relays as a $2M \times 1$ received signal vector \mathbf{Y}_d in the following matrix form

$$\mathbf{Y}_d = \mathbf{H} \underbrace{\begin{bmatrix} x_1 \\ x_2 \end{bmatrix}}_{\mathbf{x}} + \mathbf{N}_d \quad (6.2.10)$$

where

$$\mathbf{Y}_d = \begin{bmatrix} y_{1,d}(k) \\ y_{1,d}^*(k+1) \\ y_{2,d}(k) \\ y_{2,d}^*(k+1) \\ \vdots \\ y_{M,d}(k) \\ y_{M,d}^*(k+1) \end{bmatrix} \quad (6.2.11)$$

$$\mathbf{H} = \begin{bmatrix} \mathcal{G}h_{1,1}(k)h_{1,d}(k) & \mathcal{G}h_{2,1}(k)h_{1,d}(k) \\ \mathcal{G}h_{2,1}^*(k+1)h_{1,d}^*(k+1) & -\mathcal{G}h_{1,1}^*(k+1)h_{1,d}^*(k+1) \\ \mathcal{G}h_{1,2}(k)h_{2,d}(k) & \mathcal{G}h_{2,2}(k)h_{2,d}(k) \\ \mathcal{G}h_{2,2}^*(k+1)h_{2,d}^*(k+1) & -\mathcal{G}h_{1,2}^*(k+1)h_{2,d}^*(k+1) \\ \vdots & \vdots \\ \mathcal{G}h_{1,M}(k)h_{M,d}(k) & \mathcal{G}h_{2,M}(k)h_{M,d}(k) \\ \mathcal{G}h_{2,M}^*(k+1)h_{M,d}^*(k+1) & -\mathcal{G}h_{1,M}^*(k+1)h_{M,d}^*(k+1) \end{bmatrix} \quad (6.2.12)$$

and

$$\mathbf{N}_d = \begin{bmatrix} \mathcal{G}h_{1,d}(k)n_{s,1}(k) + n_{1,d}(k) \\ \mathcal{G}h_{1,d}^*(k+1)n_{s,1}^*(k+1) + n_{1,d}^*(k+1) \\ \mathcal{G}h_{2,d}(k)n_{s,2}(k) + n_{2,d}(k) \\ \mathcal{G}h_{2,d}^*(k+1)n_{s,2}^*(k+1) + n_{2,d}^*(k+1) \\ \vdots \\ \mathcal{G}h_{M,d}(k)n_{s,M}(k) + n_{M,d}(k) \\ \mathcal{G}h_{M,d}^*(k+1)n_{s,1}^*(k+1) + n_{M,d}^*(k+1) \end{bmatrix} \quad (6.2.13)$$

The $2M \times 2$ matrix \mathbf{H} represents the end-to-end channel-gain matrix of our proposed M relay-based cooperative system model and \mathbf{N}_d is a $2M \times 1$ effective noise vector. It is worthwhile to mention that the matrix \mathbf{H} is not orthogonal unless all the network fading channels are quasi-static (i.e., $\rho_{a,b} = 1 \forall (a, b)$).

6.2.3 Alamouti Space-Time-Decoder and decision statistics

The technique of the ALD [33] is based on multiplying the received signal vector by the hermitian (\mathcal{H}) (hermitian means conjugate-transpose) of the channel gain matrix such that the resulted two elements are the decision statistics needed for the demodulation process. Thus, we can obtain the space-time decoding matrix of the ALD employed at the destination of our system model by taking the hermitian of the end-to-end channel gain matrix \mathcal{H} in (6.2.10) as

$$\mathbf{H}^{\mathcal{H}} = \begin{bmatrix} \mathcal{G}h_{1,1}^*(k)h_{1,d}^*(k) & \mathcal{G}h_{2,1}^*(k)h_{1,d}^*(k) \\ \mathcal{G}h_{2,1}(k+1)h_{1,d}(k+1) & -\mathcal{G}h_{1,1}(k+1)h_{1,d}(k+1) \\ \mathcal{G}h_{1,2}^*(k)h_{2,d}^*(k) & \mathcal{G}h_{2,2}^*(k)h_{2,d}^*(k) \\ \mathcal{G}h_{2,2}(k+1)h_{2,d}(k+1) & -\mathcal{G}h_{1,2}(k+1)h_{2,d}(k+1) \\ \vdots & \vdots \\ \mathcal{G}h_{1,M}^*(k)h_{M,d}^*(k) & \mathcal{G}h_{2,M}^*(k)h_{M,d}^*(k) \\ \mathcal{G}h_{2,M}(k+1)h_{M,d}(k+1) & -\mathcal{G}h_{1,M}(k+1)h_{M,d}(k+1) \end{bmatrix}^T \quad (6.2.14)$$

where $\{.\}^T$ denotes matrix transpose. We assume that the relays and the destination receivers are capable to estimate the channel gains of their corresponding fading links over the individual signaling periods. These gains are required to construct the ALD decoding matrix $\mathbf{H}^{\mathcal{H}}$ at the destination. [45] and [46] are devoted to CSI estimation of time-selective fading channels. Now, by multiplying the received signal vector \mathbf{Y}_d in (6.2.10) by the ALD decoding matrix in (6.2.14), we obtain the required decision statistics corresponding

to the two transmitted symbols x_1 and x_2 , respectively, as

$$\begin{aligned}
\tilde{y}_1 = & \underbrace{\left(\mathcal{G}^2 \sum_{\ell=1}^M (|h_{1,\ell}(k)h_{\ell,d}(k)|^2 + |h_{2,\ell}(k+1)h_{\ell,d}(k+1)|^2) \right)}_{\beta_1} x_1 \\
& + \underbrace{\left(\mathcal{G}^2 \sum_{\ell=1}^M (h_{1,\ell}^*(k)h_{2,\ell}(k)|h_{\ell,d}(k)|^2 - h_{2,\ell}(k+1)h_{1,\ell}^*(k+1)|h_{\ell,d}(k+1)|^2) \right)}_{\zeta} x_2 \\
& + \underbrace{\sum_{\ell=1}^M (\mathcal{G}^2 h_{1,\ell}^*(k)|h_{\ell,d}(k)|^2 n_{s,\ell}(k) + \mathcal{G} h_{1,\ell}^*(k)h_{\ell,d}^*(k)n_{\ell,d}(k) + \mathcal{G}^2 h_{2,\ell}(k+1)}_{\text{effective-white-noise-term}_1 \triangleq \tilde{n}_1} \\
& \quad \times |h_{\ell,d}(k+1)|^2 n_{s,\ell}^*(k+1) + \mathcal{G} h_{2,\ell}(k+1)h_{\ell,d}(k+1)n_{\ell,d}^*(k+1)) \quad (6.2.15)
\end{aligned}$$

and

$$\begin{aligned}
\tilde{y}_2 = & \underbrace{\left(\mathcal{G}^2 \sum_{\ell=1}^M (|h_{2,\ell}(k)h_{\ell,d}(k)|^2 + |h_{1,\ell}(k+1)h_{\ell,d}(k+1)|^2) \right)}_{\beta_2} x_2 \\
& + \underbrace{\left(\mathcal{G}^2 \sum_{\ell=1}^M (h_{1,\ell}(k)h_{2,\ell}^*(k)|h_{\ell,d}(k)|^2 - h_{2,\ell}^*(k+1)h_{1,\ell}(k+1)|h_{\ell,d}(k+1)|^2) \right)}_{\zeta^*} x_1 \\
& + \underbrace{\sum_{\ell=1}^M (\mathcal{G}^2 h_{2,\ell}^*(k)|h_{\ell,d}(k)|^2 n_{s,\ell}(k) + \mathcal{G} h_{2,\ell}^*(k)h_{\ell,d}^*(k)n_{\ell,d}(k) - \mathcal{G}^2 h_{1,\ell}(k+1)}_{\text{effective-white-noise-term}_2 \triangleq \tilde{n}_2} \\
& \quad \times |h_{\ell,d}(k+1)|^2 n_{s,\ell}^*(k+1) - \mathcal{G} h_{1,\ell}(k+1)h_{\ell,d}(k+1)n_{\ell,d}^*(k+1)). \quad (6.2.16)
\end{aligned}$$

It should be noted that, in Alamouti's work [33] (non-cooperative model), it has been required the condition that the transmitter-receiver fading link must be time-invariant at least over two time-adjacent signaling periods. The reason for this is to guarantee the orthogonality

of the channel gain matrix and to obtain two separate (with no ITAI) and independent decision statistics corresponding to the two transmitted symbols in the OSTBC matrix. However, in our cooperative network model, and as a result of the relative speed among the communicating nodes, all of the network fading links are characterized as time-variant (see (6.2.2)), which violates the above condition assumed in [33]. Therefore, as it is clear from (6.2.15) and (6.2.16), the obtained decision statistics \tilde{y}_1 and \tilde{y}_2 are nonseparable for x_1 and x_2 , respectively, due to the ITAI-terms. Moreover, as an effect of the nodes mobility, \tilde{y}_1 and \tilde{y}_2 are non statistically independent. This is because that their effective noise terms \tilde{n}_1 and \tilde{n}_2 are correlated with the following conditional covariance

$$\begin{aligned}
\mathbf{COV}(\tilde{n}_1, \tilde{n}_2 | \mathcal{S}) &= \mathbb{E}[\tilde{n}_1 \tilde{n}_2^* | \mathcal{S}] \\
&= \sum_{\ell=1}^M \mathcal{G}^4 h_{1,\ell}^*(k) h_{2,\ell}(k) |h_{\ell,d}(k)|^4 \mathbb{E}[n_{s,\ell}(k) n_{s,\ell}^*(k)] + \mathcal{G}^2 h_{1,\ell}^*(k) h_{2,\ell}(k) \\
&\quad \times |h_{\ell,d}(k)|^2 \mathbb{E}[n_{\ell,d}(k) n_{\ell,d}^*(k)] - \mathcal{G}^4 h_{2,\ell}(k+1) h_{1,\ell}^*(k+1) \\
&\quad \times |h_{\ell,d}(k+1)|^4 \mathbb{E}[n_{s,\ell}^*(k+1) n_{s,\ell}(k+1)] - \mathcal{G}^2 h_{2,\ell}(k+1) h_{1,\ell}^*(k+1) \\
&\quad \times |h_{\ell,d}(k+1)|^2 \mathbb{E}[n_{\ell,d}^*(k+1) n_{\ell,d}(k+1)] \\
&= \mathcal{G}^2 N_o \sum_{\ell=1}^M h_{1,\ell}^*(k) h_{2,\ell}(k) |h_{\ell,d}(k)|^2 (\mathcal{G}^2 |h_{\ell,d}(k)|^2 + 1) - h_{2,\ell}(k+1) \\
&\quad \times h_{1,\ell}^*(k+1) |h_{\ell,d}(k+1)|^2 (\mathcal{G}^2 |h_{\ell,d}(k+1)|^2 + 1). \tag{6.2.17}
\end{aligned}$$

where $\mathcal{S} = \{h_{1,\ell}(k), h_{1,\ell}(k+1), h_{2,\ell}(k), h_{2,\ell}(k+1), h_{\ell,d}(k), h_{\ell,d}(k+1)\} \forall \ell$. The first equality in (6.2.17) is obtained under the assumption that the white noise components $n_{s,\ell}(k)$, $n_{s,\ell}(k+1)$, $n_{\ell,d}(k)$ and $n_{\ell,d}(k+1) \forall \ell$ are independent to each other. It is also worthwhile to mention that if the cooperating nodes are static (i.e., $\rho_{a,b} = 1 \forall (a, b)$) the ITAI-terms in (6.2.15) and (6.2.16) and the statistical correlation in (6.2.17) reduce to zero. This means that the decoder decision statistics \tilde{y}_1 and \tilde{y}_2 are separable to x_1 and x_2 , respectively, and also independent to each other. However, in the next section, we analyze the system SEP performance considering the more general case of mobile nodes (i.e., time-variant fading links with $\rho_{a,b} < 1 \forall (a, b)$).

6.3 System Conditional SEP Analysis

As depicted in Fig. 6.1, the destination's q -QAM demodulator uses the decision statistics \tilde{y}_1 and \tilde{y}_2 to make decision about the two transmitted symbols x_1 and x_2 , respectively. In this subsection, our target is to analyze the probability of making error in these decisions (i.e., evaluating the system SEP). First of all, in AWGN point-to-point communication system, the average SEP at the output of the q -QAM demodulator is obtained as [47, eq. (5.2-79) and eq. (5.2-78)]

$$\bar{P}_e^{\text{AWGN}} = 1 - \left(1 - 2 \left(1 - \frac{1}{\sqrt{q}} \right) Q \left(\sqrt{\frac{3}{q-1}} \bar{\gamma} \right) \right)^2 \quad (6.3.1)$$

where $\bar{\gamma} = \frac{E_s}{N_o}$ is the per-symbol average signal-to-noise-ratio (SNR) of the input decision statistic and $Q(u)$ is the Q -function. Now, we can directly use the AWGN SEP expression in (6.3.1) to evaluate the conditional SEP of our system model described in Sec. 6.2 if we (i) show that the ITAI-terms, in addition to the effective noise terms, in (6.2.15) and (6.2.16) are Gaussian (ii) obtain explicit expressions for the SINRs of the statistics \tilde{y}_1 and \tilde{y}_2 , which we do in the following:

6.3.1 Conditional SINR of the first decision statistic

It is clear from (6.2.15) that the first decision statistic \tilde{y}_1 is function of the channel gains in the set $\mathcal{S} = \{h_{1,\ell}(k), h_{1,\ell}(k+1), h_{2,\ell}(k), h_{2,\ell}(k+1), h_{\ell,d}(k), h_{\ell,d}(k+1)\} \forall \ell$. However, in order to simplify the derivation of its conditional SINR (say SINR_1), we derive it conditioned on the set $\mathcal{S}_1 = \{h_{1,\ell}(k), h_{2,\ell}(k+1), h_{\ell,d}(k), h_{\ell,d}(k+1)\}^2$. It is clear from (6.2.15) that we can now obtain SINR_1 conditioned on \mathcal{S}_1 as

$$\text{SINR}_1 | \mathcal{S}_1 = \frac{\text{P}(\text{desired signal of } x_1 | \mathcal{S}_1)}{\text{P}(\text{ITAI-term}_1 | \mathcal{S}_1) + \text{P}(\tilde{n}_1 | \mathcal{S}_1)} = \frac{|\beta_1|^2 (E_s/2)}{\text{P}(\zeta | \mathcal{S}_1) (E_s/2) + \text{Var}(\tilde{n}_1 | \mathcal{S}_1)} \quad (6.3.2)$$

²The channel gains in this set are the ones that appear as coefficients of the desired signal in the decision statistic \tilde{y}_1 in (6.2.15).

where P and Var denote the power and the variance operators, respectively. In the following we discuss how to evaluate $P(\zeta|\mathcal{S}_1)$ and $\text{Var}(\tilde{n}_1|\mathcal{S}_1)$. First, it is clear from (6.2.15) that ζ is function of the elements in \mathcal{S}_1 as well as of $h_{1,\ell}(k+1)$ and $h_{2,\ell}(k)$. Therefore, conditioned on \mathcal{S}_1 , ζ is random variable with respect to both $h_{1,\ell}(k+1)$ and $h_{2,\ell}(k)$. To find the density of ζ conditioned on \mathcal{S}_1 (which is needed first to obtain $P(\zeta|\mathcal{S}_1)$), we can first benefit from the expression of the AR1 model in (6.2.1) to write $h_{1,\ell}^*(k+1)$ in terms of $h_{1,\ell}(k)$ and $h_{2,\ell}(k)$ in terms of $h_{2,\ell}(k+1)$, respectively, as follows

$$h_{1,\ell}^*(k+1) = \rho_{s,\ell} h_{1,\ell}^*(k) + \sqrt{1 - \rho_{s,\ell}^2} e_{1,\ell}^*(k) \quad (6.3.3)$$

$$h_{2,\ell}(k) = \rho_{s,\ell} h_{2,\ell}(k+1) + \sqrt{1 - \rho_{s,\ell}^2} e_{2,\ell}(k+1). \quad (6.3.4)$$

From (6.3.3) and (6.3.4), along with the fact that $e_{1,\ell}^*(k) \sim \mathcal{CN}(0, \sigma_{1,\ell}^2)$ and $e_{2,\ell}(k+1) \sim \mathcal{CN}(0, \sigma_{2,\ell}^2)$, we can obtain the densities of $h_{1,\ell}^*(k+1)$ conditioned on $h_{1,\ell}(k)$ and that of $h_{2,\ell}(k)$ conditioned on $h_{2,\ell}(k+1)$, respectively, as follows

$$h_{1,\ell}^*(k+1) | h_{1,\ell}(k) \sim \mathcal{CN}(\rho_{s,\ell} h_{1,\ell}^*(k), (1 - \rho_{s,\ell}^2) \sigma_{1,\ell}^2). \quad (6.3.5)$$

$$h_{2,\ell}(k) | h_{2,\ell}(k+1) \sim \mathcal{CN}(\rho_{s,\ell} h_{2,\ell}(k+1), (1 - \rho_{s,\ell}^2) \sigma_{2,\ell}^2) \quad (6.3.6)$$

With the help of the densities in (6.3.5) and (6.3.6), we can now obtain the density of ζ conditioned on \mathcal{S}_1 as

$$\begin{aligned} \zeta | \mathcal{S}_1 \sim \mathcal{CN} \left(\underbrace{\mathcal{G}^2 \sum_{\ell=1}^M (\rho_{s,\ell} h_{1,\ell}^*(k) h_{2,\ell}(k+1) (|h_{\ell,d}(k)|^2 - |h_{\ell,d}(k+1)|^2))}_{\mathbb{E}[\zeta|\mathcal{S}_1] \triangleq \mu_1}, \right. \\ \left. \underbrace{\mathcal{G}^4 \sum_{\ell=1}^M ((1 - \rho_{s,\ell}^2) (\sigma_{2,\ell}^2 |h_{1,\ell}(k)|^2 |h_{\ell,d}(k)|^4 + \sigma_{1,\ell}^2 |h_{2,\ell}(k+1)|^2 |h_{\ell,d}(k+1)|^4))}_{\text{Var}[\zeta|\mathcal{S}_1] \triangleq \phi_1} \right) \end{aligned} \quad (6.3.7)$$

and thus, its conditional power, $P(\zeta \mid \mathcal{S}_1)$, can be given as

$$P(\zeta \mid \mathcal{S}_1) = |\mu_1|^2 + \phi_1. \quad (6.3.8)$$

As described in the system model section, all of the noise components $n_{s,\ell}(k)$, $n_{\ell,d}(k)$, $n_{s,\ell}^*(k+1)$ and $n_{\ell,d}^*(k+1)$ are statistically independent and each one is a ZMCSCG with variance N_o . Based on this fact, the effective noise term \tilde{n}_1 in (6.2.15) is also, (conditioned on \mathcal{S}_1) a ZMCSCG random variable, which we can find its conditional variance as

$$\text{Var}(\tilde{n}_1 \mid \mathcal{S}_1) = N_o \eta_1 \quad (6.3.9)$$

where

$$\begin{aligned} \eta_1 = \mathcal{G}^2 \sum_{\ell=1}^M & (|h_{1,\ell}(k)h_{\ell,d}(k)|^2 (\mathcal{G}^2 |h_{\ell,d}(k)|^2 + 1) + |h_{2,\ell}(k+1)h_{\ell,d}(k+1)|^2 \\ & \times (\mathcal{G}^2 |h_{\ell,d}(k+1)|^2 + 1)). \end{aligned}$$

Finally, by substituting (6.3.8) and (6.3.9) into (6.3.2), we obtain $\text{SINR}_1 \mid \mathcal{S}_1$ in its ultimate form as

$$\text{SINR}_1 \mid \mathcal{S}_1 = \frac{|\beta_1|^2 \frac{E_s}{N_o}}{(|\mu_1|^2 + \phi_1) \frac{E_s}{N_o} + 2\eta_1}. \quad (6.3.10)$$

6.3.2 Conditional SINR of the second decision statistic

Similarly as \tilde{y}_1 , \tilde{y}_2 in (6.2.16) is function of the channel gains in the set \mathcal{S} but in order to simplify the derivation of its conditional SINR (say SINR_2), we do that conditioned on the channel gains in the set $\mathcal{S}_2 = \{h_{1,\ell}(k+1), h_{2,\ell}(k), h_{\ell,d}(k), h_{\ell,d}(k+1)\}^3$. From (6.2.16),

³The channel gains in this set are the ones that appear as coefficients of the desired signal in the decision statistic \tilde{y}_2 in (6.2.16).

we can now obtain SINR_2 conditioned on \mathcal{S}_2 as

$$\text{SINR}_2 | \mathcal{S}_2 = \frac{\text{P}(\text{desired signal of } x_2 | \mathcal{S}_2)}{\text{P}(\text{ITAI-term}_2 | \mathcal{S}_2) + \text{P}(\tilde{n}_2 | \mathcal{S}_2)} = \frac{|\beta_2|^2 (E_s/2)}{\text{P}(\zeta^* | \mathcal{S}_2) (E_s/2) + \text{Var}(\tilde{n}_2 | \mathcal{S}_2)}. \quad (6.3.11)$$

It is clear from (6.2.16) that ζ^* is function of the elements in \mathcal{S}_2 as well as of $h_{1,\ell}(k)$ and $h_{2,\ell}(k+1)$. Therefore, conditioned on \mathcal{S}_2 , ζ^* is random variable in terms of both $h_{1,\ell}(k)$ and $h_{2,\ell}(k+1)$. With the help of (6.2.1), we can now obtain the densities of $h_{1,\ell}(k)$ conditioned on $h_{1,\ell}(k+1)$ and that of $h_{2,\ell}^*(k+1)$ conditioned on $h_{2,\ell}(k)$, respectively, as follows

$$h_{1,\ell}(k) | h_{1,\ell}(k+1) \sim \mathcal{CN}(\rho_{s,\ell} h_{1,\ell}(k+1), (1 - \rho_{s,\ell}^2) \sigma_{1,\ell}^2) \quad (6.3.12)$$

$$h_{2,\ell}^*(k+1) | h_{2,\ell}(k) \sim \mathcal{CN}(\rho_{s,\ell} h_{2,\ell}^*(k), (1 - \rho_{s,\ell}^2) \sigma_{2,\ell}^2). \quad (6.3.13)$$

These two densities in (6.3.12) and (6.3.13), help in obtaining the density of $\zeta^* | \mathcal{S}_2$, which is given by

$$\begin{aligned} \zeta^* | \mathcal{S}_2 \sim \mathcal{CN} \left(\underbrace{\mathcal{G}^2 \sum_{\ell=1}^M (\rho_{s,\ell} h_{1,\ell}^*(k+1) h_{2,\ell}(k) (|h_{\ell,d}(k)|^2 - |h_{\ell,d}(k+1)|^2))}_{\mathbb{E}[\zeta^* | \mathcal{S}_2] \triangleq \mu_2}, \right. \\ \left. \underbrace{\mathcal{G}^4 \sum_{\ell=1}^M ((1 - \rho_{s,\ell}^2) (\sigma_{2,\ell}^2 |h_{1,\ell}(k+1)|^2 |h_{\ell,d}(k)|^4 + \sigma_{1,\ell}^2 |h_{2,\ell}(k)|^2 |h_{\ell,d}(k+1)|^4))}_{\text{Var}[\zeta^* | \mathcal{S}_2] \triangleq \phi_2} \right). \end{aligned} \quad (6.3.14)$$

It is obvious from (6.3.14) that $\text{P}(\zeta^* | \mathcal{S}_2)$ can be given as

$$\text{P}(\zeta^* | \mathcal{S}_2) = |\mu_2|^2 + \phi_2. \quad (6.3.15)$$

As similar as \tilde{n}_1 , the effective noise term \tilde{n}_2 in (6.2.16) is also (conditioned on \mathcal{S}_2) a ZMCSCG random variable but with the following conditional variance

$$\text{Var}(\tilde{n}_2|\mathcal{S}_2) = N_o\eta_2 \quad (6.3.16)$$

where

$$\begin{aligned} \eta_2 = \mathcal{G}^2 \sum_{\ell=1}^M & (|h_{1,\ell}(k+1)h_{\ell,d}(k+1)|^2(\mathcal{G}^2|h_{\ell,d}(k+1)|^2 + 1) + |h_{2,\ell}(k)h_{\ell,d}(k)|^2 \\ & \times (\mathcal{G}^2|h_{\ell,d}(k)|^2 + 1)). \end{aligned}$$

By substituting (6.3.15) and (6.3.16) into (6.3.11), we obtain $\text{SINR}_2|_{\mathcal{S}_2}$ in its ultimate form as

$$\text{SINR}_2|_{\mathcal{S}_2} = \frac{|\beta_2|^2 \frac{E_s}{N_o}}{(|\mu_2|^2 + \phi_2) \frac{E_s}{N_o} + 2\eta_2}. \quad (6.3.17)$$

6.3.3 Conditional SEP expression

Now, without loss of generality, we can express the SEP at the output of the q -QAM demodulator of our system model conditioned on the channel gains in the set \mathcal{S} (say $P_e|\mathcal{S}$) as

$$P_e|\mathcal{S} = Pr(x_1)P_e^{\tilde{y}_1}|\mathcal{S}_1 + Pr(x_2)P_e^{\tilde{y}_2}|\mathcal{S}_2 \quad (6.3.18)$$

where $Pr(x_1)$ and $Pr(x_2)$ are the transmission probabilities of x_1 and x_2 , respectively. $P_e^{\tilde{y}_1}|\mathcal{S}_1$ and $P_e^{\tilde{y}_2}|\mathcal{S}_2$ are the conditional probabilities of symbol error decisions made by the q -QAM demodulator in estimating x_1 from \tilde{y}_1 (conditioned on \mathcal{S}_1) and in estimating x_2 from \tilde{y}_2 (conditioned on \mathcal{S}_2), respectively. By assuming equiprobable transmissions for x_1 and x_2 (i.e., $Pr(x_1) = Pr(x_2) = \frac{1}{2}$) and directly using the SEP expression in (6.3.1) to evaluate $P_e^{\tilde{y}_1}|\mathcal{S}_1$ (by replacing $\bar{\gamma}$ by $\text{SINR}_1|\mathcal{S}_1$) and $P_e^{\tilde{y}_2}|\mathcal{S}_2$ (by replacing $\bar{\gamma}$ by $\text{SINR}_2|\mathcal{S}_2$)⁴, we can

⁴This is valid because the ITAI-terms in \tilde{y}_1 and \tilde{y}_2 are distributed as Gaussian conditioned on \mathcal{S}_1 and \mathcal{S}_2 , respectively (see (6.3.7) and (6.3.14)).

obtain $P_e|\mathcal{S}$ as

$$\begin{aligned}
P_e|\mathcal{S} = & \frac{1}{2} \left[1 - \left(1 - 2 \left(1 - \frac{1}{\sqrt{q}} \right) Q \left(\sqrt{\frac{3}{q-1}} \frac{|\beta_1|^2 \frac{E_s}{N_o}}{(|\mu_1|^2 + \phi_1) \frac{E_s}{N_o} + 2\eta_1} \right) \right)^2 \right] \\
& + \frac{1}{2} \left[1 - \left(1 - 2 \left(1 - \frac{1}{\sqrt{q}} \right) Q \left(\sqrt{\frac{3}{q-1}} \frac{|\beta_2|^2 \frac{E_s}{N_o}}{(|\mu_2|^2 + \phi_2) \frac{E_s}{N_o} + 2\eta_2} \right) \right)^2 \right].
\end{aligned} \tag{6.3.19}$$

As an impact of the nodes mobility, the system SEP performance experiences sever degradation specifically at high values of the per-symbol average SNR ($\frac{E_s}{N_o}$). This degradation is mainly represented by conditional asymptotic error floors ($P_e^{\text{floor}}|\mathcal{S}$), which can be given by

$$\begin{aligned}
P_e^{\text{floor}}|\mathcal{S} = & \lim_{\frac{E_s}{N_o} \rightarrow \infty} P_e|\mathcal{S} = \frac{1}{2} \left[1 - \left(1 - 2 \left(1 - \frac{1}{\sqrt{q}} \right) Q \left(\frac{|\beta_1|^2 \sqrt{\frac{3}{q-1}}}{|\mu_1|^2 + \phi_1} \right) \right)^2 \right] \\
& + \frac{1}{2} \left[1 - \left(1 - 2 \left(1 - \frac{1}{\sqrt{q}} \right) Q \left(\frac{|\beta_2|^2 \sqrt{\frac{3}{q-1}}}{|\mu_2|^2 + \phi_2} \right) \right)^2 \right].
\end{aligned} \tag{6.3.20}$$

The obtained SEP and error floor expressions in (6.3.19) and (6.3.20) are still conditional on the network fading gains in the set \mathcal{S} . In the next section we discuss how to obtain numerical values for their averages, which are required to give an obvious picture about the SEP performance.

6.4 System Average SEP Analysis

The system average SEP (say \overline{P}_e) can be obtained from (6.3.19) as

$$\begin{aligned}
\overline{P}_e &= \mathbb{E}_{\mathcal{S}}[P_e|\mathcal{S}] \\
&= \frac{1}{2} \left[1 - \mathbb{E}_{\mathcal{S}_1} \left[\left(1 - 2 \left(1 - \frac{1}{\sqrt{q}} \right) Q \left(\sqrt{\frac{3}{q-1}} \underbrace{\frac{|\beta_1|^2 \frac{E_s}{N_o}}{(|\mu_1|^2 + \phi_1) \frac{E_s}{N_o} + 2\eta_1}}_{\text{SINR}_1|\mathcal{S}_1}} \right) \right)^2 \right] \right] \\
&\quad + \frac{1}{2} \left[1 - \mathbb{E}_{\mathcal{S}_2} \left[\left(1 - 2 \left(1 - \frac{1}{\sqrt{q}} \right) Q \left(\sqrt{\frac{3}{q-1}} \underbrace{\frac{|\beta_2|^2 \frac{E_s}{N_o}}{(|\mu_2|^2 + \phi_2) \frac{E_s}{N_o} + 2\eta_2}}_{\text{SINR}_2|\mathcal{S}_2}} \right) \right)^2 \right] \right]
\end{aligned} \tag{6.4.1}$$

where $\mathbb{E}_{\mathcal{U}}[\cdot]$ denotes the statistical expectation operator with respect to \mathcal{U} . Evaluating the last two expectations in (6.4.1) requires first deriving the probability density functions (pdfs) of both $\text{SINR}|\mathcal{S}_1$ and $\text{SINR}|\mathcal{S}_2$, which is too hard to accomplish. Therefore, by using computer Monte Carlo simulation to evaluate these two expectations (based on the sampling mean concept), we can obtain numerical values for \overline{P}_e as

$$\begin{aligned}
\overline{P}_e &= \frac{1}{2} \left[1 - \frac{1}{N} \sum_{j=1}^N \left[\left(1 - 2 \left(1 - \frac{1}{\sqrt{q}} \right) Q \left(\sqrt{\frac{3}{q-1}} \text{SINR}|\mathcal{S}_1^j \right) \right)^2 \right] \right] \\
&\quad + \frac{1}{2} \left[1 - \frac{1}{N} \sum_{j=1}^N \left[\left(1 - 2 \left(1 - \frac{1}{\sqrt{q}} \right) Q \left(\sqrt{\frac{3}{q-1}} \text{SINR}|\mathcal{S}_2^j \right) \right)^2 \right] \right]
\end{aligned} \tag{6.4.2}$$

where $\text{SINR}|\mathcal{S}_1^j$ and $\text{SINR}|\mathcal{S}_2^j$ are the generated SINRs in the j th realization and N is the number of realizations in the simulation (N is supposed to be large enough). Similarly, we use same method to obtain numerical values for the statistical average of the error floor in

(6.3.20) as

$$\begin{aligned} \overline{P}_e^{\text{floor}} = & \frac{1}{2} \left[1 - \frac{1}{N} \sum_{j=1}^N \left[\left(1 - 2 \left(1 - \frac{1}{\sqrt{q}} \right) Q \left(\frac{|\beta_1^j|^2 \sqrt{\frac{3}{q-1}}}{|\mu_1^j|^2 + \phi_1^j} \right) \right)^2 \right] \right] \\ & + \frac{1}{2} \left[1 - \frac{1}{N} \sum_{j=1}^N \left[\left(1 - 2 \left(1 - \frac{1}{\sqrt{q}} \right) Q \left(\frac{|\beta_2^j|^2 \sqrt{\frac{3}{q-1}}}{|\mu_2^j|^2 + \phi_2^j} \right) \right)^2 \right] \right]. \end{aligned} \quad (6.4.3)$$

In the numerical results section, the provided plots for the system average SEP using (6.4.2) are verified via real link-level simulation.

6.5 System Performance under Static Nodes Case

Here, we consider a special case of static (non moving) nodes in the network. In this case, and according to Jakes' autocorrelation model, all of the network fading links' correlation parameters reduce to one ($\rho_{s,\ell} = \rho_{\ell,d} = 1 \ \forall \ell$), and thereby, these fading links can be characterized as quasi-static. Under this consideration, we can also notice from (6.2.1) that

$$\begin{aligned} h_{1,\ell}(k+1) &= h_{1,\ell}(k) = h_{1,\ell} \\ h_{2,\ell}(k+1) &= h_{2,\ell}(k) = h_{2,\ell} \\ h_{\ell,d}(k+1) &= h_{\ell,d}(k) = h_{\ell,d}, \quad \forall \ell = \{1, 2, \dots, M\}. \end{aligned} \quad (6.5.1)$$

Following the channel gains description in (6.5.1), the end-to-end channel gain matrix in (6.2.12) reduces to its orthogonal (quasi-static fading) version, $\mathbf{H}^{\text{static}}$, that can be given as

$$\mathbf{H}^{\text{static}} = \begin{bmatrix} \mathcal{G}h_{1,1}h_{1,d} & \mathcal{G}h_{2,1}h_{1,d} \\ \mathcal{G}h_{2,1}^*h_{1,d}^* & -\mathcal{G}h_{1,1}^*h_{1,d}^* \\ \mathcal{G}h_{1,2}h_{2,d} & \mathcal{G}h_{2,2}h_{2,d} \\ \mathcal{G}h_{2,2}^*h_{2,d}^* & -\mathcal{G}h_{1,2}^*h_{2,d}^* \\ \vdots & \vdots \\ \mathcal{G}h_{1,M}h_{M,d} & \mathcal{G}h_{2,M}h_{M,d} \\ \mathcal{G}h_{2,M}^*h_{M,d}^* & -\mathcal{G}h_{1,M}^*h_{M,d}^* \end{bmatrix} \quad (6.5.2)$$

and the ALD decoding matrix $\mathbf{H}^{\mathcal{H}}$ in (6.2.14) reduces to

$$\mathbf{H}^{\text{static}\mathcal{H}} = \begin{bmatrix} \mathcal{G}h_{1,1}^*h_{1,d}^* & \mathcal{G}h_{2,1}^*h_{1,d}^* \\ \mathcal{G}h_{2,1}h_{1,d} & -\mathcal{G}h_{1,1}h_{1,d} \\ \mathcal{G}h_{1,2}^*h_{2,d}^* & \mathcal{G}h_{2,2}^*h_{2,d}^* \\ \mathcal{G}h_{2,2}h_{2,d} & -\mathcal{G}h_{1,2}h_{2,d} \\ \vdots & \vdots \\ \mathcal{G}h_{1,M}^*(k)h_{M,d}^* & \mathcal{G}h_{2,M}^*(k)h_{M,d}^* \\ \mathcal{G}h_{2,M}h_{M,d} & -\mathcal{G}h_{1,M}h_{M,d} \end{bmatrix}^T \quad (6.5.3)$$

Clearly, $\mathbf{H}^{\text{static}\mathcal{H}}$ in (6.5.3) diagonalizes $\mathbf{H}^{\text{static}}$ in (6.5.2), which means that, in this static nodes scenario, the ALD (as expected) is in its originally designed optimal version. This is also further verified because, under this quasi-static fading condition, the powers of the ITAI terms, $P(\zeta \mid \mathcal{S}_1)$ in (6.3.8) and $P(\zeta^* \mid \mathcal{S}_2)$ in (6.3.15), vanish. Moreover, both the derived conditional SINRs in (6.3.10) and (6.3.17) reduce to the following conditional SNR

$$\gamma^{\text{static}}|_{\mathcal{S}^{\text{static}}} = \frac{E_s \mathcal{G}^2}{2N_o} \frac{\left(\sum_{\ell=1}^M \|\mathbf{h}_{\ell}\|^2 |h_{\ell,d}|^2 \right)^2}{\sum_{\ell=1}^M ((\mathcal{G}^2 |h_{\ell,d}|^2 + 1) \|\mathbf{h}_{\ell}\|^2 |h_{\ell,d}|^2)} \quad (6.5.4)$$

where

$$\begin{aligned}\|\mathbf{h}_\ell\|^2 &= |h_{1,\ell}|^2 + |h_{2,\ell}|^2 \\ \mathcal{S}^{\text{static}} &= \{h_{1,\ell}, h_{2,\ell}, h_{\ell,d}\} \quad \forall \ell = \{1, 2, \dots, M\},\end{aligned}$$

and the conditional SEP in (6.3.19) reduces to $P_e^{\text{static}}|\mathcal{S}^{\text{static}}$ which is given by

$$P_e^{\text{static-nodes}}|\mathcal{S}^{\text{static}} = \left[1 - \left(1 - 2 \left(1 - \frac{1}{\sqrt{M}} \right) Q \left(\sqrt{\frac{3}{M-1}} \frac{|\tilde{\beta}|^2 \frac{E_s}{N_o}}{2\tilde{\eta}_1} \right) \right)^2 \right] \quad (6.5.5)$$

where

$$\tilde{\beta} = \mathcal{G}^2 \sum_{\ell=1}^M (|h_{1,\ell} h_{\ell,d}|^2 + |h_{2,\ell} h_{\ell,d}|^2)$$

and

$$\tilde{\eta} = \mathcal{G}^2 \sum_{\ell=1}^M ((\mathcal{G}^2 |h_{\ell,d}|^2 + 1) (|h_{1,\ell} h_{\ell,d}|^2 + |h_{2,\ell} h_{\ell,d}|^2)).$$

It is worthwhile to mention that the limit of (6.5.5) as $\frac{E_s}{N_o} \rightarrow \infty$ is zero (i.e., the error floor vanish) because the nodes mobility impact is removed. If we consider now another special case of a single-relay network (i.e., $M = 1$), and after doing some manipulations, the SNR in (6.5.4) can be written as

$$\gamma_{\text{single-relay}}^{\text{static}} = \frac{E_s}{2} \frac{\frac{\|\mathbf{h}_\ell\|^2}{N_o} \frac{|h_{\ell,d}|^2}{N_o}}{\frac{|h_{\ell,d}|^2}{N_o} + \frac{1}{\mathcal{G}^2 N_o}} \quad (6.5.6)$$

which is known in the literature for a system model of OSTBC transmission over single-relay quasi-static fading network [26, eq. (7)]. We conclude from this that the derived SINRs in (6.3.10) and (6.3.17) generalize [26, eq. (7)] for multiple-relay network over time-selective fading environment in case of Alamouti-OSTBC transmission.

6.6 Numerical Results and Simulation

In this section, we present numerical results for our system model average SEP performance using (6.4.2) and (6.4.3) along with the real link-level simulation results.

Figs. 6.2 and 6.3 are plots for the system average SEP versus $\frac{E_s}{N_o}$ for 4 and 64 QAM constellations, single relay ($M = 1$) network, and different relative speeds among the nodes with transmission data-rates of 9.6 kbps in Fig. 6.2 and 64 kbps Fig. 6.3. First, we can observe from these two figures that the analyzed SEP using (6.4.2) exactly matches with the real link-level simulation one, which verifies the correctness of our performed theoretical analysis. As compared with static network case (the case of 0 mph relative speeds among the cooperating nodes), the system average SEP performance is severely degraded and experiences high irreducible floors, in particular, at relatively high speeds of 50 and 80 mph. In addition, by comparing Fig. 6.3 with Fig. 6.2, we can notice that this degradation becomes less for higher transmission data-rates. This is due to the fact that increasing the transmission data-rate reduces the time-variation among the time-adjacent channel gains.

In Fig. 6.4, we consider 16-QAM constellation and 25 kbps transmission data-rate and plot the average SEP for different number of relays M and relative speeds. It is clear from this figure that the average SEP performance is improved with M as a result of the obtained diversity-gain achieved via relaying. We can also notice that despite of this general improved performance with the number of relays, the impact of the nodes mobility is still under effect whatever the number of relays is.

The target beyond Fig. 6.5 is to investigate the effect of the transmission data-rate on the SEP performance of our system with high speeds mobile nodes (for example 65 mph). We can observe from this figure that increasing the data-rate gradually reduces the impact of the nodes mobility and improves the average SEP performance so that it goes close to the performance of non-moving nodes case.

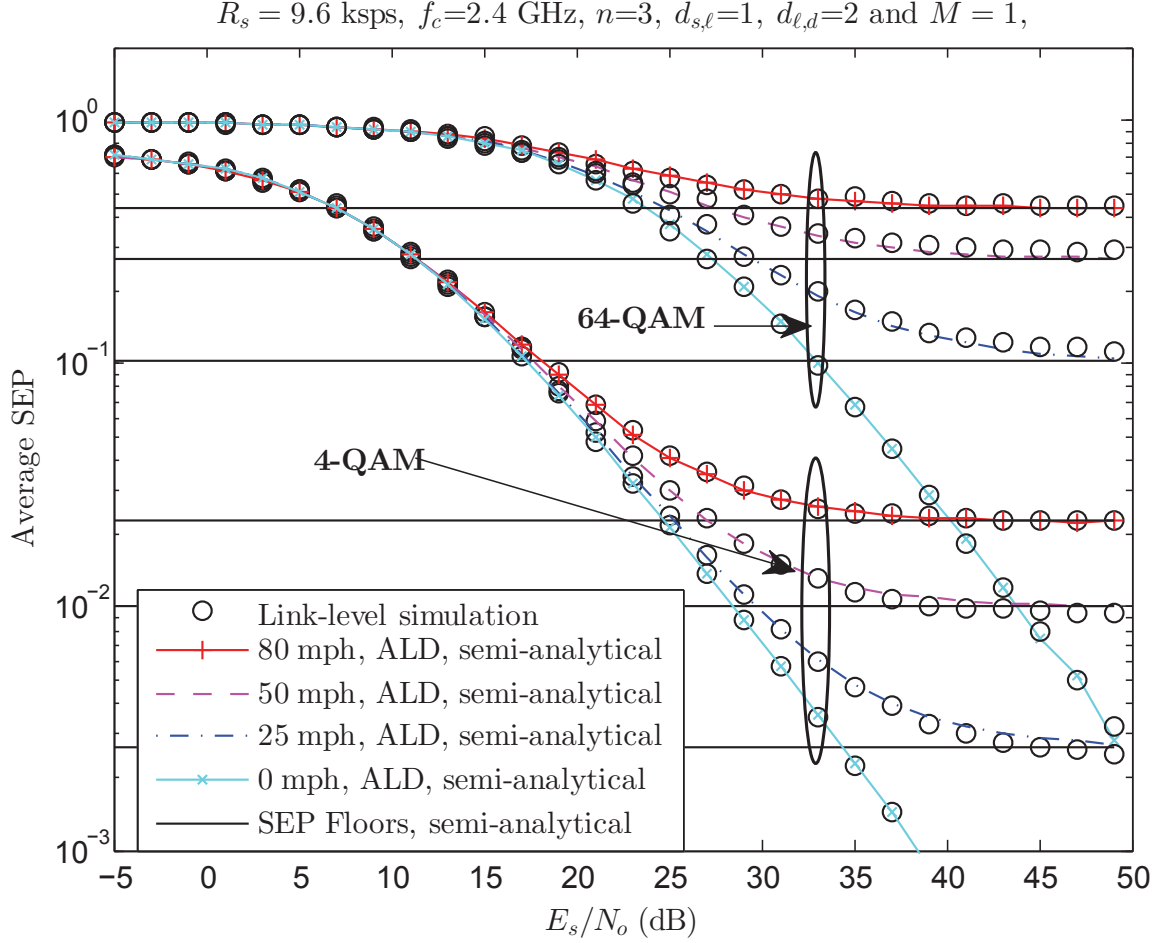


Figure 6.2. Average SEP versus E_s/N_o for $M = 1, 4$ and 64 QAM constellations, transmission data-rate $R_s = 9.6$ ksp/s, carrier frequency $f_c = 2.4$ GHz, path-loss exponent $n = 3$, normalized nodes distances $d_{s,\ell} = 1$ and $d_{\ell,d} = 2$.

6.7 Conclusion

In this chapter we have concerned in investigating the effect of the cooperating nodes mobility (their relative speeds) on the symbol error probability performance of a wireless cooperative network scenario with rectangular QAM and Alamouti-OSTBC at the source, fixed-gain amplify-and-forward protocol at the relays, and Alamouti's space-time decoder (ALD) at the destination. To take the relative speeds among the communicating nodes into account, we have modeled all of the network frequency-flat fading channels as time-selective (time-varying) using the first order autoregressive (AR1) process. We have also considered the path-loss large-scale fading model to make the network's fading environment more ag-

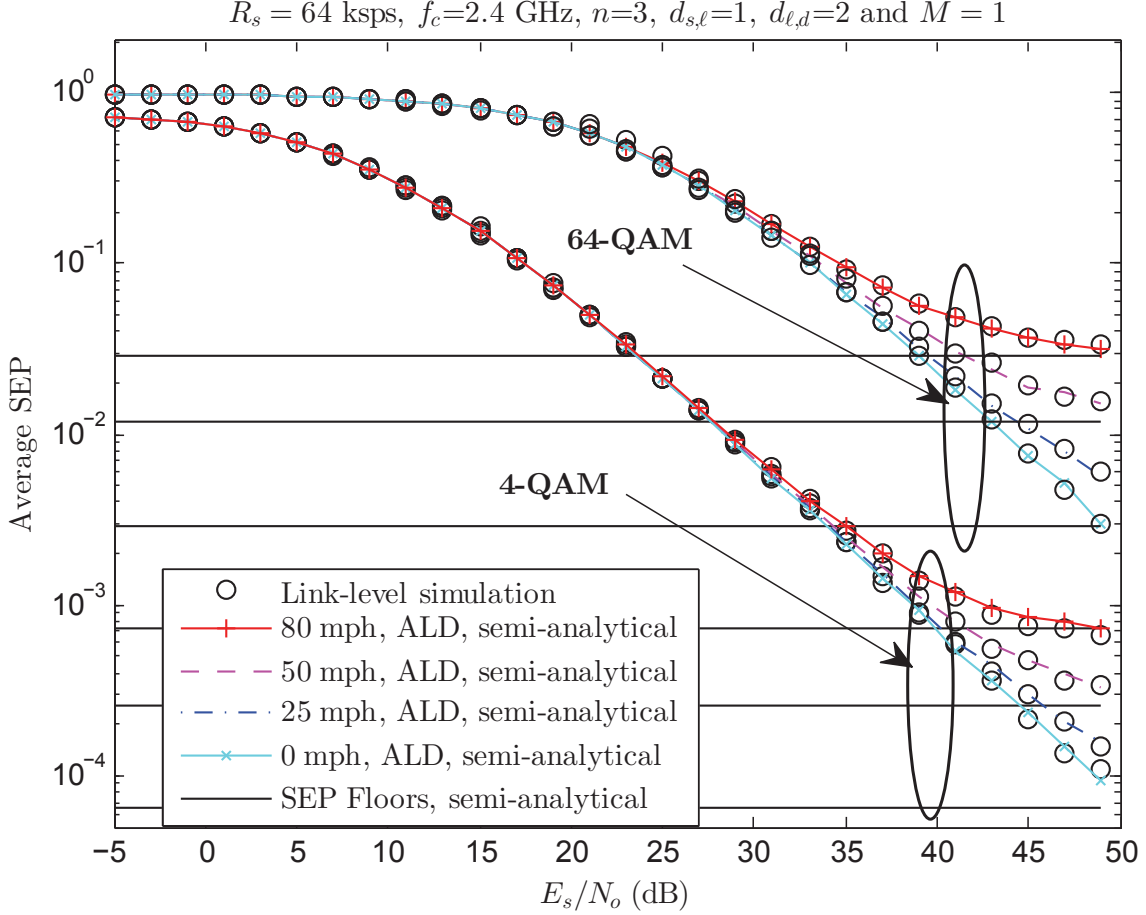


Figure 6.3. Average SEP versus E_s/N_o for $M = 1, 4$ and 64 QAM constellations, transmission data-rate $R_s = 64$ kbps, carrier frequency $f_c = 2.4$ GHz, path-loss exponent $n = 3$, normalized nodes distances $d_{s,\ell} = 1$ and $d_{\ell,d} = 2$.

gregate. Under these considerations, the overall end-to-end channel gain matrix is no longer orthogonal and the ALD provides correlated decision statistics with inter-transmit-antenna-interference (ITAI). Benefiting from the AR1 model, we have derived exact expressions for the decision statistics conditional SINRs, which have been directly used to analyze the system average SEP performance. As an impact of the nodes mobility or the ITAI, the system SEP performance is degraded and bounded by irreducible error floors no matter the number of the relays is. Moreover, as special case of static nodes network, we have shown that the end-to-end channel gain matrix reduces to its orthogonal version, the ITAI terms and the irreducible error floors vanish.

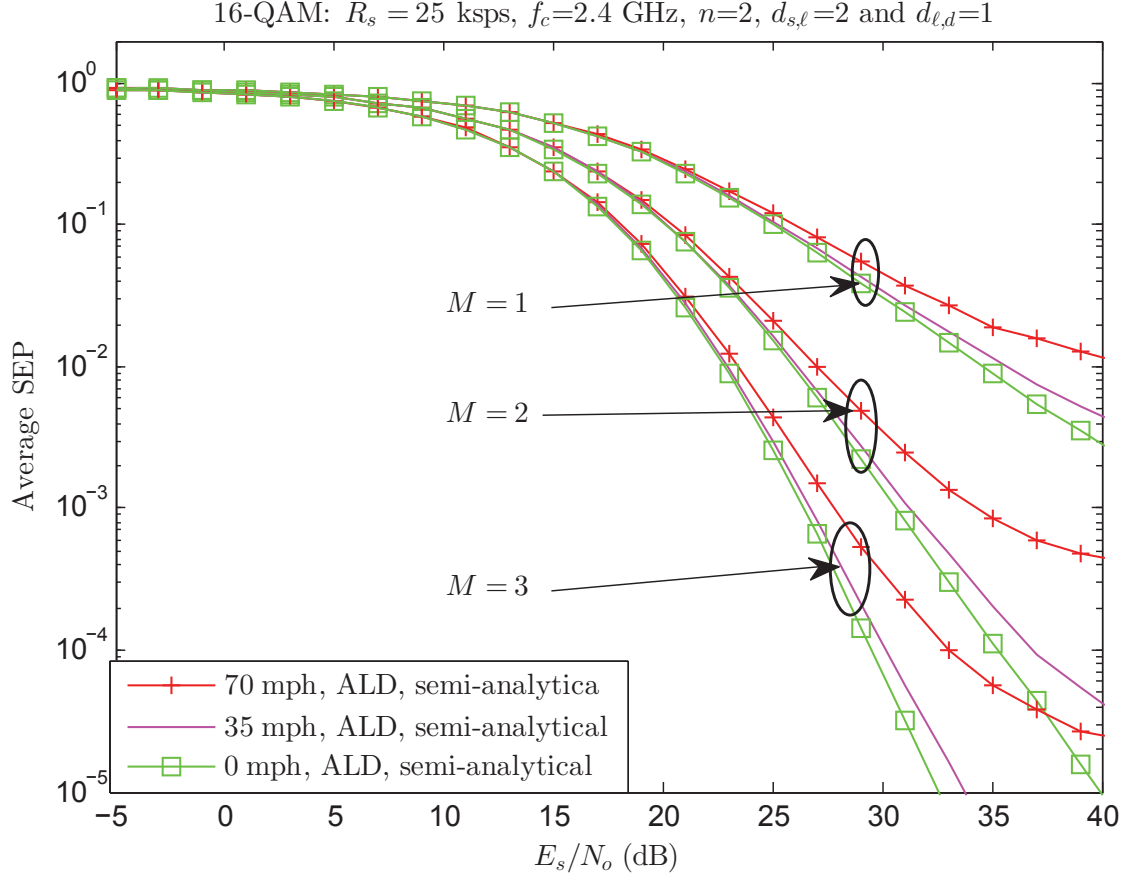


Figure 6.4. Average SEP versus E_s/N_o for $M = 1, 2$ and 3 , 16-QAM constellations, transmission data-rate $R_s = 25$ kbps, carrier frequency $f_c = 2.4$ GHz, path-loss exponent $n = 2$, normalized nodes distances $d_{s,\ell} = 2$ and $d_{\ell,d} = 1$.

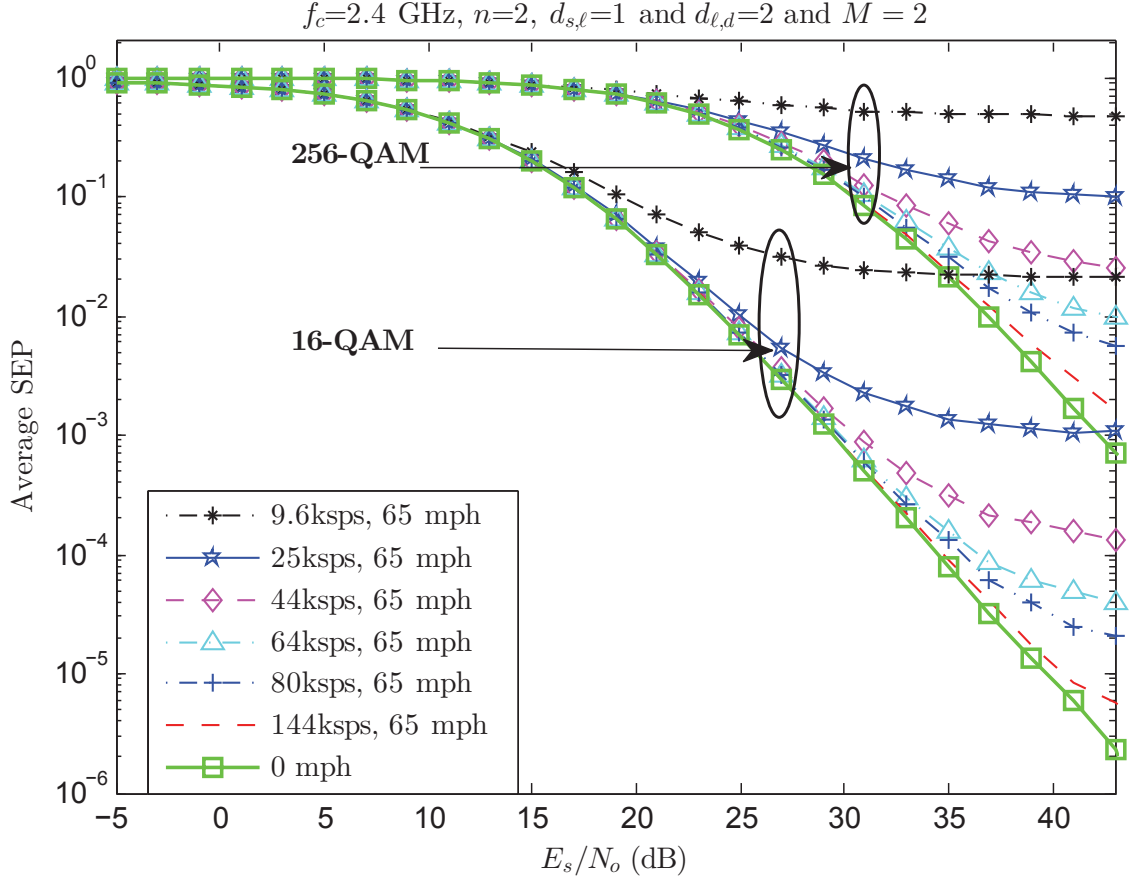


Figure 6.5. ALD Semi-analytic Average SEP versus E_s/N_o for $M = 2, 16$ and 256 QAM constellations, different transmission data-rates, carrier frequency $f_c = 2.4$ GHz, path-loss exponent $n = 2$, normalized nodes distances $d_{s,\ell} = 1$ and $d_{\ell,d} = 2$.

CHAPTER 7

Improved Performance Zero-Forcing Space-Time Decoder (ZFSTD) for High Mobility Alamouti-Type OSTBC Based AF Cooperative Systems: Decoder Design and SEP Analysis

7.1 Chapter Overview

In chapter 4, it has been shown that the SEP performance of a multiple-relay AF wireless cooperative system with Alamouti-OSTBC transmission, time-selective fading links and Alamouti's conventional space-time decoder (ALD) is severely degraded and experiences irreducible error floors. This is mainly because of the ITAI terms that appears in the ALD output's decision statistics and makes them non-separable. Based on that, we concluded that the ALD is not a suitable space-time decoder for such a system model with high nodes mobility and/or low data rates applications. Therefore, in this chapter, we propose another space-time decoder that can be applied at the destination, instead of the ALD, such that it is capable to provide separable decision statistics corresponding to the two transmitted symbols of the OSTBC matrix. In other words, it provides decision statistics without ITAI. The idea of this proposed decoder in this chapter is inspired by the notion of V-BLAST equalizers that have been proposed to perform data demultiplexing at the receiving side of MIMO communications systems [48]. Specifically, among the V-BLAST equalizers, we follow the idea of the zero-forcing-linear one to design the decoding matrix of our proposed space-time decoder. Therefore, now and on, we refer to this proposed decoder as Zero-Forcing-Space-Time-Decoder (ZFSTD). After employing the ZFSTD at the destination, we show that it achieves the required target and provides separable decision statistics. Moreover, based on these obtained statistics, we analyze the average SEP of our system model with the proposed

ZFSTD, which is also verified via real link-level simulation. As compared with the ALD, the ZFSTD provides remarkable SEP performance improvement so that it matches with that of the ALD in the quasi-static fading scenario. However, this comes at the expense of additional complexity over the ALD.

7.2 System Model

In this chapter we consider the same system model as in chapter 5 but instead of employing the ALD at the destination we propose to employ another space-time decoder, which we discuss its design and performance analysis in the following sections.

7.3 ZFSTD Decoding Matrix Design

The equalization matrix of the V-BLAST zero-forcing-equalizer, say \mathbf{G}^+ , is given as [48, Eq. (8)]

$$\mathbf{G}^+ = (\mathbf{G}^H \mathbf{G})^{-1} \mathbf{G}^H \quad (7.3.1)$$

where \mathbf{G} is the channel gain matrix of a MIMO system and $\{\cdot\}^{-1}$ denotes the matrix inverse. Now, based on our system model received signal vector in (6.2.10) and its end-to-end channel gain matrix \mathbf{H} in (6.2.12), we propose a zero-forcing-space-time-decoder (ZFSTD) that has a decoding matrix, say \mathbf{H}^+ , that follows the form of the V-BLAST zero-forcing-equalizer equalization matrix in (7.3.1) and given as

$$\mathbf{H}^+ = (\mathbf{H}^H \mathbf{H})^{-1} \mathbf{H}^H. \quad (7.3.2)$$

In order to write \mathbf{H}^+ in its ultimate form, we first multiply \mathbf{H}^H in (6.2.14) by \mathbf{H} in (6.2.12) to obtain

$$\mathbf{H}^H \mathbf{H} = \begin{bmatrix} \beta_1 & \zeta \\ \zeta^* & \beta_2 \end{bmatrix} \quad (7.3.3)$$

which is a 2×2 matrix and has the following inverse

$$(\mathbf{H}^H \mathbf{H})^{-1} = \frac{1}{\det(\mathbf{H}^H \mathbf{H})} \begin{bmatrix} \beta_2 & -\zeta \\ -\zeta^* & \beta_1 \end{bmatrix} \quad (7.3.4)$$

where

$$\det(\mathbf{H}^H \mathbf{H}) = \beta_1 \beta_2 - |\zeta|^2. \quad (7.3.5)$$

By substituting $(\mathbf{H}^H \mathbf{H})^{-1}$ in (7.3.4) and \mathbf{H}^H in (6.2.14) into (7.3.2), we obtain the proposed ZFSTD decoding matrix \mathbf{H}^+ as

$$\mathbf{H}^+ = \frac{1}{A} \begin{bmatrix} a_{11}^1 & a_{12}^1 & a_{11}^2 & a_{12}^2 & \cdots & a_{11}^M & a_{12}^M \\ a_{21}^1 & a_{22}^1 & a_{21}^2 & a_{22}^2 & \cdots & a_{21}^M & a_{22}^M \end{bmatrix} \quad (7.3.6)$$

where

$$\begin{aligned} A &= \beta_1 \beta_2 - |\zeta|^2 \\ a_{11}^\ell &= \beta_2 \mathcal{G} h_{1,\ell}^*(k) h_{\ell,d}^*(k) - \zeta \mathcal{G} h_{2,\ell}^*(k) h_{\ell,d}^*(k) \\ a_{21}^\ell &= -\zeta^* \mathcal{G} h_{1,\ell}^*(k) h_{\ell,d}^*(k) + \beta_1 \mathcal{G} h_{2,\ell}^*(k) h_{\ell,d}^*(k) \\ a_{12}^\ell &= \beta_2 \mathcal{G} h_{2,\ell}(k+1) h_{\ell,d}(k+1) + \zeta \mathcal{G} h_{1,\ell}(k+1) h_{\ell,d}(k+1) \\ a_{22}^\ell &= -\zeta^* \mathcal{G} h_{2,\ell}(k+1) h_{\ell,d}(k+1) - \beta_1 \mathcal{G} h_{1,\ell}(k+1) h_{\ell,d}(k+1). \end{aligned}$$

7.4 ZFSTD Output Decision Statistics

We can now apply the ZFSTD at the destination just by multiplying the received signal vector in (6.2.10) by the decoding matrix \mathbf{H}^+ in (7.3.6). The resulted two elements from this multiplication are the ZFSTD's decision statistics, which can be given, after some

simplifications, as

$$\tilde{z}_1 = \underbrace{\text{desired signal of } x_1}_{x_1} + \overbrace{\frac{\beta_2}{\beta_1\beta_2 - |\zeta|^2}\tilde{n}_1 - \frac{\zeta}{\beta_1\beta_2 - |\zeta|^2}\tilde{n}_2}^{\text{effective-white-noise-term}_1 \triangleq \tilde{v}_1} \quad (7.4.1)$$

and

$$\tilde{z}_2 = \underbrace{\text{desired signal of } x_2}_{x_2} + \overbrace{\frac{-\zeta^*}{\beta_1\beta_2 - |\zeta|^2}\tilde{n}_1 + \frac{\beta_1}{\beta_1\beta_2 - |\zeta|^2}\tilde{n}_2}^{\text{effective-white-noise-term}_1 \triangleq \tilde{v}_2} \quad (7.4.2)$$

It is clear from (7.4.1) and (7.4.2) that the decision statistics of the proposed ZFSTD are separable (non interfering) corresponding to x_1 and x_2 , respectively, even though the network fading links are time-selective. Therefore, this decoder has accomplished its required target.

7.5 ZFSTD SEP Performance

The q -QAM demodulator uses \tilde{z}_1 and \tilde{z}_2 to make decisions about x_1 and x_2 , respectively. Therefore, in order to analyze the SEP at the output of the q -QAM demodulator of our system model with the proposed ZFSTD (say P_e^{ZFSTD}), we need first to obtain the conditional SNRs of the statistics \tilde{z}_1 and \tilde{z}_2 . From (7.4.1) and (7.4.2), we can obtain these SNRs conditioned on the channels gains in the set \mathcal{S} , respectively, as

$$\text{SNR}_{\tilde{z}_1}|\mathcal{S} = \frac{|x_1|^2}{P(\tilde{v}_1)} = \frac{|\beta_1\beta_2 - |\zeta|^2|^2}{2|\beta_2|^2\eta_1 - 2|\zeta|^2\eta_2} \frac{E_s}{N_o} \quad (7.5.1)$$

and

$$\text{SNR}_{\tilde{z}_2}|\mathcal{S} = \frac{|x_2|^2}{P(\tilde{v}_2)} = \frac{|\beta_1\beta_2 - |\zeta|^2|^2}{2|\beta_1|^2\eta_2 - 2|\zeta|^2\eta_1} \frac{E_s}{N_o} \quad (7.5.2)$$

By assuming equiprobable transmission for x_1 and x_2 and directly using the q -QAM AWGN SEP expression in (6.3.1), we can obtain P_e^{ZFSTD} conditioned on \mathcal{S} as

$$P_e^{\text{ZFSTD}}|\mathcal{S} = \frac{1}{2} \left[1 - \left(1 - 2 \left(1 - \frac{1}{\sqrt{q}} \right) Q \left(\sqrt{\frac{3}{q-1}} \frac{|\beta_1 \beta_2 - |\zeta|^2|^2 E_s}{2|\beta_2|^2 \eta_1 - 2|\zeta|^2 \eta_2 N_o} \right) \right)^2 \right] \\ + \frac{1}{2} \left[1 - \left(1 - 2 \left(1 - \frac{1}{\sqrt{q}} \right) Q \left(\sqrt{\frac{3}{q-1}} \frac{|\beta_1 \beta_2 - |\zeta|^2|^2 E_s}{2|\beta_1|^2 \eta_2 - 2|\zeta|^2 \eta_1 N_o} \right) \right)^2 \right] \quad (7.5.3)$$

and its average can be computed following the Monte carlo method followed in section 6.4 as

$$\bar{P}_e^{\text{ZFSTD}} = \frac{1}{2} \left[1 - \frac{1}{N} \sum_{j=1}^N \left[\left(1 - 2 \left(1 - \frac{1}{\sqrt{q}} \right) Q \left(\sqrt{\frac{3}{q-1}} \frac{|\beta_1^j \beta_2^j - |\zeta^j|^2|^2 E_s}{2|\beta_2^j|^2 \eta_1^j - 2|\zeta^j|^2 \eta_2^j N_o} \right) \right)^2 \right] \right] \\ + \frac{1}{2} \left[1 - \frac{1}{N} \sum_{j=1}^N \left[\left(1 - 2 \left(1 - \frac{1}{\sqrt{q}} \right) Q \left(\sqrt{\frac{3}{q-1}} \frac{|\beta_1^j \beta_2^j - |\zeta^j|^2|^2 E_s}{2|\beta_1^j|^2 \eta_2^j - 2|\zeta^j|^2 \eta_1^j N_o} \right) \right)^2 \right] \right] \quad (7.5.4)$$

In the numerical results section it will be shown that (7.5.4) numerically matches with the quasi-static fading SEP given in (6.5.5). This means that the proposed ZFSTD completely removes the nodes mobility impact on the system SEP performance. However, this performance improvement by the ZFSTD comes at the expense of further decoding complexity required at the destination. This additional decoding complexity of the ZFSTD over the ALD is obvious if we compare their decoding matrices: \mathbf{H}^+ in (7.3.6) requires more operations to be constructed at the destination than that of $\mathbf{H}^{\mathcal{H}}$ in (6.2.14) .

7.6 ZFSTD under Static-Nodes Case

Under the special case assumption of quasi-static fading within the network under study (i.e., $\rho_{a,b} = 1 \forall (a,b)$), the proposed ZFSTD reduces to the optimal version of the ALD. This is obvious because, under this condition, the ZFSTD decoding matrix \mathbf{H}^+ in (7.3.6)

reduces as

$$\mathbf{H}^+ = \frac{1}{\beta_2} \mathbf{H}^{\text{static}\mathcal{H}} \quad (7.6.1)$$

where $\mathbf{H}^{\text{static}\mathcal{H}}$ is the decoding matrix of the optimal version of the ALD obtained in quasi-static fading scenario and given in (6.5.3). Moreover, under this scenario, the conditional SEP of the ZFSTD in (7.5.3) reduces to $P_e^{\text{static-nodes}}|\mathcal{S}^{\text{static}}$ in (6.5.5).

7.7 Numerical Results and Simulation

Here, we present numerical results along with real link-level simulation results to investigate the performance improvement by the proposed ZFSTD over the ALD and also to verify the obtained theoretical results. From Fig. 7.1 we can notice that, as compared with the severely degraded performance of the ALD due to nodes mobility with relative speeds of 65 mph, the performance of the proposed ZFSTD at that speed completely matches the system performance in the case of static nodes (0 mph relative speeds). This observation is valid for any number of relays M . Also, the SEP performance of the ZFSTD plotted using (7.5.4) show good agreement with the real link-level simulation results.

In Fig. 7.2, we compare the average SEP performance, versus the relative speeds among the nodes, between the ALD and the ZFSTD for $M=1$ and 2 and different data-rate values. It is clear from this figure that the average SEP of the ALD increases with increasing the relative speeds among the cooperating nodes while that of the ZFSTD is not affected by both the relative speeds and the data-rate values and also provides lower average SEP values.

7.8 Conclusion

In order to overcome the impact of the time-selective fading on the SEP performance of a multiple-relay AF cooperative system with Alamouti OSTBC transmission at the source and its traditional decoder at the destination (ALD), we have proposed in this chapter a zero-forcing space-time-decoder (ZFSTD) to be applied at the destination instead of ALD

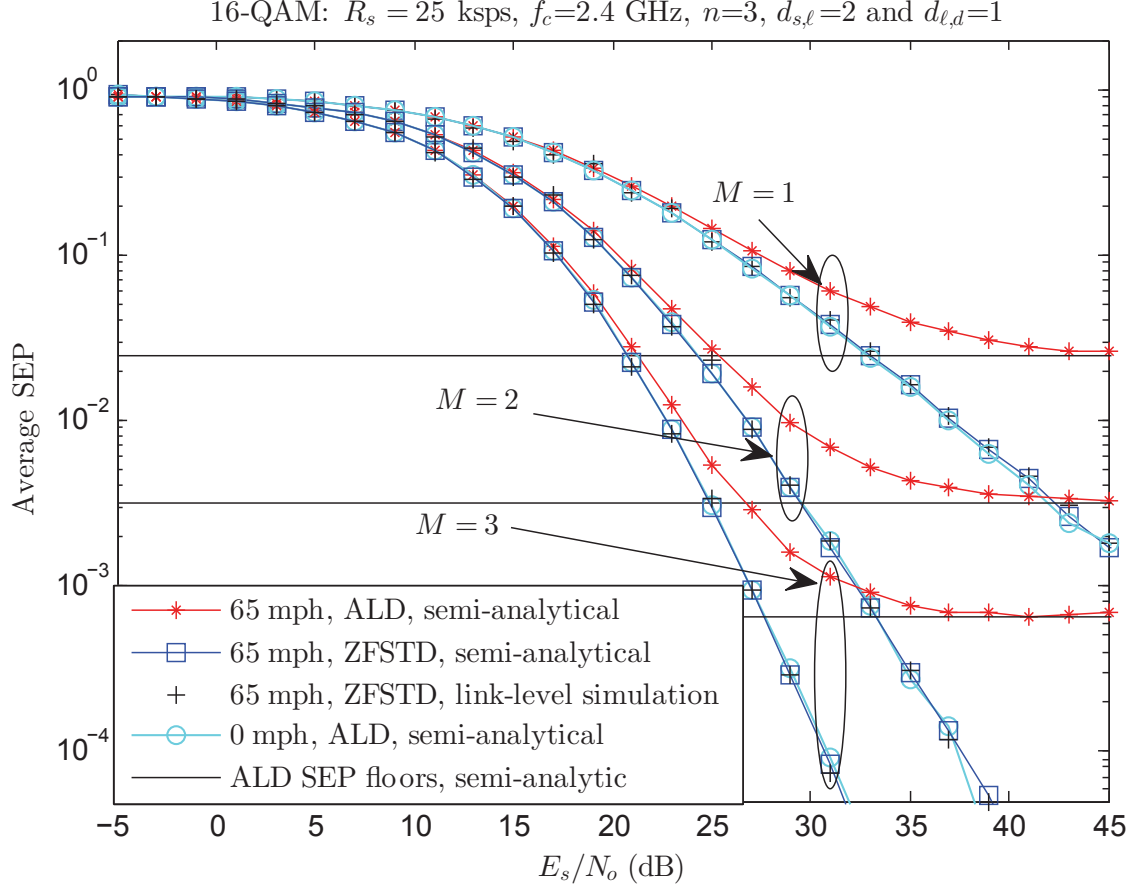


Figure 7.1. Average SEP versus E_s/N_o for both ZFSTD and ALD. $M = 1$ 2 and 3, QAM constellations size of 16, transmission data-rate $R_s = 25$ kbps, carrier frequency $f_c = 2.4$ GHz, path-loss exponent $n = 3$, normalized nodes distances $d_{s,\ell} = 2$ and $d_{\ell,d} = 1$.

and provide non interfering decision statistics. The idea of this proposed decoder is inspired by the idea of the V-BLAST zero-forcing-linear equalizer required for data demultiplexing in MIMO systems. Specifically, we have derived the decoding matrix of that decoder and obtain its output decision statistics of this proposed decoder. From these statistics we have then derived their conditional SNRs and the system SEP. As compared with the ALD performance, we have shown that the ZFSTD completely removes the impact of the time-selective fading but this comes at the expenses of additional decoding Complexity.

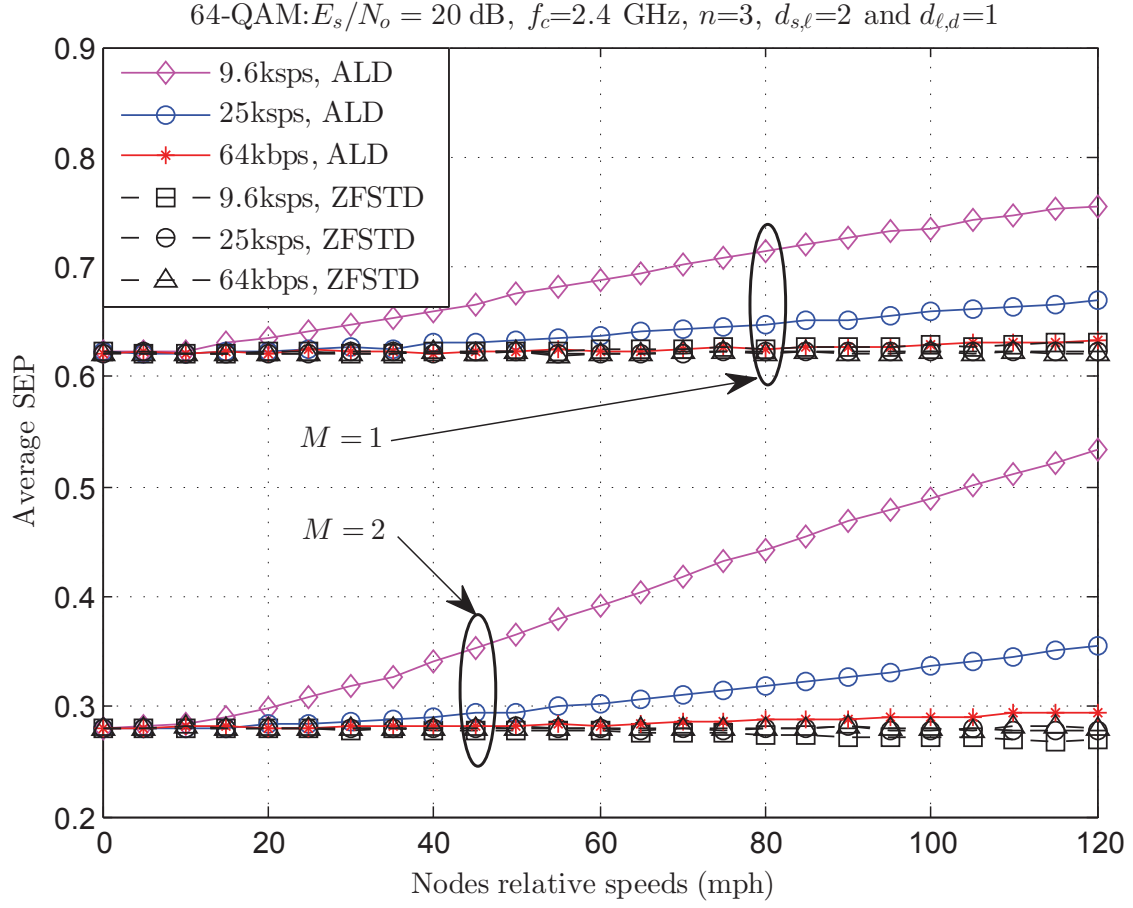


Figure 7.2. Average SEP versus nodes relative speeds for both ZFSTD and ALD with $E_s/N_o = 20$ dB, different transmission dat-rate values, $M = 1$ and 2 , QAM constellations size of 64 , carrier frequency $f_c = 2.4$ GHz, path-loss exponent $n = 3$, normalized nodes distances $d_{s,\ell} = 2$ and $d_{\ell,d} = 1$.

CHAPTER 8

Improved Performance Low-Complexity Sub-Optimal Space-Time-Decoder (SOSTD) for High Mobility Alamouti-Type OSTBC Based AF Cooperative Systems: Decoder Design and SEP Analysis

8.1 Chapter Overview

The proposed ZFSTD in chapter 6 has shown a performance improvement over the traditional Alamouti decoder (ALD) which are employed in a wireless cooperative system with multiple relays, AF protocol, time-selective fading (due to nodes mobility) and Alamouti-OSTBC transmission at the source node. This performance improvement is considerable so that it is equivalent with that of the optimal version of the ALD obtained in case of non-moving nodes network scenario (i.e., quasi-static fading). However, we have also shown in chapter 6 that this improvement requires higher processing complexity at the destination node. Therefore, in this chapter, we propose another space-time-decoder that has same complexity level as the ALD and provides very close performance to that provided by the ZFSTD. We call this low-complexity decoder as sub-optimal space-time-decoder (SOSTD). It is sub-optimal because despite it provides separable decision statistics like the ZFSTD, these statistics are statistically correlated like the ALD in the time-selective fading case.

8.2 System Model

In this chapter we consider the same system model as in chapter 5 and 6 but instead of employing the ALD or the ZFSTD at the destination we propose to employ another space-time-decoder, which we discuss its design and performance analysis in the following sections.

8.3 SOSTD Decoding Matrix Design

The idea of the proposed space-time-decoder in this chapter is based on finding a $2 \times 2M$ decoding matrix (say \mathbf{D}) such that the resulted two decision statistics from multiplying this matrix by the destination's received signal vector \mathbf{Y}_d in (6.2.11) are separable corresponding to the two transmitted symbols x_1 and x_2 . This basically can be accomplished if the resulted 2×2 matrix from multiplying \mathbf{D} by \mathbf{H} is diagonal. Therefore, we start solving for \mathbf{D} such that

$$\mathbf{D}\mathbf{H} \triangleq \begin{bmatrix} \beta_1^I & 0 \\ 0 & \beta_2^I \end{bmatrix} \quad (8.3.1)$$

where β_1^I and β_2^I are the main-diagonal elements that will be specified later after obtaining \mathbf{D}^1 . In order to simplify the problem of solving for \mathbf{D} , we first solve for a single-relay case (say ℓ th relay) by obtaining \mathbf{D}_ℓ and then extend the result for the multiple-relay case. For the ℓ th single-relay network (or dual-hop network), the ℓ th component, of the matrix \mathbf{H} in (6.2.12), reduces to

$$\mathbf{H}_\ell = \begin{bmatrix} \mathcal{G}h_{1,\ell}(k)h_{\ell,d}(k) & \mathcal{G}h_{2,\ell}(k)h_{\ell,d}(k) \\ \mathcal{G}h_{2,\ell}^*(k+1)h_{\ell,d}^*(k+1) & -\mathcal{G}h_{1,\ell}^*(k+1)h_{\ell,d}^*(k+1) \end{bmatrix} \quad (8.3.2)$$

and accordingly, we need

$$\mathbf{D}_\ell \mathbf{H}_\ell = \begin{bmatrix} \mathcal{D}_{\ell 11} & \mathcal{D}_{\ell 12} \\ \mathcal{D}_{\ell 21} & \mathcal{D}_{\ell 22} \end{bmatrix} \mathbf{H}_\ell = \begin{bmatrix} \beta_{\ell 1}^I & 0 \\ 0 & \beta_{\ell 2}^I \end{bmatrix} \quad (8.3.3)$$

where $\mathcal{D}_{\ell 11}$, $\mathcal{D}_{\ell 12}$, $\mathcal{D}_{\ell 21}$ and $\mathcal{D}_{\ell 22}$ are the elements of \mathbf{D}_ℓ and $\beta_{\ell 1}^I$ and $\beta_{\ell 2}^I$ are the main-diagonal elements of the resulted diagonal matrix. Solving for \mathbf{D}_ℓ that satisfies (8.3.3) means obtaining the intended proposed SOSTD decoding matrix for a dual-hop AF cooperative network with

¹It should be noted that solving for \mathbf{D} is only based on achieving (8.3.1) no matter how the statistical relationship between the effective noise components of the resulted decision statistics would be. Achieving (8.3.1) only grants obtaining non interfering decision statistics, which is the required target by the proposed decoder in this chapter.

Alamouti-OSTBC transmission and time-selective fading for both hops, which we do in the following. Now, in order to find the elements of \mathbf{D}_ℓ that achieves (8.3.3), we can first obtain from (8.3.3) the following two equations

$$\mathcal{D}_{\ell_{11}} \mathcal{G} h_{2,\ell}(k) h_{\ell,d}(k) + \mathcal{D}_{\ell_{12}} (-\mathcal{G} h_{1,\ell}^*(k+1) h_{\ell,d}^*(k+1)) = 0 \quad (8.3.4)$$

$$\mathcal{D}_{\ell_{21}} \mathcal{G} h_{1,\ell}(k) h_{\ell,d}(k) + \mathcal{D}_{\ell_{22}} \mathcal{G} h_{2,\ell}^*(k+1) h_{\ell,d}^*(k+1) = 0 \quad (8.3.5)$$

From (8.3.4) and (8.3.5), we can write $\mathcal{D}_{\ell_{11}}$ in terms of $\mathcal{D}_{\ell_{12}}$ and $\mathcal{D}_{\ell_{22}}$ in terms of $\mathcal{D}_{\ell_{21}}$, respectively, as

$$\mathcal{D}_{\ell_{11}} = \frac{\mathcal{D}_{\ell_{12}} \mathcal{G} h_{1,\ell}^*(k+1) h_{\ell,d}^*(k+1)}{\mathcal{G} h_{2,\ell}(k) h_{\ell,d}(k)} \quad (8.3.6)$$

$$\mathcal{D}_{\ell_{22}} = \frac{-\mathcal{D}_{\ell_{21}} \mathcal{G} h_{1,\ell}(k) h_{\ell,d}(k)}{\mathcal{G} h_{2,\ell}^*(k+1) h_{\ell,d}^*(k+1)}. \quad (8.3.7)$$

Based on (8.3.6) and (8.3.7), the matrix \mathbf{D}_ℓ that can satisfy (8.3.3) can be given in the following preliminary form

$$\mathbf{D}_\ell = \begin{bmatrix} \frac{\mathcal{D}_{\ell_{12}} \mathcal{G} h_{1,\ell}^*(k+1) h_{\ell,d}^*(k+1)}{\mathcal{G} h_{2,\ell}(k) h_{\ell,d}(k)} & \mathcal{D}_{\ell_{12}} \\ \mathcal{D}_{\ell_{21}} & \frac{-\mathcal{D}_{\ell_{21}} \mathcal{G} h_{1,\ell}(k) h_{\ell,d}(k)}{\mathcal{G} h_{2,\ell}^*(k+1) h_{\ell,d}^*(k+1)} \end{bmatrix}. \quad (8.3.8)$$

It is clear now that the form of \mathbf{D}_ℓ in (8.3.8) reduces the problem to solving only for two parameters: $\mathcal{D}_{\ell_{12}}$ and $\mathcal{D}_{\ell_{21}}$. We can now start our second step in deriving the ultimate form for \mathbf{D}_ℓ by first revealing the following corollary

Theorem 8.3.1. *The SNRs of the decision statistics resulted by applying our proposed SOSTD with the decoding matrix in (8.3.8) at the destination of the dual-hop relaying network understudy are not functions of both $\mathcal{D}_{\ell_{12}}$ and $\mathcal{D}_{\ell_{21}}$.*

Proof. The received signal vector through the ℓ th relay dual-hop link can be obtained from

(6.2.10) as

$$\begin{bmatrix} y_{\ell,d}(k) \\ y_{\ell,d}^*(k+1) \end{bmatrix} = \mathbf{H}_\ell \begin{bmatrix} x_1 \\ x_2 \end{bmatrix} + \begin{bmatrix} \mathcal{G}h_{\ell,d}(k)n_{s,\ell}(k) + n_{\ell,d}(k) \\ \mathcal{G}h_{\ell,d}^*(k+1)n_{s,\ell}^*(k+1) + n_{\ell,d}^*(k+1) \end{bmatrix}. \quad (8.3.9)$$

The proposed SOSTD is applied just by multiplying (8.3.9) by the decoding matrix \mathbf{D}_ℓ in (8.3.8), and its resulted two decision statistics (say \tilde{r}_1^ℓ and \tilde{r}_2^ℓ) can be given, respectively, as

$$\begin{aligned} \tilde{r}_1^\ell = & \overbrace{\left(\frac{\mathcal{D}_{\ell_{12}} \mathcal{G}h_{1,\ell}^*(k+1)h_{\ell,d}^*(k+1)}{\mathcal{G}h_{2,\ell}(k)h_{\ell,d}(k)} \mathcal{G}h_{1,\ell}(k)h_{\ell,d}(k) + \mathcal{D}_{\ell_{12}} \mathcal{G}h_{2,\ell}^*(k+1)h_{\ell,d}^*(k+1) \right)}^{\text{desired signal of } x_1} x_1 + \\ & \overbrace{\frac{\mathcal{D}_{\ell_{12}} \mathcal{G}h_{1,\ell}^*(k+1)h_{\ell,d}^*(k+1) \mathcal{G}h_{\ell,d}(k)n_{s,\ell}(k) + \mathcal{D}_{\ell_{12}} \mathcal{G}h_{1,\ell}^*(k+1)h_{\ell,d}^*(k+1)n_{\ell,d}(k)}{\mathcal{G}h_{2,\ell}(k)h_{\ell,d}(k)}}}_{\text{effective-white-noise-term}_1} + \\ & \mathcal{D}_{\ell_{12}} \mathcal{G}h_{\ell,d}^*(k+1)n_{s,\ell}^*(k+1) + \mathcal{D}_{\ell_{12}} n_{\ell,d}^*(k+1) \end{aligned} \quad (8.3.10)$$

$$\begin{aligned} \tilde{r}_2^\ell = & \overbrace{\left(\frac{\mathcal{D}_{\ell_{21}} \mathcal{G}h_{1,\ell}(k)h_{\ell,d}(k)}{\mathcal{G}h_{2,\ell}^*(k+1)h_{\ell,d}^*(k+1)} \mathcal{G}h_{1,\ell}^*(k+1)h_{\ell,d}^*(k+1) + \mathcal{D}_{\ell_{21}} \mathcal{G}h_{2,\ell}(k)h_{\ell,d}(k) \right)}^{\text{desired signal of } x_2} x_2 \\ & - \overbrace{\frac{\mathcal{D}_{\ell_{21}} \mathcal{G}h_{1,\ell}(k)h_{\ell,d}(k) \mathcal{G}h_{\ell,d}^*(k+1)n_{s,\ell}^*(k+1) + \mathcal{D}_{\ell_{21}} \mathcal{G}h_{1,\ell}(k)h_{\ell,d}(k)n_{\ell,d}^*(k+1)}{\mathcal{G}h_{2,\ell}^*(k+1)h_{\ell,d}^*(k+1)}}}_{\text{effective-white-noise-term}_2} + \\ & \mathcal{D}_{\ell_{21}} \mathcal{G}h_{\ell,d}(k)n_{s,\ell}(k) + \mathcal{D}_{\ell_{21}} n_{\ell,d}(k). \end{aligned} \quad (8.3.11)$$

The SNR of each of the decision statistics in (8.3.10) and (8.3.11) can be obtained as the ratio of the desired signal power over the effective-white-noise variance. Based on this and also on the fact that the white noise components $n_{s,\ell}(k)$, $n_{s,\ell}(k+1)$, $n_{\ell,d}(k)$ and $n_{\ell,d}(k+1)$ are independent and with equal variance of N_o , and after doing some manipulations and simplifications, we obtain the conditional SNRs of \tilde{r}_1^ℓ and \tilde{r}_2^ℓ conditioned on the channel gains in the set $\mathcal{S} = \{h_{1,\ell}(k), h_{1,\ell}(k+1), h_{2,\ell}(k), h_{2,\ell}(k+1), h_{\ell,d}(k), h_{\ell,d}(k+1)\}$, respectively,

as

$$\begin{aligned}
\gamma_{\tilde{r}_1^\ell} = & E_s(|\mathcal{G}h_{1,\ell}^*(k+1)h_{\ell,d}^*(k+1)|^2|\mathcal{G}h_{1,\ell}(k)h_{\ell,d}(k)|^2 \\
& + |\mathcal{G}h_{2,\ell}(k)h_{\ell,d}(k)|^2|\mathcal{G}h_{2,\ell}^*(k+1)h_{\ell,d}^*(k+1)|^2) / \\
& (2N_o(|\mathcal{G}h_{1,\ell}^*(k+1)h_{\ell,d}^*(k+1)|^2(\mathcal{G}^2|h_{\ell,d}(k)|^2 \\
& + 1) + |\mathcal{G}h_{2,\ell}(k)h_{\ell,d}(k)|^2(\mathcal{G}^2|h_{\ell,d}(k+1)|^2 + 1)))
\end{aligned} \tag{8.3.12}$$

$$\begin{aligned}
\gamma_{\tilde{r}_2^\ell} = & E_s(|\mathcal{G}h_{2,\ell}(k)h_{\ell,d}(k)|^2|\mathcal{G}h_{2,\ell}(k+1)h_{\ell,d}(k+1)|^2 \\
& + |\mathcal{G}h_{1,\ell}(k)h_{\ell,d}(k)|^2|\mathcal{G}h_{1,\ell}^*(k+1)h_{\ell,d}^*(k+1)|^2) \\
& / (2N_o(|\mathcal{G}h_{1,\ell}(k)h_{\ell,d}(k)|^2(\mathcal{G}^2|h_{\ell,d}(k+1)|^2 + 1) \\
& + |\mathcal{G}h_{2,\ell}^*(k+1)h_{\ell,d}^*(k+1)|^2(\mathcal{G}^2|h_{\ell,d}(k)|^2 + 1))).
\end{aligned} \tag{8.3.13}$$

It is clear from (8.3.12) and (8.3.13) that $\gamma_{\tilde{r}_1^\ell}$ and $\gamma_{\tilde{r}_2^\ell}$ are free of $\mathcal{D}_{\ell_{12}}$ and $\mathcal{D}_{\ell_{21}}$, which completes the proof. \square

Now, based on the above corollary and in order to eliminate the denominators in (8.3.8) we choose

$$\mathcal{D}_{\ell_{12}} = \mathcal{G}h_{2,\ell}(k)h_{\ell,d}(k) \tag{8.3.14}$$

and

$$\mathcal{D}_{\ell_{21}} = \mathcal{G}h_{2,\ell}^*(k+1)h_{\ell,d}^*(k+1) \tag{8.3.15}$$

Accordingly, the ultimate form of \mathbf{D}_ℓ is given as

$$\mathbf{D}_\ell = \begin{bmatrix} \mathcal{G}h_{1,\ell}^*(k+1)h_{\ell,d}^*(k+1) & \mathcal{G}h_{2,\ell}(k)h_{\ell,d}(k) \\ \mathcal{G}h_{2,\ell}^*(k+1)h_{\ell,d}^*(k+1) & -\mathcal{G}h_{1,\ell}(k)h_{\ell,d}(k) \end{bmatrix}. \tag{8.3.16}$$

By substituting (8.3.16) and (8.3.2) into (8.3.3), we obtain $\beta_{\ell_1}^I$ and $\beta_{\ell_2}^I$ as

$$\beta_{\ell_1}^I = \beta_{\ell_2}^I = \mathcal{G}^2 h_{1,\ell}^*(k+1) h_{\ell,d}^*(k+1) h_{1,\ell}(k) h_{\ell,d}(k) + \mathcal{G}^2 h_{2,\ell}(k) h_{\ell,d}(k) h_{2,\ell}^*(k+1) h_{\ell,d}^*(k+1). \quad (8.3.17)$$

Finally, for our M -relay network model, we can obtain the proposed SOSTD's decoding matrix \mathbf{D} defined in (8.3.1), by extension, as $\mathbf{D} = [\mathbf{D}_1, \mathbf{D}_2, \dots, \mathbf{D}_M]$ which can be written as

$$\mathbf{D} = \begin{bmatrix} \mathcal{G} h_{1,1}^*(k+1) h_{1,d}^*(k+1) & \mathcal{G} h_{2,1}^*(k+1) h_{1,d}^*(k+1) \\ \mathcal{G} h_{2,1}(k) h_{1,d}(k) & -\mathcal{G} h_{1,1}(k) h_{1,d}(k) \\ \mathcal{G} h_{1,2}^*(k+1) h_{2,d}^*(k+1) & \mathcal{G} h_{2,2}^*(k+1) h_{2,d}^*(k+1) \\ \mathcal{G} h_{2,2}(k) h_{2,d}(k) & -\mathcal{G} h_{1,2}(k) h_{2,d}(k) \\ \vdots & \vdots \\ \mathcal{G} h_{1,M}^*(k+1) h_{M,d}^*(k+1) & \mathcal{G} h_{2,M}^*(k+1) h_{M,d}^*(k+1) \\ \mathcal{G} h_{2,M}(k) h_{M,d}(k) & -\mathcal{G} h_{1,M}(k) h_{M,d}(k) \end{bmatrix}^T \quad (8.3.18)$$

8.4 SOSTD Output Decision Statistics

The decision statistic vector at the output of this proposed decoder, say $\tilde{\mathbf{R}}_d = [\tilde{r}_1, \tilde{r}_2]^T$, can be obtained by multiplying the received signal vector \mathbf{Y}_d in (6.2.10) by the decoding matrix \mathbf{D} in (8.3.18) as

$$\underbrace{\begin{bmatrix} \tilde{r}_1 \\ \tilde{r}_2 \end{bmatrix}}_{\tilde{\mathbf{R}}_d} \triangleq \mathbf{D} \mathbf{Y}_d = \underbrace{\begin{bmatrix} \beta^I & 0 \\ 0 & \beta^I \end{bmatrix}}_{\mathbf{DH}} \underbrace{\begin{bmatrix} x_1 \\ x_2 \end{bmatrix}}_{\mathbf{Y}_d} + \underbrace{\begin{bmatrix} \tilde{w}_1 \\ \tilde{w}_2 \end{bmatrix}}_{\mathbf{DN}_d \triangleq \tilde{\mathbf{W}}_d} \quad (8.4.1)$$

where

$$\beta^I = \sum_{\ell=1}^M \mathcal{G}^2 h_{1,\ell}^*(k+1) h_{\ell,d}^*(k+1) h_{1,\ell}(k) h_{\ell,d}(k) + \mathcal{G}^2 h_{2,\ell}(k) h_{\ell,d}(k) h_{2,\ell}^*(k+1) h_{\ell,d}^*(k+1) \quad (8.4.2)$$

$$\begin{aligned} \tilde{w}_1 = \sum_{\ell=1}^M \bigg(& \mathcal{G}^2 h_{1,\ell}^*(k+1) h_{\ell,d}^*(k+1) h_{\ell,d}(k) n_{s,\ell}(k) + \mathcal{G} h_{1,\ell}^*(k+1) h_{\ell,d}^*(k+1) n_{\ell,d}(k) + \\ & \mathcal{G}^2 h_{2,\ell}(k) h_{\ell,d}(k) h_{\ell,d}^*(k+1) n_{s,\ell}^*(k+1) + \mathcal{G} h_{2,\ell}(k) h_{\ell,d}(k) n_{\ell,d}^*(k+1) \bigg) \end{aligned} \quad (8.4.3)$$

$$\begin{aligned} \tilde{w}_2 = \sum_{\ell=1}^M \bigg(& \mathcal{G}^2 h_{2,\ell}^*(k+1) h_{\ell,d}^*(k+1) h_{\ell,d}(k) n_{s,\ell}(k) + \mathcal{G} h_{2,\ell}^*(k+1) h_{\ell,d}^*(k+1) n_{\ell,d}(k) - \\ & \mathcal{G}^2 h_{1,\ell}(k) h_{\ell,d}(k) h_{\ell,d}^*(k+1) n_{s,\ell}^*(k+1) - \mathcal{G} h_{1,\ell}(k) h_{\ell,d}(k) n_{\ell,d}^*(k+1) \bigg) \end{aligned} \quad (8.4.4)$$

From (8.4.1), we can write the decision statistics at the output of the proposed SOSTD as follows

$$\tilde{r}_1 = \beta^I x_1 + \tilde{w}_1 \quad (8.4.5)$$

$$\tilde{r}_2 = \beta^I x_2 + \tilde{w}_2 \quad (8.4.6)$$

which clarifies that they are separable (i.e., without ITAI) for x_1 and x_2 , respectively, and thus, the proposed decoder has achieved its target. As will be shown later in the numerical results section, by this separation the decoder provides considerable SEP improvement as compared with the ALD for any number of relays. In addition, this performance improvement does not require any additional decoding complexity at the destination. This is clear because the decoding matrices of both decoders (\mathbf{D} in (8.3.18) and $\mathbf{H}^{\mathcal{H}}$ in (6.2.14)) share same elements (i.e, require same complexity level of construction at the destination). It is also worthwhile to mention that despite that the proposed decoder provides separable decision statistics (like the optimal version of the ALD in the quasi-static fading case), it is still suboptimal because its decision statistics' noise terms \tilde{w}_1 and \tilde{w}_2 are statistically correlated with the following conditional covariance

$$\begin{aligned} \mathbf{COV}(\tilde{w}_1, \tilde{w}_2) = \mathcal{G}^2 N_o \sum_{\ell=1}^M & (h_{2,\ell}(k+1) h_{1,\ell}^*(k+1) |h_{\ell,d}(k+1)|^2 \\ & - h_{1,\ell}^*(k) h_{2,\ell}(k) |h_{\ell,d}(k)|^2). \end{aligned}$$

8.5 SOSTD SEP Performance

In order to analyze the SEP at the output of the q -QAM demodulator that uses the decision statistics \tilde{r}_1 and \tilde{r}_2 to detect x_1 and x_2 , respectively, we need first to obtain the effective SNRs of these statistics, which we can obtain them from (8.4.5) and (8.4.6) conditioned on $\mathcal{S} = \{h_{1,\ell}(k), h_{1,\ell}(k+1), h_{2,\ell}(k), h_{2,\ell}(k+1), h_{\ell,d}(k), h_{\ell,d}(k+1)\}$, respectively, as

$$\gamma_{\tilde{r}_1}|\mathcal{S} = \frac{|\beta^I x_1|^2}{\text{Var}\{\tilde{w}_1|\mathcal{S}\}} = \frac{|\beta^I|^2}{\eta_1^I} \frac{E_s}{2N_o} \quad (8.5.1)$$

$$\gamma_{\tilde{r}_2}|\mathcal{S} = \frac{|\beta^I x_2|^2}{\text{Var}\{\tilde{w}_2|\mathcal{S}\}} = \frac{|\beta^I|^2}{\eta_2^I} \frac{E_s}{2N_o} \quad (8.5.2)$$

where

$$\begin{aligned} \eta_1^I = |\mathcal{G}|^2 \sum_{\ell=1}^M & (|h_{1,\ell}(k+1)h_{\ell,d}(k+1)|^2 (\mathcal{G}^2 |h_{\ell,d}(k)|^2 + 1) \\ & + |h_{2,\ell}(k)h_{\ell,d}(k)|^2 (\mathcal{G}^2 |h_{\ell,d}(k+1)|^2 + 1)) \end{aligned} \quad (8.5.3)$$

$$\begin{aligned} \eta_2^I = |\mathcal{G}|^2 \sum_{\ell=1}^M & (|h_{2,\ell}(k+1)h_{\ell,d}(k+1)|^2 (\mathcal{G}^2 |h_{\ell,d}(k)|^2 + 1) \\ & + |h_{1,\ell}(k)h_{\ell,d}(k)|^2 (\mathcal{G}^2 |h_{\ell,d}(k+1)|^2 + 1)) \end{aligned} \quad (8.5.4)$$

Now, by assuming equiprobable transmission for x_1 and x_2 and directly using the q -QAM AWGN SEP expression in (6.3.1), we can obtain the system SEP conditioned on the channel

gains in the set \mathcal{S} as

$$\begin{aligned}
P_e|\mathcal{S} = & \frac{1}{2} \left[1 - \left(1 - 2 \left(1 - \frac{1}{\sqrt{q}} \right) Q \left(\sqrt{\frac{3}{q-1}} \underbrace{\frac{|\beta^I|^2 E_s}{\eta_1^I 2N_o}}_{\gamma_{\tilde{r}_1}|\mathcal{S}} \right) \right)^2 \right] \\
& + \frac{1}{2} \left[1 - \left(1 - 2 \left(1 - \frac{1}{\sqrt{q}} \right) Q \left(\sqrt{\frac{3}{q-1}} \underbrace{\frac{|\beta^I|^2 E_s}{\eta_2^I 2N_o}}_{\gamma_{\tilde{r}_2}|\mathcal{S}} \right) \right)^2 \right]
\end{aligned} \tag{8.5.5}$$

and its average (sampling mean) can be computed using computer Monte Carlo simulation method as

$$\begin{aligned}
\bar{P}_e = \mathbb{E}_s[P_e|\mathcal{S}] = & \frac{1}{2} \left[1 - \frac{1}{N} \sum_{j=1}^N \left[\left(1 - 2 \left(1 - \frac{1}{\sqrt{M}} \right) Q \left(\sqrt{\frac{3}{q-1}} \gamma_{\tilde{r}_1}|\mathcal{S}^j \right) \right)^2 \right] \right] \\
& + \frac{1}{2} \left[1 - \frac{1}{N} \sum_{j=1}^N \left[\left(1 - 2 \left(1 - \frac{1}{\sqrt{q}} \right) Q \left(\sqrt{\frac{3}{q-1}} \gamma_{\tilde{r}_2}|\mathcal{S}^j \right) \right)^2 \right] \right]
\end{aligned} \tag{8.5.6}$$

where $\gamma_{\tilde{r}_1}|\mathcal{S}^j$ and $\gamma_{\tilde{r}_2}|\mathcal{S}^j$ are the generated SNRs in the j th realization and N is the number of realizations in the simulation (N is supposed to be large enough). In the numerical results section, we provide real link-level simulation results to verify the method in (8.5.6).

8.6 SOSTD under Static-Nodes Case

If the fading environment in the network under study is quasi-static ($\rho_{a,b} = 1 \ \forall(a, b)$), the decoding matrix of the proposed SOSTD (\mathbf{D} in (8.3.18)) reduces to the quasi-static decoding matrix of the ALD ($\mathbf{H}^{\text{static}^{\mathcal{H}}}$ in (6.5.3)). This means that, under this fading condition, the SOSTD reduces to the optimal version of the ALD. We can also verify this because the covariance $\mathbf{COV}(\tilde{w}_1, \tilde{w}_2)$ in (8.4.7) vanish and the conditional SEP of the SOSTD in (8.5.5) reduces to that in (6.5.5) when $\rho_{a,b} = 1 \ \forall(a, b)$.

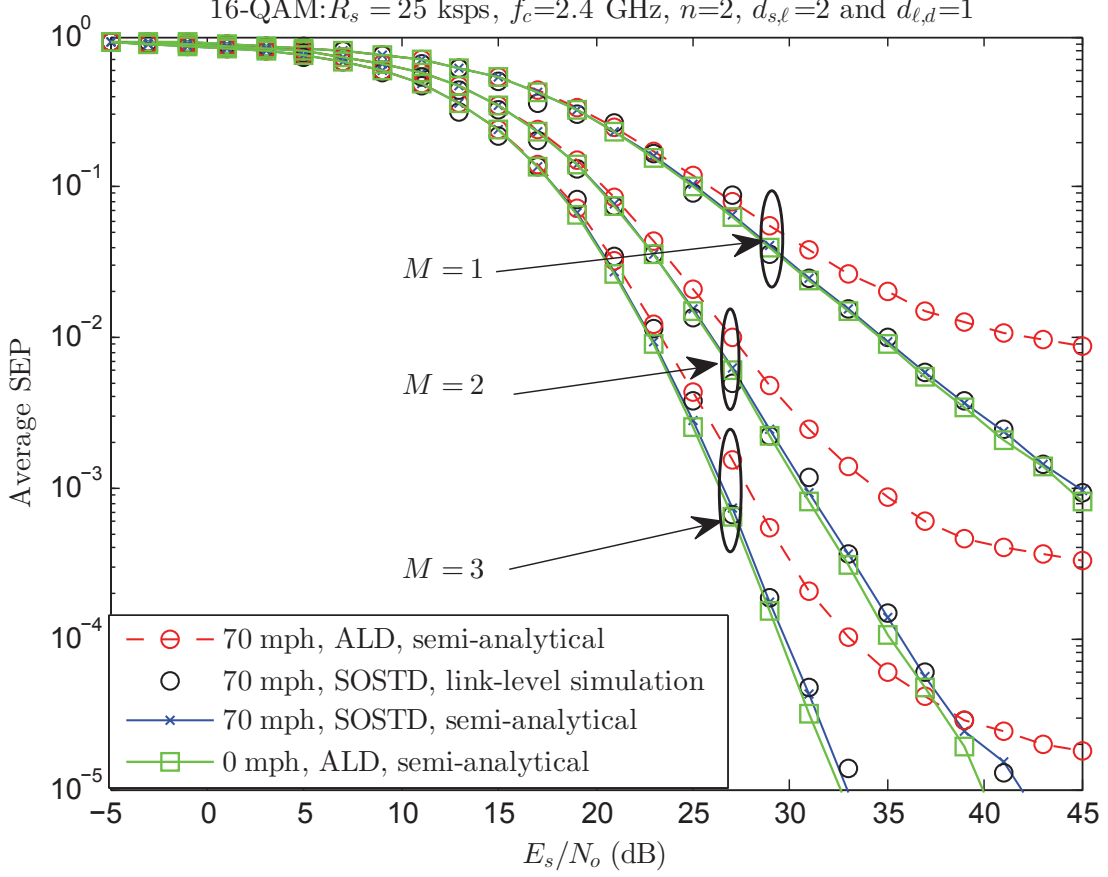


Figure 8.1. Average SEP versus E_s/N_o for both ALD and SOSTD with 0 and 70 mph relative speeds, number of relays $M = 1, 2$ and 3 , QAM constellations size of 16, transmission data-rate $R_s = 25$ kbps, carrier frequency $f_c = 2.4$ GHz, path-loss exponent $n = 2$, normalized nodes distances $d_{s,\ell} = 2$ and $d_{\ell,d} = 1$.

8.7 Numerical and Simulation Results

Here, we present numerical results along with real link-level simulation results to verify the theoretical analysis of the proposed SOSTD SER performance and to compare its performance with that of the ALD for different network scenarios.

First, Fig. 8.1 is plots for the system average SEP versus $\frac{E_s}{N_o}$ for both the SOSTD and ALD with different number of relay nodes and with transmission data rate 25 kbps. Clearly, the numerical results of SOSTD SEP performance using (8.5.6) shows very good agreement with that obtained via real link-level simulation results. As compared with the ALD in the case of mobile nodes (70 mph), the SOSTD provides remarkable SEP performance

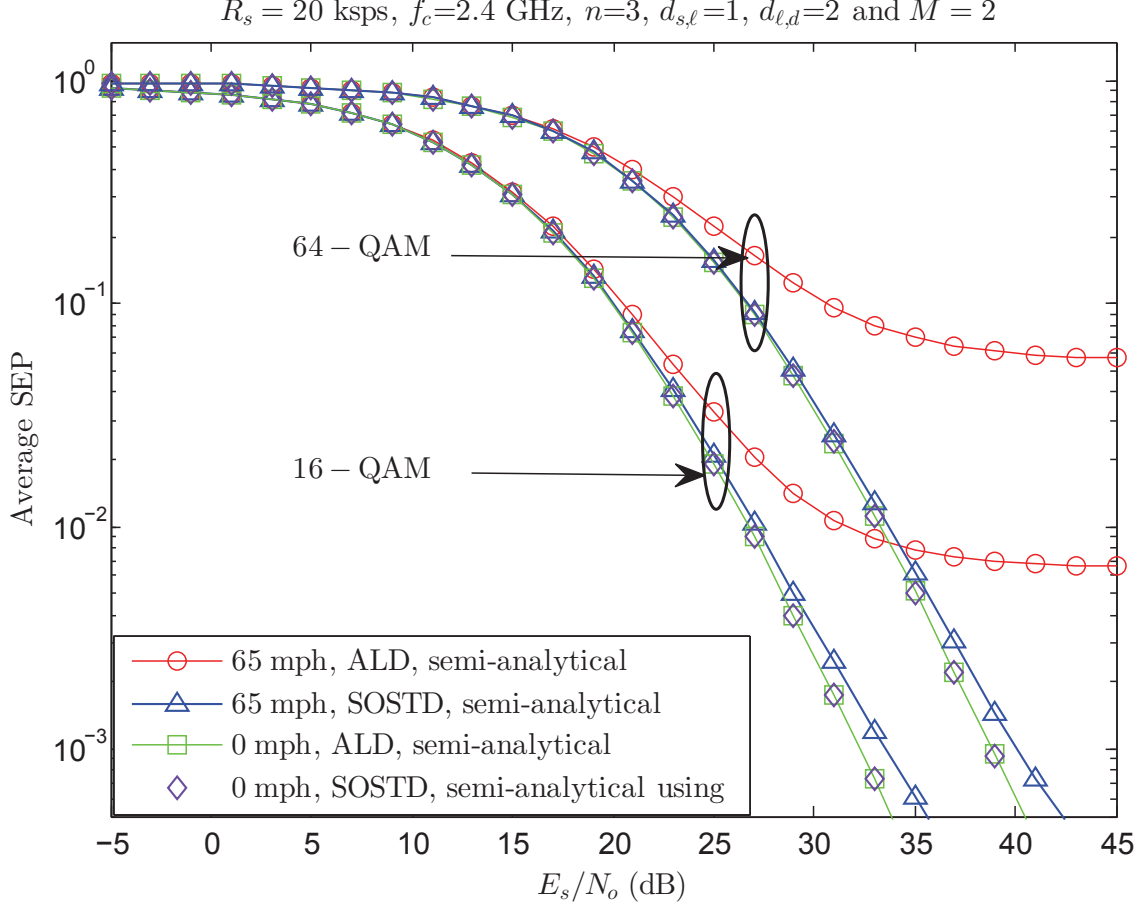


Figure 8.2. Average SEP versus E_s/N_o for both ALD and SOSTD with 0 and 60 mph relative speeds, number of relays $M = 2$, QAM constellation sizes of 16 and 64, transmission data-rate $R_s = 20$ kbps, carrier frequency $f_c = 2.4$ GHz, path-loss exponent $n = 3$, normalized nodes distances $d_{s,\ell} = 1$ and $d_{\ell,d} = 2$.

improvement which is close to that of the non-moving nodes scenario (0 mph). In addition, unlike the ALD, the SOSTD does not experience irreducible floors for any number of relay nodes. From Fig. 8.2 we can notice that the SOSTD SEP performance in case of mobile nodes is much better than that of the ALD for different QAM constellation sizes. Further, in quasi-static fading condition within the network (i.e., 0 mph relative speeds among the nodes), the SEP performance of the SOSTD matches with the ALD.

In Fig. 8.3 we plot the system SEP performance of both the SOSTD and the ALD versus nodes' relative speeds for 4 and 16 QAM constellation sizes and transmission data-rates of 9.6 and 25 kbps. Because the difference between the SEP performance of the

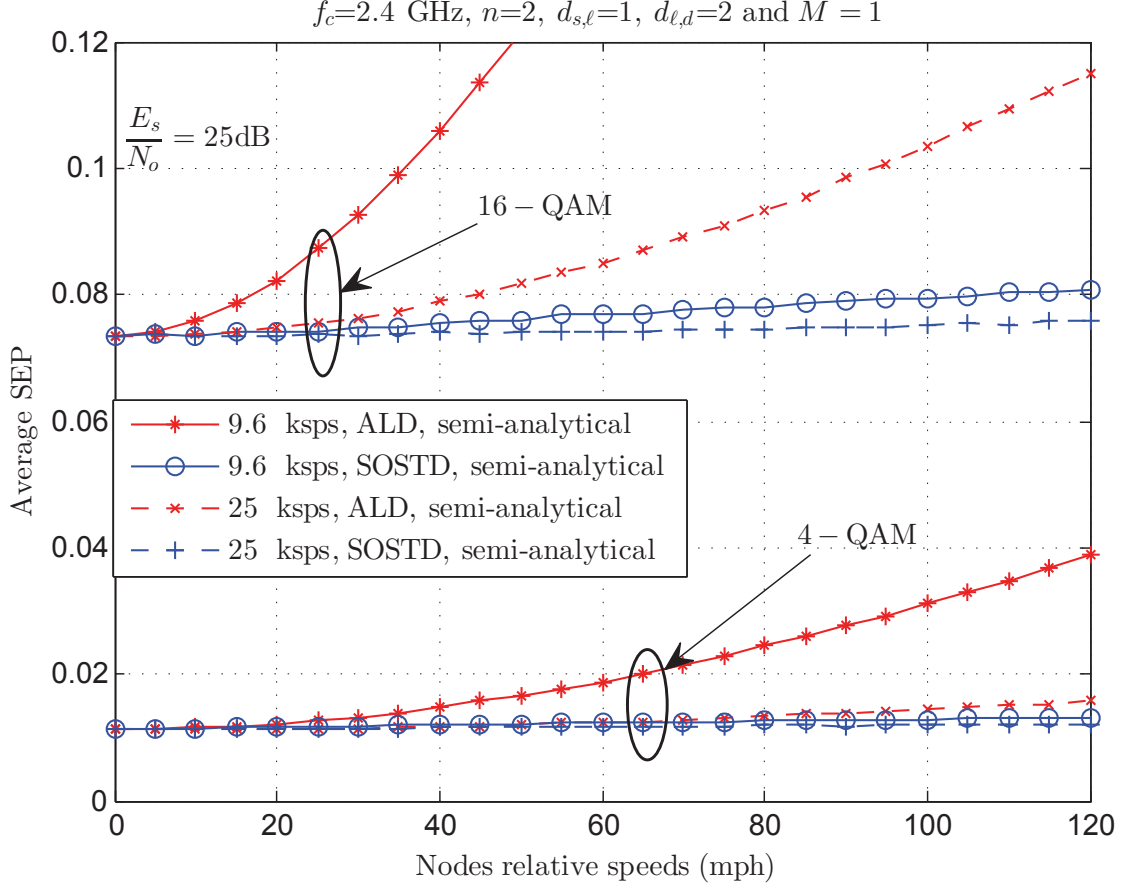


Figure 8.3. Average SEP versus nodes relative speeds for both SOSTD and ALD with $E_s/N_o = 25$ dB, different transmission data-rate values of 9.6 and 25 kbps, $M = 1$, QAM constellations size of 4 and 16, carrier frequency $f_c = 2.4$ GHz, path-loss exponent $n = 2$, normalized nodes distances $d_{s,\ell} = 1$ and $d_{\ell,d} = 2$.

SOSTD and the ALD is more obvious at medium and high regions of per-symbol average SNR, in this plot we choose E_s/N_o value of 25 dB. From this figure, we can notice the system performance improvement by the SOSTD over the ALD from several sides. First, the SOSTD provides better performance than that of the ALD for any nodes relative speed. Further, the increasing in its SEP with nodes relative speeds could be considered insignificant as compared with that of the ALD. Similarly, we can notice from Fig. 8.4 that the SOSTD provides better SEP performance over the ALD for a range of transmission data-rate values, in particular, at high nodes mobility scenario.

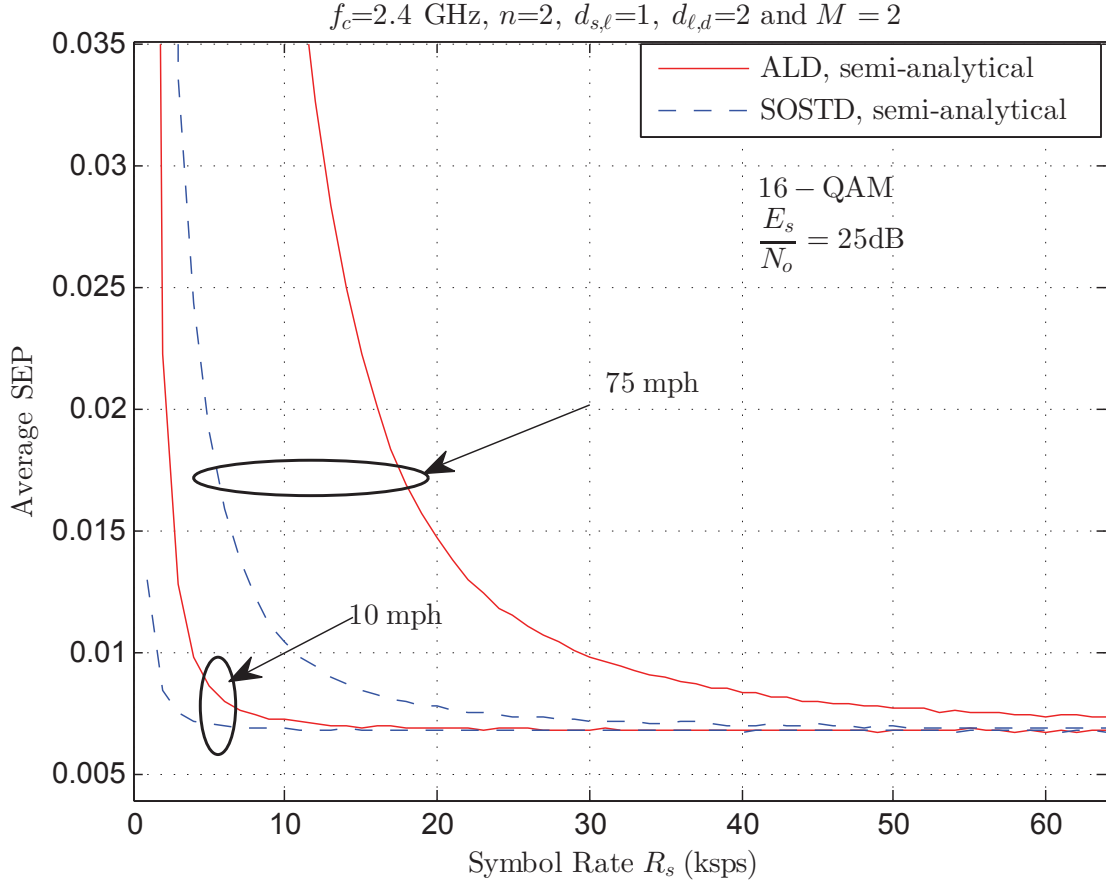


Figure 8.4. Average SEP versus transmission data-rate for both SOSTD and ALD with $E_s/N_o = 25$ dB, different nodes relative speeds of 10 and 75 mph, $M = 2$, 16-QAM constellation, carrier frequency $f_c = 2.4$ GHz, path-loss exponent $n = 2$, normalized nodes distances $d_{s,\ell} = 1$ and $d_{\ell,d} = 2$.

8.8 Conclusion

In this chapter we have derived a novel space-time-decoder that can be applied at the destination of a multiple-relay cooperative system with mobile nodes and Alamouti space-time coding at the source. This decoder is capable to provide very close SEP performance to that of the ZFSTD proposed in chapter 5 without any additional decoding complexity. In addition, we have provided theoretical analysis for its decoding matrix and SEP derivations. Comprehensive numerical and real link-level simulation results have been provided to validate these theoretical analysis and to show the SEP performance improvement by the proposed decoder.

CHAPTER 9

Alamouti-OSTBC Based M -Relay Fixed-Gain AF Cooperative Systems with Mobile Nodes and Imperfect CSI Estimation: SINR Derivation and SEP Analysis

9.1 Chapter Overview

In this chapter we follow the same OSTBC-based cooperative diversity system model as in chapter 5 but along with the assumption of time-selective fading due to nodes mobility we follow the assumption that the estimation processes at the relays and destination receivers are imperfect. Specifically, we consider an Alamouti-type OSTBC transmission over a multiple-relay fixed-gain amplify-and-forward (AF) mobile cooperative-diversity system with q -ary QAM (q -QAM) and Rayleigh frequency-flat time-selective fading channels among the cooperating nodes due to their mobility. All of these channels are modeled by the first-order-autoregressive (AR1) process and follow the standard large-scale path-loss exponent propagation model. Due to imperfect CSI estimation, the estimated channel gains at the relays and destination are assumed to be corrupted by Gaussian errors. Under these assumptions, we employ the traditional Alamouti's space-time-decoder (ALD) at the system's destination and show that the time-selective fading and the imperfect CSI estimation destroy its orthogonality and optimality as a result of the non-separable interfering terms and statistically correlated decision variables that appear at its output. By dealing with the interference terms as additional random variables, in addition to the overall background Gaussian white noise components, along with benefiting from the AR1 model, we derive exact closed-form expressions for the decision variables' instantaneous SINRs. From these SINRs, and by exploiting the central-limit-theorem (CLT), we provide very tight approximate closed-form expression for the system's symbol-error-probability (SEP) conditioned on

the channel gains in the overall system's channel gain-matrix. From this obtained conditional SEP expression, we semi-analytically (based on the sampling mean concept) compute the system's average SEP performance and verify it via realistic link-level simulation. Moreover, we show that this SEP performance is severely degraded and experiences irreducible error floors, which are also quantitatively determined. We show that, as a special case of quasi-static fading and perfect CSI estimation, the decision variables' correlation, the interference terms and the error floors all reduce to zero; i.e., ALD reduces to its originally designed optimal version in such scenario.

9.2 System Model

9.2.1 Fading link and signal model

We consider here the same mobile OSTBC-based cooperative system model as in chapter 5, which we describe it here again. We have a mobile AF cooperative system with source node S , destination node D and M relays R_1, R_2, \dots, R_M . S is equipped with two transmit antennas (e.g. corresponding to a base station), while the relays and D each equipped with single antenna and work as mobile terminals. Let $h_{i,\ell}$ and $h_{\ell,d}$ denote the channel gains for the fading links from the source i th transmit antenna ($i \in \{1, 2\}$) to the ℓ th relay and from the ℓ th relay to the destination, respectively. We assume that $h_{i,\ell}$ and $h_{\ell,d}$ have Rayleigh envelop and uniform phase, and thus, distributed as zero-mean-circularly-symmetric-complex-Gaussian (ZMCSCG); i.e., $h_{i,\ell} \sim \mathcal{CN}(0, \sigma_{i,\ell}^2)$ and $h_{\ell,d} \sim \mathcal{CN}(0, \sigma_{\ell,d}^2)$. To take into account the effect of the path-loss, $\sigma_{i,\ell}^2$ and $\sigma_{\ell,d}^2$ are given as $1/d_{s,\ell}^n$ and $1/d_{\ell,d}^n$, respectively, where $d_{s,\ell}$ and $d_{\ell,d}$ are the S - R_ℓ and R_ℓ - D distances and n is the path-loss exponent. Due to nodes mobility, all of the system's fading links (say the link from antenna a to b) are characterized as time-selective and modeled by the first order autoregressive (AR1) process as (6.2.1)

$$h_{a,b}(\tau_1) = \rho_{a,b} h_{a,b}(\tau_2) + \sqrt{1 - \rho_{a,b}^2} e_{a,b}(\tau_1) \quad (9.2.1)$$

where the pair $(a, b) \in \{(i, \ell), (\ell, d)\}$; τ_1 and τ_2 denote any two adjacent signaling period positions, the random process $e_{a,b}(k) \sim \mathcal{CN}(0, \sigma_{a,b}^2)$ is the varying-component of the associated link, and $\rho_{a,b} = \mathcal{J}_0(\frac{2\pi f_c v_{a,b}}{R_s c})$ [16] is the associated link's correlation-parameter; where $v_{a,b}$ is the relative speed between nodes a and b , R_s is the transmission symbol rate, f_c is the carrier frequency, c is the speed of light and $\mathcal{J}_0(\cdot)$ is the zeroth-order bessel function of the first kind. Observe that when $v_{a,b} = 0$, $\rho_{a,b}$ is 1, and by considering this in (9.2.1), the fading turns to be quasi-static because, in this case, $h_{a,b}(\tau_1) = h_{a,b}(\tau_2)$. Also, it is assumed that $\rho_{1,\ell} = \rho_{2,\ell} \triangleq \rho_{s,\ell}$. At S , the modulated (using q -ary QAM) complex symbol sequence $\{x_i\}$ (each with energy $E_s/2$) is parsed into code vectors $\mathbf{x} = [x_1, x_2]^T$ and then transmitted over space and time as Alamouti-OSTBC matrix [33]

$$\mathbf{X} = \begin{bmatrix} x_1 & -x_2^* \\ x_2 & x_1^* \end{bmatrix} \quad (9.2.2)$$

Broadcasting this OSTBC matrix \mathbf{X} over the cooperative system under study, based on the transmission phases described in chapter 5, results in the following $2M \times 1$ received signal vector at the destination (6.2.10)

$$\underbrace{\begin{bmatrix} y_{1,d}(k) \\ y_{1,d}^*(k+1) \\ \vdots \\ y_{M,d}(k) \\ y_{M,d}^*(k+1) \end{bmatrix}}_{\mathbf{Y}_d} = \underbrace{\mathbf{H} \begin{bmatrix} x_1 \\ x_2 \end{bmatrix}}_{\mathbf{x}} + \underbrace{\begin{bmatrix} \mathcal{G}h_{1,d}(k)n_{s,1}(k) + n_{1,d}(k) \\ \mathcal{G}h_{1,d}^*(k+1)n_{s,1}^*(k+1) + n_{1,d}^*(k+1) \\ \vdots \\ \mathcal{G}h_{M,d}(k)n_{s,M}(k) + n_{M,d}(k) \\ \mathcal{G}h_{M,d}^*(k+1)n_{s,1}^*(k+1) + n_{M,d}^*(k+1) \end{bmatrix}}_{\text{overall effective noise vector } \mathbf{N}_d} \quad (9.2.3)$$

where

$$\mathbf{H} = \begin{bmatrix} \mathcal{G}h_{1,1}(k)h_{1,d}(k) & \mathcal{G}h_{2,1}(k)h_{1,d}(k) \\ \mathcal{G}h_{2,1}^*(k+1)h_{1,d}^*(k+1) & -\mathcal{G}h_{1,1}^*(k+1)h_{1,d}^*(k+1) \\ \vdots & \vdots \\ \mathcal{G}h_{1,M}(k)h_{M,d}(k) & \mathcal{G}h_{2,M}(k)h_{M,d}(k) \\ \mathcal{G}h_{2,M}^*(k+1)h_{M,d}^*(k+1) & -\mathcal{G}h_{1,M}^*(k+1)h_{M,d}^*(k+1) \end{bmatrix}$$

is the system's end-to-end channel-gain matrix; $n_{s,\ell}(k)$, $n_{s,\ell}(k+1)$, $n_{\ell,d}(k)$ and $n_{\ell,d}(k+1)$ for all $\ell = \{1, 2, \dots, M\}$ are the background white noise samples ($\sim \mathcal{CN}(0, N_o)$) that corrupt the corresponding system fading links, and $\mathcal{G} = \sqrt{\frac{E_s}{E_s + N_o}}$ is the fixed amplification gain computed at the relays.

9.2.2 CSI estimation

Despite that the fading links in this work are assumed to be time-selective (i.e., rapidly time-varying), we assume that the relays and the destination tracking loops are capable of estimating the channel gains of their corresponding fading links over the individual signaling periods. Several algorithms have been proposed to track and estimate time-selective (time-varying) fading channel for space-time block coding [45] and [46]. However, unlike the work in chapter 5, we follow here the more practical scenario and assume that these estimation processes are imperfect (i.e., channel estimation error is significant). Thus, the estimated channel gain over the τ th signaling period, say $\hat{h}_{a,b}(\tau)$, can be related to the actual one $h_{a,b}(\tau)$ as [49]

$$\hat{h}_{a,b}(\tau) = h_{a,b}(\tau) + h_{a,b}^\epsilon(\tau) \quad (9.2.4)$$

where $h_{a,b}^\epsilon(\tau)$ is the estimation error, which is assumed to be ZMCSCG with variance $\sigma_{e_{a,b}}^2$ (i.e., $\sim \mathcal{CN}(0, \sigma_{e_{a,b}}^2)$).

9.3 ALD Decision Variables

Employing the ALD at the system's destination requires first a knowledge of the system channel-gain-matrix at the receiving side. Because in this work we assume, along with the time-selective fading assumption, imperfect channel estimation, we can write the estimated version of our system channel-gain-matrix \mathbf{H} as

$$\hat{\mathbf{H}} = \begin{bmatrix} b_{1,1}^1 & b_{1,2}^1 \\ b_{2,1}^1 & b_{2,2}^1 \\ \vdots & \vdots \\ b_{1,1}^M & b_{1,2}^M \\ b_{2,1}^M & b_{2,2}^M \end{bmatrix} \quad (9.3.1)$$

where

$$b_{1,1}^\ell = \mathcal{G}(h_{1,\ell}(k)h_{\ell,d}(k) + h_{1,\ell}(k)h_{\ell,d}^\epsilon(k) + h_{1,\ell}^\epsilon(k)h_{\ell,d}(k) + h_{1,\ell}^\epsilon(k)h_{\ell,d}^\epsilon(k))$$

$$b_{1,2}^\ell = \mathcal{G}(h_{2,\ell}(k)h_{\ell,d}(k) + h_{2,\ell}(k)h_{\ell,d}^\epsilon(k) + h_{2,\ell}^\epsilon(k)h_{\ell,d}(k) + h_{2,\ell}^\epsilon(k)h_{\ell,d}^\epsilon(k))$$

$$b_{2,1}^\ell = \mathcal{G}(h_{2,\ell}^*(k+1)h_{\ell,d}^*(k+1) + h_{2,\ell}^*(k+1)h_{\ell,d}^{\epsilon*}(k+1) \\ + h_{2,\ell}^{\epsilon*}(k+1)h_{\ell,d}^*(k+1) + h_{2,\ell}^{\epsilon*}(k+1)h_{\ell,d}^{\epsilon*}(k+1))$$

$$b_{2,2}^\ell = -\mathcal{G}(h_{1,\ell}^*(k+1)h_{\ell,d}^*(k+1) + h_{1,\ell}^*(k+1)h_{\ell,d}^{\epsilon*}(k+1) \\ + h_{1,\ell}^{\epsilon*}(k+1)h_{\ell,d}^*(k+1) + h_{1,\ell}^{\epsilon*}(k+1)h_{\ell,d}^{\epsilon*}(k+1)).$$

The last equality in (9.3.1) is obtained after substituting for $\hat{h}_{a,b}(k)$ and $\hat{h}_{a,b}(k+1)$, $\forall(a, b) \in \{(1, \ell), (2, \ell), (\ell, d)\}$, as in (9.2.4). Now, we can apply the ALD at the system's destination just by multiplying the received signal vector \mathbf{Y}_d in (9.2.3) by the hermitian of $\hat{\mathbf{H}}$ ($\hat{\mathbf{H}}^H$). The resulted two elements from this multiplication, which are the ALD's decision variables corresponding to the two transmitted symbols x_1 and x_2 , can be given after doing some

simplifications, respectively, as

$$\begin{aligned}
\tilde{y}_1 = & \underbrace{\text{desired-signal of } x_1 \triangleq \mathcal{A}_1}_{\beta_1 x_1} + \overbrace{\underbrace{\zeta x_2}_{\text{nodes-mobility-interference}} + \underbrace{\vartheta_1 x_1 + \xi_1 x_2}_{\text{imperfect-CSI-interference}}}^{\text{overall-interference-term}_1 \triangleq \mathcal{I}_1} \\
& + \overbrace{\underbrace{\tilde{n}_1}_{\text{white-noise-term}} + \underbrace{\tilde{v}_1}_{\text{imperfect-CSI-white-noise-term}}}^{\text{overall-white-noise-term}_1 \triangleq \tilde{\chi}_1}
\end{aligned} \tag{9.3.2}$$

$$\begin{aligned}
\tilde{y}_2 = & \underbrace{\text{desired-signal of } x_2 \triangleq \mathcal{A}_2}_{\beta_2 x_2} + \overbrace{\underbrace{\zeta^* x_1}_{\text{nodes-mobility-interference}} + \underbrace{\vartheta_2 x_2 + \xi_2 x_1}_{\text{imperfect-CSI-interference}}}^{\text{overall-interference-term}_2 \triangleq \mathcal{I}_2} \\
& + \overbrace{\underbrace{\tilde{n}_2}_{\text{white-noise-term}} + \underbrace{\tilde{v}_2}_{\text{imperfect-CSI-white-noise-term}}}^{\text{overall-white-noise-term}_2 \triangleq \tilde{\chi}_2}
\end{aligned} \tag{9.3.3}$$

where

$$\beta_1 = \mathcal{G}^2 \sum_{\ell=1}^M (|h_{1,\ell}(k)h_{\ell,d}(k)|^2 + |h_{2,\ell}(k+1)h_{\ell,d}(k+1)|^2) \tag{9.3.4}$$

$$\zeta = \mathcal{G}^2 \sum_{\ell=1}^M (h_{1,\ell}^*(k)h_{2,\ell}(k)|h_{\ell,d}(k)|^2 - h_{2,\ell}(k+1)h_{1,\ell}^*(k+1)|h_{\ell,d}(k+1)|^2) \tag{9.3.5}$$

$$\begin{aligned}
\vartheta_1 = & \mathcal{G}^2 \sum_{\ell=1}^M |h_{1,\ell}(k)|^2 h_{\ell,d}(k) h_{\ell,d}^{\epsilon^*}(k) + \mathcal{G}^2 \sum_{\ell=1}^M h_{1,\ell}(k) |h_{\ell,d}(k)|^2 h_{1,\ell}^{\epsilon^*}(k) \\
& + \underbrace{\mathcal{G}^2 \sum_{\ell=1}^M \frac{h_{1,\ell}(k) h_{\ell,d}(k)}{h_{1,\ell}^{\epsilon^*}(k) h_{\ell,d}^{\epsilon^*}(k)}}_{I_3^{\vartheta_1}} + \mathcal{G}^2 \sum_{\ell=1}^M |h_{2,\ell}(k+1)|^2 h_{\ell,d}^*(k+1) h_{\ell,d}^{\epsilon^*}(k+1) \\
& + \mathcal{G}^2 \sum_{\ell=1}^M h_{2,\ell}^*(k+1) |h_{\ell,d}(k+1)|^2 h_{2,\ell}^{\epsilon}(k+1) + \underbrace{\mathcal{G}^2 \sum_{\ell=1}^M \frac{h_{2,\ell}^*(k+1) h_{\ell,d}^*(k+1) h_{\ell,d}^{\epsilon}(k+1)}{+1} h_{\ell,d}^{\epsilon}(k+1)}_{I_6^{\vartheta_1}}.
\end{aligned} \tag{9.3.6}$$

$$\begin{aligned}
\xi_1 = & \mathcal{G}^2 \sum_{\ell=1}^M (h_{1,\ell}^*(k) h_{2,\ell}(k) h_{\ell,d}(k) h_{\ell,d}^{\epsilon^*}(k) + |h_{\ell,d}(k)|^2 h_{2,\ell}(k) + h_{2,\ell}(k) h_{\ell,d}(k) h_{1,\ell}^{\epsilon^*}(k) \\
& h_{\ell,d}^{\epsilon^*}(k) - h_{2,\ell}(k+1) h_{1,\ell}^*(k+1) h_{\ell,d}^*(k+1) h_{\ell,d}^{\epsilon}(k+1) - |h_{\ell,d}(k+1)|^2 \\
& h_{1,\ell}^*(k+1) h_{2,\ell}^{\epsilon}(k+1) - h_{1,\ell}^*(k+1) h_{\ell,d}^*(k+1) h_{2,\ell}^{\epsilon}(k+1) h_{\ell,d}^{\epsilon}(k+1)).
\end{aligned} \tag{9.3.7}$$

$$\begin{aligned}
\tilde{n}_1 = & \sum_{\ell=1}^M (\mathcal{G}^2 h_{1,\ell}^*(k) |h_{\ell,d}(k)|^2 n_{s,\ell}(k) + \mathcal{G} h_{1,\ell}^*(k) h_{\ell,d}^*(k) n_{\ell,d}(k) + \mathcal{G}^2 h_{2,\ell}(k+1) \\
& |h_{\ell,d}(k+1)|^2 n_{s,\ell}^*(k+1) + \mathcal{G} h_{2,\ell}(k+1) h_{\ell,d}(k+1) n_{\ell,d}^*(k+1))
\end{aligned} \tag{9.3.8}$$

$$\begin{aligned}
\tilde{v}_1 = & \sum_{\ell=1}^M \mathcal{G}^2 h_{1,\ell}^*(k) h_{\ell,d}^{\epsilon*}(k) h_{\ell,d}(k) n_{s,\ell}(k) + \sum_{\ell=1}^M \mathcal{G}^2 h_{1,\ell}^{\epsilon*}(k) h_{\ell,d}^*(k) h_{\ell,d}(k) n_{s,\ell}(k) + \sum_{\ell=1}^M \mathcal{G}^2 \\
& h_{1,\ell}^{\epsilon*}(k) h_{\ell,d}^{\epsilon*}(k) h_{\ell,d}(k) n_{s,\ell}(k) + \sum_{\ell=1}^M \mathcal{G} h_{1,\ell}^*(k) h_{\ell,d}^{\epsilon*}(k) n_{\ell,d}(k) + \sum_{\ell=1}^M \mathcal{G} h_{1,\ell}^{\epsilon*}(k) h_{\ell,d}^*(k) \\
& n_{\ell,d}(k) + \sum_{\ell=1}^M \mathcal{G} h_{1,\ell}^{\epsilon*}(k) h_{\ell,d}^{\epsilon*}(k) n_{\ell,d}(k) + \sum_{\ell=1}^M \mathcal{G}^2 h_{2,\ell}(k+1) h_{\ell,d}^{\epsilon}(k+1) h_{\ell,d}^*(k+1) \\
& n_{s,\ell}^*(k+1) + \sum_{\ell=1}^M \mathcal{G}^2 h_{2,\ell}^{\epsilon}(k+1) h_{\ell,d}(k+1) h_{\ell,d}^*(k+1) n_{s,\ell}^*(k+1) + \sum_{\ell=1}^M \mathcal{G}^2 \\
& h_{2,\ell}^{\epsilon}(k+1) h_{\ell,d}^{\epsilon*}(k) h_{\ell,d}^*(k+1) n_{s,\ell}^*(k+1) + \sum_{\ell=1}^M \mathcal{G} h_{2,\ell}(k+1) h_{\ell,d}^{\epsilon}(k+1) \\
& n_{\ell,d}^*(k+1) + \sum_{\ell=1}^M \mathcal{G} h_{2,\ell}^{\epsilon}(k+1) h_{\ell,d}(k+1) n_{\ell,d}^*(k+1) + \sum_{\ell=1}^M \mathcal{G} h_{2,\ell}^{\epsilon}(k+1) \\
& h_{\ell,d}^{\epsilon*}(k) n_{\ell,d}^*(k+1)
\end{aligned} \tag{9.3.9}$$

$$\beta_2 = \mathcal{G}^2 \sum_{\ell=1}^M (|h_{2,\ell}(k) h_{\ell,d}(k)|^2 + |h_{1,\ell}(k+1) h_{\ell,d}(k+1)|^2) \tag{9.3.10}$$

$$\begin{aligned}
\vartheta_2 = & \mathcal{G}^2 \sum_{\ell=1}^M (|h_{2,\ell}(k)|^2 h_{\ell,d}(k) h_{\ell,d}^{\epsilon*}(k) + h_{2,\ell}(k) |h_{\ell,d}(k)|^2 h_{2,\ell}^{\epsilon*}(k) + h_{2,\ell}(k) h_{\ell,d}(k) h_{2,\ell}^{\epsilon*}(k) \\
& h_{\ell,d}^{\epsilon*}(k) + |h_{1,\ell}(k+1)|^2 h_{\ell,d}^*(k+1) h_{\ell,d}^{\epsilon*}(k+1) + h_{1,\ell}^*(k+1) |h_{\ell,d}(k+1)|^2 \\
& h_{1,\ell}^{\epsilon}(k+1) + h_{1,\ell}^*(k+1) h_{\ell,d}^*(k+1) h_{\ell,d}^{\epsilon}(k+1) h_{\ell,d}^{\epsilon}(k+1))
\end{aligned} \tag{9.3.11}$$

$$\begin{aligned}
\xi_2 = & \mathcal{G}^2 \sum_{\ell=1}^M (h_{2,\ell}^*(k) h_{1,\ell}(k) h_{\ell,d}(k) h_{\ell,d}^{\epsilon*}(k) + |h_{\ell,d}(k)|^2 h_{1,\ell}(k) h_{2,\ell}^{\epsilon*}(k) + h_{1,\ell}(k) h_{\ell,d}(k) \\
& h_{2,\ell}^{\epsilon*}(k) h_{\ell,d}^{\epsilon*}(k) - h_{1,\ell}(k+1) h_{2,\ell}^*(k+1) h_{\ell,d}^*(k+1) h_{\ell,d}^{\epsilon}(k+1) - |h_{\ell,d}(k+1)|^2 \\
& h_{2,\ell}^*(k+1) h_{1,\ell}^{\epsilon}(k+1) - h_{2,\ell}^*(k+1) h_{\ell,d}^*(k+1) h_{1,\ell}^{\epsilon}(k+1) h_{\ell,d}^{\epsilon}(k+1))
\end{aligned} \tag{9.3.12}$$

$$\begin{aligned} \tilde{n}_2 = \sum_{\ell=1}^M & (\mathcal{G}^2 h_{2,\ell}^*(k) |h_{\ell,d}(k)|^2 n_{s,\ell}(k) + \mathcal{G} h_{2,\ell}^*(k) h_{\ell,d}^*(k) n_{\ell,d}(k) - \mathcal{G}^2 h_{1,\ell}(k+1) |h_{\ell,d}(k+1)|^2 \\ & n_{s,\ell}^*(k+1) - \mathcal{G} h_{1,\ell}(k+1) h_{\ell,d}(k+1) n_{\ell,d}^*(k+1)) \end{aligned} \quad (9.3.13)$$

$$\begin{aligned} \tilde{v}_2 = \mathcal{G} \sum_{\ell=1}^M & (\mathcal{G} h_{2,\ell}^*(k) h_{\ell,d}^{\epsilon*}(k) h_{\ell,d}(k) n_{s,\ell}(k) + \mathcal{G} h_{2,\ell}^{\epsilon*}(k) h_{\ell,d}^*(k) h_{\ell,d}(k) n_{s,\ell}(k) + \mathcal{G} h_{2,\ell}^{\epsilon*}(k) \\ & h_{\ell,d}^{\epsilon*}(k) h_{\ell,d}(k) n_{s,\ell}(k) + h_{2,\ell}^*(k) h_{\ell,d}^{\epsilon*}(k) n_{\ell,d}(k) + h_{2,\ell}^{\epsilon*}(k) h_{\ell,d}^*(k) n_{\ell,d}(k) + h_{2,\ell}^{\epsilon*}(k) \\ & h_{\ell,d}^{\epsilon*}(k) n_{\ell,d}(k) - \mathcal{G} h_{1,\ell}(k+1) h_{\ell,d}^{\epsilon}(k+1) h_{\ell,d}^*(k+1) n_{s,\ell}^*(k+1) - \mathcal{G} h_{1,\ell}^{\epsilon}(k+1) \\ & h_{\ell,d}(k+1) h_{\ell,d}^*(k+1) n_{s,\ell}^*(k+1) - \mathcal{G} h_{1,\ell}^{\epsilon}(k+1) h_{\ell,d}^{\epsilon*}(k) h_{\ell,d}^*(k+1) n_{s,\ell}^*(k+1) \\ & - h_{1,\ell}(k+1) h_{\ell,d}^{\epsilon}(k+1) n_{\ell,d}^*(k+1) - h_{1,\ell}^{\epsilon}(k+1) h_{\ell,d}(k+1) n_{\ell,d}^*(k+1) \\ & - h_{1,\ell}^{\epsilon}(k+1) h_{\ell,d}^{\epsilon*}(k) n_{\ell,d}^*(k+1)) \end{aligned} \quad (9.3.14)$$

Because in this work we follow the more practical assumptions of time-selective fading environment and imperfect CSI estimation processes at the relays and the destination, the obtained decision variables \tilde{y}_1 and \tilde{y}_2 are nonseparable for x_1 and x_2 , respectively (see the interference terms \mathcal{I}_1 and \mathcal{I}_2). The imperfect CSI estimation assumption also adds additional white noise components to these decision variables, which are \tilde{v}_1 and \tilde{v}_2 . Moreover, as an impact of both the time-selective fading and the imperfect channel estimation, \tilde{y}_1 and \tilde{y}_2 are non independent. This is because that their effective noise terms $\tilde{\chi}_1$ and $\tilde{\chi}_2$ are correlated and have conditional covariance given by (9.3.15). It is worthwhile to mention that if the system's fading environment is quasi-static (i.e., $\rho_{a,b} = 1 \forall(a,b)$) and the estimation processes are perfect (i.e., $(h_{\epsilon_{a,b}}(\tau) = 0 \forall(a,b))$) the interference terms \mathcal{I}_1 and \mathcal{I}_2 , the imperfect-estimation white noise terms \tilde{v}_1 and \tilde{v}_2 and the statistical correlation in (9.3.15) reduce to zero. This means that \tilde{y}_1 and \tilde{y}_2 are separable corresponding to x_1 and x_2 , respectively, and also independent to each other (in this case, the ALD is optimal ML). However, in the following section, we analyze the SEP performance of this system considering the more general scenarios of time-selective fading (i.e., $\rho_{a,b} < 1 \forall(a,b)$) and imperfect estimation

$(h_{\epsilon_{a,b}}(\tau) \neq 0)$, which has not been done before in the literature.

$$\begin{aligned}
\mathbb{E}[\tilde{\chi}_1 \tilde{\chi}_2^* | \tilde{\mathcal{S}}] &= \mathcal{G}^2 N_o \sum_{\ell=1}^M (h_{1,\ell}^*(k) h_{2,\ell}(k) |h_{\ell,d}(k)|^2 (\mathcal{G}^2 |h_{\ell,d}(k)|^2 + \\
&1) - h_{2,\ell}(k+1) h_{1,\ell}^*(k+1) |h_{\ell,d}(k+1)|^2 (\mathcal{G}^2 |h_{\ell,d}(k+1)|^2 + 1)) + \\
&(\mathcal{G}^2 h_{1,\ell}^*(k) |h_{\ell,d}(k)|^2 (h_{2,\ell}(k) h_{\ell,d}^\epsilon(k) h_{\ell,d}^*(k) + h_{2,\ell}^\epsilon(k) h_{\ell,d}(k) h_{\ell,d}^*(k) + \\
&h_{2,\ell}^\epsilon(k) h_{\ell,d}^\epsilon(k) h_{\ell,d}^*(k)) + h_{1,\ell}^*(k) h_{\ell,d}^*(k) (h_{2,\ell}(k) h_{\ell,d}^\epsilon(k) + h_{2,\ell}^\epsilon(k) h_{\ell,d}(k) + \\
&h_{2,\ell}^\epsilon(k) h_{\ell,d}^\epsilon(k)) - \mathcal{G}^2 h_{2,\ell}(k+1) |h_{\ell,d}(k+1)|^2 (h_{1,\ell}^*(k+1) h_{\ell,d}^{\epsilon*}(k+1) h_{\ell,d}(k+1) + \\
&h_{1,\ell}^{\epsilon*}(k+1) h_{\ell,d}^*(k+1) h_{\ell,d}(k+1) + h_{1,\ell}^{\epsilon*}(k+1) h_{\ell,d}^\epsilon(k+1) h_{\ell,d}(k+1)) - \\
&h_{2,\ell}(k+1) h_{\ell,d}(k+1) (h_{1,\ell}^*(k+1) h_{\ell,d}^{\epsilon*}(k+1) + h_{1,\ell}^{\epsilon*}(k+1) h_{\ell,d}^\epsilon(k+1) + \\
&h_{1,\ell}^{\epsilon*}(k+1) h_{\ell,d}^*(k+1) + h_{1,\ell}^{\epsilon*}(k+1) h_{\ell,d}^\epsilon(k+1) h_{\ell,d}^*(k+1))) + \\
&(\mathcal{G}^2 h_{2,\ell}(k) |h_{\ell,d}(k)|^2 (h_{1,\ell}^*(k) h_{\ell,d}^{\epsilon*}(k) h_{\ell,d}(k) + h_{1,\ell}^{\epsilon*}(k) h_{\ell,d}^*(k) h_{\ell,d}(k) + \\
&h_{1,\ell}^{\epsilon*}(k) h_{\ell,d}^{\epsilon*}(k) h_{\ell,d}(k)) + h_{2,\ell}(k) h_{\ell,d}(k) (h_{1,\ell}^*(k) h_{\ell,d}^{\epsilon*}(k) + h_{1,\ell}^{\epsilon*}(k) h_{\ell,d}^*(k) + \\
&h_{1,\ell}^{\epsilon*}(k) h_{\ell,d}^{\epsilon*}(k)) - \mathcal{G}^2 h_{1,\ell}^*(k+1) |h_{\ell,d}(k+1)|^2 (h_{2,\ell}(k+1) h_{\ell,d}^\epsilon(k+1) h_{\ell,d}^*(k+1) + \\
&h_{2,\ell}^\epsilon(k+1) h_{\ell,d}(k+1) h_{\ell,d}^*(k+1) + h_{2,\ell}^\epsilon(k+1) h_{\ell,d}^{\epsilon*}(k+1) h_{\ell,d}^*(k+1) + \\
&h_{2,\ell}^\epsilon(k+1) h_{\ell,d}^\epsilon(k+1) h_{\ell,d}(k+1) + h_{2,\ell}^\epsilon(k+1) h_{\ell,d}^\epsilon(k+1) h_{\ell,d}^{\epsilon*}(k+1) h_{\ell,d}^*(k+1)) - \\
&h_{1,\ell}^*(k+1) h_{\ell,d}^*(k+1) (h_{2,\ell}(k+1) h_{\ell,d}^\epsilon(k+1) + h_{2,\ell}^\epsilon(k+1) h_{\ell,d}(k+1) + \\
&h_{2,\ell}^\epsilon(k+1) h_{\ell,d}^\epsilon(k+1) h_{\ell,d}^{\epsilon*}(k+1) h_{\ell,d}^*(k+1))) + (\mathcal{G}^2 (h_{1,\ell}^*(k) h_{\ell,d}^{\epsilon*}(k) h_{\ell,d}(k) + \\
&h_{1,\ell}^{\epsilon*}(k) h_{\ell,d}^*(k) h_{\ell,d}(k) + h_{1,\ell}^{\epsilon*}(k) h_{\ell,d}^{\epsilon*}(k) h_{\ell,d}(k)) (h_{2,\ell}(k) h_{\ell,d}^\epsilon(k) h_{\ell,d}^*(k) + \\
&h_{2,\ell}^\epsilon(k) h_{\ell,d}(k) h_{\ell,d}^*(k) + h_{2,\ell}^\epsilon(k) h_{\ell,d}^\epsilon(k) h_{\ell,d}^*(k)) + (h_{1,\ell}^*(k) h_{\ell,d}^{\epsilon*}(k) + \\
&h_{1,\ell}^{\epsilon*}(k) h_{\ell,d}^*(k) + h_{1,\ell}^{\epsilon*}(k) h_{\ell,d}^{\epsilon*}(k)) (h_{2,\ell}(k) h_{\ell,d}^\epsilon(k) + h_{2,\ell}^\epsilon(k) h_{\ell,d}(k) + \\
&h_{2,\ell}^\epsilon(k) h_{\ell,d}^\epsilon(k)) - \mathcal{G}^2 (h_{2,\ell}(k+1) h_{\ell,d}^\epsilon(k+1) h_{\ell,d}^*(k+1) + h_{2,\ell}^\epsilon(k+1) h_{\ell,d}(k+1) h_{\ell,d}^*(k+1) + \\
&h_{2,\ell}^\epsilon(k+1) h_{\ell,d}^{\epsilon*}(k+1) h_{\ell,d}^*(k+1)) (h_{1,\ell}^*(k+1) h_{\ell,d}^{\epsilon*}(k+1) h_{\ell,d}(k+1) + \\
&h_{1,\ell}^{\epsilon*}(k+1) h_{\ell,d}^*(k+1) h_{\ell,d}(k+1) + h_{1,\ell}^{\epsilon*}(k+1) h_{\ell,d}^\epsilon(k+1) h_{\ell,d}(k+1)) - \\
&(h_{2,\ell}(k+1) h_{\ell,d}^\epsilon(k+1) + h_{2,\ell}^\epsilon(k+1) h_{\ell,d}(k+1) + h_{2,\ell}^\epsilon(k+1) h_{\ell,d}^{\epsilon*}(k+1) h_{\ell,d}^*(k+1)) (h_{1,\ell}^*(k+1) h_{\ell,d}^{\epsilon*}(k+1) + \\
&h_{1,\ell}^{\epsilon*}(k+1) h_{\ell,d}^*(k+1) + h_{1,\ell}^{\epsilon*}(k+1) h_{\ell,d}^\epsilon(k+1) h_{\ell,d}^*(k+1)))
\end{aligned} \tag{9.3.15}$$

where

$$\tilde{\mathcal{S}} = \mathcal{S} \cup \mathcal{S}^\epsilon$$

$$\mathcal{S} = \{h_{1,\ell}(k), h_{1,\ell}(k+1), h_{2,\ell}(k), h_{2,\ell}(k+1), h_{\ell,d}(k), h_{\ell,d}(k+1) : \forall \ell = 1, 2 \dots, M\}$$

$$\mathcal{S}^\epsilon = \{h_{1,\ell}^\epsilon(k), h_{1,\ell}^\epsilon(k+1), h_{2,\ell}^\epsilon(k), h_{2,\ell}^\epsilon(k+1), h_{\ell,d}^\epsilon(k), h_{\ell,d}^\epsilon(k+1) : \forall \ell = 1, 2 \dots, M\}.$$

(9.3.16)

9.4 System Conditional SEP Analysis

The decision variables \tilde{y}_1 in (9.3.2) and \tilde{y}_2 in (9.3.3) are used by the destination q -QAM demodulator to make decisions about the two transmitted symbols x_1 and x_2 , respectively. Here, we use these two decision variables to analyze the system symbol error probability (SEP) at the q -QAM demodulator output. However, due to the complicated form of the decision variables \tilde{y}_1 in (9.3.2) and \tilde{y}_2 in (9.3.3), which complicates deriving the SEP of the system model under study from scratch, we propose here an approach that allows us to directly utilize the AWGN SEP expression in (6.3.1) in evaluating this system SEP. Basically, this proposed approach is based on (i) deriving explicit closed-form expressions for the SINRs of the variables \tilde{y}_1 and \tilde{y}_2 (ii) showing that the overall-interference terms (\mathcal{I}_1 and \mathcal{I}_2) and the overall-white-noise terms ($\tilde{\chi}_1$ and $\tilde{\chi}_2$) in (9.3.2) and (9.3.3) are complex-Gaussian or fairly approximated as complex-Gaussian, which we do in the following subsections.

9.4.1 Conditional SINR of the first decision statistic

It is clear from (9.3.2) that the decision variable \tilde{y}_1 is a function of the channel gains in the set $\tilde{\mathcal{S}} = \{h_{1,\ell}(k), h_{1,\ell}(k+1), h_{2,\ell}(k), h_{2,\ell}(k+1), h_{\ell,d}(k), h_{\ell,d}(k+1), h_{1,\ell}^\epsilon(k), h_{1,\ell}^\epsilon(k+1), h_{2,\ell}^\epsilon(k), h_{2,\ell}^\epsilon(k+1), h_{\ell,d}^\epsilon(k), h_{\ell,d}^\epsilon(k+1) : \forall \ell = 1, 2 \dots, M\}$. However, in order to simplify the derivation of its conditional SINR (say γ_1), we propose to derive it conditioned on the set $\mathcal{S}_1 = \{h_{1,\ell}(k), h_{2,\ell}(k+1), h_{\ell,d}(k), h_{\ell,d}(k+1) : \forall \ell = 1, 2 \dots, M\}$ ¹. It is clear now from

¹The channel gains in this set are the ones that appear as coefficients of the desired-signal term in the decision variable \tilde{y}_1 in (9.3.2).

(9.3.2) that $\gamma_1|\mathcal{S}_1$ can be expressed as

$$\begin{aligned}\gamma_1|\mathcal{S}_1 &= \frac{P(\mathcal{A}_1|\mathcal{S}_1)}{P(\mathcal{I}_1|\mathcal{S}_1) + P(\tilde{\chi}_1|\mathcal{S}_1)} \\ &= \frac{|\beta_1|^2(E_s/2)}{P(\zeta|\mathcal{S}_1)(E_s/2) + P(\vartheta_1|\mathcal{S}_1)(E_s/2) + P(\xi_1|\mathcal{S}_1)(E_s/2) + P(\tilde{n}_1|\mathcal{S}_1) + P(\tilde{v}_1|\mathcal{S}_1)}\end{aligned}\quad (9.4.1)$$

where P denotes the power operator. In the following we discuss how we can evaluate $P(\zeta|\mathcal{S}_1)$, $P(\vartheta_1|\mathcal{S}_1)$, $P(\xi_1|\mathcal{S}_1)$, $P(\tilde{n}_1|\mathcal{S}_1)$ and $P(\tilde{v}_1|\mathcal{S}_1)$. First, it is clear from (9.3.5) that ζ is a function of the elements in \mathcal{S}_1 as well as of $h_{1,\ell}(k+1)$ and $h_{2,\ell}(k)$. Therefore, conditioned on \mathcal{S}_1 , ζ is a random variable with respect to both $h_{1,\ell}(k+1)$ and $h_{2,\ell}(k)$. To find $P(\zeta|\mathcal{S}_1)$, we propose first to utilize the expression of the AR1 model in (9.2.1) to write $h_{1,\ell}^*(k+1)$ in terms of $h_{1,\ell}(k)$ and $h_{2,\ell}(k)$ in terms of $h_{2,\ell}(k+1)$, respectively, as follows

$$h_{1,\ell}^*(k+1) = \rho_{s,\ell}h_{1,\ell}^*(k) + \sqrt{1 - \rho_{s,\ell}^2}e_{1,\ell}^*(k+1) \quad (9.4.2)$$

$$h_{2,\ell}(k) = \rho_{s,\ell}h_{2,\ell}(k+1) + \sqrt{1 - \rho_{s,\ell}^2}e_{2,\ell}(k). \quad (9.4.3)$$

By substituting (9.4.2) and (9.4.3) into (9.3.5), we can expand ζ as

$$\begin{aligned}\zeta &= \underbrace{\mathcal{G}^2 \sum_{\ell=1}^M (\rho_{s,\ell}h_{1,\ell}^*(k)h_{2,\ell}(k+1)(|h_{\ell,d}(k)|^2 - |h_{\ell,d}(k+1)|^2))}_{\mu_1} \\ &+ \underbrace{\mathcal{G}^2 \sum_{\ell=1}^M (\sqrt{1 - \rho_{s,\ell}^2}h_{1,\ell}^*(k)|h_{\ell,d}(k)|^2e_{2,\ell}(k) - \sqrt{1 - \rho_{s,\ell}^2}h_{2,\ell}(k+1)|h_{\ell,d}(k+1)|^2e_{1,\ell}^*(k+1))}_{\psi_1}\end{aligned}\quad (9.4.4)$$

It is obvious from (9.4.4) that because $e_{1,\ell}^*(k+1) \sim \mathcal{CN}(0, \sigma_{1,\ell}^2)$ and $e_{2,\ell}(k) \sim \mathcal{CN}(0, \sigma_{2,\ell}^2)$, $\zeta|\mathcal{S}_1$ is a non-zero mean complex Gaussian with mean μ_1 and variance given as

$$\begin{aligned} \text{Var}[\zeta | \mathcal{S}_1] = \text{Var}[\psi_1 | \mathcal{S}_1] = \mathcal{G}^4 \sum_{\ell=1}^M & \left((1 - \rho_{s,\ell}^2) (\sigma_{2,\ell}^2 |h_{1,\ell}(k)|^2 \right. \\ & \left. |h_{\ell,d}(k)|^4 + \sigma_{1,\ell}^2 |h_{2,\ell}(k+1)|^2 |h_{\ell,d}(k+1)|^4 \right). \end{aligned} \quad (9.4.5)$$

Given ζ in (9.4.4), the power of $\zeta | \mathcal{S}_1$ can be obtained as

$$\text{P}(\zeta | \mathcal{S}_1) = |\mu_1|^2 + \text{Var}[\psi_1 | \mathcal{S}_1]. \quad (9.4.6)$$

The parameter ϑ_1 in (9.3.6) is function of the elements in \mathcal{S}_1 as well as of the estimation errors $h_{1,\ell}^\epsilon(k)$, $h_{2,\ell}^\epsilon(k+1)$, $h_{\ell,d}^\epsilon(k)$ and $h_{\ell,d}^\epsilon(k+1)$. Therefore, $\vartheta_1|\mathcal{S}_1$ is random variable with respect to these estimation errors. Since $h_{a,b}^\epsilon(\tau) \sim \mathcal{CN}(0, \sigma_{e_{a,b}}^2) \quad \forall (a, b) \in \{(1, \ell), (2, \ell), (\ell, d)\}$ and $\tau \in \{k, k+1\}$, we can evaluate the mean and the variance of $\vartheta_1|\mathcal{S}_1$, respectively, as follows

$$\text{E}[\vartheta_1|\mathcal{S}_1] = 0 \quad (9.4.7)$$

$$\begin{aligned} \text{Var}[\vartheta_1|\mathcal{S}_1] = \mathcal{G}^4 \sum_{\ell=1}^M & \left(|h_{1,\ell}(k)|^4 |h_{\ell,d}(k)|^2 \sigma_{e_{\ell,d}}^2 + |h_{1,\ell}(k)|^2 |h_{\ell,d}(k)|^4 \sigma_{e_{1,\ell}}^2 + |h_{1,\ell}(k)|^2 \right. \\ & |h_{\ell,d}(k)|^2 \sigma_{e_{1,\ell}}^2 \sigma_{e_{\ell,d}}^2 + |h_{2,\ell}(k+1)|^4 |h_{\ell,d}(k+1)|^2 \sigma_{e_{\ell,d}}^2 + |h_{2,\ell}(k+1)|^2 \\ & \left. |h_{\ell,d}(k+1)|^4 \sigma_{e_{2,\ell}}^2 + |h_{2,\ell}(k+1)|^2 |h_{\ell,d}(k+1)|^2 \sigma_{e_{2,\ell}}^2 \sigma_{e_{\ell,d}}^2 \right) \end{aligned} \quad (9.4.8)$$

and thus, its power can be given by

$$\text{P}(\vartheta_1|\mathcal{S}_1) = \text{Var}[\vartheta_1|\mathcal{S}_1]. \quad (9.4.9)$$

Moreover, we can notice from (9.3.6) that the densities of the terms of ϑ_1 , conditioned on \mathcal{S}_1 , are complex-Gaussian (specifically ZMCSCG) except the terms $I_3^{\vartheta_1}$ and $I_6^{\vartheta_1}$. $I_3^{\vartheta_1}|\mathcal{S}_1$ is

sum of multiplications of two ZMCSCG random variables; $h_{1,\ell}^{\epsilon^*}(k)$ and $h_{\ell,d}^{\epsilon^*}(k)$, while $I_6^{\vartheta_1}|\mathcal{S}_1$ is sum of multiplications of the two ZMCSCG random variables $h_{2,\ell}^{\epsilon^*}(k+1)$ and $h_{\ell,d}^{\epsilon^*}(k+1)$. However, with the help of the central-limit-theorem (CLT) [50], $I_3^{\vartheta_1}|\mathcal{S}_1$ can be approximated as ZMCSCG random variable (see Appendix A). Similarly as $I_3^{\vartheta_1}|\mathcal{S}_1$, $I_6^{\vartheta_1}|\mathcal{S}_1$ can be also approximated as ZMCSCG, and thus, $\vartheta_1|\mathcal{S}_1$ can be fairly approximated as ZMCSCG as well. As can be seen from (9.3.7), ξ_1 conditioned on \mathcal{S}_1 is random variable with respect to $h_{1,\ell}(k+1)$, $h_{2,\ell}(k)$, $h_{1,\ell}^{\epsilon}(k)$, $h_{2,\ell}^{\epsilon}(k+1)$, $h_{\ell,d}^{\epsilon}(k)$ and $h_{\ell,d}^{\epsilon}(k+1) \forall \ell$. Now, in order to simplify the evaluation of its power $P(\xi_1|\mathcal{S}_1)$, we first substitute (9.4.2) and (9.4.3) into (9.3.7), which leads to expanding ξ_1 as

$$\begin{aligned} \xi_1 = & \underbrace{\sum_{\ell=1}^M \mathcal{G}^2 \rho_{s,\ell} h_{2,\ell}(k+1)}_{I_1^{\xi_1}} + \underbrace{\sum_{\ell=1}^M \mathcal{G}^2 \sqrt{1 - \rho_{s,\ell}^2} h_{1,\ell}^*(k)}_{I_2^{\xi_1}} + \underbrace{\sum_{\ell=1}^M \mathcal{G}^2 \rho_{s,\ell} h_{2,\ell}(k+1)}_{I_3^{\xi_1}} \\ & + \underbrace{\sum_{\ell=1}^M \mathcal{G}^2 \sqrt{1 - \rho_{s,\ell}^2} |h_{\ell,d}(k)|^2}_{I_4^{\xi_1}} + \underbrace{\sum_{\ell=1}^M \mathcal{G}^2 \rho_{s,\ell} h_{2,\ell}(k+1) h_{\ell,d}(k)}_{I_5^{\xi_1}} \\ & + \underbrace{\sum_{\ell=1}^M \mathcal{G}^2 \sqrt{1 - \rho_{s,\ell}^2} h_{\ell,d}(k)}_{I_6^{\xi_1}} - \underbrace{\sum_{\ell=1}^M \mathcal{G}^2 \rho_{s,\ell} h_{1,\ell}^*(k) h_{2,\ell}(k+1)}_{I_7^{\xi_1}} \\ & - \underbrace{\sum_{\ell=1}^M \mathcal{G}^2 \sqrt{1 - \rho_{s,\ell}^2} h_{2,\ell}(k+1) h_{\ell,d}^*(k+1)}_{I_8^{\xi_1}} - \underbrace{\sum_{\ell=1}^M \mathcal{G}^2 \rho_{s,\ell} h_{1,\ell}^*(k)}_{I_9^{\xi_1}} \\ & - \underbrace{\sum_{\ell=1}^M \mathcal{G}^2 \sqrt{1 - \rho_{s,\ell}^2} |h_{\ell,d}(k+1)|^2}_{I_{10}^{\xi_1}} - \underbrace{\sum_{\ell=1}^M \mathcal{G}^2 \rho_{s,\ell} h_{1,\ell}^*(k) h_{\ell,d}^*(k+1)}_{I_{11}^{\xi_1}} \\ & - \underbrace{\sum_{\ell=1}^M \mathcal{G}^2 \sqrt{1 - \rho_{s,\ell}^2} h_{\ell,d}^*(k+1) h^{\epsilon}_{2,\ell}(k+1)}_{I_{12}^{\xi_1}}. \end{aligned} \quad (9.4.10)$$

It is shown now from (9.4.10) that $\xi_1|\mathcal{S}_1$ is random variable with respect to $e_{2,\ell}(k)$, $e_{1,\ell}(k+1)$, $h_{1,\ell}^\epsilon(k)$, $h_{2,\ell}^\epsilon(k+1)$, $h_{\ell,d}^\epsilon(k)$ and $h_{\ell,d}^\epsilon(k+1) \forall \ell$. $e_{2,\ell}(k) \sim \mathcal{CN}(0, \sigma_{2,\ell}^2)$, which we can evaluate its mean and variance, after doing some simplifications, respectively, as

$$\mathbb{E}[\xi_1|\mathcal{S}_1] = 0 \quad (9.4.11)$$

$$\begin{aligned} \text{Var}(\xi_1|\mathcal{S}_1) = & \mathcal{G}^4 \sum_{\ell=1}^M \left((|h_{1,\ell}(k)|^2 |h_{\ell,d}(k)|^2 \sigma_{e_{\ell,d}}^2 + |h_{\ell,d}(k)|^4 \sigma_{e_{1,\ell}}^2 + |h_{\ell,d}(k)|^2 \sigma_{e_{1,\ell}}^2 \sigma_{e_{\ell,d}}^2) \right. \\ & (\rho_{s,\ell}^2 |h_{2,\ell}(k+1)|^2 + (1 - \rho_{s,\ell}^2) \sigma_{2,\ell}^2) + (|h_{2,\ell}(k+1)|^2 |h_{\ell,d}(k+1)|^2 \\ & \sigma_{e_{\ell,d}}^2 + |h_{\ell,d}(k+1)|^4 \sigma_{e_{2,\ell}}^2 + |h_{\ell,d}(k+1)|^2 \sigma_{e_{2,\ell}}^2 \sigma_{e_{\ell,d}}^2) (\rho_{s,\ell}^2 |h_{1,\ell}(k)|^2 \\ & \left. + (1 - \rho_{s,\ell}^2) \sigma_{1,\ell}^2) \right). \end{aligned} \quad (9.4.12)$$

and thereby, its power is given as

$$\mathbb{P}(\xi_1|\mathcal{S}_1) = \text{Var}[\xi_1|\mathcal{S}_1]. \quad (9.4.13)$$

We can notice from (9.4.10) that, conditioned on \mathcal{S}_1 , the terms $I_1^{\xi_1}$, $I_3^{\xi_1}$, $I_7^{\xi_1}$ and $I_9^{\xi_1}$ are exact ZMCSCG while the remaining terms are not. However, as similar as approximating $I_3^{\theta_1}|\mathcal{S}_1$ as ZMCSCG as in Appendix A, we can approximate $I_2^{\xi_1}|\mathcal{S}_1$, $I_4^{\xi_1}|\mathcal{S}_1$, $I_5^{\xi_1}|\mathcal{S}_1$, $I_8^{\xi_1}|\mathcal{S}_1$, $I_{10}^{\xi_1}|\mathcal{S}_1$ and $I_{11}^{\xi_1}|\mathcal{S}_1$ as so. The remaining two terms $I_6^{\xi_1}|\mathcal{S}_1$ and $I_{12}^{\xi_1}|\mathcal{S}_1$ are sums of multiplications of three ZMCSCG random variables, which, can be also approximated with the help of the CLT as ZMCSCG (see Appendix B). Finally, we can conclude that $\xi_1|\mathcal{S}_1$ in (9.4.10) can be fairly approximated as complex-Gaussian. The noise term \tilde{n}_1 in (9.3.8) is function of the channel gains in the set \mathcal{S}_1 as well as of the the noise components $n_{s,\ell}(k)$, $n_{\ell,d}(k)$, $n_{s,\ell}^*(k+1)$ and $n_{\ell,d}^*(k+1)$ for all ℓ . Because $n_{s,\ell}(k)$, $n_{\ell,d}(k)$, $n_{s,\ell}^*(k+1)$ and $n_{\ell,d}^*(k+1)$ for all ℓ are statistically independent and distributed as ZMCSCG with variance N_o (i.e., $\mathcal{CN}(0, N_o)$),

$\tilde{n}_1|\mathcal{S}_1$ is ZMCSCG random variable which has the the following conditional power

$$\begin{aligned} \text{P}(\tilde{n}_1|\mathcal{S}_1) \triangleq \text{Var}(\tilde{n}_1|\mathcal{S}_1) = N_o \mathcal{G}^2 \sum_{\ell=1}^M & \left(|h_{1,\ell}(k)h_{\ell,d}(k)|^2 (\mathcal{G}^2 |h_{\ell,d}(k)|^2 + 1) + \right. \\ & \left. |h_{2,\ell}(k+1)h_{\ell,d}(k+1)|^2 (\mathcal{G}^2 |h_{\ell,d}(k+1)|^2 + 1) \right). \end{aligned} \quad (9.4.14)$$

The term \tilde{v}_1 in (9.3.9) is, conditioned on \mathcal{S}_1 , a random variable with respect to $n_{s,\ell}(k)$, $n_{\ell,d}(k)$, $n_{s,\ell}^*(k+1)$, $n_{\ell,d}^*(k+1)$ as well as to $h_{1,\ell}^\epsilon(k)$, $h_{2,\ell}^\epsilon(k+1)$, $h_{\ell,d}^\epsilon(k)$ and $h_{\ell,d}^\epsilon(k+1)$. Given that $n_{s,\ell}(k)$, $n_{\ell,d}(k)$, $n_{s,\ell}^*(k+1)$, $n_{\ell,d}^*(k+1)$ are $\sim \mathcal{CN}(0, N_o)$; and $h_{a,b}^\epsilon(\tau) \sim \mathcal{CN}(0, \sigma_{e_{a,b}}^2)$ $\forall (a,b) \in \{(1,\ell), (2,\ell), (\ell,d)\}$ and $\tau \in \{k, k-1\}$, the mean, variance and power of $\tilde{v}_1|\mathcal{S}_1$ can be evaluated, respectively, as

$$\text{E}[\tilde{v}_1|\mathcal{S}_1] = 0 \quad (9.4.15)$$

$$\begin{aligned} \text{Var}(\tilde{v}_1|\mathcal{S}_1) = \mathcal{G}^4 N_o \sum_{\ell=1}^M & \left((|h_{\ell,d}(k)|^2 + 1) (|h_{1,\ell}(k)|^2 \sigma_{e_{\ell,d}}^2 + |h_{\ell,d}(k)|^2 \sigma_{e_{1,\ell}}^2 + \sigma_{e_{1,\ell}}^2 \sigma_{e_{\ell,d}}^2) + \right. \\ & \left. (|h_{\ell,d}(k+1)|^2 + 1) (|h_{2,\ell}(k+1)|^2 \sigma_{e_{\ell,d}}^2 + |h_{\ell,d}(k+1)|^2 \sigma_{e_{2,\ell}}^2 + \sigma_{e_{2,\ell}}^2 \sigma_{e_{\ell,d}}^2) \right) \end{aligned} \quad (9.4.16)$$

and

$$\text{P}(\tilde{v}_1|\mathcal{S}_1) = \text{Var}(\tilde{v}_1|\mathcal{S}_1). \quad (9.4.17)$$

By approximating the non complex-Gaussian terms of \tilde{v}_1 as ZMCSCG (as similar as approximating $I_3^{\theta_1}|\mathcal{S}_1$ and $I_6^{\xi_1}|\mathcal{S}_1$) we can approximate $\tilde{v}_1|\mathcal{S}_1$ as ZMCSCG as $\mathcal{CN}(0, \text{Var}(\tilde{v}_1|\mathcal{S}_1))$. Finally, by substituting (9.4.6), (9.4.9), (9.4.13), (9.4.14) and (9.4.17) into (9.4.1), and after doing some simplifications, we can obtain the ultimate form of $\gamma_1|\mathcal{S}_1$ in terms of channel gains in set \mathcal{S}_1 , system links' correlation parameters $\rho_{a,b}$, estimation errors variances $\sigma_{e_{a,b}}^2$,

and $\frac{E_s}{N_o}$ as

$$\begin{aligned}
\gamma_1|\mathcal{S}_1 = & \frac{\left| \sum_{\ell=1}^M (|h_{1,\ell}(k)h_{\ell,d}(k)|^2 + |h_{2,\ell}(k+1)h_{\ell,d}(k+1)|^2) \right|^2 \frac{E_s}{N_o}}{\left| \sum_{\ell=1}^M (\rho_{s,\ell} h_{1,\ell}^*(k) h_{2,\ell}(k+1) (|h_{\ell,d}(k)|^2 - |h_{\ell,d}(k+1)|^2)) \right|^2 \frac{E_s}{N_o} +} \\
& \sum_{\ell=1}^M ((1 - \rho_{s,\ell}^2)(\sigma_{2,\ell}^2 |h_{1,\ell}(k)|^2 |h_{\ell,d}(k)|^4 + \sigma_{1,\ell}^2 |h_{2,\ell}(k+1)|^2 |h_{\ell,d}(k+1)|^4) \\
& + \sigma_{e_{\ell,d}}^2 |h_{1,\ell}(k)|^4 |h_{\ell,d}(k)|^2 + |h_{1,\ell}(k)|^2 |h_{\ell,d}(k)|^4 \sigma_{e_{1,\ell}}^2 + \\
& |h_{1,\ell}(k)|^2 |h_{\ell,d}(k)|^2 \sigma_{e_{1,\ell}}^2 \sigma_{e_{\ell,d}}^2 + |h_{2,\ell}(k+1)|^4 |h_{\ell,d}(k+1)|^2 \sigma_{e_{\ell,d}}^2 + \\
& |h_{2,\ell}(k+1)|^2 |h_{\ell,d}(k+1)|^4 \sigma_{e_{2,\ell}}^2 + |h_{2,\ell}(k+1)|^2 |h_{\ell,d}(k+1)|^2 \sigma_{e_{2,\ell}}^2 \sigma_{e_{\ell,d}}^2 + \\
& (|h_{1,\ell}(k)|^2 \sigma_{e_{\ell,d}}^2 |h_{\ell,d}(k)|^2 + |h_{\ell,d}(k)|^4 \sigma_{e_{1,\ell}}^2 + |h_{\ell,d}(k)|^2 \sigma_{e_{1,\ell}}^2 \sigma_{e_{\ell,d}}^2) (\rho_{s,\ell}^2 |h_{2,\ell}(k+1)|^2 \\
& + (1 - \rho_{s,\ell}^2) \sigma_{2,\ell}^2) + (|h_{2,\ell}(k+1)|^2 |h_{\ell,d}(k+1)|^2 \sigma_{e_{\ell,d}}^2 + |h_{\ell,d}(k+1)|^4 \sigma_{e_{2,\ell}}^2 \\
& + |h_{\ell,d}(k+1)|^2 \sigma_{e_{2,\ell}}^2 \sigma_{e_{\ell,d}}^2) (\rho_{s,\ell}^2 |h_{1,\ell}(k)|^2 + (1 - \rho_{s,\ell}^2) \sigma_{1,\ell}^2) \frac{E_s}{N_o} + \\
& 2 \sum_{\ell=1}^M (|h_{1,\ell}(k)h_{\ell,d}(k)|^2 (|h_{\ell,d}(k)|^2 + \frac{1}{\mathcal{G}^2}) + |h_{2,\ell}(k+1)h_{\ell,d}(k+1)|^2 (|h_{\ell,d}(k+1)|^2 \\
& + \frac{1}{\mathcal{G}^2}) + (|h_{\ell,d}(k)|^2 + 1)(|h_{1,\ell}(k)|^2 \sigma_{e_{\ell,d}}^2 + \sigma_{e_{1,\ell}}^2 |h_{\ell,d}(k)|^2 + \sigma_{e_{1,\ell}}^2 \sigma_{e_{\ell,d}}^2) + \\
& (|h_{\ell,d}(k+1)|^2 + 1)(|h_{2,\ell}(k+1)|^2 \sigma_{e_{\ell,d}}^2 + |h_{\ell,d}(k+1)|^2 \sigma_{e_{2,\ell}}^2 + \sigma_{e_{2,\ell}}^2 \sigma_{e_{\ell,d}}^2))
\end{aligned} \tag{9.4.18}$$

The instantaneous SINR $\gamma_1|\mathcal{S}_1$ is a random variable in terms of $h_{1,\ell}(k)$, $h_{2,\ell}(k+1)$, $h_{\ell,d}(k)$, $h_{\ell,d}(k+1)$: $\forall \ell = 1, 2 \dots, M$, which are Rayleigh distributed gains, and because of its very complicated form, deriving its probability-density-function (pdf) or moment-generating-function (mgf) is intractable.

9.4.2 Conditional SINR of the second decision statistic

Similarly as \tilde{y}_1 , \tilde{y}_2 in (9.3.3) is function of the channel gains in the set $\tilde{\mathcal{S}}$ described in (9.3.16). However, in order to simplify the derivation of its conditional SINR, say γ_2 , we do that conditioned on the channel gains in the set $\mathcal{S}_2 = \{h_{1,\ell}(k+1), h_{2,\ell}(k), h_{\ell,d}(k), h_{\ell,d}(k+1)\}^2$.

²The channel gains in this set are the ones that appear as coefficients of the desired-signal term in the decision statistic \tilde{y}_2 in (9.3.3).

From (9.3.3), we can now obtain γ_2 conditioned on \mathcal{S}_2 as

$$\begin{aligned}\gamma_2|\mathcal{S}_2 &= \frac{P(\mathcal{A}_2|\mathcal{S}_2)}{P(\mathcal{I}_2|\mathcal{S}_2) + P(\tilde{\chi}_2|\mathcal{S}_2)} \\ &= \frac{|\beta_2|^2(E_s/2)}{P(\zeta^*|\mathcal{S}_2)(E_s/2) + P(\vartheta_2|\mathcal{S}_2)(E_s/2) + P(\xi_2|\mathcal{S}_2)(E_s/2) + P(\tilde{n}_2|\mathcal{S}_2) + P(\tilde{v}_2|\mathcal{S}_2)}.\end{aligned}\tag{9.4.19}$$

It is clear from (9.3.5) that the conjugate of ζ is function of the elements in \mathcal{S}_2 as well as of $h_{1,\ell}(k)$ and $h_{2,\ell}(k+1)$. Therefore, conditioned on \mathcal{S}_2 , ζ^* is random variable in terms of both $h_{1,\ell}(k)$ and $h_{2,\ell}(k+1)$. With the help of the AR1 model in (9.2.1), we can write $h_{1,\ell}(k)$ in terms of $h_{1,\ell}(k+1)$ and $h_{2,\ell}^*(k+1)$ in terms of $h_{2,\ell}(k)$, respectively, as follows

$$h_{1,\ell}(k) = \rho_{s,\ell}h_{1,\ell}(k+1) + \sqrt{1 - \rho_{s,\ell}^2}e_{1,\ell}(k)\tag{9.4.20}$$

$$h_{2,\ell}^*(k+1) = \rho_{s,\ell}h_{2,\ell}^*(k) + \sqrt{1 - \rho_{s,\ell}^2}e_{2,\ell}^*(k+1).\tag{9.4.21}$$

By substituting (9.4.20) and (9.4.21) into (9.3.5), we can express ζ^* as

$$\zeta^* = \underbrace{\frac{\mathcal{G}^2 \sum_{\ell=1}^M (\rho_{s,\ell}h_{1,\ell}(k+1)h_{2,\ell}^*(k))}{(|h_{\ell,d}(k)|^2 - |h_{\ell,d}(k+1)|^2)}}_{\mu_2} + \underbrace{\frac{\mathcal{G}^2 \sum_{\ell=1}^M (\sqrt{1 - \rho_{s,\ell}^2}h_{2,\ell}^*(k)|h_{\ell,d}(k)|^2e_{1,\ell}(k) - \sqrt{1 - \rho_{s,\ell}^2}h_{1,\ell}(k+1)|h_{\ell,d}(k+1)|^2e_{2,\ell}^*(k+1))}{\psi_2}}_{\psi_2}\tag{9.4.22}$$

Because $e_{1,\ell}^*(k) \sim \mathcal{CN}(0, \sigma_{1,\ell}^2)$ and $e_{2,\ell}^*(k+1) \sim \mathcal{CN}(0, \sigma_{2,\ell}^2)$, ζ^* in (9.4.22) is, conditioned on \mathcal{S}_2 , a non-zero mean complex-Gaussian with mean μ_2 and variance $\text{Var}[\psi_2 | \mathcal{S}_2]$ that is given by

$$\text{Var}[\psi_2 | \mathcal{S}_2] = \mathcal{G}^4 \sum_{\ell=1}^M ((1 - \rho_{s,\ell}^2)(\sigma_{2,\ell}^2|h_{1,\ell}(k+1)|^2|h_{\ell,d}(k)|^4 + \sigma_{1,\ell}^2|h_{2,\ell}(k)|^2|h_{\ell,d}(k+1)|^4)).\tag{9.4.23}$$

We can now obtain $P(\zeta^*|\mathcal{S}_2)$ as

$$P(\zeta^*|\mathcal{S}_2) = |\mu_2|^2 + \text{Var}[\psi_2 | \mathcal{S}_2]. \quad (9.4.24)$$

The element ϑ_2 in (9.3.11) is function of the elements in \mathcal{S}_2 as well as of the estimation errors $h_{2,\ell}^\epsilon(k)$, $h_{1,\ell}^\epsilon(k+1)$, $h_{\ell,d}^\epsilon(k)$ and $h_{\ell,d}^\epsilon(k+1)$. Thus, $\vartheta_2|\mathcal{S}_2$ is random variable with respect to these estimation errors, and we can evaluate its mean, variance and power, respectively, as

$$E[\vartheta_2|\mathcal{S}_2] = 0 \quad (9.4.25)$$

$$\begin{aligned} \text{Var}(\vartheta_2|\mathcal{S}_2) = \mathcal{G}^4 \sum_{\ell=1}^M & \left(|h_{2,\ell}(k)|^4 |h_{\ell,d}(k)|^2 \sigma_{e_{\ell,d}}^2 + |h_{2,\ell}(k)|^2 |h_{\ell,d}(k)|^4 \sigma_{e_{2,\ell}}^2 + |h_{2,\ell}(k)|^2 \right. \\ & |h_{\ell,d}(k)|^2 \sigma_{e_{2,\ell}}^2 \sigma_{e_{\ell,d}}^2 + |h_{1,\ell}(k+1)|^4 |h_{\ell,d}(k+1)|^2 \sigma_{e_{\ell,d}}^2 + |h_{1,\ell}(k+1)|^2 \\ & \left. |h_{\ell,d}(k+1)|^4 \sigma_{e_{1,\ell}}^2 + |h_{1,\ell}(k+1)|^2 |h_{\ell,d}(k+1)|^2 \sigma_{e_{1,\ell}}^2 \sigma_{e_{\ell,d}}^2 \right) \end{aligned} \quad (9.4.26)$$

$$P(\vartheta_2|\mathcal{S}_2) = \text{Var}(\vartheta_2|\mathcal{S}_2). \quad (9.4.27)$$

By following the same CLT-based approach we followed to approximate $\vartheta_1|\mathcal{S}_1$ as ZMCSCG, $\vartheta_2|\mathcal{S}_2$ can be fairly approximated as ZMCSCG as $\mathcal{CN}(0, \text{Var}(\vartheta_2|\mathcal{S}_2))$. ξ_2 in (9.3.12), conditioned on \mathcal{S}_2 , is random variable with respect to $h_{2,\ell}(k+1)$, $h_{1,\ell}(k)$, $h_{2,\ell}^\epsilon(k)$, $h_{1,\ell}^\epsilon(k+1)$, $h_{\ell,d}^\epsilon(k)$ and $h_{\ell,d}^\epsilon(k+1)$, and by expanding $h_{1,\ell}(k)$ and $h_{2,\ell}^*(k+1)$ as in (9.4.20) and (9.4.21),

respectively, we can expand it as

$$\begin{aligned}
\xi_2 = & \mathcal{G}^2 \sum_{\ell=1}^M (\rho_{s,\ell} h_{1,\ell}(k+1) h_{2,\ell}^*(k) h_{\ell,d}(k) h_{\ell,d}^{\epsilon^*}(k) + \sqrt{1 - \rho_{s,\ell}^2} h_{2,\ell}^*(k) h_{\ell,d}(k) h_{\ell,d}^{\epsilon^*}(k) e_{1,\ell}(k) \\
& + \rho_{s,\ell} h_{1,\ell}(k+1) |h_{\ell,d}(k)|^2 h_{2,\ell}^{\epsilon^*}(k) + \sqrt{1 - \rho_{s,\ell}^2} |h_{\ell,d}(k)|^2 h_{2,\ell}^{\epsilon^*}(k) e_{1,\ell}(k) + \rho_{s,\ell} \\
& h_{1,\ell}(k+1) h_{\ell,d}(k) h_{2,\ell}^{\epsilon^*}(k) h_{\ell,d}^{\epsilon^*}(k) + \sqrt{1 - \rho_{s,\ell}^2} h_{\ell,d}(k) h_{2,\ell}^{\epsilon^*}(k) h_{\ell,d}^{\epsilon^*}(k) e_{1,\ell}(k) \\
& - \rho_{s,\ell} h_{2,\ell}^*(k) h_{1,\ell}(k+1) h_{\ell,d}^*(k+1) h_{\ell,d}^{\epsilon}(k+1) - \sqrt{1 - \rho_{s,\ell}^2} h_{1,\ell}(k+1) h_{\ell,d}^*(k+1) \\
& h_{\ell,d}^{\epsilon}(k+1) e_{2,\ell}^*(k+1) - \rho_{s,\ell} h_{2,\ell}^*(k) |h_{\ell,d}(k+1)|^2 h_{1,\ell}^{\epsilon}(k+1) - \sqrt{1 - \rho_{s,\ell}^2} \\
& |h_{\ell,d}(k+1)|^2 h_{1,\ell}^{\epsilon}(k+1) e_{2,\ell}^*(k+1) - \rho_{s,\ell} h_{2,\ell}^*(k) h_{\ell,d}^*(k+1) h_{1,\ell}^{\epsilon}(k+1) h_{\ell,d}^{\epsilon}(k+1) \\
& - \sqrt{1 - \rho_{s,\ell}^2} h_{\ell,d}^*(k+1) h_{1,\ell}^{\epsilon}(k+1) h_{\ell,d}^{\epsilon}(k+1) e_{2,\ell}^*(k+1)). \tag{9.4.28}
\end{aligned}$$

This clarifies that $\xi_2|\mathcal{S}_2$ is random variable with respect to $e_{1,\ell}(k)$, $e_{2,\ell}(k+1)$, $h_{2,\ell}^{\epsilon}(k)$, $h_{1,\ell}^{\epsilon}(k+1)$, $h_{\ell,d}^{\epsilon}(k)$ and $h_{\ell,d}^{\epsilon}(k+1)$. Based on this, we obtain the mean, variance and power of $\xi_2|\mathcal{S}_2$, respectively, as

$$\mathbb{E}[\xi_2|\mathcal{S}_2] = 0 \tag{9.4.29}$$

$$\begin{aligned}
\text{Var}(\xi_2|\mathcal{S}_2) = & \mathcal{G}^4 \sum_{\ell=1}^M ((|h_{2,\ell}(k)|^2 |h_{\ell,d}(k)|^2 \sigma_{e_{\ell,d}}^2 + |h_{\ell,d}(k)|^4 \sigma_{e_{2,\ell}}^2 + |h_{\ell,d}(k)|^2 \sigma_{e_{2,\ell}}^2 \sigma_{e_{\ell,d}}^2) \\
& (\rho_{s,\ell}^2 |h_{1,\ell}(k+1)|^2 + (1 - \rho_{s,\ell}^2) \sigma_{1,\ell}^2) + (|h_{1,\ell}(k+1)|^2 |h_{\ell,d}(k+1)|^2 \sigma_{e_{\ell,d}}^2 \\
& + |h_{\ell,d}(k+1)|^4 \sigma_{e_{1,\ell}}^2 + |h_{\ell,d}(k+1)|^2 \sigma_{e_{1,\ell}}^2 \sigma_{e_{\ell,d}}^2) (\rho_{s,\ell}^2 |h_{2,\ell}(k)|^2 + \\
& (1 - \rho_{s,\ell}^2) \sigma_{2,\ell}^2)) \tag{9.4.30}
\end{aligned}$$

$$\mathbb{P}(\xi_2|\mathcal{S}_2) = \text{Var}(\xi_2|\mathcal{S}_2). \tag{9.4.31}$$

Similarly as $\xi_1|\mathcal{S}_1$, we can use the CLT and approximate $\xi_2|\mathcal{S}_2$ as $\mathcal{CN}(0, \text{Var}(\xi_2|\mathcal{S}_2))$. Like \tilde{n}_1 , \tilde{n}_2 in (9.3.13) is function of the components $n_{s,\ell}(k)$, $n_{\ell,d}(k)$, $n_{s,\ell}^*(k+1)$ and $n_{\ell,d}^*(k+1) \forall \ell$, and

thus, conditioned on \mathcal{S}_2 , it is ZMCSCG random variable and we can obtain its conditional power as

$$\begin{aligned} P(\tilde{n}_2|\mathcal{S}_2) &\triangleq \text{Var}(\tilde{n}_2|\mathcal{S}_2) = N_o \mathcal{G}^2 \sum_{\ell=1}^M (|h_{1,\ell}(k+1)h_{\ell,d}(k+1)|^2 (\mathcal{G}^2 |h_{\ell,d}(k+1)|^2 + 1) \\ &\quad + |h_{2,\ell}(k)h_{\ell,d}(k)|^2 (\mathcal{G}^2 |h_{\ell,d}(k)|^2 + 1)). \end{aligned} \quad (9.4.32)$$

From (9.3.14), we can observe that $\tilde{v}_2|\mathcal{S}_2$ is random variable with respect to $n_{s,\ell}(k)$, $n_{\ell,d}(k)$, $n_{s,\ell}^*(k+1)$, $n_{\ell,d}^*(k+1)$, $h_{2,\ell}^\epsilon(k)$, $h_{1,\ell}^\epsilon(k+1)$, $h_{\ell,d}^\epsilon(k)$ and $h_{\ell,d}^\epsilon(k+1)$, and after doing some simplification, we can obtain its mean, variance and power, respectively, as

$$E(\tilde{v}_2|\mathcal{S}_2) = 0 \quad (9.4.33)$$

$$\begin{aligned} \text{Var}(\tilde{v}_2|\mathcal{S}_2) &= \mathcal{G}^4 N_o \sum_{\ell=1}^M ((|h_{\ell,d}(k)|^2 + 1)(|h_{2,\ell}(k)|^2 \sigma_{e_{\ell,d}}^2 + |h_{\ell,d}(k)|^2 \sigma_{e_{2,\ell}}^2 + \sigma_{e_{2,\ell}}^2 \sigma_{e_{\ell,d}}^2) + \\ &\quad (|h_{\ell,d}(k+1)|^2 + 1)(|h_{1,\ell}(k+1)|^2 \sigma_{e_{\ell,d}}^2 + |h_{\ell,d}(k+1)|^2 \sigma_{e_{1,\ell}}^2 + \sigma_{e_{1,\ell}}^2 \sigma_{e_{\ell,d}}^2)) \end{aligned} \quad (9.4.34)$$

$$P(\tilde{v}_2|\mathcal{S}_2) = \text{Var}(\tilde{v}_2|\mathcal{S}_2). \quad (9.4.35)$$

By substituting (9.4.24), (9.4.27), (9.4.31), (9.4.32) and (9.4.35) into (9.4.19), we obtain the ultimate form of $\gamma|\mathcal{S}_2$ as

$$\begin{aligned} \gamma_2|\mathcal{S}_2 = & \frac{\left| \sum_{\ell=1}^M (|h_{2,\ell}(k)h_{\ell,d}(k)|^2 + |h_{1,\ell}(k+1)h_{\ell,d}(k+1)|^2) \right|^2 \frac{E_s}{N_o}}{\left(\left| \sum_{\ell=1}^M (\rho_{s,\ell} h_{2,\ell}^*(k) h_{1,\ell}(k+1) (|h_{\ell,d}(k)|^2 - |h_{\ell,d}(k+1)|^2)) \right|^2 \frac{E_s}{N_o} + \right. \\ & \sum_{\ell=1}^M ((1 - \rho_{s,\ell}^2)(\sigma_{1,\ell}^2 |h_{2,\ell}(k)|^2 |h_{\ell,d}(k)|^4 + \sigma_{2,\ell}^2 |h_{1,\ell}(k+1)|^2 |h_{\ell,d}(k+1)|^4) \\ & + \sigma_{e_{\ell,d}}^2 |h_{2,\ell}(k)|^4 |h_{\ell,d}(k)|^2 + |h_{2,\ell}(k)|^2 |h_{\ell,d}(k)|^4 \sigma_{e_{2,\ell}}^2 + \\ & |h_{2,\ell}(k)|^2 |h_{\ell,d}(k)|^2 \sigma_{e_{2,\ell}}^2 \sigma_{e_{\ell,d}}^2 + |h_{1,\ell}(k+1)|^4 |h_{\ell,d}(k+1)|^2 \sigma_{e_{1,\ell}}^2 + \\ & |h_{1,\ell}(k+1)|^2 |h_{\ell,d}(k+1)|^2 \sigma_{e_{1,\ell}}^2 \sigma_{e_{\ell,d}}^2 + |h_{1,\ell}(k+1)|^2 |h_{\ell,d}(k+1)|^2 \sigma_{e_{1,\ell}}^2 \sigma_{e_{\ell,d}}^2 + \\ & (|h_{2,\ell}(k)|^2 \sigma_{e_{\ell,d}}^2 |h_{\ell,d}(k)|^2 + |h_{\ell,d}(k)|^4 \sigma_{e_{2,\ell}}^2 + |h_{\ell,d}(k)|^2 \sigma_{e_{2,\ell}}^2 \sigma_{e_{\ell,d}}^2) (\rho_{s,\ell}^2 |h_{1,\ell}(k+1)|^2 \\ & + (1 - \rho_{s,\ell}^2) \sigma_{1,\ell}^2) + (|h_{1,\ell}(k+1)|^2 |h_{\ell,d}(k+1)|^2 \sigma_{e_{\ell,d}}^2 + |h_{\ell,d}(k+1)|^4 \sigma_{e_{1,\ell}}^2 \\ & + |h_{\ell,d}(k+1)|^2 \sigma_{e_{1,\ell}}^2 \sigma_{e_{\ell,d}}^2) (\rho_{s,\ell}^2 |h_{2,\ell}(k)|^2 + (1 - \rho_{s,\ell}^2) \sigma_{2,\ell}^2) \left. \right) \frac{E_s}{N_o} + \\ & 2 \sum_{\ell=1}^M (|h_{2,\ell}(k)h_{\ell,d}(k)|^2 (|h_{\ell,d}(k)|^2 + \frac{1}{\mathcal{G}^2}) + |h_{1,\ell}(k+1)h_{\ell,d}(k+1)|^2 (|h_{\ell,d}(k+1)|^2 + \frac{1}{\mathcal{G}^2}) \\ & + (|h_{\ell,d}(k)|^2 + 1)(|h_{2,\ell}(k)|^2 \sigma_{e_{\ell,d}}^2 + \sigma_{e_{2,\ell}}^2 |h_{\ell,d}(k)|^2 + \sigma_{e_{2,\ell}}^2 \sigma_{e_{\ell,d}}^2) + \\ & (|h_{\ell,d}(k+1)|^2 + 1)(|h_{1,\ell}(k+1)|^2 \sigma_{e_{\ell,d}}^2 + |h_{\ell,d}(k+1)|^2 \sigma_{e_{1,\ell}}^2 + \sigma_{e_{1,\ell}}^2 \sigma_{e_{\ell,d}}^2)) \end{aligned} \quad (9.4.36)$$

which also has intractable form to derive its pdf.

9.4.3 Conditional SEP expression

Without loss of generality, we can express the overall SEP at the output of the q -QAM demodulator, conditioned on the channel gains in the set \mathcal{S} described in (9.3.16), say $P_e|\mathcal{S}$, as

$$P_e|\mathcal{S} = Pr(x_1)P_e^{\tilde{y}_1}|\mathcal{S}_1 + Pr(x_2)P_e^{\tilde{y}_2}|\mathcal{S}_2 \quad (9.4.37)$$

where $Pr(x_1)$ and $Pr(x_2)$ are the symbol transmission probabilities of x_1 and x_2 , respectively; and $P_e^{\tilde{y}_1}|\mathcal{S}_1$ and $P_e^{\tilde{y}_2}|\mathcal{S}_2$ are the conditional probabilities of symbol error decisions made by the q -QAM demodulator in estimating x_1 from \tilde{y}_1 (conditioned on \mathcal{S}_1) and in estimating x_2 from \tilde{y}_2 (conditioned on \mathcal{S}_2), respectively. By assuming equiprobable symbol transmissions for x_1

and x_2 , i.e., $Pr(x_1) = Pr(x_2) = \frac{1}{2}$, and directly using the AWGN-system's SEP expression in (6.3.1) to evaluate $P_e^{\tilde{y}_1}|\mathcal{S}_1$ (by replacing $\bar{\gamma}$ by $\gamma_1|\mathcal{S}_1$) and $P_e^{\tilde{y}_2}|\mathcal{S}_2$ (by replacing $\bar{\gamma}$ by $\gamma_2|\mathcal{S}_2$)³, we can obtain $P_e|\mathcal{S}$ in the following (approximate) closed-form as

$$P_e|\mathcal{S} = 1 - \frac{1}{2} \left(\left(1 - 2 \left(1 - \frac{1}{\sqrt{q}} \right) Q \left(\sqrt{\frac{3}{q-1}} \gamma_1 |\mathcal{S}_1 \right) \right)^2 - \left(1 - 2 \left(1 - \frac{1}{\sqrt{q}} \right) Q \left(\sqrt{\frac{3}{q-1}} \gamma_2 |\mathcal{S}_2 \right) \right)^2 \right). \quad (9.4.38)$$

As an impact of the nodes mobility and/or the imperfect channel estimation, the system's SEP performance experiences sever degradation especially at high values of the per-symbol average SNR $\frac{E_s}{N_o}$. This degradation is mainly represented by irreducible conditional symbol error floors $P_e^F|\mathcal{S}$ that can be evaluated as

$$P_e^F|\mathcal{S} = \lim_{\frac{E_s}{N_o} \rightarrow \infty} P_e|\mathcal{S} = 1 - \frac{1}{2} \left(\left(1 - 2 \left(1 - \frac{1}{\sqrt{q}} \right) Q \left(\sqrt{\frac{3}{q-1}} \gamma_1^F |\mathcal{S}_1 \right) \right)^2 - \left(1 - 2 \left(1 - \frac{1}{\sqrt{q}} \right) Q \left(\sqrt{\frac{3}{q-1}} \gamma_2^F |\mathcal{S}_2 \right) \right)^2 \right) \quad (9.4.39)$$

³This is valid because, in \tilde{y}_1 and \tilde{y}_2 , the terms ζ_{x_2} , \tilde{n}_1 , $\zeta_{x_1}^*$ and \tilde{n}_2 are complex-Gaussian and, as discussed in subsections 9.4.1 and 9.4.2, the terms $\vartheta_1 x_1$, $\xi_1 x_2$, \tilde{v}_1 , $\vartheta_2 x_2$, $\xi_2 x_1$ and \tilde{v}_2 are fairly approximated with the help of the CLT as complex-Gaussian.

where

$$\begin{aligned}
\gamma_1^F |\mathcal{S}_1| &= \lim_{\frac{E_s}{N_o} \rightarrow \infty} \gamma_1 |\mathcal{S}_1| \\
&= \frac{\left| \sum_{\ell=1}^M (|h_{1,\ell}(k)h_{\ell,d}(k)|^2 + |h_{2,\ell}(k+1)h_{\ell,d}(k+1)|^2) \right|^2}{\left| \sum_{\ell=1}^M (\rho_{s,\ell} h_{1,\ell}^*(k) h_{2,\ell}(k+1) (|h_{\ell,d}(k)|^2 - |h_{\ell,d}(k+1)|^2)) \right|^2 +} \\
&\quad \sum_{\ell=1}^M ((1 - \rho_{s,\ell}^2) (\sigma_{2,\ell}^2 |h_{1,\ell}(k)|^2 |h_{\ell,d}(k)|^4 + \sigma_{1,\ell}^2 |h_{2,\ell}(k+1)|^2 |h_{\ell,d}(k+1)|^4) \\
&\quad + \sigma_{e_{\ell,d}}^2 |h_{1,\ell}(k)|^4 |h_{\ell,d}(k)|^2 + |h_{1,\ell}(k)|^2 |h_{\ell,d}(k)|^4 \sigma_{e_{1,\ell}}^2 + \\
&\quad |h_{1,\ell}(k)|^2 |h_{\ell,d}(k)|^2 \sigma_{e_{1,\ell}}^2 \sigma_{e_{\ell,d}}^2 + |h_{2,\ell}(k+1)|^4 |h_{\ell,d}(k+1)|^2 \sigma_{e_{\ell,d}}^2 + \\
&\quad |h_{2,\ell}(k+1)|^2 |h_{\ell,d}(k+1)|^4 \sigma_{e_{2,\ell}}^2 + |h_{2,\ell}(k+1)|^2 |h_{\ell,d}(k+1)|^2 \sigma_{e_{2,\ell}}^2 \sigma_{e_{\ell,d}}^2 + \\
&\quad (|h_{1,\ell}(k)|^2 \sigma_{e_{\ell,d}}^2 |h_{\ell,d}(k)|^2 + |h_{\ell,d}(k)|^4 \sigma_{e_{1,\ell}}^2 + |h_{\ell,d}(k)|^2 \sigma_{e_{1,\ell}}^2 \sigma_{e_{\ell,d}}^2) (\rho_{s,\ell}^2 |h_{2,\ell}(k+1)|^2 \\
&\quad + (1 - \rho_{s,\ell}^2) \sigma_{2,\ell}^2) + (|h_{2,\ell}(k+1)|^2 |h_{\ell,d}(k+1)|^2 \sigma_{e_{\ell,d}}^2 + |h_{\ell,d}(k+1)|^4 \sigma_{e_{2,\ell}}^2 + \\
&\quad |h_{\ell,d}(k+1)|^2 \sigma_{e_{2,\ell}}^2 \sigma_{e_{\ell,d}}^2) (\rho_{s,\ell}^2 |h_{1,\ell}(k)|^2 + (1 - \rho_{s,\ell}^2) \sigma_{1,\ell}^2)) \\
\end{aligned} \tag{9.4.40}$$

$$\begin{aligned}
\gamma_2^F |\mathcal{S}_2| &= \lim_{\frac{E_s}{N_o} \rightarrow \infty} \gamma_2 |\mathcal{S}_2| \\
&= \frac{\left| \sum_{\ell=1}^M (|h_{2,\ell}(k)h_{\ell,d}(k)|^2 + |h_{1,\ell}(k+1)h_{\ell,d}(k+1)|^2) \right|^2}{\left| \sum_{\ell=1}^M (\rho_{s,\ell} h_{2,\ell}^*(k) h_{1,\ell}(k+1) (|h_{\ell,d}(k)|^2 - |h_{\ell,d}(k+1)|^2)) \right|^2 +} \\
&\quad \sum_{\ell=1}^M ((1 - \rho_{s,\ell}^2) (\sigma_{1,\ell}^2 |h_{2,\ell}(k)|^2 |h_{\ell,d}(k)|^4 + \sigma_{2,\ell}^2 |h_{1,\ell}(k+1)|^2 |h_{\ell,d}(k+1)|^4) \\
&\quad + \sigma_{e_{\ell,d}}^2 |h_{2,\ell}(k)|^4 |h_{\ell,d}(k)|^2 + |h_{2,\ell}(k)|^2 |h_{\ell,d}(k)|^4 \sigma_{e_{2,\ell}}^2 + \\
&\quad |h_{2,\ell}(k)|^2 |h_{\ell,d}(k)|^2 \sigma_{e_{2,\ell}}^2 \sigma_{e_{\ell,d}}^2 + |h_{1,\ell}(k+1)|^4 |h_{\ell,d}(k+1)|^2 \sigma_{e_{\ell,d}}^2 + \\
&\quad |h_{1,\ell}(k+1)|^2 |h_{\ell,d}(k+1)|^4 \sigma_{e_{1,\ell}}^2 + |h_{1,\ell}(k+1)|^2 |h_{\ell,d}(k+1)|^2 \sigma_{e_{1,\ell}}^2 \sigma_{e_{\ell,d}}^2 + \\
&\quad (|h_{2,\ell}(k)|^2 \sigma_{e_{\ell,d}}^2 |h_{\ell,d}(k)|^2 + |h_{\ell,d}(k)|^4 \sigma_{e_{2,\ell}}^2 + |h_{\ell,d}(k)|^2 \sigma_{e_{2,\ell}}^2 \sigma_{e_{\ell,d}}^2) (\rho_{s,\ell}^2 |h_{1,\ell}(k+1)|^2 \\
&\quad + (1 - \rho_{s,\ell}^2) \sigma_{1,\ell}^2) + (|h_{1,\ell}(k+1)|^2 |h_{\ell,d}(k+1)|^2 \sigma_{e_{\ell,d}}^2 + |h_{\ell,d}(k+1)|^4 \sigma_{e_{1,\ell}}^2 + \\
&\quad |h_{\ell,d}(k+1)|^2 \sigma_{e_{1,\ell}}^2 \sigma_{e_{\ell,d}}^2) (\rho_{s,\ell}^2 |h_{2,\ell}(k)|^2 + (1 - \rho_{s,\ell}^2) \sigma_{2,\ell}^2)) \\
\end{aligned} \tag{9.4.41}$$

9.5 System Average SEP Analysis

The system's average SEP, say \bar{P}_e , can be obtained from the conditional SEP in (9.4.38) as

$$\begin{aligned} \bar{P}_e = \mathbb{E}_{\mathcal{S}}[P_e|\mathcal{S}] = 1 - \frac{1}{2} & \left(\mathbb{E}_{\mathcal{S}_1} \left[\left(1 - 2 \left(1 - \frac{1}{\sqrt{q}} \right) Q \left(\sqrt{\frac{3}{q-1}} \gamma_1 | \mathcal{S}_1 \right) \right)^2 \right] \right. \\ & \left. - \mathbb{E}_{\mathcal{S}_2} \left[\left(1 - 2 \left(1 - \frac{1}{\sqrt{q}} \right) Q \left(\sqrt{\frac{3}{q-1}} \gamma_2 | \mathcal{S}_2 \right) \right)^2 \right] \right) \end{aligned} \quad (9.5.1)$$

where $\mathbb{E}_{\mathcal{U}}[\cdot]$ denotes the statistical expectation operator with respect to \mathcal{U} . Evaluating the last two expectations in (9.5.1) requires first deriving the pdfs of both $\gamma|\mathcal{S}_1$ in (9.4.18) and $\gamma|\mathcal{S}_2$ in (9.4.36), which, as we mentioned before, is too hard to accomplish. Therefore, we propose here to use semi-analytical computation for \bar{P}_e , based on the sampling mean concept, as

$$\begin{aligned} \bar{P}_e = 1 - \frac{1}{2} & \left(\frac{1}{N} \sum_{j=1}^N \left(\left(1 - 2 \left(1 - \frac{1}{\sqrt{q}} \right) Q \left(\sqrt{\frac{3}{q-1}} \gamma_1 | \mathcal{S}_1^j \right) \right)^2 \right. \right. \\ & \left. \left. - \left(1 - 2 \left(1 - \frac{1}{\sqrt{q}} \right) Q \left(\sqrt{\frac{3}{q-1}} \gamma_2 | \mathcal{S}_2^j \right) \right)^2 \right) \right) \end{aligned} \quad (9.5.2)$$

where $\gamma_1|\mathcal{S}_1^j$ and $\gamma_2|\mathcal{S}_2^j$ are the generated SINRs in the j th realization obtained by (9.4.18) and (9.4.36), respectively, and N is the number of realizations in the simulation ($N = 10^6$ in our numerical results). In the numerical results section, we provide realistic link-level simulations to validate the semi-analytical results obtained based on (9.5.2). Similarly, we

can semi-analytically compute average values for $P_e^F|\mathcal{S}$ in (9.4.39) as

$$\begin{aligned} \overline{P}_e^F = \mathbb{E}_s[P_e^F|\mathcal{S}] = 1 - \frac{1}{2} \left(\frac{1}{N} \sum_{j=1}^N \left(\left(1 - 2 \left(1 - \frac{1}{\sqrt{q}} \right) Q \left(\sqrt{\frac{3}{q-1}} \gamma_1^F | \mathcal{S}_1^j \right) \right)^2 \right. \right. \\ \left. \left. - \left(1 - 2 \left(1 - \frac{1}{\sqrt{q}} \right) Q \left(\sqrt{\frac{3}{q-1}} \gamma_2^F | \mathcal{S}_2^j \right) \right)^2 \right) \right) \end{aligned} \quad (9.5.3)$$

where $\gamma_1^F|\mathcal{S}_1^j$ and $\gamma_2^F|\mathcal{S}_2^j$ are the generated SINRs in the j th realization obtained by (??) and (??), respectively.

9.6 Numerical Results and Simulation

In this section, we present numerical results along with realistic link-level simulations to validate the accuracy of our derived expressions and to show the impact of both the high nodes mobility; i.e., the time-selective fading impact, and the imperfect channel estimation on the SEP performance of the OSTBC-based cooperative system under study. We provide these results in terms of the QAM constellation size q , the number of relays M , the estimation error variances $\sigma_{e_{a,b}}^2$, the nodes' relative speeds $v_{a,b}$ in mph, the transmission symbol-rate R_s in kbps, the carrier frequency f_c in GHz, the path loss exponent n , the cooperating nodes normalized distances $d_{a,b}$. Further, moving nodes and static-nodes cases are related to time-selective and quasi-static fading cases, respectively.

Fig. 9.1 shows numerical plots for the system's average SEP performance versus the per-symbol average $\frac{E_s}{N_o}$ with single relay ($M = 1$), 4-ary and 64-ary QAM constellations, and transmission symbol-rate of 44 kbps (which is corresponding to narrowband channels). We can first observe that the results plotted using (9.5.2) provides a perfect match with the exact results obtained via practical link-level simulation, which corroborates the correctness of the derived SINRs exact expressions and the tightness of the approximations followed using the CLT. This figure also shows that, as compared with the system's SEP performance under the static-nodes (0 mph relative speeds) and perfect channel estimation ($\sigma_{e_{s,\ell}}^2 = \sigma_{e_{\ell,d}}^2 = 0$)

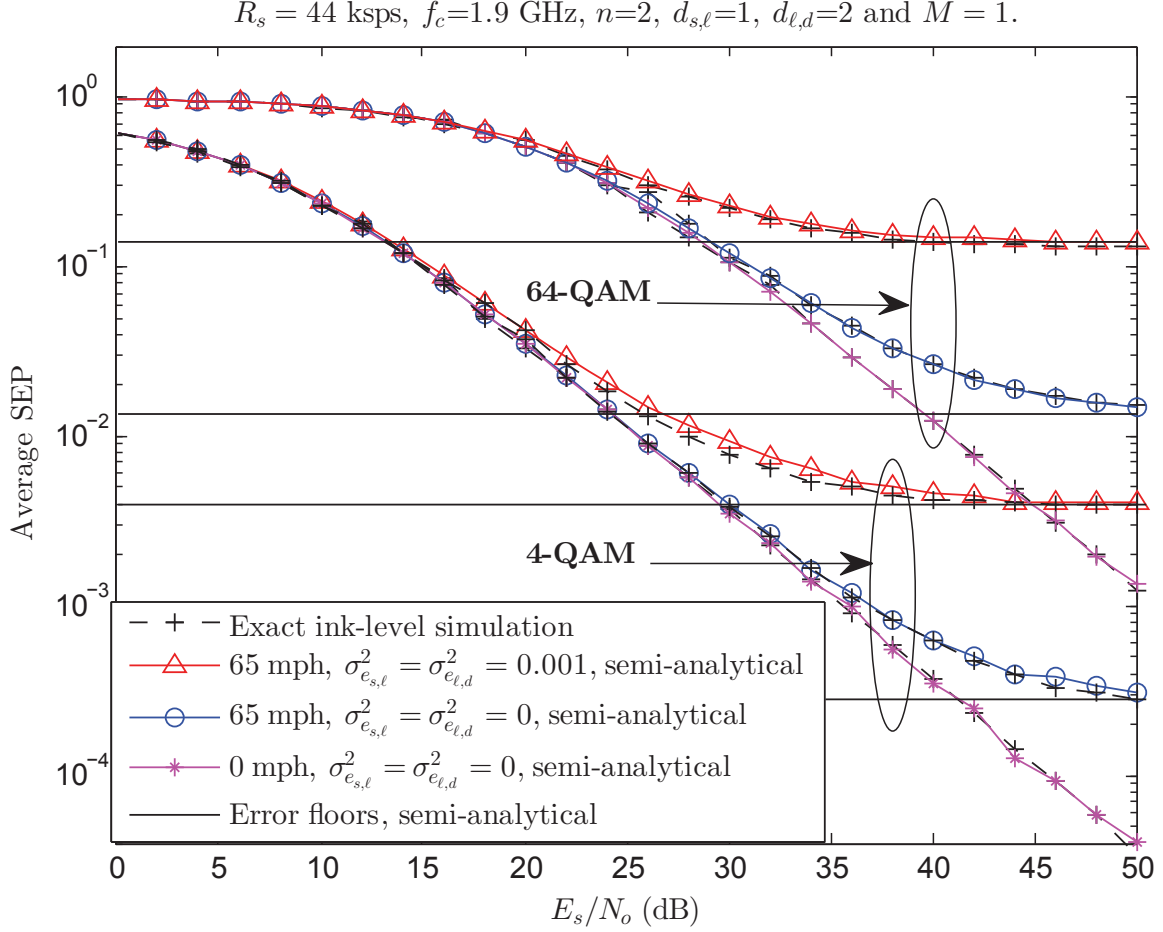


Figure 9.1. Average SEP versus E_s/N_o for $M = 1$ and 4 and 64 -QAM, transmission data-rate $R_s = 44$ ksp/s, carrier frequency $f_c = 1.9$ GHz, path-loss exponent $n = 2$, normalized nodes distances $d_{s,\ell} = 1$ and $d_{\ell,d} = 2$.

scenario, the nodes relatively high mobility, for e.g., with relative speeds of 65 mph, degrades the system SEP performance, in particular, at high values of $\frac{E_s}{N_o}$ (starting from 30 dB) and limits it by floors. Moreover, under the significance of the channel estimation error; i.e., imperfect channel estimation scenario with for e.g. $\sigma_{e_{s,\ell}}^2 = \sigma_{e_{\ell,d}}^2 = 0.001$, the system's SEP performance is further degraded, almost, starting from $\frac{E_s}{N_o} = 18$ dB and limited by higher floors.

In Fig. 9.2, we plot the system average SEP versus $\frac{E_s}{N_o}$ with 16 -QAM constellation showing the effect of the increase in the channel estimation error variance for different M values. It is obvious that the system's average SEP performance is improved with M as a

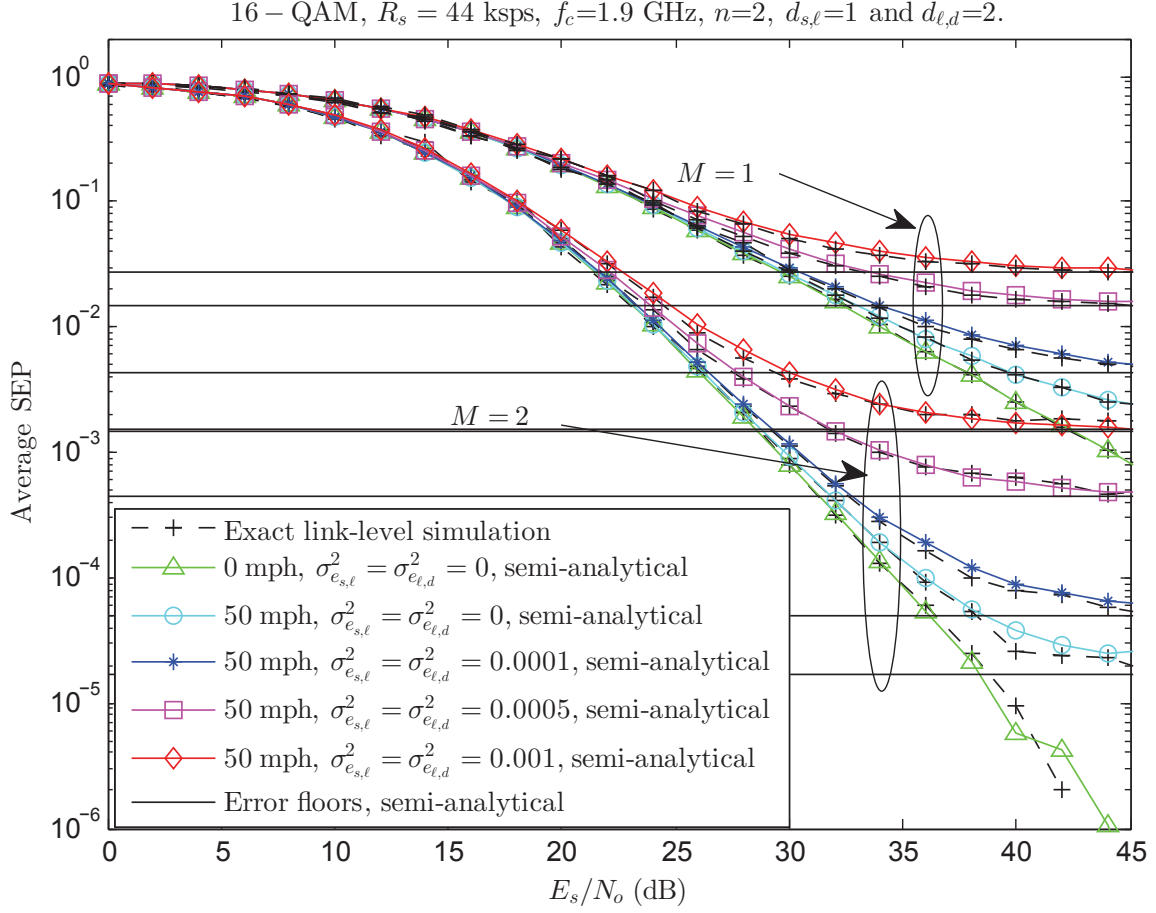


Figure 9.2. Average SEP versus E_s/N_o for $M = 1$ and 2 , 16 QAM constellations, transmission data-rate $R_b = 44$ kbps, carrier frequency $f_c = 1.9$ GHz, path-loss exponent $n = 2$, normalized nodes distances $d_{s,\ell} = 1$ and $d_{\ell,d} = 2$.

result of the increased diversity-gain achieved via the relaying process. However, the harmful impact of both the nodes mobility and the imperfect channel estimation still exist for any number of relays M , where, it is clear that the small increase in the estimation error variance, for e.g., from 0.0001 to 0.0005, causes a significant performance degradation. Also, a high agreement between the semi-analytically results and link-level simulations is notable.

Fig. 9.3 shows plots the system average SEP versus the nodes relative speeds in mph, for 16-ary and 64-ary QAM constellations, $M = 1$, $R_s = 9.6$ and 25 kbps, and $\frac{E_s}{N_o} = 20$ dB, considering both perfect and imperfect channel estimation scenarios. It is clear that, regardless of the other parameters, the increase in the nodes speeds degrades the system average

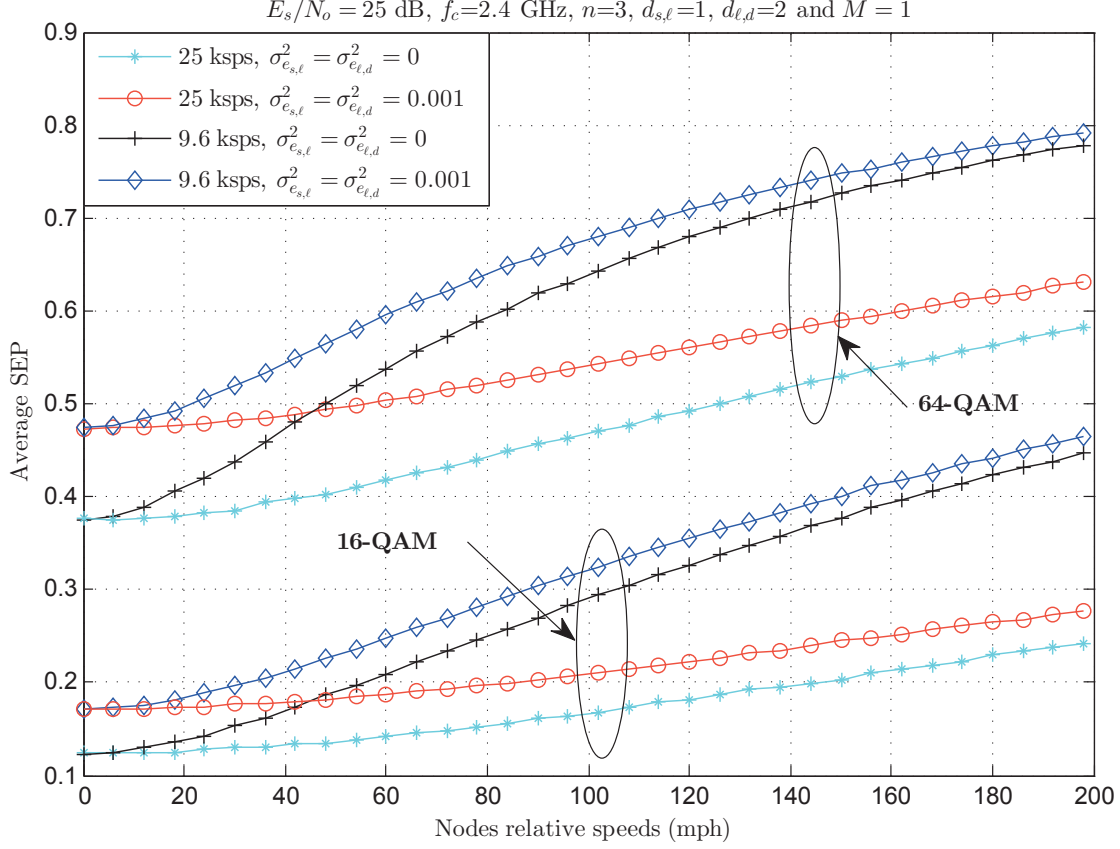


Figure 9.3. Average SEP versus nodes relative speeds in mph with $E_s/N_o = 25$ dB, different transmission data-rate values of 9.6 and 25 ksps, $M = 1$, QAM constellations size of 16 and 64, carrier frequency $f_c = 2.4$ GHz, path-loss exponent $n = 3$, normalized nodes distances $d_{s,\ell} = 1$ and $d_{\ell,d} = 2$.

SEP performance. However, for fixed transmission data-rate, the system SEP performance is worse in the case of imperfect channel estimation even though the estimation error variance is relatively small (for e.g., $\sigma_{e_{s,\ell}}^2 = \sigma_{e_{\ell,d}}^2 = 0.001$). On the other hand, for fixed estimation error variance, the system SEP performance is improved and the speed of its degradation by increasing the nodes speeds is less when the transmission data-rate is higher (compare the * curve with the + one). This is because of the fact that increasing the transmission data-rate increases the fading links' correlation parameters, which reduces the likelihood of the time-selective fading to occur (see (9.2.1) for more clarification). This also could be notified from Fig. 9.4, where, for a fixed relative speed and channel estimation error variance, the improvement in the system error performance is fast with increasing the transmission

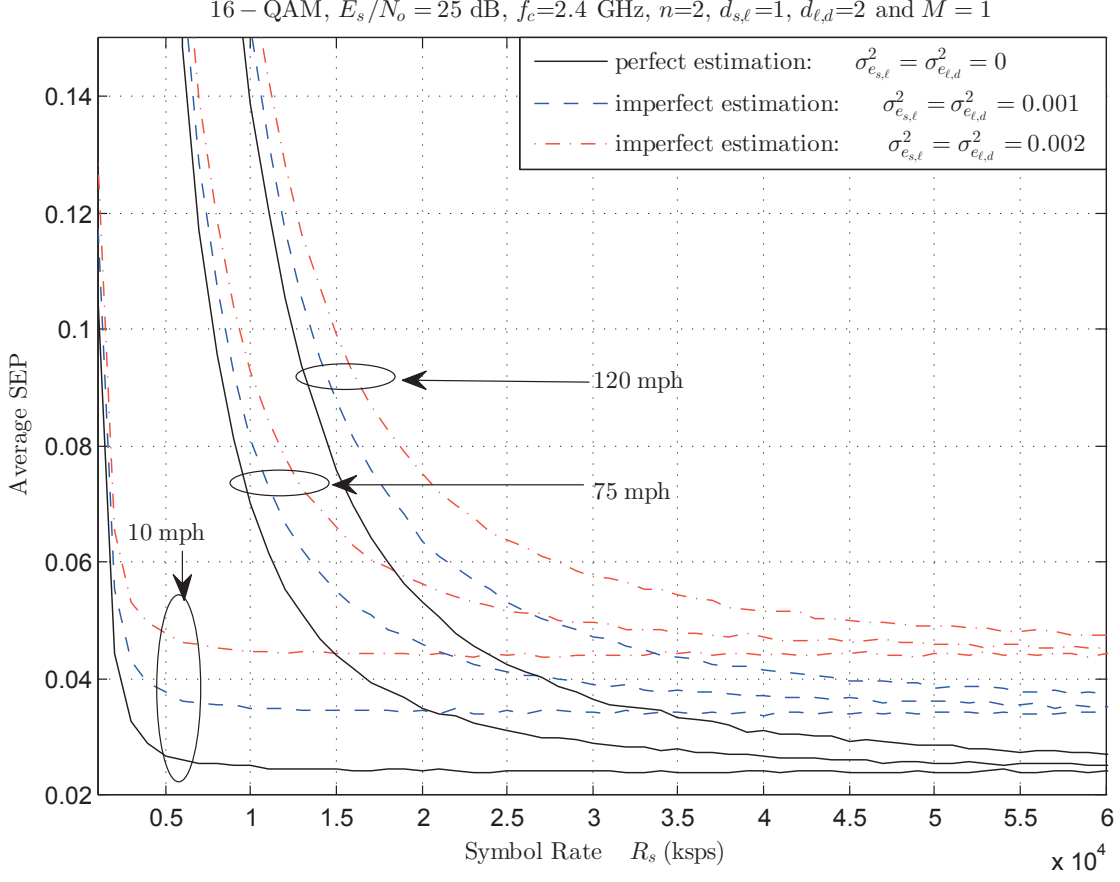


Figure 9.4. Average SEP versus transmission data-rate in kbps with $E_s/N_o = 25$ dB, different nodes relative speeds of 10, 75 and 120 mph, $M = 1$, 16-QAM constellation, carrier frequency $f_c = 2.4$ GHz, path-loss exponent $n = 2$, normalized nodes distances $d_{s,\ell} = 1$ and $d_{\ell,d} = 2$.

data-rate.

9.7 Conclusion

In this chapter, we have investigated the influence of the more practical scenarios of both nodes-mobility and imperfect CSI estimation on the SEP performance of an Alamouti-type OSTBC-based multiple-relay fixed-gain AF cooperative-diversity system with q -ary QAM. All of the system's multipath links are characterized by frequency-flat and, due to nodes-mobility, by time-selective (i.e., rapidly time-varying) fading channels using the AR1 process. Due to the imperfect CSI estimation, all of the estimated channel gains at the system's relays and destination are assumed to be corrupted by Gaussian errors. For such

a system model, we have employed the ALD at its destination and shown that, due to nodes-mobility and imperfect CSI estimation, this ALD is no longer optimal ML and provides interfering and statistically correlated decision variables. Exploiting the AR1 model, we have first derived exact closed-form expressions of effective SINRs associated with these decision variables, which generalize an SNR expression that is well known in the literature for such a system under the special scenario of static-nodes, perfect estimation and single-relay. Moreover, benefiting from the central-limit-theorem (CLT), we have provided a tight approximate closed-form expression for the system's conditional SEP at the q -QAM demodulator's output by directly using the obtained SINRs along with the already known SEP expression of the AWGN q -QAM systems. Furthermore, from the obtained conditional SEP expression, it is revealed that the nodes-mobility and/or the imperfect CSI estimation severely degrade the system SEP performance by irreducible error floors that appear irrespective of the number of the relay nodes. Because of the intractability in deriving closed-form probability density functions of the obtained SINRs, due to their very complicated forms, we have proposed a semi-analytical computation of the system's average SEP using the exact conditional SEP expression based on the sampling mean concept. Numerical results for the system's semi-analytical average SEP along with realistic link-level simulations have been also provided to validate the accuracy of the derived expressions and to demonstrate the system's performance under several scenarios.

Part III:
Dissertation Conclusions and Proposed Future Work

CHAPTER 10

Dissertation Conclusions and Proposed Future Work

10.1 Dissertation Conclusions

In this dissertation, we have discussed several problems related to evaluating and improving the performance of several emerging models for wireless amplify-and-forward (AF) cooperative-based communication systems taking into account the effects of different practical issues; including, nodes mobility (either low or high), channel estimations (either perfect or imperfect), and speeds of receivers channel tracking loops (either slow or fast). We have developed extensive approaches and analytical techniques to quantitatively evaluate the impacts of these practical issues on the performance of wireless AF cooperative systems by deriving new closed-form expressions for different system performance metrics. We have also proposed several innovative receiving designs aiming to mitigating the high nodes mobility effects on the performance of AF cooperative systems and improving their overall performance.

This dissertation contains two parts and in the following we summarize the contributions of each part:

- In the first part of this dissertation several scenarios for multiple-relay single-antenna-nodes AF cooperative communication systems that employ MRC combining at the destination and operate in mobile environments have been considered, and extensive analyses of different performance measures have been presented. The performance of these considered system scenarios have been studied taking into account the impacts of the nodes mobility, the estimation errors, and the speed of the receivers tracking

loops that estimate the individual channel gains. Under these impacts, tight approximate novel and general closed-form expressions for the systems per-block average bit error rate (BER), outage probability, and channel capacity have been derived. ALL of the derived performance expressions are functions of the nodes relative speeds, the transmission data rates, the channel estimation errors, and the speeds of the receivers tracking loops, and thus, they generalize many previously published literature results. With the help of these expressions we have analytically shown that the wireless AF cooperative communication systems performance is severally affected by the high nodes mobility (in particular when the channel estimations are imperfect), where the systems BERs and outage probabilities experience irreducible floors while their channel capacities experience ceilings. These expressions also helped us to investigate the impacts of different nodes mobility scenarios on the AF cooperative systems performance, where interesting and useful observations have been reported. These observations are related to which nodes are mobile and which are static, which cooperative protocol is followed; the regular protocol or the best-relay-selection one, which amplification gain category is employed at the relay, the variable-gain or fixed-gain. Moreover, the case of equipping the receivers with fast tracking loops feature has been assumed and it has been shown that such assumption has great capability of reducing the high nodes mobility effects.

- In this second part of the dissertation, we have dealt with evaluating and improving the performance of an emerging system model that combines both techniques of Alamouti-type orthogonal-space-time-block-code (Alamouti-OSTBC) and cooperative transmission and works under the influence of high nodes mobility. The classical Alamouti space-time decoder (ALD) is first employed at the destination and an approach that simplifies analyzing its overall error performance has been developed, where a closed-form expression for its conditional SEP performance has been derived and used to compute its average SEP performance semi-analytically. This derived expression is

novel and reduces to already derived existing literature results under the special case of negligible nodes mobility. Using the derived SEP expression, we have shown that the ALD is no longer optimal and experiences irreducible error floors when the nodes mobility is high. Therefore, in the second part of this dissertation, we have also proposed two space-time decoders to be employed instead of the ALD such that they can overcome with this high nodes mobility effect. These two decoders are the zero-forcing-space-time-decoder (ZFSTD) and the sub-optimal-space-time-decoder (SOSTD). The ZFSTD has shown its capability of completely suppressing the nodes mobility impact but at the expense of additional decoding complexity. On the other hand, the SOSTD can highly reduce the high nodes mobility effect without the need of any additional decoding complexity.

The work in this dissertation presents a valuable contribution to the wireless cooperative communications literature, in terms of performance evaluation and improvement. Moreover, the obtained results in this work are of great importance for network design engineers. They provide with closed-form expressions that help in cooperative-based networks planning rather than running time-consuming simulation algorithms. They also shed light on network performance behavior under the influence of mobile nodes speeds (e.g., in-town or highway mobile vehicles) and provide with perfect solutions to alleviate these influences.

10.2 Proposed Future Work

Possible extensions to this work can be summarized in the following points:

- Extending the error performance analyses carried out for coherent detectors to non-coherent or differentially coherent detectors, and investigating their error performance under the nodes mobility effect.
- Extending the study carried out for amplify-and-forward cooperative networks to decode-and-forward cooperative networks and investigating how their performance is affected by nodes mobility and imperfect CSI estimations.

- Extending the analyses conducted for narrowband channels to wideband channels (i.e., high data rate transmission) along with employing the orthogonal-frequency-division-modulation (OFDM) technique.
- Extending the 2x2 Alamouti-type OSTBC code to generalized OSTBC codes, and evaluating and improving their performance under the nodes mobility influences.

BIBLIOGRAPHY

BIBLIOGRAPHY

- [1] C. Patel and G. Stuber, "Channel estimation for amplify and forward relay based co-operation diversity systems," *Wireless Communications, IEEE Transactions on*, vol. 6, no. 6, pp. 2348–2356, June 2007.
- [2] F. Gao, T. Cui, and A. Nallanathan, "On channel estimation and optimal training design for amplify and forward relay networks," *Wireless Communications, IEEE Transactions on*, vol. 7, no. 5, pp. 1907–1916, May 2008.
- [3] Y. Wu and M. Patzold, "Performance analysis of cooperative communication systems with imperfect channel estimation," in *Communications, 2009. ICC '09. IEEE International Conference on*, June 2009, pp. 1–6.
- [4] Z. Hadzi-Velkov, D. S. Michalopoulos, G. K. Karagiannidis, and R. Schober, "On the effect of outdated channel estimation in variable gain relaying: Error performance and papr," *Wireless Communications, IEEE Transactions on*, vol. 12, no. 3, pp. 1084–1097, March 2013.
- [5] S. Ikki, S. Al-Dharrab, and M. Uysal, "Error probability of df relaying with pilot-assisted channel estimation over time-varying fading channels," *Vehicular Technology, IEEE Transactions on*, vol. 61, no. 1, pp. 393–397, Jan 2012.
- [6] M. Mohammadi, P. Sadeghi, T. Lamahewa, and M. Ardebilipour, "Impact of unknown time-varying fading on the information rates of amplify and forward cooperative systems," *Wireless Communications, IEEE Transactions on*, vol. 12, no. 1, pp. 146–157, January 2013.
- [7] J. Cavers, "An analysis of pilot symbol assisted modulation for rayleigh fading channels [mobile radio]," *Vehicular Technology, IEEE Transactions on*, vol. 40, no. 4, pp. 686–693, Nov 1991.
- [8] Y. Chen and N. Beaulieu, "Optimum pilot symbol assisted modulation," *Communications, IEEE Transactions on*, vol. 55, no. 8, pp. 1536–1546, Aug 2007.
- [9] H. S. Wang, "On verifying the first-order markovian assumption for a rayleigh fading channel model," in *Universal Personal Communications, 1994. Record., 1994 Third Annual International Conference on*, Sep 1994, pp. 160–164.
- [10] M. Tsatsanis, G. Giannakis, and G. Zhou, "Estimation and equalization of fading channels with random coefficients," in *Acoustics, Speech, and Signal Processing, 1996. ICASSP-96. Conference Proceedings., 1996 IEEE International Conference on*, vol. 2, May 1996, pp. 1093–1096 vol. 2.

- [11] R. Iltis, "Joint estimation of pn code delay and multipath using the extended kalman filter," *Communications, IEEE Transactions on*, vol. 38, no. 10, pp. 1677–1685, Oct 1990.
- [12] X. Zhou, T. A. Lamahewa, and P. Sadeghi, "Kalman filter-based channel estimation for amplify and forward relay communications," in *Signals, Systems and Computers, 2009 Conference Record of the Forty-Third Asilomar Conference on*, Nov 2009, pp. 1498–1502.
- [13] D. Michalopoulos, H. Suraweera, G. Karagiannidis, and R. Schober, "Amplify-and-forward relay selection with outdated channel estimates," *Communications, IEEE Transactions on*, vol. 60, no. 5, pp. 1278–1290, May 2012.
- [14] K. S. Gomadam and S. Jafar, "Impact of mobility on cooperative communication," in *Wireless Communications and Networking Conference, 2006. WCNC 2006. IEEE*, vol. 2, April 2006, pp. 908–913.
- [15] M. Avendi and H. Nguyen, "Performance of differential amplify-and-forward relaying in multinode wireless communications," *Vehicular Technology, IEEE Transactions on*, vol. 62, no. 8, pp. 3603–3613, Oct 2013.
- [16] W. C. Jakes and D. C. Cox, Eds., *Microwave Mobile Communications*. Wiley-IEEE Press, 1994.
- [17] H. Yomo and E. de Carvalho, "A csi estimation method for wireless relay network," *Communications Letters, IEEE*, vol. 11, no. 6, pp. 480–482, June 2007.
- [18] J. Laneman, D. Tse, and G. W. Wornell, "Cooperative diversity in wireless networks: Efficient protocols and outage behavior," *Information Theory, IEEE Transactions on*, vol. 50, no. 12, pp. 3062–3080, Dec 2004.
- [19] P. Anghel and M. Kaveh, "Exact symbol error probability of a cooperative network in a rayleigh-fading environment," *Wireless Communications, IEEE Transactions on*, vol. 3, no. 5, pp. 1416–1421, Sept 2004.
- [20] M. Hasna and M.-S. Alouini, "End-to-end performance of transmission systems with relays over rayleigh-fading channels," *Wireless Communications, IEEE Transactions on*, vol. 2, no. 6, pp. 1126–1131, Nov 2003.
- [21] —, "Harmonic mean and end-to-end performance of transmission systems with relays," *Communications, IEEE Transactions on*, vol. 52, no. 1, pp. 130–135, Jan 2004.
- [22] S. Ikki and M. Ahmed, "Performance analysis of cooperative diversity wireless networks over nakagami-m fading channel," *Communications Letters, IEEE*, vol. 11, no. 4, pp. 334–336, April 2007.
- [23] T. Nechiporenko, K. Phan, C. Tellambura, and H. Nguyen, "On the capacity of rayleigh fading cooperative systems under adaptive transmission," *Wireless Communications, IEEE Transactions on*, vol. 8, no. 4, pp. 1626–1631, April 2009.

- [24] M.-S. Alouini and A. Goldsmith, "Capacity of rayleigh fading channels under different adaptive transmission and diversity-combining techniques," *Vehicular Technology, IEEE Transactions on*, vol. 48, no. 4, pp. 1165–1181, Jul 1999.
- [25] M. Tsatsanis, G. Giannakis, and G. Zhou, "Estimation and equalization of fading channels with random coefficients," in *Acoustics, Speech, and Signal Processing, 1996. ICASSP-96. Conference Proceedings., 1996 IEEE International Conference on*, vol. 2, May 1996, pp. 1093–1096 vol. 2.
- [26] S. Chen, W. Wang, X. Zhang, and Z. Sun, "Performance analysis of ostbc transmission in amplify-and-forward cooperative relay networks," *Vehicular Technology, IEEE Transactions on*, vol. 59, no. 1, pp. 105–113, Jan 2010.
- [27] A. Bletsas, A. Khisti, D. Reed, and A. Lippman, "A simple cooperative diversity method based on network path selection," *Selected Areas in Communications, IEEE Journal on*, vol. 24, no. 3, pp. 659–672, March 2006.
- [28] S. S. Ikki and M. H. Ahmed, "Performance of multiple-relay cooperative diversity systems with best relay selection over rayleigh fading channels," *EURASIP J. Adv. Signal Process*, vol. 2008, pp. 145:1–145:7, Jan. 2008. [Online]. Available: <http://dx.doi.org/10.1155/2008/580368>
- [29] S. Ikki and M. Ahmed, "Performance analysis of adaptive decode-and-forward cooperative diversity networks with best-relay selection," *Communications, IEEE Transactions on*, vol. 58, no. 1, pp. 68–72, January 2010.
- [30] M. Yuksel and E. Erkip, "Multiple-antenna cooperative wireless systems: A diversity-multiplexing tradeoff perspective," *Information Theory, IEEE Transactions on*, vol. 53, no. 10, pp. 3371–3393, Oct 2007.
- [31] P. Jayasinghe, L. Jayasinghe, M. Juntti, and M. Latva-aho, "Performance analysis of optimal beamforming in fixed-gain af mimo relaying over asymmetric fading channels," *Communications, IEEE Transactions on*, vol. 62, no. 4, pp. 1201–1217, April 2014.
- [32] V.-B. Pham, "Space-time block code design for lte-advanced systems," *Transactions on Emerging Telecommunications Technologies*, 2013.
- [33] S. Alamouti, "A simple transmit diversity technique for wireless communications," *Selected Areas in Communications, IEEE Journal on*, vol. 16, no. 8, pp. 1451–1458, Oct 1998.
- [34] V. Tarokh, H. Jafarkhani, and A. Calderbank, "Space-time block codes from orthogonal designs," *Information Theory, IEEE Transactions on*, vol. 45, no. 5, pp. 1456–1467, Jul 1999.
- [35] T. Q. Duong, G. C. Alexandropoulos, H.-J. Zepernick, and T. A. Tsiftsis, "Orthogonal space-time block codes with csi-assisted amplify-and-forward relaying in correlated nakagami-fading channels," *Vehicular Technology, IEEE Transactions on*, vol. 60, no. 3, pp. 882–889, 2011.

- [36] L. Jayasinghe, N. Rajatheva, P. Dharmawansa, and M. Latva-aho, "Dual hop mimo ostbc communication over rayleigh-rician channel," in *Vehicular Technology Conference (VTC Spring), 2011 IEEE 73rd*, May 2011, pp. 1–5.
- [37] S. Frattasi, H. Fathi, F. Fitzek, R. Prasad, and M. Katz, "Defining 4g technology from the users perspective," *Network, IEEE*, vol. 20, no. 1, pp. 35–41, Jan 2006.
- [38] Z. Liu, X. Ma, and G. Giannakis, "Space-time coding and kalman filtering for time-selective fading channels," *Communications, IEEE Transactions on*, vol. 50, no. 2, pp. 183–186, Feb 2002.
- [39] F.-C. Zheng and A. Burr, "Signal detection for orthogonal space-time block coding over time-selective fading channels: a pic approach for the gi systems," *Communications, IEEE Transactions on*, vol. 53, no. 6, pp. 969–972, June 2005.
- [40] G. de Abreu, H. Orchiai, and R. Kohno, "Linear maximum likelihood decoding of space-time block coded ofdm systems for mobile communications," *Communications, IEE Proceedings-*, vol. 151, no. 5, pp. 447–459, Oct 2004.
- [41] T. Tran and A. Sesay, "A generalized linear quasi-ml decoder of ostbcs for wireless communications over time-selective fading channels," *Wireless Communications, IEEE Transactions on*, vol. 3, no. 3, pp. 855–864, May 2004.
- [42] G. Villardi, G. de Abreu, and R. Kohno, "Modified orthogonal space-time block codes for time-selective fading channels," in *Signals, Systems and Computers, 2005. Conference Record of the Thirty-Ninth Asilomar Conference on*, October 2005, pp. 1243–1247.
- [43] G. Villardi, G. de Abreu, R. Kohno, and H. Harada, "Stbcs with orthogonal decoder for highly time-selective channels," *Consumer Electronics, IEEE Transactions on*, vol. 56, no. 2, pp. 380–387, May 2010.
- [44] M. Hasna and M.-S. Alouini, "A performance study of dual-hop transmissions with fixed gain relays," vol. 3, no. 6, Nov 2004, pp. 1963–1968.
- [45] M. Tsatsanis, G. Giannakis, and G. Zhou, "Estimation and equalization of fading channels with random coefficients," in *Acoustics, Speech, and Signal Processing, 1996. ICASSP-96. Conference Proceedings., 1996 IEEE International Conference on*, vol. 2, May 1996, pp. 1093–1096 vol. 2.
- [46] A. Enescu and V. Koivunen, "Time-varying channel tracking for space-time block coding," in *Vehicular Technology Conference, 2002. VTC Spring 2002. IEEE 55th*, vol. 1, 2002, pp. 294–297 vol.1.
- [47] J. Proakis and M. Salehi, *Digital Communications*, ser. McGraw-Hill higher education. McGraw-Hill Education, 2007. [Online]. Available: <http://books.google.com/books?id=HroiQAAACAAJ>

- [48] E. Guerrero, G. Tello, and F. Yang, "Simulation and performance analysis for ordering algorithm in zf and mmse detectors for v-blast architectures," in *Computer Science and Network Technology (ICCSNT), 2011 International Conference on*, vol. 1, Dec 2011, pp. 59–64.
- [49] V. Tarokh, A. Naguib, N. Seshadri, and A. R. Calderbank, "Space-time codes for high data rate wireless communication: performance criteria in the presence of channel estimation errors, mobility, and multiple paths," *Communications, IEEE Transactions on*, vol. 47, no. 2, pp. 199–207, 1999.
- [50] A. Papoulis and S. U. Pillai, "Probability, random variables and stochastic processes," 2002.
- [51] M. K. Simon, *Probability distributions involving Gaussian random variables: A handbook for engineers and scientists*. Springer Science & Business Media, 2007.

APPENDIX

Appendix A

Approximating $I_3^{\vartheta_1}|\mathcal{S}_1$ as ZMCSCG

First, since $h_{1,\ell}^{\epsilon^*}(k)$ and $h_{\ell,d}^{\epsilon^*}(k)$ are ZMCSCG, we can express them as

$$h_{1,\ell}^{\epsilon^*}(k) = h_{1,\ell}^{\epsilon^*}(k)_{\Re} + jh_{1,\ell}^{\epsilon^*}(k)_{\Im} \text{ and } h_{\ell,d}^{\epsilon^*}(k) = h_{\ell,d}^{\epsilon^*}(k)_{\Re} + jh_{\ell,d}^{\epsilon^*}(k)_{\Im} \quad (\text{A.1})$$

where \Re and \Im denote the real part and imaginary part, respectively, $h_{1,\ell}^{\epsilon^*}(k)_{\Re}$ and $h_{1,\ell}^{\epsilon^*}(k)_{\Im}$ are $\mathcal{N}(0, \frac{\sigma_{e_{1,\ell}}^2}{2})$ and $h_{\ell,d}^{\epsilon^*}(k)_{\Re}$ and $h_{\ell,d}^{\epsilon^*}(k)_{\Im}$ are $\mathcal{N}(0, \frac{\sigma_{e_{\ell,d}}^2}{2})$. By substituting (A.1) into the term $I_3^{\vartheta_1}$ given in (9.3.6), we can expand it as

$$\begin{aligned} I_3^{\vartheta_1} = & \underbrace{\sum_{\ell=1}^M \mathcal{G}^2 h_{1,\ell}(k) h_{\ell,d}(k) h_{1,\ell}^{\epsilon^*}(k)_{\Re} h_{\ell,d}^{\epsilon^*}(k)_{\Re}}_{I_{3\ 1}^{\vartheta_1}} - \underbrace{\sum_{\ell=1}^M \mathcal{G}^2 h_{1,\ell}(k) h_{\ell,d}(k) h_{1,\ell}^{\epsilon^*}(k)_{\Im} h_{\ell,d}^{\epsilon^*}(k)_{\Im}}_{I_{3\ 2}^{\vartheta_1}} \\ & + j \left(\underbrace{\sum_{\ell=1}^M \mathcal{G}^2 h_{1,\ell}(k) h_{\ell,d}(k) h_{1,\ell}^{\epsilon^*}(k)_{\Re} h_{\ell,d}^{\epsilon^*}(k)_{\Im}}_{I_{3\ 3}^{\vartheta_1}} + \underbrace{\sum_{\ell=1}^M \mathcal{G}^2 h_{1,\ell}(k) h_{\ell,d}(k) h_{1,\ell}^{\epsilon^*}(k)_{\Im} h_{\ell,d}^{\epsilon^*}(k)_{\Re}}_{I_{3\ 4}^{\vartheta_1}} \right). \end{aligned} \quad (\text{A.2})$$

But, according to [51, Ch. (6)], if W_1 and W_2 are two independent zero-mean Gaussian random variables with variances σ_1^2 and σ_2^2 , respectively, then $U = W_1 W_2$ is a zero-mean random variable with variance $\sigma_1^2 \sigma_2^2$ and exact pdf of

$$f_U(u) = \frac{1}{\pi \sigma_1^2 \sigma_2^2} K_0 \left(\frac{|u|}{\sigma_1^2 \sigma_2^2} \right)$$

where $K_0(k)$ is the 0th order modified bessel function of the second kind. Based on this Gaussian random variables property, and conditioned on $h_{1,\ell}(k)$ and $h_{\ell,d}(k)$, each of $I_{3\ 1}^{\vartheta_1}$,

$I_{3\ 2}^{\vartheta_1}$, $I_{3\ 3}^{\vartheta_1}$ and $I_{3\ 4}^{\vartheta_1}$ in (A.2) is a sum of M independent but non-identically distributed zero-mean random variables such that the ℓ th one (say U_ℓ) has and pdf of

$$f_{U_\ell}(u) = \frac{1}{\pi \mathcal{G}^4 |h_{1,\ell}(k)|^2 |h_{\ell,d}(k)|^2 \frac{\sigma_{e_{1,\ell}}^2}{2} \frac{\sigma_{e_{\ell,d}}^2}{2}} K_o \left(\frac{|u|}{\mathcal{G}^4 |h_{1,\ell}(k)|^2 |h_{\ell,d}(k)|^2 \frac{\sigma_{e_{1,\ell}}^2}{2} \frac{\sigma_{e_{\ell,d}}^2}{2}} \right).$$

According to the CLT, we can now approximate the density of each of $I_{3\ 1}^{\vartheta_1} - I_{3\ 2}^{\vartheta_1}$ and $I_{3\ 3}^{\vartheta_1} + I_{3\ 4}^{\vartheta_1}$ as $\mathcal{N}\left(0, 2\mathcal{G}^4 \sum_{\ell=1}^M |h_{1,\ell}(k)|^2 |h_{\ell,d}(k)|^2 \frac{\sigma_{e_{1,\ell}}^2}{2} \frac{\sigma_{e_{\ell,d}}^2}{2}\right)$, and accordingly, the density of $I_3^{\vartheta_1}$ in (A.2) can be approximated as ZMCSCG as

$$\sim \mathcal{CN}\left(0, 4\mathcal{G}^4 \sum_{\ell=1}^M |h_{1,\ell}(k)|^2 |h_{\ell,d}(k)|^2 \frac{\sigma_{e_{1,\ell}}^2}{2} \frac{\sigma_{e_{\ell,d}}^2}{2}\right).$$

Appendix B

Approximating $I_6^{\xi_1}|\mathcal{S}_1$ and $I_{12}^{\xi_1}|\mathcal{S}_1$ as ZMCSCG

By substituting (A.1) and $e_{2,\ell}(k) = e_{2,\ell}(k)_{\Re} + je_{2,\ell}(k)_{\Im}$ into $I_6^{\xi_1}$ given in (9.4.10), we can expand $I_6^{\xi_1}$ as

$$\begin{aligned}
I_6^{\xi_1} = & \underbrace{\sum_{\ell=1}^M \mathcal{G}^2 \sqrt{1 - \rho_{s,\ell}^2} h_{\ell,d}(k) h_{1,\ell}^{\epsilon*}(k)_{\Re}}_{I_{6\ 1}^{\xi_1}} - \underbrace{\sum_{\ell=1}^M \mathcal{G}^2 \sqrt{1 - \rho_{s,\ell}^2} h_{\ell,d}(k) h_{1,\ell}^{\epsilon*}(k)_{\Im}}_{I_{6\ 2}^{\xi_1}} \\
& - \underbrace{\sum_{\ell=1}^M \mathcal{G}^2 \sqrt{1 - \rho_{s,\ell}^2} h_{\ell,d}(k) h_{1,\ell}^{\epsilon*}(k)_{\Re}}_{I_{6\ 3}^{\xi_1}} - \underbrace{\sum_{\ell=1}^M \mathcal{G}^2 \sqrt{1 - \rho_{s,\ell}^2} h_{\ell,d}(k) h_{1,\ell}^{\epsilon*}(k)_{\Im}}_{I_{6\ 4}^{\xi_1}} \\
& + j \left(\underbrace{\sum_{\ell=1}^M \mathcal{G}^2 \sqrt{1 - \rho_{s,\ell}^2} h_{\ell,d}(k) h_{1,\ell}^{\epsilon*}(k)_{\Re}}_{I_{6\ 5}^{\xi_1}} - \underbrace{\sum_{\ell=1}^M \mathcal{G}^2 \sqrt{1 - \rho_{s,\ell}^2} h_{\ell,d}(k)}_{I_{6\ 6}^{\xi_1}} \right. \\
& \left. + \underbrace{\sum_{\ell=1}^M \mathcal{G}^2 \sqrt{1 - \rho_{s,\ell}^2} h_{\ell,d}(k) h_{1,\ell}^{\epsilon*}(k)_{\Re}}_{I_{6\ 7}^{\xi_1}} + \underbrace{\sum_{\ell=1}^M \mathcal{G}^2 \sqrt{1 - \rho_{s,\ell}^2} h_{\ell,d}(k) h_{1,\ell}^{\epsilon*}(k)_{\Im}}_{I_{6\ 8}^{\xi_1}} \right).
\end{aligned} \tag{B.1}$$

Conditioned on $h_{\ell,d}(k)$, each term in (B.1) is a sum of M independent but non-identically distributed random variables where the ℓ th one of them (say D_{ℓ}) has mean zero, variance

$\mathcal{G}^4(1 - \rho_{s,\ell}^2)|h_{\ell,d}(k)|^2 \frac{\sigma_{e_{1,\ell}}^2}{2} \frac{\sigma_{e_{\ell,d}}^2}{2} \frac{\sigma_{2,\ell}^2}{2}$ and exact pdf of

$$f_{D_\ell}(d) = \frac{1}{2\sqrt{2}\pi^{3/2}\mathcal{G}^4(1 - \rho_{s,\ell}^2)|h_{\ell,d}(k)|^2 \frac{\sigma_{e_{1,\ell}}^2}{2} \frac{\sigma_{e_{\ell,d}}^2}{2} \frac{\sigma_{2,\ell}^2}{2}} \times G_{0,3}^{3,0} \left(\frac{d^2}{8\mathcal{G}^4(1 - \rho_{s,\ell}^2)|h_{\ell,d}(k)|^2 \frac{\sigma_{e_{1,\ell}}^2}{2} \frac{\sigma_{e_{\ell,d}}^2}{2} \frac{\sigma_{2,\ell}^2}{2}} \middle| 0, 0, 0 \right)$$

where $G_{p,q}^{m,n}$ denotes the Meijer G-functions. Now, according to CLT, we can approximate the density of each of $I_{6,1}^{\xi_1} - I_{6,2}^{\xi_1} - I_{6,3}^{\xi_1} - I_{6,4}^{\xi_1}$ and $I_{6,5}^{\xi_1} - I_{6,6}^{\xi_1} + I_{6,7}^{\xi_1} + I_{6,8}^{\xi_1}$ as $\mathcal{N}\left(0, 4\mathcal{G}^4(1 - \rho_{s,\ell}^2)|h_{\ell,d}(k)|^2 \frac{\sigma_{e_{1,\ell}}^2}{2} \frac{\sigma_{e_{\ell,d}}^2}{2} \frac{\sigma_{2,\ell}^2}{2}\right)$, and accordingly, the density of $I_6^{\xi_1}$ in (B.1) can be approximated as ZMCSCG as $\sim \mathcal{CN}\left(0, 8\mathcal{G}^4(1 - \rho_{s,\ell}^2)|h_{\ell,d}(k)|^2 \frac{\sigma_{e_{1,\ell}}^2}{2} \frac{\sigma_{e_{\ell,d}}^2}{2} \frac{\sigma_{2,\ell}^2}{2}\right)$. Similarly, we can approximate the density of $I_{12}^{\xi_1}$ in (9.4.10), conditioned on $h_{\ell,d}(k+1)$, as $\sim \mathcal{CN}\left(0, 8\mathcal{G}^4(1 - \rho_{s,\ell}^2)|h_{\ell,d}(k+1)|^2 \frac{\sigma_{e_{2,\ell}}^2}{2} \frac{\sigma_{e_{\ell,d}}^2}{2} \frac{\sigma_{1,\ell}^2}{2}\right)$.

VITA

Yazid Khattabi was born in Ajloun, Jordan, in 1985. He received the Bachelor degree (with highest honors) in Electrical Engineering with emphasis in Electronics and Communications and the Master degree in Electrical Engineering with emphasis in Wireless Communications both from Jordan University of Science and Technology (JUST), Irbid, Jordan, in 2008 and 2010, respectively.

From March 2011 to December 2012, he was a communication and electronics design engineer at King Abdullah II Design and Development Bureau (KADDB), Amman, Jordan. During the period of 2013-2016, he was with the Center for Wireless Communications (CWC) at the University of Mississippi, Oxford, MS, USA, as a Research Assistant where he pursued his Ph.D. degree in Electrical Engineering. His research interest includes several areas in wireless communications with emphasis on the performance evaluation and improvement of mobile cooperative communication systems over fading channels.

In recognition of his research work at the University of Mississippi, Mr. Khattabi is the recipient of the University of Mississippi Summer Research Assistantship Award in 2014 and 2016, and the recipient of the Dissertation Fellowship from the Graduate School in Spring 2016. He is also the recipient of the Best Poster Award at the 2015 Broadband Wireless Access & Applications Center (BWAC) Workshop, January 2015, Oxford, MS, USA. Mr. Khattabi served as a reviewer for several refereed international journals and conferences and currently he is an IEEE student member.